Culture of human pluripotent stem cells and neural networks in 3D using an optogenetic approach and a hydrogel model

A thesis presented for the degree of Doctor of Philosophy

by

Si Yuen Lee

Jesus College

Department of Oncology
and
Institute of Biomedical Engineering
University of Oxford

Hillary Term 2015/2016

Dedication

In loving memory of my late father

To the heavenly father with grateful thanks for His unconditional love

To Homo sapiens – be kind to one another, tenderhearted and forgiving one another

Acknowledgement

1. Dari Kuantan ke Menara Mimpi

Sesat Jalan di Neraka Api

Walau saudari bermulia hati

Jangan dibuli sesuka hati

`

2. Jadi hamba bayar tuan gaji

Dihina disingkir suatu hari

Ribut kencang kekalkan janji

Ingat keluarga sayangkan diri

3. Terbang tinggi cara hidup

Helang cedera jadi teladan

Tanya Yesus makna hidup

Kevin dikorban demi jawapan

4. Berjalan bersama Emmanuel

Manis, masam, pahit, pedas

Henna, Sarah, Willie, Eunice

Suka duka ditempuh bersama

5. Keluar tanah Mesir hamba dilindungi

Janji Tuhanku tidak dilupai

Guru membina aku disanjungi

Akar umbiku tidak dilupai

Declaration

I declare that this thesis is wholly my own work.

Supervision

Supervisor:
Leonard W. Seymour
Department of Oncology (Clinical Pharmacology)

Co-supervisor:
Hua Ye
Institute of Biomedical Engineering (IBME)

Lab-supervisor:
Julian H. George
Institute of Biomedical Engineering (IBME)

Abstract

Development of optogenetically controllable human neural network models can provide an investigative system that is relevant to the human brain. Conventional cultures of neural networks in two-dimensions (2D) have major limitations of scale. For instance, the soma of neurons in 2D is unrealistically flattened and both axon and dendrite outgrowth is restricted. Using a combination of tissue engineering techniques and the inclusion of optogenetically modified human induced pluripotent stem cell (hiPSC)-derived neural progenitor cells (NPCs), the development of a three-dimensional (3D) human neural culture model within a defined 3D microenvironment is investigated in this study.

Light-sensitive neurons were successfully generated by transducing Channelrhodopsin-2 (ChR2) into human iPSC-derived NPCs and neuroblastoma cells (SH-SY5Y) using lentiviral transduction. The use of neuron specific promoters for synapsin-1 (SYN1) and calcium-calmodulin kinase II (CaMKII) in driving the expression of ChR2-Yellow Florescent Protein (YFP) within the mixed neuronal populations from hiPSC-derived neurons (Axol cells) were compared. Viability of the cells at 7 day-post-infection was 80% - 97% in all conditions tested. In line with published literature, transduction efficiency of neurons at day 14 was found to be 3% - 7% for plasmids containing the SYN1 promoter and 2% - 5% for plasmids containing the CaMKII promoter. An increase in promoter driven ChR2-YFP expression was evaluated over 28 days as the neural subpopulations matured. Stably ChR2 expression continued through-out higher passages ($\geq P_{10}$) and possibly for periods up to several months. Both SYN1 and CaMKII promoters were found to drive the expression of ChR2 in Axol cells targeting inhibitory and excitatory neurons, respectively.

3D culture systems to support cell growth and optogenetic application were developed and characterised. Alginate hydrogel functionalised with short peptide sequence arginine-glycine-aspartate (RGD), and small molecules such as Rho Kinase inhibitor (ROCKi) and ZVAD were incorporated to increase the viability of human pluripotent stem cells (hPSCs). Investigation of cell response reveals that a flow rate of 3 ml/min and an alginate concentration of 1.8% (w/v) are optimal and that stem cell survival is significantly improved through incorporation of RGD and ROCKi. Interestingly, ChR2-YFP expression of Axol and SY5Y cells was detectable when transferred to the 3D culture system.

The optogenetically modified neurons were found responsive to light stimulation, showing firing patterns and calcium events typical of early developing neurons (e.g. mixed and burst waves; single and multipeak spikes). Neuronal activities were assessed using calcium imaging. Higher numbers of calcium events were associated with CaMKII driven ChR2-YFP expression than with SYN1 in Axol cells. However, calcium activity in SH-SY5Y cells was most noticeable in neurons expressing ChR2-YFP driven by the SYN1 promoter. In primary rodent neuronal cultures, synchronous calcium firing with repetitive action potentials (APs) resulted from ChR2-YFP expression was driven by both SYN1 and CaMKII promoter upon light stimulation. By combining multi-approaches, we report for the first time on the generation of an *in vitro* hiPSC-derived neural network model in 3D using functionalised alginate hydrogel and involving optogenetic targeting. Expression of ChR2-YFP was found driven by both SYN1 and CaMKII promoter in the RGD-alginate bead system that cultured with Axol cells.

Table of Contents

List of Figures

5.0 Neurophysiological investigation of human neural networks in 2D and 3D 118

List of Tables

List of Abbreviations

AAV	Adeno-associated viruses
ACSF	Artificial cerebrospinal fluid
Alg	Alginate
AM ester	Acetoxymethyl ester
AMPA	α-amino-3-hydroxy-5-methylisoxazole-4-propionic acid
ANOVA	Analysis of variance
AP	Action potential
ATP	Adenosine triphosphate
Axol	Human induced pluripotent stem cell-derived neural progenitor cells
BDNF	Brain-derived neurotrophic factor
BRs	Bacteriorhodopsins
BSA	Bovine serum albumin
Ca2+/CaM	Calcium/Calmodulin complex
CaMKII	Calcium/calmodulin-dependent protein kinase type II
ChoP	Channelopsin
ChR2	Channelrhodopsin-2
CNS	Central nervous system
cRGD	cyclic Arginine-Glycine-Aspartate
DAPI	6-diamidino-2-phenylindole
DIV	Day in vitro
DMEM	Dulbecco's modified eagle's medium
DMSO	di-methylsulfoxide

DNA	Deoxyribonucleic acid
DRG	Dorsal root ganglion
ECM	Extracellular matrix
EDC	Carbodiimide hydrochloride
EDTA	Ethylenediaminetetraacetic acid
EF1a	Elongation factor-1 alpha
EFG	Epidermal growth factor
env	envelop
ER	Endoplasmic reticulum
ERK	Extracellular signal regulated kinase
EPSC	Excitatory postsynaptic current
EPSP	Excitatory postsynaptic potential
EtBr	Ethidium bromide
EtOH	Ethanol
E8	Chemically defined E8 medium
FAK	Focal adhesion kinase
FBS	Fetal bovine serum
FGF-2	Fibroblast growth factor-2
FITC	Fluorescein isothiocyanate
Fig.	Figure
FRET	Fluorescence resonance energy transfer
GABA	γ-aminobutyric acid
GFAP	Glial fibrillary acidic protein

GFP	Green fluorescent protein
HEK 293FT	Human embryonic kidney 293FT cell line
HIV	Human immunodeficiency virus
HRs	Halorhodopsins
hESCs	Human embryonic stem cells
hPSCs	Human pluripotent stem cells
hrs	Hours
ICM	Inner cell mass
iPSC	Induced pluripotent stem cells
IF	Immunofluorescent
ITR	Inverted terminal repeat
kDa	kilo Dalton
KCl	Potassium chloride
Kd	Dissociation constant
KSR	Knockout serum replacer
LB	Lysogeny broth
LED	Light-emitting diode
LiCl	Lithium chloride
LN	Laminin
LP	Lentiviral particle
LRRK2	Leucine-rich repeat protein kinase-2
LTRs	Long terminal repeats
LV	Lentivirus

MAPK	Mitogen-activated protein kinase
MNK1	MAPK-interacting protein kinases-1
MEA	Multielectrode array
MEFs	Mouse embryonic fibroblasts
MEM	Minimal essential medium
mEPSC	Miniature excitatory postsynaptic current
MLC	Myosin light chain
MSK1	Mitogen-, stress-activated protein kinase-1
MOI	Multiplicity of infection
MSCs	Mesenchymal stem cells
Mw	Molecular weight
NPC	Neural progenitor stem cells
NGF	Nerve growth factor
NMDA	N-methyl-D-aspartate
NS	Neural stem cells
ORF	Open reading frame
PBS	Phosphate buffered saline
PBST	Phosphate puffered saline with tween 20
PEG	Poly(ethylene glycol)
Pen-Strep	Penicillin-streptomycin
PFA	Paraformaldehyde
PF127	Pluronic acid
PI	Propidium iodide
pol	Protease

Pol II	Polymerase II
PRK2	Protein kinase C-related kinase 2
PSD	Post-synaptic density
PVA	Poly(vinyl alcohol)
RA	Retinoic acid
RGD	Arginine-Glycine-Aspartate
RNA	Ribonucleic acid
ROCK	Rho-associated protein kinase
ROCKi	Rho-associated protein kinase inhibitor
ROI	Region of interest
rcf	elative centrifugal force or x g-force
rpm	revolutions per minute
SCC	Saline-sodium citrate buffer
SD	Standard deviation
SEM	Standard error of mean
S.O.C	Super optimal broth with catabolite repression
SYN1	Synapsin 1
SY5Y	Neuroblastoma (SH-SY5Y cell line)
TGF- β	Transforming growth factor-β
Tuj1	Neuron-specific class III beta-tubulin
vGlut1	Vesicular glutamate transporter 1
vGlut2	Vesicular glutamate transporter 2
WPRE	Woodchuck hepatitis virus (WHP) posttranscriptional regulatory element

YFP	Yellow fluorescent protein
ZVAD	zVAD-fmk (caspase-3 inhibitor)

1.0 Introduction

1.1 Overview

Investigating the function of complex cortical neural circuits is currently only possible through use of animal models, where investigations are typically performed either on tissue slices dissected from live brains or through direct stimulation and recording of neural circuits in animal brains *in-situ*. It is also possible to investigate neural cell function in 2D culture of neurons derived from disassociated animal brain tissue that display neuron-like properties such as the rat and mouse cell lines (PC12, NG108-15, and F11 cells) or the human neuroblastoma cell lines (SH-SY5Y, NT2, and REN cells). However, all these models have a number of disadvantages. For instance, the results obtained from animal studies are not equivalent to investigations carried out in human tissue, and the use of carcinoma-derived cell lines cannot recapitulate the responses found in healthy human neurons and glia cells. To this end, the development of a human cortical culture model derived from human pluripotent stem cells (hPSCs) would be a fundamental step forwards benefiting neuroscience research, producing functional neurons for treating neurodegenerative diseases or damaged brain tissues.

Considering the self-renewal capacity of hPSCs, direct neuronal differentiation protocols of hPSCs, and selective stimulation of grafted cells, it is anticipated that neuronal functions and integration of these cells into a native circuitry or a new habitat may achieve when combined with optogenetics, the method of the year 2010. Before the introduction of optogenetics, little was known about the functional integration of transplanted stem cell-derived neurons as a unit of the brain circuitry. However, optogenetics can tackle this challenge by genetically modified stem cells that respond to light both *in vitro* and *in vivo*.

The work performed in this thesis describes the development and optimisation of optogenetic modified human neuronal networks derived from hPSCs in a 3D culture model using hydrogels for the first time. The transparent alginate hydrogels allow for optical analysis of cells in culture and the physical properties of alginate hydrogels can be tailored to regulate diffusion around the cells, leading to higher cell viability. In addition, the culture and expansion of hPSCs have many challenges, some of which may be overcome through use of 3D culture systems. Current culture systems for hPSCs utilise mouse embryonic fibroblast (MEF) feeder layers to support stem cell attachment and growth. Stem cells grown as spheroids in culture without MEF feeder layers are tend to differentiate away from the stem cell phenotype. However, modified alginate hydrogels enhance adhesion of hPSCs and allow expansion of stem cell spheroids that may mitigate the requirement for feeder layer culture. Peptide functionalised alginate incorporated with small molecules were among the strategies used to create a chemically defined 3D culture system in this project.

A key property of the neural network model is that it should support the stimulation and recording of neuronal firing (action potential activity). This can be achieved through non-invasive optical techniques (optogenetics) both in 2D and 3D cultures. In the present study, the use of calcium dyes (calcium imaging) for recording neuronal activity and expression of light sensitive channelrhodopsin 2 (ChR2) ion channels is investigated upon optical stimulation in monolayer culture and 3D hydrogel model.

Targeting of specific cell types in the mix populations of human brain tissue or neuronal populations derived from hPSCs is feasible using optogenetics. For example, inhibitory and excitatory neurons which involve in neural network firing can be labelled with neuron-specific promoters (synapsin1 and Ca^{2+}/calmodulin-dependent protein kinase II α) linked to ChR2.

Establishing methods to control light-activated ChR2 expression is a novel area and essential in this study.

We therefore hypothesised that optogenetics may enable the assessment of neuronal activity of differentiated neurons derived from hiPSCs in a 3D alginate hydrogel system.

1.2 Optogenetics

Karl Deisseroth (together with Edward Boyden) have defined optogenetics as: the *"Combination of optical and genetic method to obtain gain or loss in function of well-defined events in specific cells of living tissue"* [1].

This method is based on membrane bound light responsive proteins named opsins, which was first implemented in neurons in 2005 [2]. Earlier, in 1979, Francis Crick predicted that to fully investigate the complexity of the brain, there would be a demand to inactivate one specific cell type without altering the functions of others [3]. Despite cell type specificity, the circuits of the brain should have fast kinetics to provide high temporal control of the neural activity.

Although electrical stimulation with electrodes provides high temporal resolution to inhibit or excite single action potentials (APs) in neurons, it is difficult to achieve specific control of single cell types due to the general electrical influence of the electrodes on their surroundings. Pharmacological and genetic approaches are able to target specific cell types, but have slow kinetics to control discrete spiking in neurons [4]. Conventional methods to modulate neurons such as electrical stimulation, pharmacological and genetic techniques have not yet successfully combined both the cell type specificity and fast kinetics that are required for precise control of neural circuits. Each of these methods has major drawbacks, however, optogenetics enables the combination of fast elements from the electrical stimulation and high selectivity from genetic techniques. This subsequently provides a new approach for precision control of the brain [5].

1.2.1 Rhodopsins – photoreceptors in optogenetics

The most commonly used opsins are Bacteriorhodopsins (BRs), Halorhodopsins (HRs) and Channelrhodopsin (ChRs). Opsins are seven-transmembrane-helix proteins that form a pocket in which the chromophore retinal is covalently linked (this complex is known as rhodopsin, a photoreceptor) [6]. The opsin genes are classified into two groups: microbial (type I proteins) and animal (type II proteins). Type I proteins are found in archaea, eubacterium, fungi and algae, whereas type II proteins are expressed in mammalian cells. Type II proteins indirectly control transmembrane ion currents by coupling to G-protein based signal transduction pathways. Type I proteins (BRs, HRs and ChRs) are not bound to these signal transduction pathways but depend on their direct-light-activated regulators of transmembrane ion conductance. BRs pump protons from the cytoplasm to the extracellular medium to drive adenosine triphosphate (ATP) synthesis via light energy that harvests from a pH gradient over the membrane [6, 7], supporting membrane hyperpolarisation. HRs (derived from *Natronomonas Pharaonis*, NpHR) are light-driven inward specific chloride (Cl^-) pumps that support the silencing of neural activity in response to yellow light [8]. In contrast, ChRs (derived from *Chlamydomonas reinhardtii*) are light-driven inward non-specific cation channels (Ca^{2+}, H^+, K^+, Na^+) supporting neural depolarisation in response to blue light [9]. ChRs are highly utilised in neuroscience research due to the expression of ChRs in neurons can trigger APs within milliseconds [10].

1.2.2 Channelrhodopsin-2 (ChR2) – optogenetic actuators of neural activity

ChR2 (Fig. 1.1), a light-gated nonspecific cation channel, was the first depolarising opsin successfully expressed in mammalian neurons. It absorbs blue light (350 - 550 nm, average 470 nm) [10], and triggers a conformational change from the transition of low-energy all-trans-retinal chromophore complex to the higher energy 13-cis-retinal [10]. Subsequently, transmembrane

proteins are activated, opening a channel (size ≥ 6Å) and allowing the passive transport of cations. This change leads to cell membrane depolarisation and generation of APs firing. When the light is turned off, the 13-cis-retinal form returns to the all-trans form within milliseconds, closing the channel and terminating the flow of cations [2, 10-13].

ChR2 is an attractive tool to depolarise neurons because: (1) the channel can be quickly and reversibly activated by light illumination [11, 14], therefore, single APs can be generated with a brief pulse of blue light and no long lasting residual effects are seen from stimulation. (2) ChR2 can be expressed in specific cells through the use of promoters and enhancer elements [13, 15-17]. (3) Genetically modified ChR2 variants are available to meet different needs with each having unique advantages.

ChR2 can pair with channelrhodopsin-1 (VChR1, derived from *Volvox carteri*) as a powerful tool for controlling neuronal activity [4]. This is because VChR1 is significantly light sensitive at 589 nm, a wavelength which ChR2 (470 nm) unresponsive to. Both ChR2 (deactivation time constant ~12 ms) and VChR1 (deactivation time constant ~120 ms) are able to transduce trains of millisecond-duration light flashes into defined spike trains (30–50 Hz) [2, 13, 18]. They are normally utilised to direct control spiking rather than temporary modulate the intracellular biochemical activity. Due to sufficient spectral separation, ChR2 also paired with NpHR which can be expressed in the same neurons simultaneously to enable bi-directional optical control of neuronal activity [4].

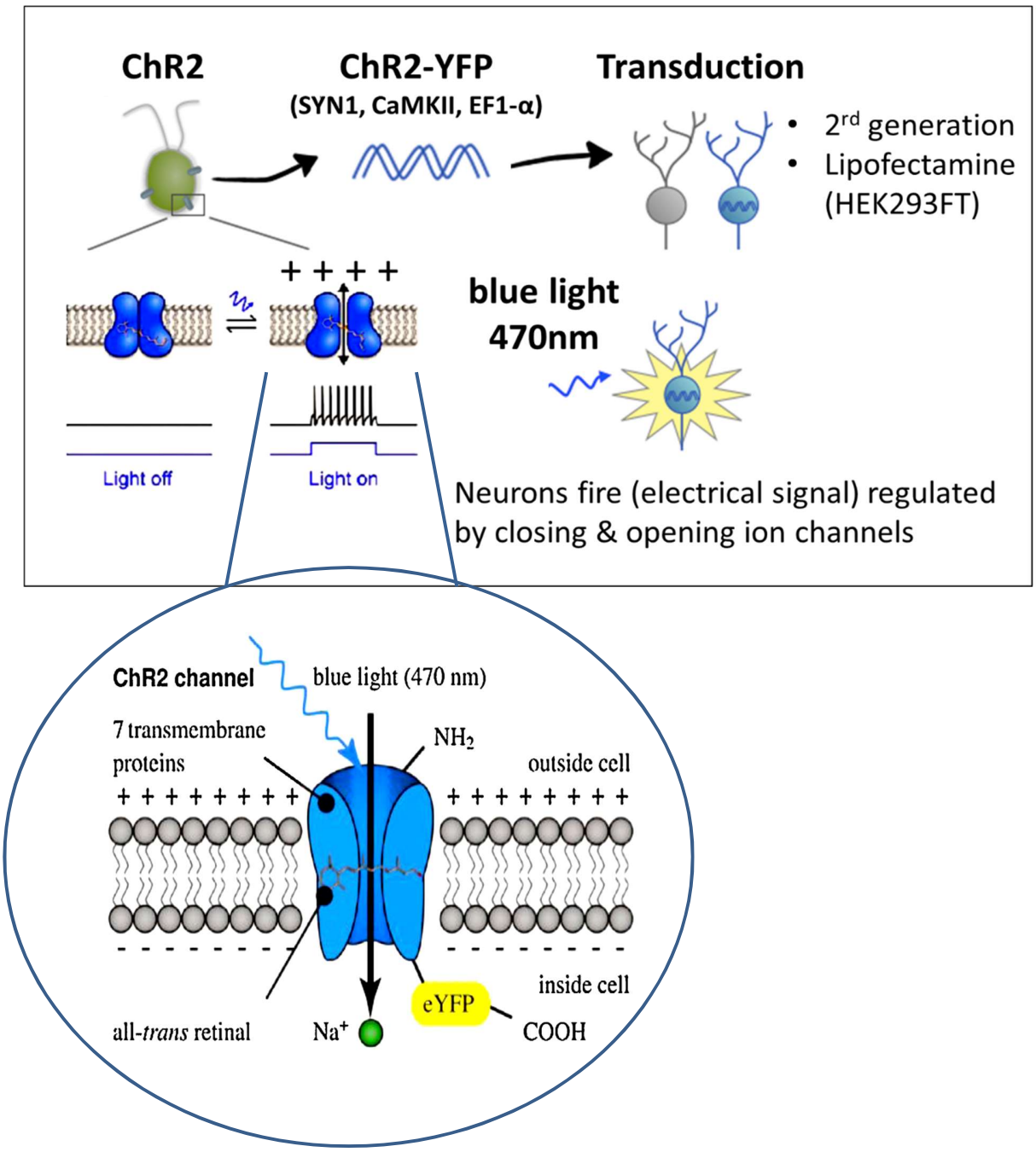

Figure 1.1: Channelrhodopsin-2 (ChR2).

ChR2 (found in the eyespot of green algae) has been used recently to map the functional circuit of neural system. It consists of 7 transmembrane proteins fused to YFP. When photo-stimulated with blue light at 470 nm, the ion channel opens followed by ultra-fast membrane depolarisation and calcium influx, subsequently generating an action potential (AP). ChR2-SYN1, -CaMKII and –EF1a were constructed and packaged using lentiviruses through second generation transfection onto HEK293FT cells in this project (credit: Stanford University, adapted from Dugue, G.P. et al., 2012 and LaLumiere, R.T. et al., 2011) [19, 20].

1.2.3 The variants of ChR2

The functions of ChR2 can be engineered, expanded and refined by altering their absorption spectral properties, conductance and kinetics (faster or slower open-state lifetimes). Wild type ChR2 is a light-switched cation-selective ion channel. The channel opens rapidly after absorption of a photon to generate a large permeability for cations. Mutations, however, permit more rapid gating of ChR2, allowing AP firing up to 200 Hz [21] and flexibility in regulating neuronal activity via different wavelengths of light [22]. One point mutation, H134R in ChR2 [23], has been shown to result in two to three times improved cellular photocurrents, but at the cost of slow deactivation [23]. A number of C128 point mutants of ChR2 demonstrated profound bi-stability, converting a brief pulse of light into a stable step in membrane potential [21]. At the stable state, transduced cells are responsive to light at lower intensity (>100×) because of delayed exit of these proteins from the open state [21]. When compared to wild type ChR2, the C128 mutants are activated faster by blue light (470 nm), and the photocurrents evoked by the opening of ChR2-C128A and ChR2-C128S can be superiorly inactivated by green light (542 nm). This created a step-function opsin (SFO) which is very useful for light-controlled stimulation of cells [24].

On the other hand, Andre Berndt et al. have discovered substitution of threonine-to-cysteine at position 159 (ChR2-T159C) that can produce very large photocurrents and sensitize neurons to very low light intensities [22]. Many optophysiological experiments are limited due to the relatively small photocurrent. Combination of E123T and T159C yielded a double mutant (ChR2-be) that sustained optical stimulation of hippocampal pyramidal neurons (≥60 Hz). Another ChR2 variant, calcium translocating channelrhodopsin (CatCh) which possesses a point mutation at L132C, is able to accelerate response time and increase light sensitivity (70x more than wild-type) in voltage response [25].

1.2.4 Delivery of ChR2 to target cells

There are three main methods to deliver genes coding for light sensitive proteins (e.g. ChR2) into target cells such as transfection, viral transduction and the creation of transgenic animal lines. These delivery methods are all commonly used, each with their own advantages and limitations. Targeted cellular expression can be achieved by using specific promoters, delivering a location specific injection, or by restricting activation through targeted light delivery [21].

Transfection is a non-viral method of introducing the gene into host cells which includes electroporation, liposomal transfection, DNA microinjection and calcium phosphate precipitation. Such methods are relatively safe as they do not involve infectious biological agents. Effectiveness in achieving high expression on the targeted cell and practical issues for *in vivo* use, however, are two significant limitations [26].

Viral transduction alternatively, is widely applied by using recombinant viruses containing ChR2 gene. Several viral vectors have been utilised experimentally including adenoviruses [27], adeno-associated viruses (AAV), retroviruses [28] and lentiviruses [29, 30]. Among the viral vectors, lentivirus (LV) and adeno-associated virus (AAV) have been chosen for introducing excitatory and inhibitory opsins to *in-vivo* tissue [11]. The viral vector is injected to the area of interest in the brain, and subsequently infects most of the cells in the vicinity of the injection site because these viruses are capable of infecting both dividing and non-dividing cells. [31].

1.2.5 Recombinant adeno-associated virus (rAAV) as transfer vector

To date, recombinant adeno-associated virus (rAAV) gene delivery has been successfully used to express ChR2 in mouse retinal neurons and hippocampal neurons. The expression was reported to be stable for a year [32, 33]. Furthermore, genetic modules introduced into rAAV are found to be less prone to epigenetic gene silencing [34]. Due to their high rate of infectivity, rAAVs can be used to deliver multiple genes into the same neurons in selective brain regions [35]. This widens the experimental possibilities that other genes (which act as biosensors for different signaling systems, such as for calcium [36, 37] and neurotransmitter release [38]) could also be introduced into the same neuron using rAAV. The availability of different AAV serotypes offers additional means of selectively targeting different neuron types [35, 39, 40]. This may useful for the investigation of functional brain circuits in living animals. The low immunogenicity of rAAVs have made rAAV gene delivery suitable for the therapeutic treatment of neurological diseases in human [41]. Use of rAAVs as transfer vectors have been less applied in human stem cells compared to lentiviruses.

1.2.6 Lentivirus (LV) as transfer vector

Lentiviral (LV) vectors are more widely exploited in hPSC research than rAAVs due to several advantages and features. LV vectors have been proven to efficiently target dividing cells and stably integrate into the host genome of human embryonic stem cells (hESCs) [42]. The lentiviruses (LVs) including human, equine, simian and feline immunodeficiency viruses are a genus of the Retroviridae family. LVs can target the nucleus of both dividing and non-dividing cells without causing the breakdown of the nuclear membrane for genome integration (as required by gammaretroviruses). In comparison to other viruses, lentiviral long terminal repeats (LTRs) are less prone to methylation and gene silencing, enabling long-term control over viral transcription [43].

The lentiviral genome consists of a positive-sense single-stranded RNA (ssRNA) encoding core *gag* (capsid), *pol* (protease, reverse transcriptase, and integrase) and *env* (envelope) genes, as well as a number of accessory genes. The accessory genes are not involved in the generation of recombinant vector systems, however *gag*, *pol* and an *env* are used for effective recombinant viral packaging. Packaging of viruses can be improved by triple (2nd generation) or quadruple (3rd generation) transfection of human embryonic kidney cells (HEK293) [44]. *Gag* and *pol* genes (from HIV), and *env* (vesicular stomatitis virus glycoprotein, VSV-G) are provided in trans proteins that are packaged into recombinant virions.

The recombinant viral genome contains desired transgenes (e.g. ChR2) and promoter elements (e.g. SYN1, CaMKII, EF1a) with a packaging signal and modified LTRs. In general, recombinant LV particles contain minimal viral RNA (≤ 40%), transgene/s and regulators (promoters and/or enhancers) packaged with reverse transcriptase, protease and integrase proteins in a lentiviral capsid studded with envelope glycoprotein. Viral particles harvested from the packaging cell media can be used directly for transduction or concentrated by ultracentrifugation before use.

The efficiency of lentiviral-mediated gene transfer to any cell type depends on the vector and cellular target. Uptake of the viral particle relies upon various factors including the affinity of the viral envelope for target cell surface receptors, endocytosis, transfer, integration and expression of the viral genome within the target cells. Efficiency of LV transduction in hPSCs is measured based on transgene expression. Further improvement of transgene expression is possible at lower multiplicities of infection (MOIs) by optimising earlier steps in transduction. In addition, changing the *env* glycoprotein can be used to alter viral tropism to selectively transduce hESCs or neural derivatives. Although VSV-G is the most commonly used envelope, the RD114 glycoprotein from

endogenous feline leukemia virus and the GALV glycoprotein from gibbon ape leukemia virus, have both shown selective tropism for hESCs [45]. LVs pseudotyped with rabies or LCMV glycoproteins exhibit tropism for neurons [46] and astrocytes [47] derived from rodents, respectively.

Although hESCs and their neural progeny have been efficiently transduced by LV vectors, the stability of transduction throughout neural differentiation and maturation is also regulated by the promoters which drive transgene expression. The following section will discuss the role of cell type specific promoters.

1.2.7 Cell type-specific promoters

The use of cell type-specific promoters to restrict gene expression of a specified cell population within the brain remains an attractive approach [48, 49]. Gene expression is regulated by genetic sequences preceding the gene that codes for a protein (called promoters). Transcription factors bind to the promoter to trigger the transcription into mRNA. The sets of transcription factors which regulate the gene expression can specify a cell type. The amount of expression is control by the number of transcription factors dedicated to one promoter. There are neuronal populations that express one specific type of protein. The promoter of such protein can link to a transgene in a vector. Expression of this transgene will then be directed to the cell type of interest only even though the virus has the potential to infect all cells.

There are numerous neuron-specific promoters available to target different type of neurons being applied to transgenic animals and viral vectors. For instance, the Ca^{2+}/calmodulin-dependent protein kinase II α (CaMKII α) has been used to target excitatory pyramidal neurons [50] and the Parvalbumin (PV) promoter has been used to target a certain class of interneurons [51]. Human synapsin I (SYN1) has been instrumental to visualise and sort neurons from the mixed population but is not specific to any neuronal subtype as SYN1 targets both inhibitory and excitatory neurons

(Table 1.1). Other neuron-specific promoters include rat tubulin alpha I (Ta1) [52], rat neuron-specific enolase (NSE) [53] and human platelet-derived growth factor-beta chain (PDGF-B) promoters [54]. These promoters are known to be specific for neuronal expression, but the transcriptional activities are relatively weaker than viral promoters such as cytomegalovirus (CMV) promoter which is also a pan cellular promoter. The neuron-specific promoters are less likely to activate host cell defences, and have better stability and longevity of gene expression than viral promoters.

Promoters	Targeting cell types
Ca^{2+}/calmodulin-dependent protein kinase II α (CaMKII α)	Excitatory/Glutamatergic neurons
Parvalbumin (PV)	Interneurons
Human synapsin I (SYN1)	Pan-neuronal promoter (Inhibitory/GABAergic and Excitatory/Glutamatergic neurons)
Rat Tubulin alpha I (Ta1)	Neuron-specific or neuroprotective promoter (neurons)
Rat neuron-specific enolase (NSE)	Neuron-specific promoter (neurons) 20-30% non-neurons are targeted
Human platelet-derived growth factor-beta chain (PDGF-B)	Neuron-specific promoter (neurons)

Table 1.1: Type of promoters and specific cell targeting

1.3 Human pluripotent stem cells (hPSCs)

Human pluripotent stem cells (hPSC) have the capacity for indefinite self-renewal and differentiation into all cell types (approximately 200 cell types of the body) that form the tissue of developing fetus. These fundamental characteristics make hPSCs a potential source of cells for regenerative medicine, cell therapy, drug discovery and disease modelling.

1.3.1 Human embryonic stem cells (hESCs)

Human embryonic stem cells (hESCs) were first isolated in 1998 by Thomson et al. based on the development of embryonic culture in *in vitro* fertilisation (IVF) [55]. Isolation of the inner cell mass (ICM) from blastocysts (Fig. 1.2a) have produced hESCs and the progress in non-human primate stem cell culture have contributed to the development of hESC models [56, 57]. These cells possess characteristics of self-renewal and pluripotency. Self-renewal refers to the ability to remain in an uncommitted or undifferentiated stage, allowing unlimited yield and long-term maintenance. Pluripotency of hESCs is defined as their ability to differentiate into derivatives of the three germ lineages i.e. ectoderm, mesoderm, and endoderm [58]**.** The commonly used markers of pluripotent cells are Oct4 (POU5F1) [59], Nanog [60], SOX2 [61], TRA-1-60, SSEA3 and SSEA4 [62]. hESCs can be transplanted into an immune-compromised mouse to test their pluripotency. A benign tumor or teratoma consisting of derivatives of all three germ lineages will develop if the transplanted cells are pluripotent [63].

Although these cells are a promising candidate cell source for the generation of all cell types, hESC derivation remains ethically controversial and encounters a limited supply of donor human embryos. Therefore, the discovery of hiPSCs with remarkable similarity to hESCs that derived from somatic tissues was a significant advance [64, 65].

1.3.2 Human induced pluripotent stem cells (hiPSCs)

In contrast to hESCs, hiPSCs are derived by reprogramming of somatic cells to a pluripotent state through the overexpression of four transcription factors i.e. Oct4, Sox2, Klf4 and Myc (Fig. 1.2b). This technique does not involve the destruction of embryos, and therefore circumvents the ethical issue surrounding hESC derivation [66-68]. Moreover, cell lines can be easily obtained from adult somatic cells with genetic backgrounds to create patient-specific hiPSCs with a lower risk of immune rejection [69-75].

The hiPSCs are similar to hESCs in terms of their self-renewal and pluripotency capability, morphology, culture environment, surface marker expression, and *in vivo* teratoma formation [64, 65]. Despite these similarities, the functional and molecular equivalence of hiPSCs and hESCs required assessment due to the reports of variability in the *in vitro* differentiation of hiPSCs. For example, a reduced and more variable yield of neural [76] and cardiovascular progeny [77] has been observed in hiPSCs, irrespective of the presence of reprogramming transgenes in the hiPSC genome. Furthermore, hiPSC-derived early blood progenitor and endothelial cells appear to undergo premature senescence [77, 78]. Thus, differentiation methods and efficiency are crucial to drive these cells toward the targeted cell types. Neural differentiation of hPSCs and potential applications in the treatment of neurodegeneration diseases are detailed in the following section (section 1.6).

a) Embryonic stem cell (ESC) derivation

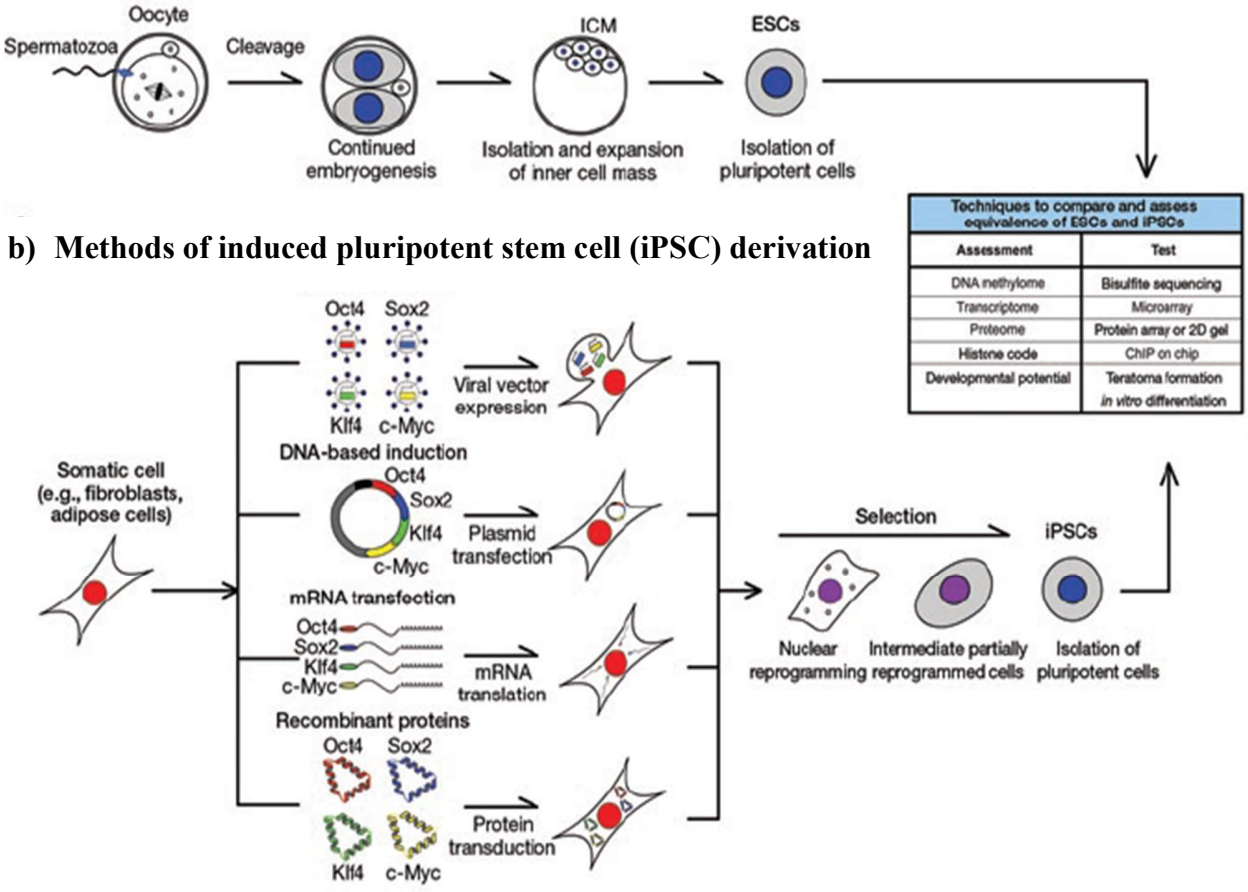

Techniques to compare and assess equivalence of ESCs and iPSCs	
Assessment	**Test**
DNA methylome	Bisulfite sequencing
Transcriptome	Microarray
Proteome	Protein array or 2D gel
Histone code	ChIP on chip
Developmental potential	Teratoma formation *in vitro* differentiation

Figure 1.2: Derivation protocols of human embryonic stem cell (hESC) and human induced pluripotent stem cell (hiPSC).

(a) ESCs are isolated from the ICM of the blastocyst, whilst (b) iPSCs can be derived from several somatic cell types using various reprogramming techniques such as viral vector expression, plasmid transfection, mRNA translation and protein transduction. The equivalence of hESCs and iPSCs at the molecular and functional levels are determined using assays as listed in the table on the right (adapted from Narsinh, K.H. et al., 2011) [79].

1.3.3 Optogenetics in hPSCs and neuroscience

Optogenetics allows fast control of precisely defined events in biological systems from a single cell to different parts of whole tissue in animals upon light illumination. A number of studies have been published to elucidate brain functions and dysfunctions [80-82]. Although this method has been used to target neurons within the neural networks in order to understand the mechanism of specific neurons in brain function, it has been extended to stem cell research and therapy.

The combination of optogenetics and human pluripotent stem cells (hPSCs) opened up opportunities in stem cell research and its integration in new circuit as a cell-based treatment strategy for neurodegenerative and cardiovascular disorders. Recently, some studies showed that engineered stem cells expressing exogenous light-activated opsins were used in hPSC and neuroscience research including tracking the differentiation of stem cells, functional analysis of ESCs and iPSCs derived graft, and testing the functional integration of PSC-derived neurons into a native circuitry [80, 82, 83]. With the risen of non-invasive approach involving transcranial excitation or inhibition, optogenetics enable non-invasive control of engineered stem cell.

Before the clinical use for cell replacement therapy, fully functional integration and natural behaviour of grafted stem cell-derived neurons in the native circuitry should be examined. Traditional tools like histochemical and immunohistochemical methods cannot ascertain full electrophysiological connection in an intact animal. One of the first attempts has been made by Weick and colleagues to create pluripotent cell line that expressed ChR2 up to 6 months under neuron-specific promoter that could be optically regulated when differentiated to neurons [84].

1.4 The microenvironment for human pluripotent stem cell (hPSC) culture

The fate and organisation of human pluripotent stem cells (hPSCs) in the body are regulated through interactions with neighboring cells, surrounding extracellular matrix (ECM), and soluble biochemical cues in a three-dimensional (3D) microenvironment [85, 86]. Therefore, it is crucial to mimic cell-, tissue- and organ-specific niches such as *in vivo*-like cellular structures, properties and organisations by modulating the physiochemical culture environment [87-90]. In general, the growth of any cells *in vitro* requires three main factors i.e. (a) growth media, (b) extracellular matrices and (c) environmental factors.

Growth medium, as one of the most important components in the culture of hPSCs, has undergone a dynamic evolution since it was used for human embryonic stem cells (hESCs) [55]. A serum-free, xenogeneic-free, and chemically defined medium is a goal to achieve for supporting the growth of all hPSC lines. Previous hESC media contain fetal bovine serum (FBS) and undefined secretory components from mouse embryonic fibroblasts (MEFs). Recently, xenogeneic elements in the media [91-93] have been replaced with Activin A, Nodal and fibroblast growth factor-2 (FGF-2) in a chemically defined condition for the propagation of hESCs. The knock-out serum replacement (KSR) is widely used with FGF-2 to support feeder-based hPSC culture. However, Thomson et al. have established feeder-free conditions using a defined culture medium (termed TeSR1) containing FGF-2, lithium chloride (LiCl), transforming growth factor-β (TGF-β), γ-aminobutyric acid (GABA), and pipeolic acid [94]. They later developed a chemically defined E8 medium (E8), a derivative of TeSR1 consisting of only eight elements excluding both β-mercaptoethanol and serum albumin. The combination of E8 medium with the use of ethylenediaminetetraacetic acid (EDTA) in passaging may suitable for culturing a wide range of hPSC lines [95, 96].

Extracellular substrates include organic matrices from animal cells, human matrix proteins, synthetic surfaces, hydrogels, and commercially defined xenogeneic-free components. Among the available commercial products such as CELLstart (fibronectin components of human origin, Invitrogen), StemAdhere (a defined matrix with human proteins produced in human cells, Primorigen Biosciences) and Synthemax-R Surface (a synthetic peptide acrylate-coating surface, Corning), the most widely used extracellular substrate for feeder-free culture of hPSCs is matrigel (BD Biosciences). Matrigel is a basement membrane matrix rich in type I and IV collagens, laminin, entactin, matrix metalloproteinases, heparan sulfate proteoglycan, undefined growth factors and chemical compounds [97-99]. However, it is a semi-chemically defined and xenogeneic substrate that may limit its use for clinical-grade hPSC cultures.

On the other hand, recombinant vitronectin is a defined substrate that promotes hESC self-renewal via adhesion with αVβ5 integrin [100]. There is also evidence showing that specific laminin isoforms (laminin-511 and LM-511) may sustain long-term hPSC growth for more than 20 passages [101]. The current use of laminin for both hPSC maintenance and expansion is limited, therefore new methods utilising synthetic surfaces are being developed to stimulate the effects of ECM proteins on hPSC growth.

*S*ynthetic surfaces (on two-dimensional, 2D culture) are designed to modulate the major signal transduction pathways and to conjugate with peptides (e.g. laminin peptides) that are required for hPSC growth [102, 103]. Further modification of synthetic surfaces could facilitate the development of chemically defined conditions to expand clinical-grade hPSCs at low cost. For example, Jaenisch et al. coated a cell culture plastic surface using UV/ozone radiation, producing a significantly improved quantity of hPSCs (a threefold increase) under fully defined conditions when compared with feeder-based culture [104]. Several research groups have developed new surface

substrates such as high-affinity cyclic arginine-glycine-aspartate (cRGD) peptide surfaces that contain the RGD integrin recognition motifs [105], synthetic peptide-acrylate surfaces [106] and synthetic polymer coating with poly[2-(methacryloyloxy)ethyl dimethyl-(3-sulfopropyl)ammonium hydroxide] (PMEDSAH) [107] for long-term maintenance of hPSCs. These advancements allowed for fully synthetic environmental cues that support long-term culture of clinical-grade hPSCs to be achieved. Types of ECM proteins or ligands for surface coating that support long-term hPSC culture are presented in Table 1.2.

Other environmental factors, including both physical and physiological environments that encourage hPSC growth are: temperature, humidity, osmosity, acidity, surface integrity, cell density, gas diffusion exchange, modes of multicellular associations, consumption of oxygen, mechanical force and electrical stimulation.

Substrates	ECM proteins or Ligands	CAM (s)	References
Tissue culture polystyrene (TCP)	Vitronectin	αVβ3/5 intergrins, GAGs	100
	Laminin-511	α6β1 integrin	101
	Laminin E8 fragments	-	108
	Fibronectin	α5β1 integrin	109
	Collagen+fibronectin+laminin+vitronectin	-	94
	Poly(L-lysine)	-	110
	E-cadherin-IgG1Fc (StemAdhere^{TM})	E-cadherin	111
Amine-modified TCP	Cyclic-CRGDC	-	105
UV-treated TCP	Adsorbed serum proteins, vitronectin	-	104
Acylate monomer-coated TCP	KGGNGEPRGDTYRAY (Corning)	αVβ5	106
	KGGPQVTRGDVFTMP	αVβ3/5	106
	Vitronectin	Integrins, GAGs	112
Self-assembled monolayers	GKKQRFRHRNRKG	HSPGs	113
	LTTAPKLPKVTR	GAGs	114
Amino-propylmethacrylamide hydrogels	BSA + non-specific proteins (adsorbed from media)	-	115
Polyacrylamide hydrogel	GKKQRFRHRNRKG	HSPGs	116
PMEDSH	Uniform (Adsorbed growth factors)	-	117

Table 1.2: Reports of extracellular matrix (ECM) proteins or ligands and their interactions with cell adhesion molecules to promote long-term culture of hPSCs.

The whole ECM proteins, fragments, fusion proteins and peptides presented by amine-modified or acrylate monomer coated TCP, protein-fouling hydrogels and polymers have demonstrated the capability to support hPSC culture by interacting with several integrins, E-cadherins and/or heparan sulphate proteoglycans. Key references have been listed for each adhesion surface (adapted from Lambshead, J.W. et al., 2013) [118].

1.4.1 Extracellular matrix (ECM) : laminins (LNs)

Extracellular matrix proteins, especially the basement membranes, are an important part of *in vivo* niches for the differentiation, maintenance and function of somatic cells and stem cells. Laminins (LNs), the main component of basement membranes, belong to a family of heterotrimeric glycoproteins which compose of alpha (α), beta (β) and gamma (γ) chains that are twisted to form either a cruciform or a T-shaped structure. The combination of 5α, 4β and 3γ chains (αβγ) has formed 15 different LN subtypes [101, 106, 111] which are named according to chain composition. For example, LN-511 consists of α5, β1 and γ1 chains.

Different LNs show distinct expression patterns of spatiotemporal as well as tissue-specific locations and functions. LN-111 is found in the early embryo, certain epithelial cells [119] and matrigel components. LN-211 and LN-221 are located in the basement membranes of muscle cells and motor-neuron synapses [120]. LN-332 is specific for sub-epithelial basement membranes [121], LN-411 is found in sub-endothelial basement membranes [122] whilst LN-511 is ubiquitous [123] (Table 1.3). Apart from mouse LN-111, LNs are difficult to isolate in native forms from tissues. Some recombinant proteins [124-126] have been recently produced from human LNs.

LN proteins including peptides derived from RGD (Arg-Gly-Asp), IKVAV (Ile-Lys-Val-Ala-Val), AG-10 (NPWHSIYITRFG), C-16 and AG-73 (RKRLQVQLSIRT) have been suggested as hPSC culture surfaces because they contain multiple cell-binding motifs that interact with integrins and proteoglycans expressed by hPSCs [101, 106, 127]. For example, LN-511, -332 and −111 (which interact with integrin α6β1) were reported to support both culture and differentiation of hPSCs into 3 germ layers for at least 10 passages. However, LN-211 (α3β1) and −411 (α7β1) failed to promote cell adhesion [101, 128]. LN-511 is the most commonly used subtype which has been

demonstrated to support long-term hPSC culture in different chemically-defined media and hESC lines [101, 129].

Peptides derived from AG-10, C-16 and AG-73 mediated adhesion of hPSCs in defined media are able to support growth for up to few passages by engaging different integrin subtypes or heparan sulphates [127]. Another peptide (RNIAEIIKDI) derived from the γ-chain has successfully promoted attachment of hPSCs in defined xenogeneic-free media. However, IKVAV-containing peptide is found to adhere hPSCs poorly [103, 106]. Several reports of hPSC culture on LN-derived subunits reflect how hPSCs can attach to the different binding sites with different affinities. The maintenance of pluripotency also depends on other properties such as cell adhesion molecule-mediated interactions with the culture surface.

Table 1.3: Laminins are found in different tissue-specific locations.

Laminins (LNs)	Sources
LN-111	Early embryo, certain epithelial and muscle cells
LN-211 and LN-221	Basement membranes of muscle cells and motor-neuron synapses
LN-332	Sub-epithelial basement membranes
LN-411	Sub-endothelial basement membranes
LN-511	Ubiquitous

LNs show distinct expression patterns of spatiotemporal as well as tissue-specific locations and functions. LN-111, -332 and -511 (α6β1) support culture and differentiation of hPSCs into 3 germ layers (≥10 passages) while LN-211 (α3β1) and -411 (α7β1) have failed to promote cell adherence.

1.4.2 Synthetic peptides: arginine-glycine-aspartate (RGD)

Feeder cells, protein substrates (Matrigel) [130] and individual ECM proteins such as vitronectin [100], fibronectin [131] and laminin [128] are currently used to culture hPSCs. The main function of these substrates is to provide a surface that supports integrin-mediated cell attachment, which can protect hPSCs against apoptosis caused by anoikis [132]. However, the undefined nature of these substrates may lead to potential infectious agents or host immune responses in therapeutic application. These issues can be circumvented by using chemically synthesised peptides. Synthetic peptides containing RGD integrin recognition sequence [133] can mimic the function of ECM proteins in cell attachment. The linear GRGDSP peptide has been used as a substrate for this purpose on hPSCs [134]. When compared to the linear GRGDSP, cyclic RGD peptide (CRGDC) has been shown to achieve 10-fold greater potency in supporting cell adhesion [135]. RGD and other peptides ligands (YIGSR and IKVAV) have also been reported to be crucial in neural progenitor cell survival and differentiation [136, 137].

As anchoring molecules, the tripeptide motif RGD was identified by Pierschbacher and Rouslahti as a minimal essential cell adhesion peptide sequence in fibronectin [133]. Since then, cell adhesive RGD sites were identified in many other ECM proteins, including vitronectin, fibrinogen, collagen, laminin, von Willebrand factor, osteopontin, tenascin and bone sialoprotein as well as in membrane proteins [134]. The RGD sequence is not the universal cell recognition motif but it has broad distribution and usage. The conformation of the RGD containing loop and its flanking amino acids are mainly responsible for their different integrin affinity [134].

Cell adhesion is mediated by integrin through ligand binding, cell spreading (cell flattens and its plasma membrane spreads), organisation of actin cytoskeleton (into microfilament bundles), and formation of focal adhesions (ECM was link to actin cytoskeleton molecules) [138].

Formation of focal adhesions can activate focal adhesion kinase (FAK), extracellular signal regulated kinase (ERK), small Rho GTPases, phosphatidyl inositol 4- phosphate 5-kinase (PIP 5-kinase) and mitogen-activated protein kinase (MAPK) pathways [139-142].

1.4.3 Small molecules inhibit apoptosis of hPSCs

Traditionally, it has been suggested that hPSC self-renewal and long-term maintenance are induced through a combination of signals such as cytokines, feeder cells, fetal bovine serum (FBS) and growth factors. Differentiation of hPSCs can be triggered in the absence of these key signaling cues [143]. It is now, however, accepted that self-renewal is the default pathway in mouse ESCs. ESC self-renewal can be maintained by simply blocking differentiation cues which has been demonstrated in the ERK/MAPK, FGF-4 and glycogen synthase kinase 3 (GSK-3) pathways [143, 144]. Similar strategies have also been applied to hESCs by utilising multiple small molecules to inhibit certain signaling pathways including apoptosis to increase cell survivability [145, 146].

Recent studies suggest that single cell dissociation triggers Rho-associated kinase (ROCK)-dependent myosin hyperactivation and cell death, inhibiting this pathway can prevent apoptosis [147] (Fig. 1.3). A small molecule inhibitor of the ROCK, namely Y-27632 (ROCKi), was found to enhance the survival of dissociated hESCs at 10 μM [148]. In sublethal concentrations (<100 μM), ROCK inhibitors Y-27632 and fasudil inhibited apoptosis in established glioblastoma cell line (U87-MG), in patient-derived glioblastoma xenoline (JX12), and in primary glioblastoma cell line (SMC448) [149]. The protection provided by ROCK inhibitors allows for a greater cell yield after these cells undergo stress when culture *in vitro*. In addition, other researchers have shown that ROCK inhibition induced cytoskeletal and pro-survival responses in non-cancerous astrocytes [150]. The anti-apoptotic effect of Y-27632 was also demonstrated in feeder-free culture and its effect in pro-expansion in most stem cell types, suggesting that it can be incorporated into 3D cultures

[148, 151]. On the other hand, Lamas and colleagues recently showed that expansion of human adipose stem cells (hADSCs) is not enhanced in the presence of ROCK inhibitors Y-27632 after 24 hours of culture [152]. The effect of Y-27632 in hADSCs is concentration-dependent and continuously treatment in the cultures decreases the number of cells.

ROCK inhibitors such as thiazovivin (Tzv; a 2,4-disubstituted thiazole) and pyrintegrin (Ptn; a 2,4-disubstituted pyrimidine) were found to enhance survival following dissociation of hESCs more than 30-fold, without adversely affecting pluripotency over long-term culture in chemically defined medium [153, 154]. Both increase cell adhesion to ECM (e.g. Matrigel or laminin) without the use of gelatin. The findings suggested that integrin-mediated cell–ECM interactions form the basis of survival niche for hESCs. In addition, small molecules PD0325901 (for ERK inhibition) and SB203580 (a p38 kinase inhibitor) have greatly reduced cell death upon dissociation, supporting the growth of hESCs and demonstrating stable cell-surface E-cadherin interactions [155].

Other key mediators of apoptosis are caspases; cysteine proteases cleave their substrates at aspartic acid residues leading to execute programmed cell death or cytokine activations. The mechanisms can be regulated upstream through signals that induce activation of zymogen, or downstream by inhibitors that prevent them from their substrates [156]. The distinct morphological changes of cells undergoing apoptosis are cell shrinkage, chromatin hypercondensation, chromosome cleavage into nucleosomal fragments, violent plasma membrane blebbing, and packaging of cellular contents into membrane-enclosed vesicles (apoptotic bodies) that subsequently phagocytosed by the surrounding cells leading to cell death [157].

Caspases are classified into two groups in mammals, the initiator caspases such as caspase-9, and the effector caspases such as caspases-3 and -7. The activation of an effector caspase

(caspase-3 or -7) is performed by an initiator caspase (caspase-9) through an internal cleavage to separate the large and small subunits. An initiator caspase, however, is auto-activated under apoptotic conditions, which usually facilitated by multicomponent complexes [158, 159]. X-linked inhibitor of apoptosis (XIAP) is found as the most potent inhibitor of caspases-3 and -7 *in vitro*, while c-inhibitor-apoptosis-protein (c-IAP1 or c-IAP2) has an inhibitory constant (approximately 100-fold weaker than XIAP) [160, 161].

In addition, a number of specific and broad-spectrum synthetic peptide caspase inhibitors were recently developed. Peptides are linked to chemical groups to block the amino acids as well as to improve cell permeability, stability and efficacy. Among these inhibitors are (1) single O-methyl-aspartate residue e.g. benzyloxycarbonyl-aspartyl(OMe)-fluoromethylketone (Boc-Asp-FMK) [162], (2) tri-peptides e.g. Boc-val-ala-asp(OMe)-fluoromethylketone (z-VAD-FMK) [163] and (3) tetrapeptides e.g. Tyr-val-ala-asp(OMe)-fluoromethylketone (YVAD-FMK) [163]. The mechanism of caspase inhibition by IAPs and ZVAD-FMK is described in figure 1.4.

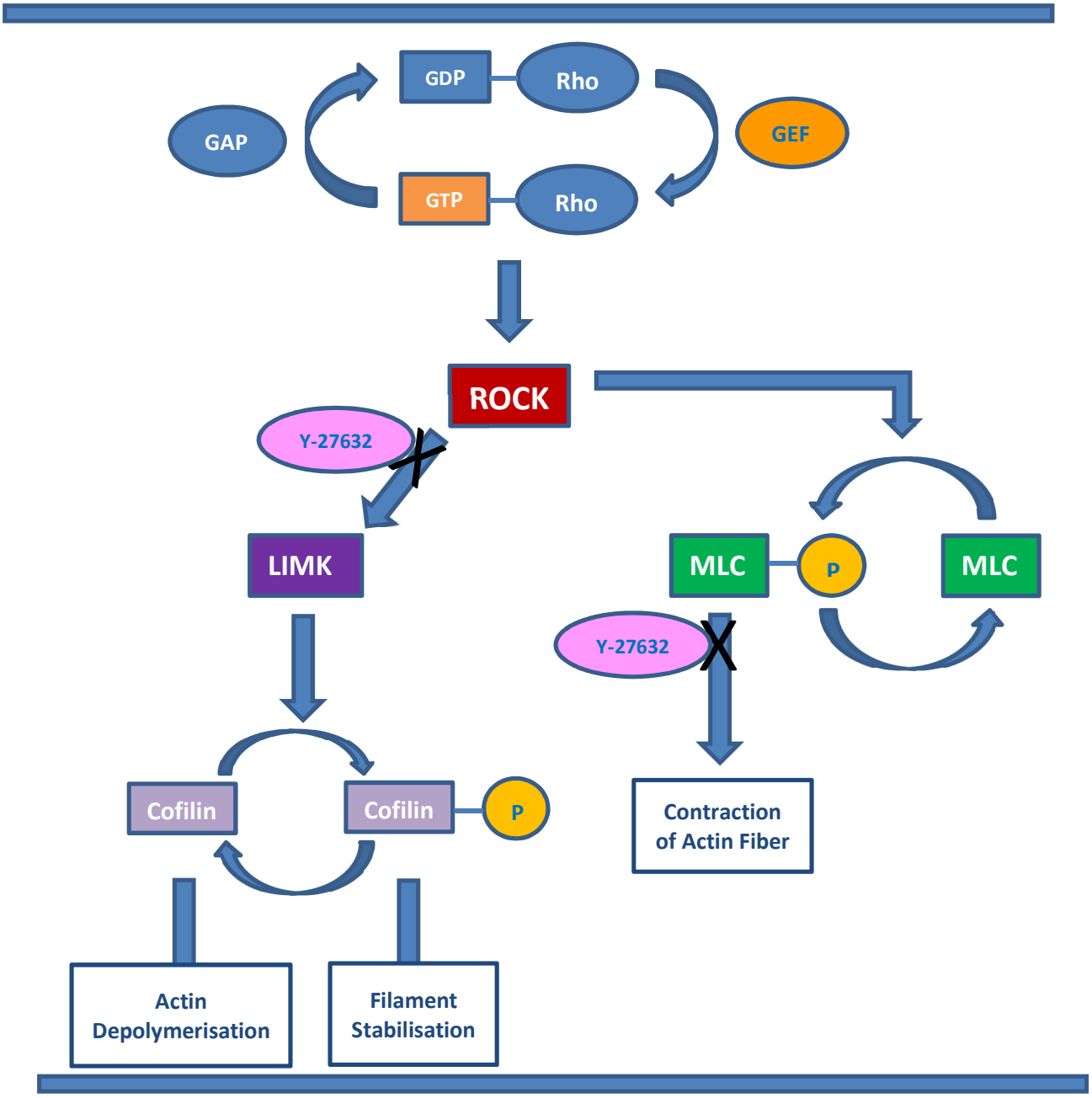

Figure 1.3: Regulation of cellular function by the rho-associated protein kinase (ROCK) pathway and the use of ROCK inhibitor (ROCKi).
ROCK activation via Rho guanine exchange factor (GEF) phosphorylates myosin light chain (MLC), leading to actin-myosin interactions which cause cellular contraction. Small molecule Y-27632 inhibitor is sensitive to MLC-P, inhibits downstream signaling to prevent contraction of actin fiber and membrane blebbing, subsequently increase survival of hPSCs from dissociation-induced apoptosis. Stimulation of ROCK also leads to activation of LIMK, which in turn phosphorylates cofilin/actin-depolymerizing factor (ADF), thereby inactivating its actin-depolymerisation activity. This will stabilize actin filaments and increase their numbers. Actin monomers that are required to continue actin polymerisation for cell migration become less. ROCK inhibitor Y-27632 can prevent the loss of actin monomers over time, and decreased stable filaments to promote cell migration. (Modified from Ohgush, M. and Sasai, Y., 2011; Riento, K. and Ridley, A.J., 2003) [147, 164].

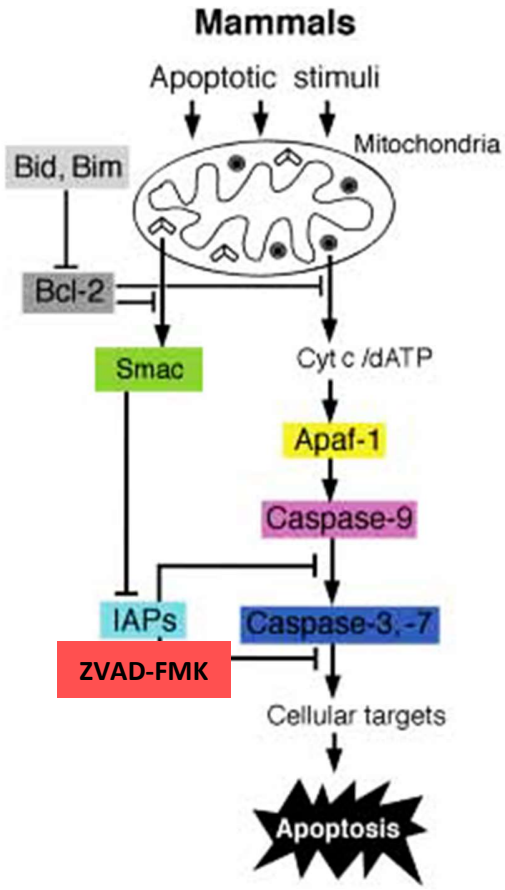

Figure 1.4: Caspase inhibition by IAPs and ZVAD-FMK in a conserved apoptotic pathway of mammals.

IAPs and ZVAD-FMK bind to the process end of the large subunit of caspase 9, its dimerisation and subsequent activation are blocked. These small molecules can also bind to the active catalytic sites of effector caspases, i.e. caspase 3/7 and thereby preventing their activity (Adapted from Shi, Y., 2004) [157].

1.5 Three-dimensional (3D) cell cultures of hPSCs

Human pluripotent stem cells (hPSCs) can be cultured *in vitro* and differentiated into all cell types, thus providing a promising cell source for cell therapies, tissue engineering, and drug discovery. Current 2D cell cultures, however, are suffering from inert heterogeneity, limited scalability and a lack of reproducibility, and are therefore unable to provide a sufficient number of high quality hPSCs and progeny [85, 165]. A promising approach is to move cell culture from 2D to 3D which has more advantages than conventional 2D systems [85, 166].

Various 2D culture systems involve the use of tissue culture plastics (TCPs) or synthetic biomaterial surfaces. The 2D systems enable control of long-term clonal growth and multi-lineage differentiations of hPSCs [87], but often induce early developmental structures such as neural rosettes [165]. Unexpectedly, 3D culture systems utilising functional biomaterials produce a defined niche that recapitulate the native cell microenvironment. These systems have been shown to improve viability and regenerative potential of hESC-derived multipotent stem cells after *in vivo* implantation [166, 167]. 3D cultures of hPSCs are also ideal for modelling human diseases related to abnormal ECM remodelling during development and ageing [168]. In addition, 3D spatiotemporal patterning and organisation of cytosystems in embryonic development, tissue morphogenesis, and organogenesis can only be simulated in a 3D environment using functional biomaterials of appropriate properties [169]. For example, 3D culturing enables the generation of organoid cultures containing mixed ectodermal derivatives which can recapitulate the cytoarchitecture of the developing nervous system as well as the complexity and functionality of *in vivo* neural circuits [170-172].

To date, several 3D culture systems have been developed for hPSCs and neural derivatives such as cell aggregates in suspension culture [173-175], cells on microcarriers [176, 177], cells in alginate

microencapsulates, and cells on polymeric scaffolds coated with matrix proteins [178]. Whilst these 3D systems have achieved some degrees of success, many challenges still lie ahead for better enhancements.

1.5.1 Hydrogel

3D scaffolds are designed to recapitulate native cellular microenvironment for *in vitro* cell culture. Among these, hydrogel provides crosslinked networks that possess high water contents and has demonstrated a distinct efficiency as scaffold for 3D cell culture. Hydrogel scaffolds are made from natural and/or synthetic materials with each possessing its own advantages and limitations. Due to their ability to simulate the nature of soft tissues, hydrogels are a highly attractive material for developing synthetic ECM analogues. The crosslinked polymer chains possess a high water content and facilitate transport of oxygen, nutrients, waste and soluble factors [179]. In addition, many hydrogel scaffolds can be formed under mild, cytocompatible conditions and are easily modified to acquire cell adhesion ligands, desired viscoelasticity and degradability [180].

Natural hydrogel scaffolds are derived from biological sources, proteins and ECM components such as collagen [181], fibrin [182], hyaluronic acid [183], chitosan [184], alginate [185] and silk fibrils [186]. They are inherently biocompatible and bioactive due to the presence of numerous endogenous factors which can enhance cellular functions including cell viability, proliferation and development [187]. However, tuning their material properties such as mechanics and biochemical characteristics can be challenging since they degrade or shrink quickly.

Alternatively, hydrogel scaffolds can be formed from synthetic materials such as poly(ethylene glycol) (PEG) [188], poly(vinyl alcohol) (PVA) [189] and poly(2-hydroxy ethyl methacrylate) [190]. PEG hydrogel scaffolds, for example, have been shown to maintain the viability

of encapsulated cells and allowing for ECM deposition as they degrade [191]. This demonstrates that synthetic hydrogel scaffolds can function as 3D cell culture platforms. One issue with hydrogel scaffolds however is that they lack endogenous factors that promote cell behavior and function of human stem cells [192], hence modification of both natural and synthetic hydrogel scaffolds is needed in order to improve the properties and characteristics of the materials. Types of the common used natural and synthetic materials for hPSC self-renewal, survival, differentiation and application are listed in Table 1.4.

Biomaterials	Application	Pore size or diameter (µm)	Young's modulus (kPa)	References
Alginate	Vascular tissue differentiation	50-100	500-1136 (dry state)	[193]
	Transplantation into infarcted myocardium, rat	±100	NA	[194]
Alginate-chitosan complex	Self-renewal	±65	±600	[195]
Collagen	Liver tissue differentiation	30-50	2-100	[196]
Dextran	Vascular tissue differentiation	NA	1.5-6.0	[197]
Hyaluronic acid	Self-renewal	30-50	2-100	[198]
	Transplantation into cartilage, rat	NA	NA	[199]
Matrigel	Transplantation into infracted myocardium, rat	NA	NA	[200]
	Transplantation subcutaneously, mouse	NA	NA	[201]
	Intestinal differentiation and organization	NA	NA	[202]
Poly(glycerol sebacate)	Vascular differentiation	20-200	40-60	[203]
PEG	Cartilage tissue differentiation	0.01-0.10	0.3-4.0	[166]
	Self-renewal, mouse	NA	0.02-1.00	[204]
	Transplantation into infracted myocardium, rat	0.1	4.0	[205]
PLLA mixed with PLGA	Neuronal, cartilage, liver & skeletal muscle tissue differentiation	225-500	65-500	[206, 207]
	Transplantation intramuscular, mouse and rat	225-500	65-500	[206]
	Cardiomyocyte differentiation and 3D organization	212-600	NA	[208]

Table 1.4: Biomaterials for hPSC self-renewal, differentiation, application and transplantation.

Physical properties and references of each material have been provided (adapted from Kraehenbuehl, T.P. et al., 2011) [209]. NA = not available.

1.5.2 Alginate

Alginates are natural polysaccharides which have been used as synthetic ECMs of hydrogel [210]. Alginates consist of α-L-guluronic acid (G units) and (1-4)-linked β-D-mannuronic acid (M units) monomers that vary in amount and sequential distribution along the polymer chain depending on the alginate type [211]. The alginate molecule is a block copolymer composed of sequential G units (G-blocks), sequential M units (M-blocks), and alternating M and G units (MG-blocks). Divalent cations of calcium bind between the G-blocks of adjacent alginate chains, creating ionic interchain bridges that cause gelling of alginate solutions (Fig. 1.5).

Encapsulation of cells within alginate hydrogel allows for production of a high-density cell culture as well as exchange of oxygen, nutrients and stimuli across the membrane. Moreover, the cells can be protected from external risks such as antibodies released from the host [187, 212]. Alginate hydrogel has been demonstrated to support expansion and differentiation of hESCs [213, 214]. It has also been shown to promote better growth, differentiation, maturation and even protein secretion of various cell types including mouse ESCs, hESCs and mesenchymal stem cells (MSCs) [213, 215].

However, other studies have reported the limitations of using alginate because it lacked of cell-specific bioactive molecules that required by certain cell types to adhere, migrate and proliferate [216, 217]. For example, C2C12 (mouse myoblast) and MDCK (canine kidney) cell lines did not proliferate in the alginate hydrogel [217]. To overcome this limitation, bioactive elements such as peptides and growth factors have been incorporated into alginate hydrogel network to mediate specific cell functions [218, 219].

a

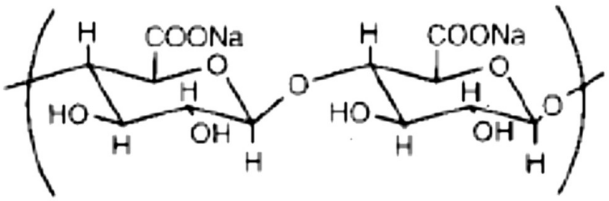

b

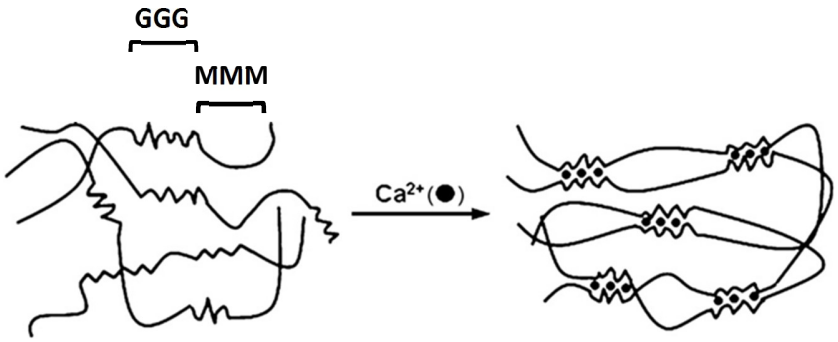

Figure 1.5: Alginate structure and formation.

(a) Chemical structure of sodium alginate. (b) Alginate hydrogels are prepared by ionic cross-linking; only Guluronate blocks (GGG) participate in the formation of corrugated egg-box-like structure with the interspace in which calcium ions are bound. MMM: Mannuronate blocks (adapted from Lee, K.Y. and Mooney, D.J., 2007) [220].

1.6 Neurons derived from hPSCs and neuroblastoma cells

Human pluripotent stem cells (hPSCs; i.e human embryonic stem cells, hESCs and human induced pluripotent stem cells, hiPSCs) can give rise to neurons. Current studies not only show that a neuronal subtype or neurons of interest can be made from hPSCs, but that these cells can mimic the various developmental stages, and therefore provide insights into the pathogenesis of neurodevelopmental diseases [76, 221, 222].

Neural development can be categorised into three main stages: neural induction, specification and maturation. Each stage can be modelled and manipulated *in vitro*. The specific neuronal cell fates can be selectively enhanced in hPSCs and other neuronal cell types (e.g. neuroblastoma) using differentiation strategies as described in the following sections.

1.6.1 Neuron

Neuron or nerve cell is an electrically excitable cell that consists of a cell body or soma, dendrites and an axon which transmits information through electrical and chemical signals (Fig. 1.6) [223]. A single neuron connects to other cells via synapse and the connections form neural networks. The neurons maintain voltage gradients across their membranes by metabolically driven ion pumps which combine with ion channels in their membranes to generate extracellular-intracellular concentration differences of ions. Changes in the cross-membrane voltage generate action potential (AP) which travels rapidly along the axon, and activates synaptic connections with other neurons upon it arrives. The action potential triggers release of neurotransmitters and activates membrane depolarisation.

Type of neurons can be classified based on the production of neurotransmitters such as:

a. Cholonergic neurons release acetylcholine from presynaptic neurons into the synaptic cleft.

b. GABAergic neurons release GABA (gamma aminobutyric acid) which is a neuroinhibitor in the centre nervous system that allow chloride ions to enter the post synaptic neuron.
c. Glutametergic neurons release glutamate which is one or two primary excitatory amino acid neurotransmitter causing AMPA (permeable to sodium ions) and NMDA (permeable to calcium ions) receptor activation, mediating fast synaptic transmission.
d. Dopaminergic neurons release dopamine that acts on D1 type Gs- and Gi-coupled receptors, regulate both pre- and post-synaptic neurotransmission.
e. Serotonergic neurons release serotonin (5-Hydroxytryptamine, 5-HT) which can act as excitatory or inhibitory.

Generally, neurons do not undergo cell division, they are mostly generated by special types of stem cells. Glial cells such as astrocytes in star shape have been recently shown to convert into neurons may attribute to pluripotency characteristic. Current strategies to generate new neurons *in vitro* are focused on neural differentiation of human stem cells.

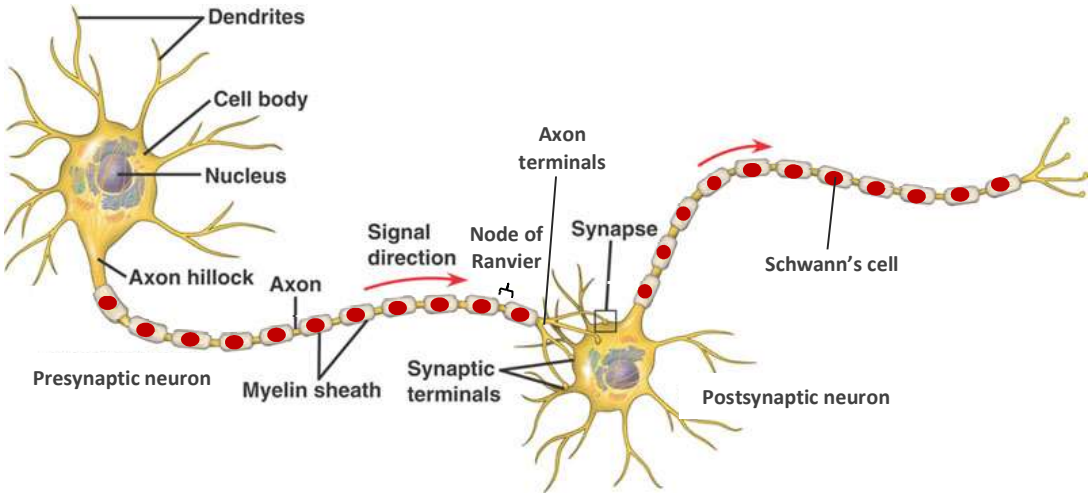

Figure 1.6: Schematic of neurons.

A neuron consists of a cell body (soma), branching dendrites (signal receivers) and an axon which conduct the nerve signal to the end (axon terminals). Myelin is produced by Schwann's cells to increase transmission speed along the axon. It coats the axon with a period break called nodes of Ranvier (modified from http://biomedicalengineering.yolasite.com/neurons.php) and Frederic, M. et al, 2010) [223] .

1.6.2 Neural differentiation of hESCs

When compared to the murine ESCs, the culture and differentiation methods of hESCs are more challenging and labour intensive. Current research is focused on the establishment of serum-free and feeder cell-free expansion as well as efficient differentiation of hESCs. In common with the murine ESCs, hESCs give rise to neural subtype when embryoid bodies (EBs) differentiate spontaneously, and the mesodermal lineages are often observed [224].

Differentiation of neurons from murine ESCs involves several weeks of culture. Recent work performed by Conti et al. has isolated stable neural stem cells (NS) or precursor populations from murine ESCs and further induced differentiation to a terminal stage [225]. This is possible due to the expansion of NS cells in fibroblast growth factor-2 (FGF-2) and epidermal growth factor (EGF) allowing the long-term stabilisation of NS cells. NS cells are classified as multipotent neural progenitors, which may be a more appropriate starting point for the derivation of neurons. Another possible strategy to identify and isolate progenitors from PSCs is to use reporters that are driven by lineage-specific promoters for specific neural subtypes, such as dopaminergic neurons and cortical neurons [226-228].

The *in vitro* derivation of neural lineages from hESCs is dependent upon the exposure of the cells to exogenous signals and substrates which mimic the conditions in a developing embryo. Indirect and direct methods have been used to differentiate hESCs into neuroectodermal-like cells.

The indirect method is to maintain hESCs in culture for more than a week without passaging to allow spontaneous differentiation into all three germ lineages. Differentiation toward neuroepithelial-like cells can be identified by a rosette-like morphology which contains columnar epithelial cells that are organised radially [229]. Neural rosettes express neuroectodermal markers (PAX6 and SOX1) during neural induction [230]. The cells can then be isolated and cultured in

suspension to form aggregates called ‘‘neurospheres’’ [231]. A feeder-free suspension culture of hESCs forms clusters of cells known as embryoid bodies (EBs), which can also differentiate toward any of the three germ lineages. This technique is commonly used to determine pluripotency *in vitro* [232].

Directed neural induction of hESCs involves culturing cells on a feeder layer of murine embryonic fibroblasts or stromal cells (MEFs, PA-6 or MS-5 cell lines) [233]. These stromal feeder layers secrete factors that promote neural induction. Recent research however, has moved from feeder layer systems to direct culturing of hESCs on laminin substrates in media containing neural-inducing factors [234]. Fibronectin substrates are used for glial differentiation and mitogenic factors are maintained for a certain period [231]. Directed systems are widely adopted due to the fact that hESC differentiation is directed toward the neural lineage ectoderm instead of mesoderm or endoderm. An example of directed differentiation of hPSCs to cerebral cortex neurons performed by Shi, Y. and colleagues is summarised in Table 1.5 [235]. In general, this differentiation system is useful for obtaining neurons and glial cells. Heterogeneous cell populations still present however; hence genetic modification of hESCs and their progeny to intrinsically drive their differentiation toward specific lineages is an option.

Mature neurons and glial cells can be characterised by their morphology and expression of specific neuronal (b-III tubulin, TUJ1, MAP2) and glial markers (GFAP and S100b), respectively [231]. At terminal stage, specific mature neuronal cell types can be identified, and the efficiency of the neuronal differentiation methods can be determined. The ESC-derived models may not be identical to native neurons *in vivo,* but their phenotypes will be close enough to provide advanced pharmacological and neurodegenerative models. At present, it is impossible to obtain cultures that

are homogeneous for drug screening and tissue regeneration applications, but the technology of directed differentiation is progressing rapidly and reductions in heterogeneity are possible.

Phase 1: Preparing cultures of hPSCs (21 days)			
D0	D1	D2	D10 D21
Plate MEFs MEF medium Dish: 6-well dish	Thaw and plate hPSCs Medium: MEFs-conditioning hPSC + ROCKi Use until D23	Medium: + FGF – ROCKi Change daily Incubation: 4 – 6 days Observations: Colonies (1mm) formed	Dissociation: dispase Sub-culture: on MEFs 1:6 in ratio Medium: change daily Incubation: 4 – 6 days or more
Phase 2: Neural Induction (12 days)			
D22	D23	D35	D36
Dish: 12-well dishes coat with CELLStart Colonies: dissociate into small fragments Seeding density: high Plate 5/6 wells of 12-well plate with cells from one 6-well plate	Medium: Neural induction Use until D36 Change daily Incubation: 12 days	Observations: hPSCs (large nuclei) were replaced with neuroepithelial cells (smaller nuclei) Uniform neuroepithelial cell layer formed Sub-culture: split cells from each single 12-well dish into a laminin-coated 35mm dish Dissociation: dispase	Medium: neural maintenance
Phase 3: NPC expansion and differentiation (20 days)			
D36	D43	D47	D56-66 D116-126
Observations: Neural rosette structure appeared	Medium: Neural maintenance + 20 ng/ml of FGF	Sub-culture: split cells onto laminin-coated 35mm dish Expand after 4 -6 days of culture Medium: Neural maintenance Dissociation: dispase	Observations: Neurons accumulate outside of the rosettes Incubation: up to 50-60 days from last splitting Medium: Neural maintenance Change daily Dissociation: accutase

Table 1.5: Directed differentiation of human pluripotent stem cells to cerebral cortex neurons and neural networks in 2D culture that involves three phases.
(a) Phase 1 (21 days): culture and expansion of hPSCs onto MEFs required FGF with/without ROCK inhibitor at different stages. (b) Phase 2 (12 days): Neural Induction of hPSCs is begin with the use of neural induction medium in CellStart-coated dish following the change to neural maintenance medium in laminin-coated dish. (c) Phase 3 (20 days): NPC expansion and differentiation in neural maintenance medium with 20 ng/ml of FGF, and plated onto a laminin-coated dish. Typical morphology of neurons from the formation of neural rosette to mature neuron phenotypes and neural branching was observed. Prolong culture and incubation from day 56 to 126 can increase neuron maturation and cell proliferation (protocol is adapted from Shi, Y. et al., 2012) [235].

1.6.3 Neural differentiation of hiPSCs

Human induced pluripotent stem cells (hiPSCs) derived from somatic cells have great potential to treat neurodegenerative diseases. However, the development of differentiation strategies that can generate disease-relevant subtypes of neurons is a recent challenge. Progress has been made to produce enriched populations of dopaminergic neurons and spinal motor neurons to model Parkinson disease (PD) and amyotrophic lateral sclerosis (ALS), respectively [72, 236-239].

In the case of Parkinson's disease, iPSC-derived dopaminergic neurons gave positive therapeutic effect on a rodent Parkinson's disease model as a proof of principle in using iPSCs as sources of cell replacement therapy. On the other hand, spinal muscular atrophy (SMA) is one of the first human neurodegenerative diseases that was characterised in an iPSC-based *in-vitro* disease model [240]. Ebert et al. generated iPSCs from fibroblasts of a SMA patient and using the patient's unaffected mother as a normal control [241]. Human iPSCs from the SMA patient and his control were differentiated into motor neurons, and his identity was confirmed through immunostaining for mature motor neurons.

In addition, given the fact that *in vitro* studies of the central nervous system (CNS) tissue are difficult in motor neuron disease (MND) patients, hence differentiation of patient-derived iPSCs into motor neurons offers an experimental approach to better understanding of the mechanisms and pathogenesis of MND. Motor neurons (MNs) differentiated from patient-derived iPSCs resemble relevant disease phenotypes. Transplantation of iPSC-derived MNs into CNS tissue in animal models is feasible [68, 69].

Furthermore, cortical pyramidal neurons and forebrain interneurons have been differentiated from hiPSCs using strategies that recapitulate the *in vivo* developmental process for cellular therapy [221, 222, 235, 242, 243]. Since hiPSCs resemble to hESCs, established neuronal

differentiation protocols could be applied on both cells [235]. Beyond iPSC technology, recent efforts are being made to generate neurons directly from fibroblasts or other somatic cells using neuron-specific transcription factors, which can avoid making iPSCs as an intermediate cell type.

1.6.4 Neural differentiation of neuroblastoma cells

Live, adult human neurons for functional and interventional studies are unavailable, thus different immortalised cell lines are used as an alternative. These cell lines such as the frequently used neuroblastoma cell line (SH-SY5Y), lack of the features that define neurons *in vivo* including neuronal morphology, inhibited cell division, and expression of neuron-specific markers. The expression and distribution of neuron-specific proteins are rare in SH-SY5Y cells at levels comparable to mature neurons [244].

Neuroblastoma cells can be differentiated into several different phenotypes based on the treatment *in vitro* (differentiation protocol in this project refers to Fig. 1.7). Commonly used differentiation agents are phorbol esters and retinoic acid (RA) [75], growth factors include brain derived neurotrophic factor (BDNF), nerve growth factor (NGF), and neuregulins [245-247]. Other differentiation factors are vitamin D metabolite 1,25-dihydroxycholecalciferol (VitD3) and cholesterol [248-250]. The recent approach of improving neuronal differentiation involves culturing SH-SY5Y cells in a three-dimensional (3D) environment [251] such as an extracellular matrix (ECM) hydrogel, which provides cell support and substances that promote differentiation.

Each of the stimuli mentioned above induces neuronal differentiation and demonstrates neuron-like morphology but less functional expression. One more promising approach is to use a combination of several stimuli to generate mature neurons, allowing the functional study of neural activities such as neurotransmission, microtubule function and axonal transport [244].

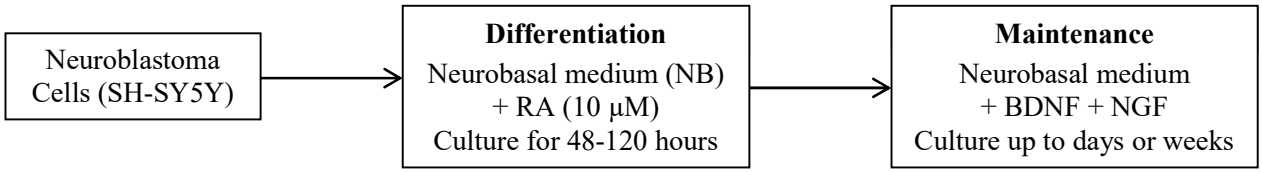

Figure 1.7: Schematic of neural differentiation from neuroblastoma cells (SH-SY5Y) to cortical neurons.

SH-SY5Y cells were cultured and expanded in neurobasal medium, differentiation to cortical neurons were triggered when RA (10 μM) was added into the medium and cultured up to 120 hours. The differentiated cells were further matured in maintenance medium consists of BDNF and NGF for days or weeks before use.

.

1.7 Calcium in neurons and electrophysiological analyses

Calcium has vital roles in neuronal connections. Neurons exploit the spatial and temporal differences of calcium signals to associate with electrical activity. Synaptic transmitters released from the presynaptic neuron activate the receptors on the postsynaptic membrane, and opening of calcium channels links this chemical event to electrical changes of the cell [252]. Calcium influx into mature neurons affects synaptic function, acting both at the synapse and within the nucleus [253]. There is a ten-thousand-fold difference in calcium concentration across the cell membrane (100 nM in the cytoplasm and 1mM outside the cell). Calcium influx from outside is restricted to synapses and sometimes transduced to the nucleus to induce gene expression, subsequently leading to global structural changes. Calcium concentration found in the endoplasmic reticulum (ER) is up to 1000 nM [254] and the ER could serve as an internal calcium store [255].

Calcium is not free to diffuse in the cell, as there are various calcium binding proteins buffering the movement of calcium. Most of the calcium that enters the cytoplasm is rapidly bound to cytosolic buffers such as calbindin, calretinin and parvalbumin. Cytosolic buffers are involved in shaping the amplitude and duration of calcium signals. This is particularly important in neurons as calcium signals are largely confined to synapses.

1.7.1 Calcium imaging

Activity-induced calcium signals expand from the starting site to the nucleus to initiate gene responses. Light-induced calcium signals however, propagate from the cell membrane. Therefore, visualisation of cytosolic and nuclear calcium is of great relevance in understanding the cellular behaviour as well as the behaviours of neuronal networks upon different stimuli.

For the past decade, improvements have been made in the design of calcium indicators. There are two major groups of calcium indicators: (1) synthetic fluorescence calcium indicators

(SFCIs), and (2) genetically encoded calcium indicators (GECIs). The SFCIs cover a wide range of calcium indicators with different fluorescent excitation/emission spectra, dynamics and capacities. Fura-2 is a ratiometric and sensitive indicator dye for measuring intracellular calcium [256]. Fura-2 has an excitation ratio at 340/380 nm allowing for accurate measurements of the intracellular calcium concentration. Fluo-3 and Fluo-4 are excited by visible-light with excitation at 488 nm from argon-ion laser sources. Their wide fluorescence intensity increases response to calcium binding. X-rhod-1 is a red dye (excitation peak at 576 nm and emission peak at 602 nm) with low affinity to calcium (Kd=700 nM).

GECIs are used as an alternative to SFCIs as they can be easily targeted to specific cell types or subcellular compartments with neural-specific promoters. Since they are expressed by cells, these calcium indicators are compatible with long-term and repetitive *in vivo* measurements. GECIs consist of a calcium-binding domain (calmodulin or troponin C, TnC), fused to either one or two fluorescent proteins. GECIs fused to two fluorescent proteins show that calcium binding regulates fluorescence resonance energy transfer (FRET) between fluorescent proteins. GECIs fused to single fluorescent protein demonstrate the fluorescence intensity of a circularly permuted fluorescent protein (cpFP) is controlled by calcium binding-dependent changes in the chromophores environment [257].

1.7.2 Patch clamp

The membranes of neurons contain ion channels that regulate the movement of charge, thereby controlling neuron firing. Functional connectivity of neurons, the electrical and biophysical properties of ion channels in the neurons can be analysed using patch clamp recording. In this method, a glass micropipette is placed against a patch of the cell membrane and aspiration

is applied to form a high-resistance seal. Patch clamp configurations are decided based on research interests.

In the cell-attached mode, the membrane patch remains intact for the recording of ion channels within the patch and action potentials (APs). When the pipette loosely attached to the membrane, APs in neurons can be recorded without changing the composition of cytoplasm. A pore-forming agent (e.g. amphotericin) is used to create a perforated patch, to establish electrical continuity and to prevent dialysis of intracellular proteins. The whole-cell mode however, is most commonly used. Strong aspiration is briefly applied to disrupt the membrane patch for electrical and molecular access to the intracellular space. There are two main configurations: (1) voltage-clamp, in which the voltage is held constantly enabling the analysis of ionic currents, and (2) current-clamp, in which the current is regulated allowing the analysis of changes in membrane potential.

1.8 Summary

Application of pluripotent stem cell (PSC)-derived neurons in regenerative medicine, disease modeling and drug discovery requires integration of these cells into complex functional human networks. This has been addressed by tissue engineering approaches where PSCs were used to generate miniature 3D model of human organs [258]. However, one of the most important properties of neurons is their ability to form functional synapses for neurotransmission which is remains largely unexplored especially in hPSC-based model systems. Recent studies have started to integrate optogenetics, a non-invasive tool that allows for light-stimulation and millisecond-precise activation of genetically targeted neuronal populations [2, 6] into hPSC-based regenerative medicine paradigms [80, 259, 260].

The work carried out in this thesis was split into two major parts:

- **Optogenetically modified neurons differentiated from human pluripotent stem cells (hPSCs) in 2D and 3D culture systems to achieve cortical neural function.**
  A strategy for stimulating and recording of neurons in 3D culture was achieved by virally transducing human iPSC derived neural progenitor cells to express the membrane light-sensitive ion channel protein (ChR2), and optically stimulating the cells with blue light (470nm) whilst recording neural calcium transients using calcium imaging. This strategy was further extended to investigate the use of cell type-specific promoters that selectively target neuronal subpopulations within the mixed cultures consisting of progenitor, neuronal and glial cells after differentiation. ChR2 expression was restricted to neuronal subpopulations (GABAergic neurons) using SYN1 specific promoter, and to the excitatory neuronal subpopulation (glutamatergic neurons) using CAMKII specific promoter. The performance and targeting efficiency of these promoters were compared in this study.

- **Optimisation of defined culture environment in 3D alginate hydrogel system that facilitates cell survival and expansion of hPSCs.**
  In the 3D culture of hPSCs, a defined microenvironment was improved through encapsulation of cells in alginate hydrogels conjugated with RGD peptides and incorporation of small molecules (ROCK or/and ZVAD inhibitor).

In summary, we hypothesised that the novel non-invasive approach - optogenetics may enable the assessment of neuronal activity of differentiated mature neurons from hiPSCs in a 3D culture system using functionalised alginate hydrogels. The specific aims of this thesis are summarised as:

1. To establish an optogenetic approach in controlling ChR2-YFP expression of functional human neurons and networks in a 2D and 3D model.
2. To assess efficiency of lentiviral transduction and positive expression of ChR2-YFP in human iPSC-derived neurons driven by SYN1 and CaMKII promoters.
3. To improve a 3D culture system using peptide functionalised-alginate hydrogel incorporating with small molecules for hPSCs and neurons.

2.0 Materials and Methods

2.1 Materials and general reagents

The materials and reagents used in this thesis are listed in Appendix 1: List of Materials and Reagents.

2.2 Cell isolation, culture and maintenance

2.2.1 Primary cells

2.2.1.1 Mouse Embryonic fibroblasts (MEFs)

Mouse embryonic fibroblasts (MEFs) were used as a feeder layer for hESCs culture and were provided by the James Martin Stem Cell Facility, Oxford University at passage 0 and expanded up to passage 3 before mitotically inactivated using mitomycin C. The treated MEFs (3.3×10^5 cells/ml) were cultured on a 0.1% gelatin coated dish in MEFs medium, incubated at 37°C for a day prior to seeding with human embryonic stem cells (hESCs).

2.2.1.2 Neurons (mouse hippocampus and DRG)

The dissociated hippocampal cells and spinal cord or dorsal root ganglion (DRG) tissue was isolated from E14.5-day pregnant mice by Fabio Biachi working in conjunction with the Department of Physiology, Anatomy and Genetics, Oxford according to local established ethical policies. Briefly, individual embryos were separated by cutting uterus between embryo locations, kept in cold neural basal media (NB media) on ice and then sacrificed by decapitation. An incision was made in embryo head to expose the brain and to dissect it in half via the sagittal midline. The meninges were removed, and the hippocampus was located and removed using forceps and

microscissors into NB media on ice. For spinal cord or DRG neurons, the embryo was placed flat with the ventral facing upwards. The limbs and organs, rib cage, other pre-ossified structure and meninges were removed from the spinal cord. Individual DRG was then isolated using a fine forceps and placed in NB media on ice.

Hippocampi and DRGs were placed in NB media and centrifuged at low speed (500 rcf) for 2 min. The media was discarded, 1 ml of trypsin was added for 25 min of incubation in a water bath at 37°C, and stirred every 5 min to create a homogeneous mixture. The enzymatic activity was neutralized by adding 1 ml fetal bovine serum (FBS) and the tissues were triturated using a fine Pasteur pipette coated with FBS to obtain a single cell suspension. The cells were collected by centrifugation at 1000 rcf for 5 min, and the cell pellet was re-suspended in complete NB media prior to being plated onto PLO/laminin coated surfaces.

2.2.2 Cell lines

2.2.2.1 Human embryonic stem cells, hESCs

Human embryonic stem cells, hESCs (HUES-1, HUES-2, HUES-3 and HUES-4 cell lines) were obtained from Harvard University, Melton Lab, MA, USA. One million hESCs were thawed and re-suspended in 1 ml hESCs medium gently with minimal pipetting, dropped into the MEFs feeder layer dish, incubated at 37°C without disturbance for the first day of seeding. Cells were treated with Rho-associated protein kinase inhibitor (ROCKi), Y-27632 (Calbiochem, California, USA) to a final concentration of 10 μM. For routine culture and maintenance, medium was changed daily (replaced with 50% of fresh medium) for 6 days before being sub-cultured or transferred to matrigel (feeder free culture) in mTeSR1 medium (Stemcell Technologies Inc., France). The mTeSR1 medium was changed daily until cells reached 80% confluency, and then passaged as single cells using accutase (Invitrogen, USA). Cells were sub-cultured and expanded

to a sufficient number for the subsequent experiments. HUES-2 cell line was successfully raised and maintained in the lab for the whole project.

2.2.2.2 Human iPSC-derived neurons (Axol)

Human induced pluripotent stem cell-derived neurons (Axol-13 and Axol-15 from two different healthy donors) were purchased from Axol Bioscience, Cambridge, UK. The cells were thawed and then cultured at a seeding density of 50,000 cm^2 in the laminin coated 6-well plate (Sigma, USA) and Axol plating-XF medium. After 24 hours, the cultures were maintained in Axol neural maintenance-XF medium (up to 50 days) or differentiated in Axol neural differentiation-XF medium for 72 hrs.

2.2.2.3 Human neuroblastoma cells (SH-SY5Y)

Human neuroblastoma cell line (SH-SY5Y, purchased from ATCC® CRL-2266™) is a subline of the parental line *SK-N-SH* (ATCC® HTB-11™). These cells were cultured and maintained in complete medium which was then replaced by neuronal differentiation medium (refer Appendix 2 – List of medium).

2.2.2.4 Human embryonal kidney cells (HEK 293FT)

The human embryonal kidney 293 FT cell line (HEK 293FT) was purchased from Invitrogen, USA. It is a host for lentiviral production attributed to its stably expression of SV40 large T antigen from the pCMVSPORT6Tag.neo plasmid. The cells were thawed and plated into a T-75 cm^2 flask containing 10 ml of complete medium without Geneticin, incubated overnight at 37ºC and replaced with fresh complete medium containing 500 µg/ml Geneticin. The cells were cultured until 80-90% confluent and sub-cultured to a minimum of 3 passages before use in other applications.

2.3 Cell treatment and transfection

2.3.1 Sub-cloning into lentiviral vector

DNA plasmids coding for chanelrhodopsin-2 (ChR2) and its mutants were obtained from Karl Deisseroth, Department of Bioengineering and Howard Hughes Medical Institute, Stanford University, California, USA, for the hChR2 and Peter Hegemann, Institute of Biology, Experimental Biophysics, Humboldt-University, Berlin, Germany, for the ChR2-T159C mutant.

These plasmids were integrated into a lentiviral expression system provided by Dr. David Nagel at Aston University by sub-cloning the coding sequences into the lentiviral expression vector with synapsin 1 (SYN1), calcium/calmodulin-dependent protein kinase type II (CaMKII) and elongation factor-1 alpha (EF1a) promoter. ChR2 was sub-cloned into the lentiviral vector with the EcoR1, Not1 and HindIII restriction sites (refer Appendix 3). The assembled plasmids were a kind gift from Dr. Eric Hill and Dr. David Nagel at Aston University, UK. The yellow fluorescent protein (YFP) and green fluorescent protein (GFP) label were used as an indicator for positive expression. Polymerase chain reaction and sequencing of the virus constructs were performed by Dr. David Nagel.

2.3.2 Plasmid manipulation: bacteria transformation

The plasmids were diluted with water in a 1:10 ratio (recommended amount is 1 to 10 ng DNA) whilst the DH5α bacteria were thawed and 50 µl was aliquot to another pre-chilled Eppendorf tube. One µl each of the diluted plasmids (1:10 ratio stock) was added to the DH5α bacteria tube, incubated on ice for 15 or 30 min. The cells were heat-shocked in a 42˚C water bath for 42 seconds without shaking and placed on ice for 2 min. Total 750 µl of S.O.C. medium or LB medium was added into the cells at room temperature, and then incubated in a shaker-incubator at 225 rpm and 37˚C for an hour. The cells were then aliquoted and 4 drops were placed onto the LB

plates contained ampicillin, inoculated in 3 different directions. The cells were left at room temperature for 10 min to adhere onto the LB plate before being transferred into the incubator at 37˚C for overnight.

Cell colonies formed on the LB plate after 12 hrs incubation and were stored at 4ºC. A single colony was picked from the LB plate using sterile filter tip and dropped into 5 ml medium in a 15 ml falcon tube, incubated in a shaker at 37ºC, 225 rpm overnight and then kept at 4ºC. Total 125 ml of sterile LB-broth was prepared in a conical flask which contained ampicillin (125 ul in 125 ml, final stock concentration of ampicillin = 100 mg/ml or 50 mg/ml). The plasmids (i.e. psPAX2 or pMD2.G) were then added, incubated in a shaker at 37ºC, 225 rpm overnight. The bacterial cells were harvested by centrifugation at 6000 x g for 15 min at 4˚C. The supernatant was discarded and purified using Maxiprep; alternatively, the pellet was stored at -20°C.

2.3.3 Maxiprep plasmid purification

Maxiprep plasmid purification was performed by according to the protocol stated in Qiagen plasmid purification kit (catalogue 12963 & 12965 manual). The pelleted bacteria were completely re-suspended in 8 ml buffer P1 (P1+ RNase A solution stored at 4˚C), buffer P2 was added and gently mixed by inverting until the lysate appeared viscous before incubating at room temperature for 3 min. Total 8 ml of Buffer S3 was added to the Lysate and mixed by inverting 4-6 times (The solution was further mixed until completely colourless if LyseBlue reagent was been added). The QIAfilter cartridge was placed into a 15 ml falcon tube, lysate was transferred to the QIAfilter cartridge and incubated at room temperature for 10 min. Qiagen Plasmids Plus spin columns were placed into the QIAvac 24 Plus device connected to a vacuum pump and tube extenders were inserted into each column. A plunger was gently inserted into the QIAfilter Cartridge and the cell lysate was filtered into the collection tube. The cleared lysate was then added with 5 ml Buffer

BB, mixed by inverting 4-6 times before being transferred to a QIAGEN Plasmid Plus spin column on the QIAvac 24 plus. Approximately 300 - 600 mbar of vacuum pressure was applied until the liquid was drawn through all columns. The tube extender was removed, 0.7 ml Buffer ETR was added and vacuum pressure was applied until the liquid has been drawn through all columns in order to wash the DNA. This step was repeated with 0.7 ml Buffer PE, following by centrifugation of the column at 10,000x g for 1 min in a tabletop microcentrifuge to completely remove the residual wash buffer. The QIAGEN Plasmids Plus spin column was placed into a clean 2 ml Eppendorf tube, 400 ul Buffer EB or water was added to the centre of the spin column, and centrifuged for 1 min to elute the DNA. The eluted DNA was stored at 4˚C for immediate use or kept in aliquots at -20°C for long-term storage.

2.4 Lentiviral production: virus making

2.4.1 HEK cell transfected with Lipofectamine-2000

The ChR2 gene was fused to YFP and cloned into a lentivirus expression plasmid with cell type-specific promoter (i) human synapsin 1 promoter (pLenti-synapsin1-hChr2-(E123T-T159C)-EYFP-WPRE) and (ii) excitatory glutametergic neuron promoter (pLenti-CaMKII-hChr2 (E123T-T159C)-EYFP-WPRE), driving ChR2-YFP expression in the cells. The universal or constitutive promoter of human origin i.e. human elongation factor-1 alpha (EF1a) was included in the study.

Replication incompetent lentiviruses were produced via second generation packaging system containing the promoter and gene of interest (i.e., SYN1-ChR2-YFP, CaMKII-ChR2-YFP and EF1a-ChR2-GFP), the viral helper plasmid (psPAX2), and the pseudotyping plasmid (pMD2.G, encoding the coat protein VSV-G). Briefly, HEK 293FT cells (Invitrogen, USA) were plated in three T-75 flasks in DMEM medium (comprising 10% FBS + 1% penicillin-streptomycin). At 100% confluence, cells were transfected with DNA using lipofectamine-2000: 10 µg of plasmid containing the promoter and gene of interest, 10 µg of pSPAX2, and 10 µg of pMD2.G were mixed with 75 µl of lipofectamine-2000 and 1.5 ml of Opti-MEM. After 24 hrs, the cells were washed with DMEM and 15 ml of virus production media was added (comprising Opti-MEM with GlutaMAX-I + 1% penicillin-streptomycin, 1% sodium pyruvate, and 1% sodium bicarbonate). Approximately 48 hrs later, the supernatant was harvested after centrifugation at 500 g for 10 min, and then filtered through a 0.45-micron filter (pre-wetted with DMEM). The filtrated virus was then aliquoted to Eppendorf tubes for storage at −80°C.

2.4.2 Virus titration

The detection and quantification of HIV-1 core protein in viral supernatants was performed using an enzyme immunoassay, HIV p24 antigen ELISA (Cell Biolabs' QuickTiter™ Lentivirus Titer Kit). According the manufacturer, free p24 remained in supernatant when complexes formed with ViraBind™ lentivirus reagents, only the amount of lentivirus associated p24 was measured.

The p24 antigen standard (concentration range: 100 ng/ml – 1 ng/ml) was prepared by diluting p24 stock solution and incubated 30 min at 37°C. The lentiviral samples were diluted in OPTI-MEM at 1:50 with ViraBind™ Lentivirus Reagent A (10 µl) and mixed by inverting. Reagent B (10 µl) was then added immediately, incubated for 30 min at 37°C before centrifuging for 5 min at 12,000 rpm. The supernatant was removed and the pellet was dissolved in 250 µl of Sample Diluent, and then incubated for 30 min at 37°C to inactivate the viruses. Each lentiviral sample, HIV p24 standard, blank and control medium was assayed in duplicate. Total 100 µl of inactivated lentiviral sample or p24 antigen standard was added to an anti-p24 antibody coated plate. The plate was sealed and incubated overnight at 4˚C. The reagents in the wells were discarded and washed 3 times with 250 µl 1X Wash Buffer per well with thorough aspiration between each wash. Diluted FITC-Conjugated Anti-p24 Monoclonal Antibody (100 ul) was added to each well and incubated at room temperature for 1 hr on an orbital shaker. The wells were washed 3 times, and incubated with 100 ul of diluted HRP-Conjugated Anti-FITC Monoclonal Antibody at room temperature for 1 hr. The well strips were washed and 100 µl of warm Substrate Solution was added immediately then the wells were incubated at room temperature on an orbital shaker (actual incubation time varied from 2-30 min). The enzyme reaction was stopped by adding 100 µl of Stop Solution into each well when the well changed colour. Results were read immediately, optical density of each well was measured at 450 nm (primary wave length, 560 nm

as secondary wave length) using a spectrophotometer (Wallace Victor^2 reader and software). Lentiviral particle (LP) was obtained by calculating the lentivirus titer (VP/ml) as stated in the manufacture manual sheet.

2.5 Cell transduction

Axol and SY5Y cells were transduced with ChR2-YFP or ChR2-GFP transgenes using lentiviruses under the control of elongation factor 1-alpha (EF1a, universal) promoter, synapsin-1 (SYN1, pan-neuronal) promoter and calmodulin-dependent protein kinase type II (CaMKII, glutametergic neurons) promoter, which had been generated as previously described (section 2.7.1). The amount of viruses used in the transduction was MOI-1 and MOI-2, respectively for first infection in 24 hrs and second infection in the next 24 hrs. Transduction efficiency was evaluated using fluorescent microscopy and flow cytometry after 14 days of transduction. Cell viability was measured with trypan blue staining and by a cell counting.

2.6 Immunofluorescent staining (IF)

Cells (Axol and SY5Y) were fixed with 4% paraformaldehyde in PBS for 30 min at room temperature. Fixation was stopped by washing cells three times with PBS, pH 7.4. The cells were permeabilised and blocked (5% BSA, 0.2% Triton-X100 and 0.1% Tween 20 in PBS) for 1 hr and incubated overnight in primary antibody solution at 4°C. Cells were washed three times with wash buffer (0.2% BSA, 0.2% Triton-X100 and 0.1% Tween 20 in PBS) and then blocked with 10% goat serum in wash buffer for 30 min. Secondary antibody solution was added and cells were incubated at room temperature for 2 hrs. Finally, cells were washed three times with washing buffer and 300 µl of 6-diamidino-2-phenylindole (DAPI) was added. Pictures were taken using confocal microscopy (Zeiss-LSM 780, Germany) and ZEN light 2013 software.

Primary antibodies were mouse anti-neuron-specific class III beta-tubulin (Tuj1) (1:1000; abcam, Cambridge, UK, www.abcam.com), mouse anti-γ-aminobutyric acid B receptor 1(GABA-B-R1) (1:50; abcam), rabbit anti-S100B (1:200; abcam), rabbit anti-glial fibrillary acidic protein (GFAP) (1:2500; abcam), and rabbit anti-vesicular glutamate transporter 1 (vGlut1) (1:100; abcam). Alexa Fluor®568-conjugated goat anti-mouse, Alexa Fluor®649-conjugated goat-anti rabbit and Alexa Fluor®488-conjugated goat anti-rabbit secondary antibodies were all used at 1:500 (Invitrogen, Life Technologies, Grand Island, NY, www.lifetechnoogies.com) (Table 2.1; Appendix 4). Negative control of the samples was prepared in the same staining protocol containing no primary antibody, only with secondary antibody incubated in the samples. SY5Y cells could be used as a positive control in the study for comparison.

Cell type/component of neuron	Phenotypic markers
Neural cytoskeleton	III-beta tubulin (TuJ-1)
Astrocytes	Glial fibrillary acidic protein (GFAP)
Glutamatergic/excitatory neurons	Vesicular glutamate transporter 1 or 2 (vGlut1 or vGlut2)
GABAergic/inhibitory neurons	γ-aminobutyric acid B receptor 1(GABA)
Nuclei	DAPI

Table 2.1: Phenotypic markers for the identification of specific neuronal cell types in the culture.

Indirect immunofluorescent staining using primary and secondary antibodies with optimised concentration or dilution were suggested in section 2.6 and Appendix 4.

2.7 Flow cytometry

Cells were pre-treated as described in section 2.5 before quantifying by flow cytometry for assessing the efficiency of transduction. Untreated cells or non-transduced cells were used as a negative control and setting gating region. Negative control cells stained with primary without secondary antibody to check non-specific binding of primary whilst treated cells stained without primary to check non-specific binding of secondary antibody. Total events acquired are 10,000 cells defined as number of particle detected by the instrument in one sample.

The cells were stained with primary antibodies as described in section 2.6 for immunophenotyping (refer Appendix 4 – List of antibodies). The protein markers were used according to the stated concentration or dilution. PerCP-Cy5.5-conjugated goat anti-mouse IgG_{2a} (1:400, Santa Cruz) and Alexa Fluor®649-conjugated goat anti-rabbit (1:500, Invitrogen) were secondary antibodies used in flow cytometry (BD FACSCanto™) analysis and the data was analysed with BD CellQuest™ Pro Software.

Since multiple dyes were used in flow cytometry and the concern is positively by spectral overlap, therefore a fluorescence-minus-one control (FMO) was preferred than isotype control in which all antibodies are included except the one suspect is most prone to error from spectral overlap. Isotype control is not use to determine positive versus negative cells or as a gating control in the experiments. There are useful for demonstrating that there was poor blocking of the cells, and they can be eliminated when carefully titration of reagents yielded highest positive signals in bright population, whilst spread was reduced in the negative population.

2.8 Calcium imaging

Photo-activation of ChR2-expressing cells was initially investigated using X-Rhod-1, AM (Invitrogen, X14210). The dye (0.5 uM) was added to the culture for 20 min before imaging, and then replaced with artificial cerebrospinal fluid (ACSF). The dye was solubilised in DMSO, sonicated and diluted in 10 ml ACSF to 4 uM stock (ACSF: NaCl = 121 mM; KCl = 4.2 mM; NaH_2PO_4 = 0.5 mM; $CaCl_2$ = 1.1 mM; $MgCl_2$ = 0.3 mM; D-glucose = 20 mM). The images were obtained by EM-CCD (electron multiplying-charge coupled device) camera at 10 frames/sec with an exposure time of 60 ms/frame. In sync with calcium imaging, illumination of 20 ms duration was delivered over a whole test area at 1 Hz or 0.2Hz.

Live calcium imaging was also performed with CAL-590 (AM, Mw-1129.86, 5 x 50 µg package, ATT Bioquest, 20510). Transduced and non-transduced Axol, SY5Y and primary neurons were incubated with CAL-590 AM at a concentration of 10 µM in ACSF for 40 min at room temperature. The cells were washed and ACSF was added for imaging using Carl Zeiss 780 confocal microscope. The set up was as follows: 20x objective, Zoom 1, 512 x 512 format, 8 bit resolution, xyt scan mode, 400 Hz speed, 1.0 airy pinhole, frame average 1, line average 4 for image, and 1 for time lapse imaging. Virus transduced cells were excited with 594 nm laser for Ca^{2+} indicator (CAL-590 AM) and 488 nm laser (at 20% of laser) to see the yellow fluorescence from YFP whilst 100% of 488 nm laser was set to stimulate the ChR2-YFP. Emission fluorescence was collected at 550/590 nm for CAL-590 AM. Time lapse imaging was set with a stimulation of 1.635 sec and a total of 200 frames were recorded at the basal Ca^{2+} level recording.

To optimise the fluorescence signal (F) as well as to test the dye loading efficiency, cells stained with CAL-590 AM in ACSF solution were added with 50 M ionomycin (Sigma-Aldrich, USA) during imaging. The stock of the dye was prepared with Pluronic F-127 to help disperse the

acetoxymethyl (AM) esters. Different concentrations of the dye (1, 4, 8 and 10 μM) were evaluated. After imaging, data was analysed offline with ZEN and ImageJ software (NIH). For the virus transduced groups, only YFP positive cells were analysed and included in the presented results.

2.9 ChR2 stimulation

In calcium imaging using X-Rhod-1 AM, light stimulation was achieved by a custom-built light-emitting diode (LED) device that used a blue LED (470 nm; Thor Labs) directly placed 2–5 mm from the ChR2-expressing neurons. Power to the LED was delivered through a current-controlled custom built LED driver and Arduino UNO microprocessor system. In calcium imaging using CAL-590 AM, light stimulation was applied through efficient blue light excitation (470-490 nm) of a confocal microscope equipped with argon lasers.

2.10 Cell scaffold

2.10.1 Alginate

High molecular weight ultrapure alginate (Pronova-MVG) was obtained from Pronova Biomedical, Oslo, Norway (Mw = 231 kDa, high guluronic acid content, medium viscosity >322 cP). Low molecular weight alginate was obtained from Sigma-Aldrich, St Louis, MO (Mw = 12-80 kDa, low guluronic acid content, low viscosity 100-300 cP).

2.10.2 Fabrication of alginate hydrogel

Alginate was dissolved in 0.9% (w/v) sodium chloride (NaCl) at 60°C for 6 hours, autoclaved and left overnight before being used. A stock solution of alginate was prepared at a concentration of 2.0% (w/v), and diluted to 1.2, 1.4, 1.6 and 1.8% (w/v), respectively. Alginate solutions were transferred to a 5 ml syringe, which was connected to a syringe pump (Harvard

apparatus, USA) with flow rate set at 2, 2.5 and 3 ml/min. To polymerise the gel into beads, the solutions were then extruded into a stirred bath of 102 mM calcium chloride ($CaCl_2$) via a 30 gauge needle at each of the flow rates and gently stirred for 7 min at room temperature. The beads were washed with sodium chloride twice and immersed in phosphate buffer saline (PBS, pH = 7.4) for microscopic analysis.

2.11 Physical characterisation of alginate hydrogel

2.11.1 Measurement of bead diameter

Alginate beads were characterised using microscopic analysis (Nikon eclipse Ti, Japan) to measure the diameter of beads. Mean diameter (n = 50) was calculated to determine the bead size at different concentrations (1.2, 1.4, 1.6, 1.8 and 2.0%) and flow rates (2, 2.5 and 3 ml/min).

2.11.2 Swelling test

The initial weight of alginate hydrogels (1.8% w/v) were recorded at day 0 (W_i) prior to immersion in 2 ml of PBS, pH = 7.4 for 1, 3, 7 and 14 days at 37 °C. At each time point, the gel beads (per ml) were taken out of the solution. The swollen samples were blotted using filter paper to remove the excess water remaining on the surface of the hydrogels, and then weighed (W_s). The swelling ratio of the alginate beads was defined as the ratio of the weight increase ($W_s - W_i$) to the initial weight (W_i) according to following equation:

$$\text{Swelling (\%)} = ((W_s - W_i) / W_i) \times 100 \text{ (\%)}$$

where W_i represents the initial weight at day 0 and W_s represents the swollen weight of the hydrogels at each time point.

2.11.3 *In vitro* degradation of alginate

The degradation experiments were conducted by incubating the hydrogels (1.8% w/v) in PBS at 37°C and by determining the weight loss after recovery of the samples at predetermined time intervals. At the investigated time points (1, 3, 5, 7 and 14 days), the samples (per ml) were removed from the medium and the surface of hydrogels was blotted dry gently with filter paper, frozen and lyophilised before being weighed. The degradation was assessed by measuring the weight loss ratio (%), which was defined with the following equation [261]:

$$\text{Weight loss (\%)} = ((W_i - W_d) / W_i) \times 100 \text{ (\%)}$$

where W_i represents the initial weight at day 0 and W_d represents the dry weight of the hydrogels at each time point.

2.11.4 Analysis of protein diffusion

Bovine serum albumin (BSA, Mw = 66 kDa) and laminin (LN, Mw = 400 kDa) were physically entrapped in the alginate beads devoid of cells. The diffusion rate of entrapped BSA and LN was assessed with the advanced protein assay (ADVA01, Cytoskeleton). BSA and LN were prepared at 5, 10, 20, 40 and 80 µg per ml in alginate solution (1.8% w/v). The BSA-alginate and LN-alginate were extruded into 102mM $CaCl_2$ for 7 min at room temperature to form beads. The beads were washed twice before immersion in 1 ml of PBS and incubated at 37°C. The solution was taken from each well at 1 and 7 days, transferred to a 96-well plate and mixed with ADV01 solution in the ratio of 4:1 according to the protocols in the manual. The samples were placed in the spectrophotometer reader and the absorbance was read at 590 nm. The concentrations of the proteins were calculated by referring to the standard curve of BSA. The amount of proteins retained by the beads was obtained by subtracting the amount of proteins diffused into the solution from the initial loaded proteins.

2.11.5 Functionalisation of alginate with RGD peptides

RGD peptide was conjugated to alginate via an amide bond between the terminal amine (NH_2) of peptide and the carboxylate (COOH) on alginate. The immobilisation of RGD onto alginate utilised the aqueous 1-ethyl-3-[3-dimethylaminopropyl] carbodiimide (EDC) chemistry as referred to the experiments reported by Rowley et al. [217]. Briefly, Sulfo-NHS (0.1 mmol), EDC (0.2 mmol) and RGD peptide were added into the Alginate-MES buffer, the reaction was performed for 20 hrs. Alginate-MES solution was prepared by mixing 1% (v/v) alginate solution in 0.1 M MES buffer (0.3 M NaCl, pH = 6.5) for 12 hrs. The use of Sulfo-NHS in the reaction can stabilise the reactive EDC-intermediate against competitive hydrolysis, thereby achieving high efficiency of peptide binding. The RGD-alginate solution was purified by dialysis (3500 MWCO) against distilled water (dH_2O) in decreasing salt solution concentrations for 3 days and then lyophilised for 1 day. The resultant solid RGD-alginate was stored desiccated until use. Validation of the conjugated RGD with amino acid analysis was performed using a service provided by Alta Bioscience Ltd. (results attached in Appendix 5).

2.12 Cell growth and survival in alginate hydrogel

2.12.1 Encapsulation of cells (HUES-2 and astrocytes)

The effect of cell seeding density (1 x 10^6, 2 x 10^6 and 3 x 10^6 cells/ml) was previously assessed in our group, and an optimal encapsulation density was found to be 2 x 10^6 cells/ml. The hESCs (HUES-2 derived from feeder-free layers) were harvested as single cells using accutase, re-suspended in 1.8% alginate and RGD-alginate solutions, prior to extrusion into 102 mM $CaCl_2$ at a flow rate 3 ml/min (refer to section 2.10.2: Fabrication of alginate hydrogel). Beads encapsulated with hESCs were then rinsed with PBS twice, transferred to a 6-well dish and cultured in a chemically-defined condition (using mTeSR1 medium and ROCKi). In order to

compare RGD modified alginate and unmodified alginate using HUES-2, another cell type (astrocytes) were cultured in alginate as a control in the study. Culture medium was changed daily and the beads withdrawn from culture (500 µl per well) at different time points for the following studies.

2.12.2 Three-dimensional culture systems and cell seeding (SY5Y cells)

Cell culture systems in three-dimensional (3D) environments were made from alginate hydrogel into (i) channel system (channel-alginate, Ch-Alg): channels within the alginate hydrogel were created using a fine needle (30G); cells were encapsulated within hydrogel and also seeded onto the surface, and (ii) microcarrier system (Mc-Alg): alginate beads were placed in a stack position and cells were seeded directly on the surface of the beads. These 3D culture systems were used for neuronal culture and growth (tested with SY5Y cells) in comparison to the earlier developed RGD peptide functionalised alginate beads (section 2.11.5). Schematic of the 3D culture systems was illustrated in Figure 2.1. Each of these constructs was placed in a well surrounded or supported by 1% agarose gel (w/v) made in $CaCl_2$ solution. Presto blue assay and live-dead cell staining were performed to assess cell viability and localisation.

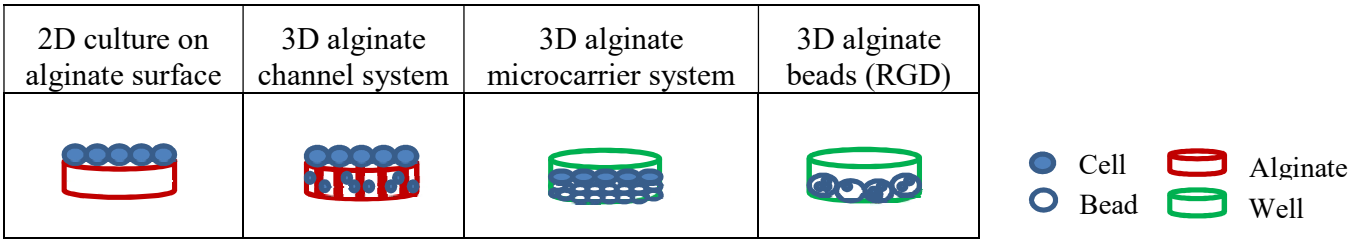

Figure 2.1: 3D culture systems for neurons (SY5Y cells) using alginate hydrogels.

Channel (Ch-Alg), microcarrier (Mc-Alg) and bead system (RGD-Alg) were seeded and encapsulated with SY5Y cells compared to the standard control 2D culture on alginate surface.

2.12.3 Viability analysis

Method-1: Trypan blue dye exclusion staining was used for cell viability analysis and cell counting in the study (for 2D or monolayer culture). This technique is the standard methodology based on the principle that live (viable) cells do not take up trypan blue whereas dead (non-viable) cells do. Cells were routinely counted manually with a hemocytometer. A cell suspension was prepared in 1 ml PBS solution at pH 7.4. Then 900 µl of Trypan Blue solution 0.4% (Sigma) was added to 100 µl of the cell suspension (dilution factor = 10), and mixed thoroughly for 5 minutes. A small amount of trypan blue-cell suspension mixture was transferred to both chambers of the hemocytometer with the cover-slip in place. All the cells in the 1 mm centre square and four 1 mm corner squares were counted (chamber 1 and repeated for chamber 2) with a separate count of viable and non-viable cells. Total cells and cell viability were obtained from the following formula:

a) Total cells: The average count per square x dilution factor (10) x 10^4 (count 10 squares) x 1 ml (original volume)
b) Cell viability: Total viable cells (unstained)/total cells (stained and unstained) x 100%

Method-2: Calcein-AM and propidium iodide (PI), (Sigma Aldrich, Missouri, USA) staining was performed to assess the viability of encapsulated hESCs, which stained viable cells green and dead cells red. The hESC-alginate constructs were removed from culture, stained with calcien-AM and PI solution at 37°C for 1 hr. The constructs were rinsed and immersed in PBS for confocal imaging (Zeiss-LSM 710) using ZEN light 2011 software. Pictures were taken at the equatorial plane using a 5 x objective. The percentage of surviving cells was determined by the number of green signals divided by the total number of cells (green and red signals) at a sectional-view using ImageJ (National Institutes of Health, Bethesda, MD). The experiments were carried out in triplicate for three independent tests, and results were analysed using Prism5.

Method-3: Presto blue assay (Invitrogen, Life Technology) was carried out to evaluate viability, proliferation and cytotoxicity. Cell-scaffold constructs were rinsed with PBS buffer briefly and gently before stained with 300 µl of Presto blue solution in a single well of 24-well plate for 90-120 min incubation. Total 100 µl of the solution was aspirated and then transferred into a 96-well plate for absorbance reading at the excitation/emission wavelength of 570/600 nm. The constructs were washed with culture medium and replaced with fresh medium to keep the cells in culture. Data from this experiment was collected at day-1, -3, -7 and -14.

2.12.4 Apoptosis analysis

The event of cell death induced by apoptosis in the alginate beads was evaluated using flow cytometry. Encapsulated hESCs were treated with caspase inhibitor, ZVAD (Z-VAD-FMK, Enzo Life Sciences) in the presence and absence of ROCK inhibitor (ROCKi). ROCKi alone served as a control group. The final concentration of ZVAD and ROCKi at 10 µM each were incorporated into the 3D system, and incubated overnight. The cells were then de-capsulated (with 50 mM EDTA and 10 mM HEPES in PBS or alginase) and collected for propidium iodide, PI staining at 4°C in the dark. The cells were washed and incubated in cytofix/cytoperm at 4°C for 20 min. The cells were washed with perm/wash solution twice before being stained with caspase 3-FITC antibody (diluted with wash buffer in a 1:5 ratio, BD Biosciences, USA) for 30 min in the dark. Finally, the cells were washed twice in perm/wash solution, fixed with 1% formaldehyde and analysed with flow cytometry. Unstained cells were prepared as control groups.

2.13 Statistical analyses

Average values and the standard error of mean (±SEM) or standard deviation (SD) of three independent experiments were determined based on the study performed. Significance was tested by two-way analysis of variance (ANOVA), the p-values denote as *=$p<0.05$, **=$p<0.01$, ***=$p<0.001$, n.s. = non-significant. Experiments were performed in triplicate (n) and at least three independence tests (N).

3.0 Generation and characterisation of optogenetically modified human iPSC-derived neurons expressing ChR2 under the control of SYN1, CaMKII and EF1a promoter

Introduction:

Current therapy for neurodegenerative diseases such as Parkinson's and Alzheimer's disease has been focused on full behavioral recovery which requires functional integration of grafted dopamine or cortical neurons into diseased host circuits [262, 263]. Optogenetics is a novel non-invasive tool to validate the functional neuronal integration (known as graft-mediated neuronal network repair) which involves optical stimulation. Optical stimulation of heterogeneous brain tissue can be achieved in a cell type-specific manner using channelrhodopsin-2 (ChR2) under the control of different promoters.

The rise in the use of optogenetic techniques has enabled greater control over the stimulation of individual neurons both *in vitro* and *in vivo* [264, 265]. However, when ChR2 is transduced into the mixed neuronal cultures derived from human iPSC containing glutamatergic (excitatory) and GABAergic (inhibitory) neurons, neuron firing may inhibit with optical stimulation. This is because a GABAergic neuron will silence all surrounding neurons that it synapses with, therefore the results of stimulating mixed populations of neurons cannot be easily predicted if the distribution and connectivity of excitatory and inhibitory neurons within the population is variable. This is a considerable challenge in population of neurons derived from human iPS progenitor cells as the resulting mix of cell types will vary from culture to culture. It should be possible to overcome this drawback by targeting sub-population of neurons using promoters specific to neuronal cell type. For instance, human synapsin 1 (SYN1) is associated to

all type neurons including GABAergic and glutamatergic neurons whilst calcium/calmodulin-dependent protein kinase II (CaMKII) promoter is specific to glutamatergic neurons [266-268].

To apply this technique in hPSC-derived neurons, we adopted a strategy to explore optogenetic modification and functional assessment in 2D culture, including molecular targeting of specific neurons such as glutamatergic and GABAergic cells, subsequently leading to the development of an *in vitro* 3D model using hydrogel matrix to recapitulate some aspects of human brain.

The goal of this study was to assess lentiviral transduction of Axol (human iPSC-derived neurons) and SY5Y (neuroblastoma) cells expressing ChR2 under the regulation of two different cell type-specific promoters i.e. human synapsin 1 (SYN1) and calcium/calmodulin-dependent protein kinase II (CaMKII). To allow simple visualisation of ChR2 expression, it is encoded as a fusion protein with yellow fluorescent protein (ChR2-YFP). The differentiated Axol and SY5Y cells which have been transduced with ChR2 are characterised in this chapter and the expression of neuronal cellular subtypes were further assessed with neuronal markers, and correlated with the levels of ChR2 observed. We hypothesised that the differentiated Axol cells could be optogenetically modified and demonstrated positive expression of ChR2-YFP (driven by CaMKII) not only in 2D culture but in a 3D culture system. This chapter was focused on human stem cell engineering, manipulation and characterisation of neural subpopulations. In addition, SY5Y cells were also included as a control group to show positive expression of ChR2 under the control of all promoters.

3.1 Identification of an optimal transduction protocol

3.1.1 Lentiviruses mediated expression of ChR2-YFP in neurons derived from human iPSCs (Axol cells)

The experimental setup in this chapter enables the potential of optogenetics in human iPSC derived neurons (Axol cells) to be targeted under the control of cell type-specific promoters, for example SYN1 and CaMKII as well as the universal promoter EF1a. Cell viability together with the resulting expression level was investigated under different transduction condition i.e. Multiplicity of Infection 2 (MOI-2) without re-infection [M2H0]; Multiplicity of Infection 2 (MOI-2) with re-infection at MOI-2 [M2H2], and Multiplicity of Infection 1 (MOI-1) with re-infection at MOI-1 [M1H1]. Higher cell viability (>90%) remained at M1H1 and M2H2 than M2H0 in all promoters tested (Fig. 3.1a) using the Trypan Blue exclusion test. The data (M1H1 and M2H2) suggests that re-infection does not lead to increase cell death.

Flow cytometry results indicated that ChR2-YFP expression level was higher in Axol cells driven by pSYN1-ChR2-YFP (6.5%) than pCaMKII-ChR2-YFP (2-5%) from day 7-28 after transduction (Fig. 3.1b), indicating that pan neuronal promoter SYN1 is stronger than CaMKII. An example of the results obtained from dot plot was shown in Appendix-6. The positive control EF1a-ChR2-GFP construct driven expression 2 fold (>13%) higher when compared to pSYN1-ChR2-YFP and pCaMKII-ChR2-YFP due to all cell types in the culture were highly expressing it. Transduction condition M2H2 and M1H1 which involved re-infection were more efficient than M2H0, displayed higher ChR2 expression. On day 14 after transduction, Axol cells showed strong ChR2 expression (Fig. 3.2) and mature neuronal morphology (glutamatergic and GABAergic cells) in all promoters. Confocal microscopy demonstrated the distribution of ChR2-YFP/GFP expression in the cells and dendrites.

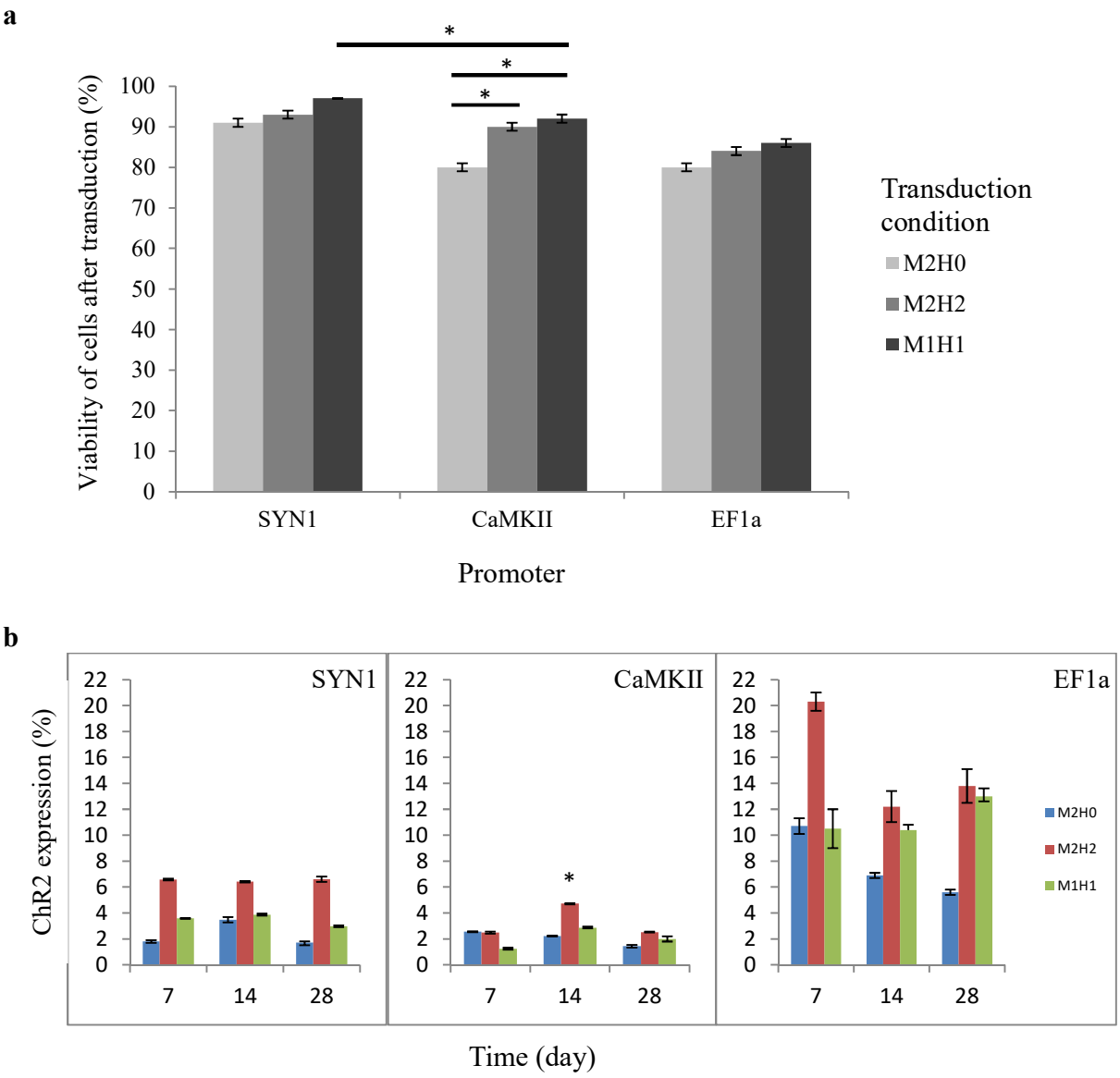

Figure 3.1: Human iPSC-derived neurons (Axol) achieved higher cell viability and stronger ChR2 expression (%) in the transduction conditions of M2H2 and M1H1 than M2H0, under the regulation of different promoters.

Day 14 post-transduction was selected as the best time point for light stimulation due to the strong expression of ChR2-YFP signal.
(a) Axol cells were transduced with pSYN1-ChR2-YFP, pCaMKII-ChR2-YFP and pEF1a-ChR2-GFP plasmids. Viability of the cells was calculated using trypan blue excursion test after 7 days of transduction. Transduction conditions: M2H0 (Multiplicity of Infection-2 without re-infection); M2H2 (Multiplicity of Infection-2 with re-infection at MOI-2), M1H1 (Multiplicity of Infection-1 with re-infection at MOI-1), n=3.
(b) Transduction efficiency was performed using flow cytometry and positive ChR2 expression in the cells was quantified. The universal promoter, EF1a was served as a positive control. Significance was tested by ANOVA; * = $p<0.05$; error bars denote standard error of deviation (±SD), n=3.

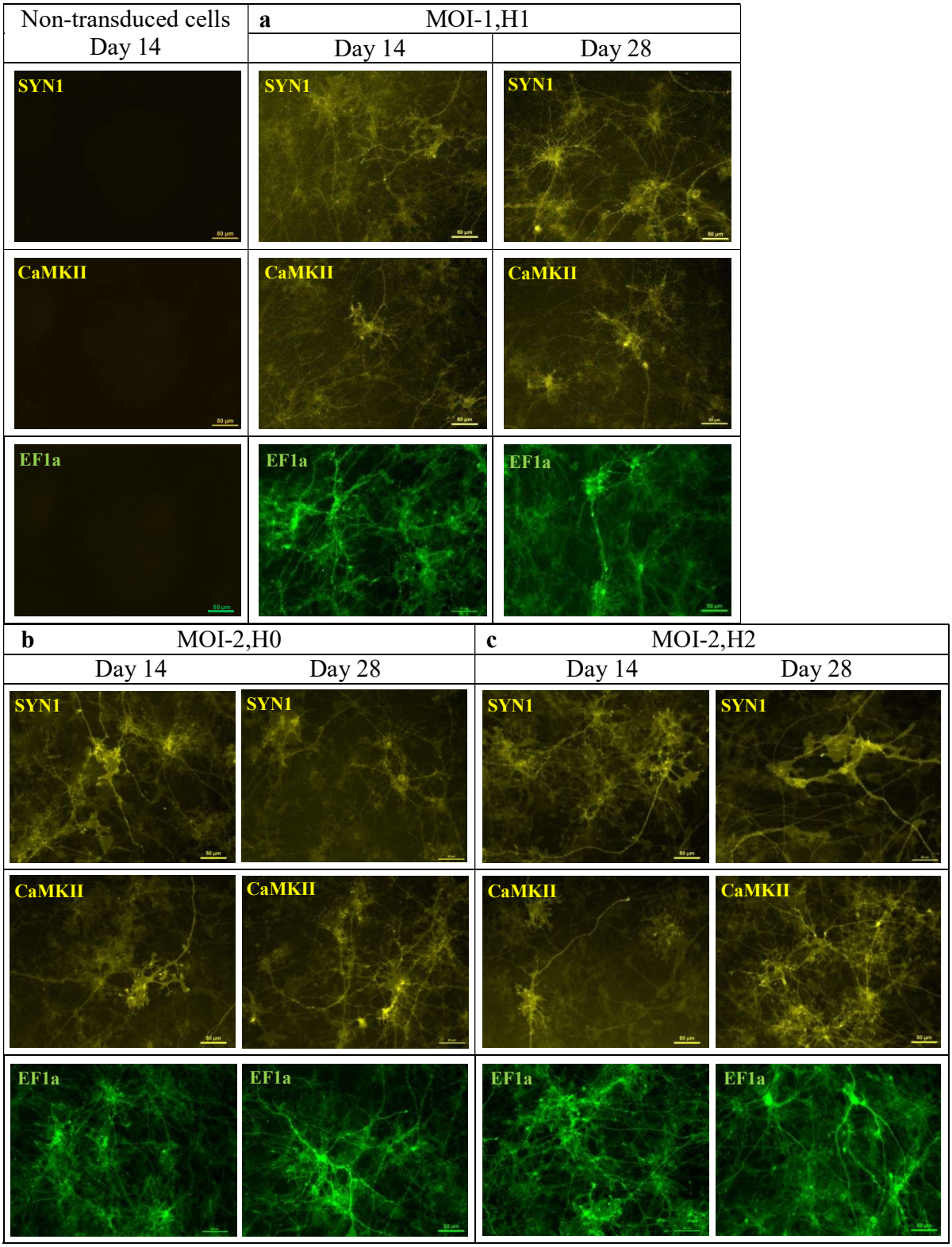

Figure 3.2: Positive expression of ChR2-YFP-SYN1, ChR2-YFP-CaMKII and ChR2-GFP-EF1a in Axol cells after 14 and 28 days of transduction.
ChR2 distributed evenly in the culture, Axol cells were transduced at different conditions (a) M1H1, (b) M2H0 and (c) M2H2. The cells were imaged using a fluorescence microscope (Nikon Eclipse T_i-E, Japan). Negative control showed no expression in untreated or non-transduced cells. Scale bar: 50 µM.

3.1.2 Lentiviruses mediated expression of ChR2-YFP in neurons derived from neuroblastoma cells (SY5Y)

The potential to apply optogenetics in human neurons and the efficiency of transduction were further evaluated using neuroblastoma cells (SY5Y) which are robust. Transduction condition with re-infection at M1H1 and M2H2 shows high cell viability (> 85%) in transduced SY5Y cells (Fig. 3.3a). Data shows that SY5Y cells containing pSYN1-ChR2-YFP remained the most viable group up to 14 days after transduction (> 92%). Although pCaMKII-ChR2-YFP and pEF1a-ChR2-GFP have lower cell viability than pSYN1-ChR2-YFP on day 7, the cells recovered and increased viability up to 93% on day 14.

Flow cytometry revealed that ChR2-YFP expression level at M2H2 was higher in cells driven by pSYN1-ChR2-YFP and pEF1a-ChR2-GFP than pCaMKII-ChR2-YFP cells on 7 and 28 days of transduction (Fig. 3.3b). The low expression level of pCaMKII-ChR2-YFP was further confirmed by the images captured using confocal microscopy (Fig. 3.3c), suggesting that CaMKII is a weaker cell type-specific promoter as previously reported by Dittgen, T. el al., and Rein, M.L. and Deussing, J.M. [267, 269]

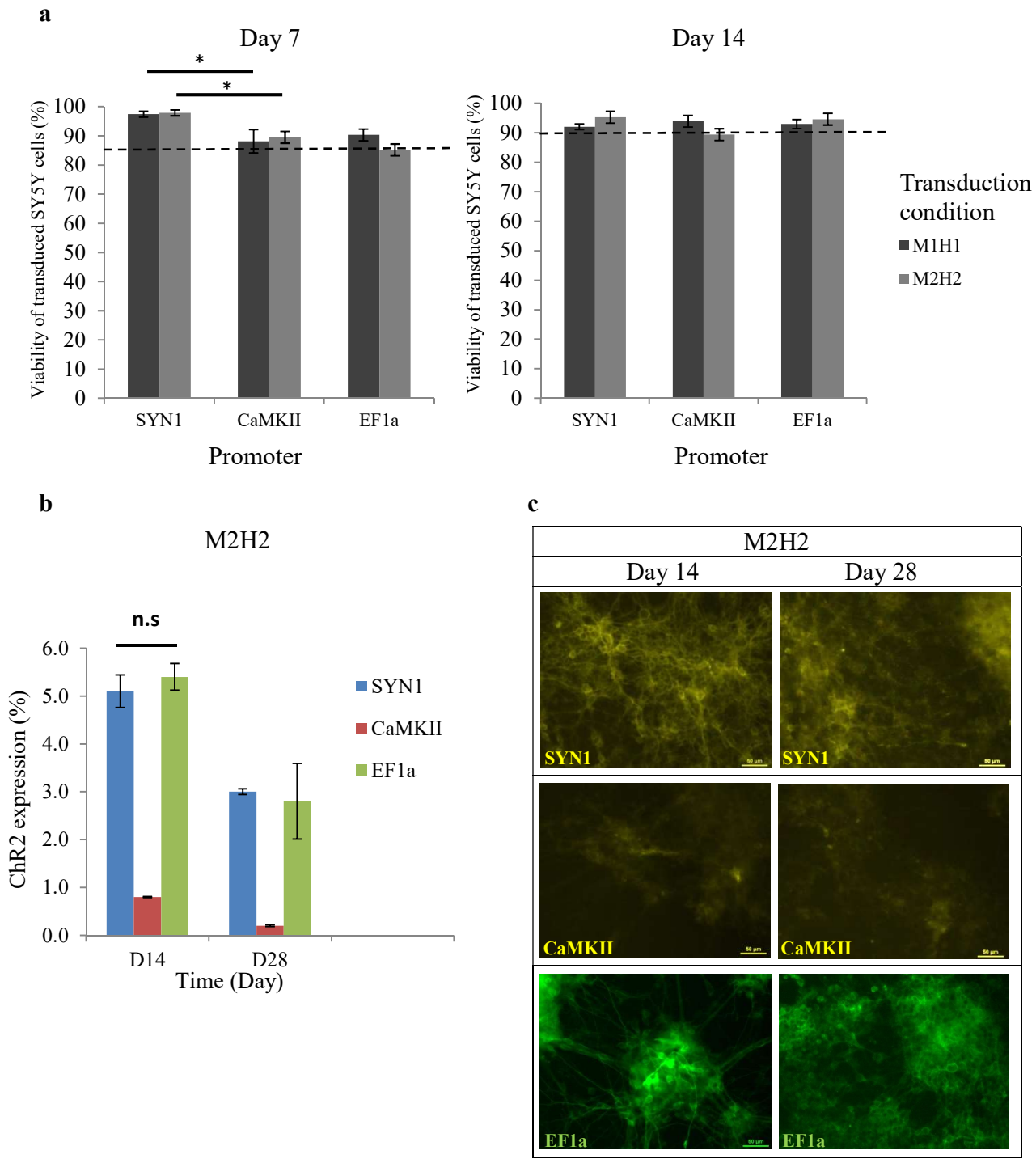

Figure 3.3: Human neuroblastoma (SY5Y) cells with different promoters demonstrated a high percentage of viability (>85%) and positive expression of ChR2.
(a) Cell viability of lentiviral transduced SY5Y cells was analysed using trypan blue exclusion test after 7 and 14 days of transduction at the conditions of M1H1 and M2H2 (n=3). (b) Efficiency of transduction was evaluated using flow cytometry on day 14 and 28 post-transduction (n=3). ANOVA test was used to determine significance, n.s = non-significant; * = $p<0.05$ was considered statistically significant. Error bars denote standard deviation (±SD). (c) pCaMKII-ChR2-YFP showed a distinct low expression in SY5Y cells. Fluorescence imaging of cells was performed using fluorescence microscopy (Nikon Eclipse T_i-E, Japan). Scale bar: 50 µm.

3.2 Sub-classes of differentiated Axol and SY5Y cells were identified with neural markers

3.2.1 Maturation of neurons (Axol cells) derived from hiPSCs was increased over passages in the culture

Neural induction of Axol cells have been adapted in this study according to the manufacturer's protocol [235], and it was assessed whether pro-long period of neural differentiation enhanced maturation of neurons by increased passaging. The later-passage iPSC-derived neurons exhibited notably greater neuronal marker expression (vGlut1) and less progenitor stem cell markers (Nestin and Pax6) than early-passage iPSC-derived neurons (Fig. 3.4a).

Expression of Pax-6 and Nestin decreased from 65-80% at passage 6 to approximately 20% at passage 10 (Fig. 3.4b). On the contrary, vGlut1 increased from 10% to approximately 65% in total neuronal population. The extended passaging has given rise to more functional neurons in the culture whilst reducing progenitor stem cells has enhanced Axol maturation, displayed morphological and phenotypical similarity to primary neurons.

3.2.2 Optogenetic modified Axol cells exhibited characteristics of mature neurons

In order to better characterise cellular phenotype, immunofluorescent staining on transduced Axol cells under the regulation of different promoters (between passages 8-10) was performed. Confocal microscopy imaging revealed that the transgene ChR2-YFP was expressed efficiently in both pSYN1-ChR2-YFP and pCaMKII-ChR2-YFP driven Axol cells. The cells stained strongly positive for the mature neural markers ßIII-tubulin (TuJ1) and glial fibrillary acidic protein (GFAP) (Fig. 3.5), and low expression of both GABAergic (GABA) and glutamatergic cells (vGlut1) (Fig. 3.6).

Flow cytometry analysis for these neural markers shows the differentiated Axol cells consist of higher percentage of neurons in pCaMKII-ChR2-YFP (~52%) than pSYN1-ChR2-YFP (~38%) and pEF1a-ChR2-GFP (~45%). Progenitor stem cells are still present in the culture with percentage between 38% - 46%. The neurons in each group expressed approximately 25% of TuJ1 and 45% of GFAP, respectively. The neurons also exhibited 10% of GABA and 70-80% of vGlut1 (Fig. 3.7c). Data obtained from flow cytometry in dot plot were attached in Appendix 7.

3.2.3 Optogenetic modified SY5Y cells expressed positive neural markers

Similar to human iPSC-derived neurons, transduced neuroblastoma (SY5Y) cells also expressed mature neural markers and ChR2 which is optically excitable in culture. The heterogeneous SY5Y cells exhibited positive staining of TuJ1 and vGlut2 with a lack of expression of GABA after differentiation (Fig. 3.8). The TuJ1-positive cells displayed normal neural branching and their proper nuclei suggesting that transduced SY5Y cells are non-degenerated (Fig. 3.9). Flow cytometry data revealed that approximately 10% of GABAergic and 15% of glutamategic cells present in pSYN1-ChR2-YFP regulated SY5Y cells, similar to pCaMKII-ChR2-YFP and pEF1a-ChR2-YFP (Fig. 3.10).

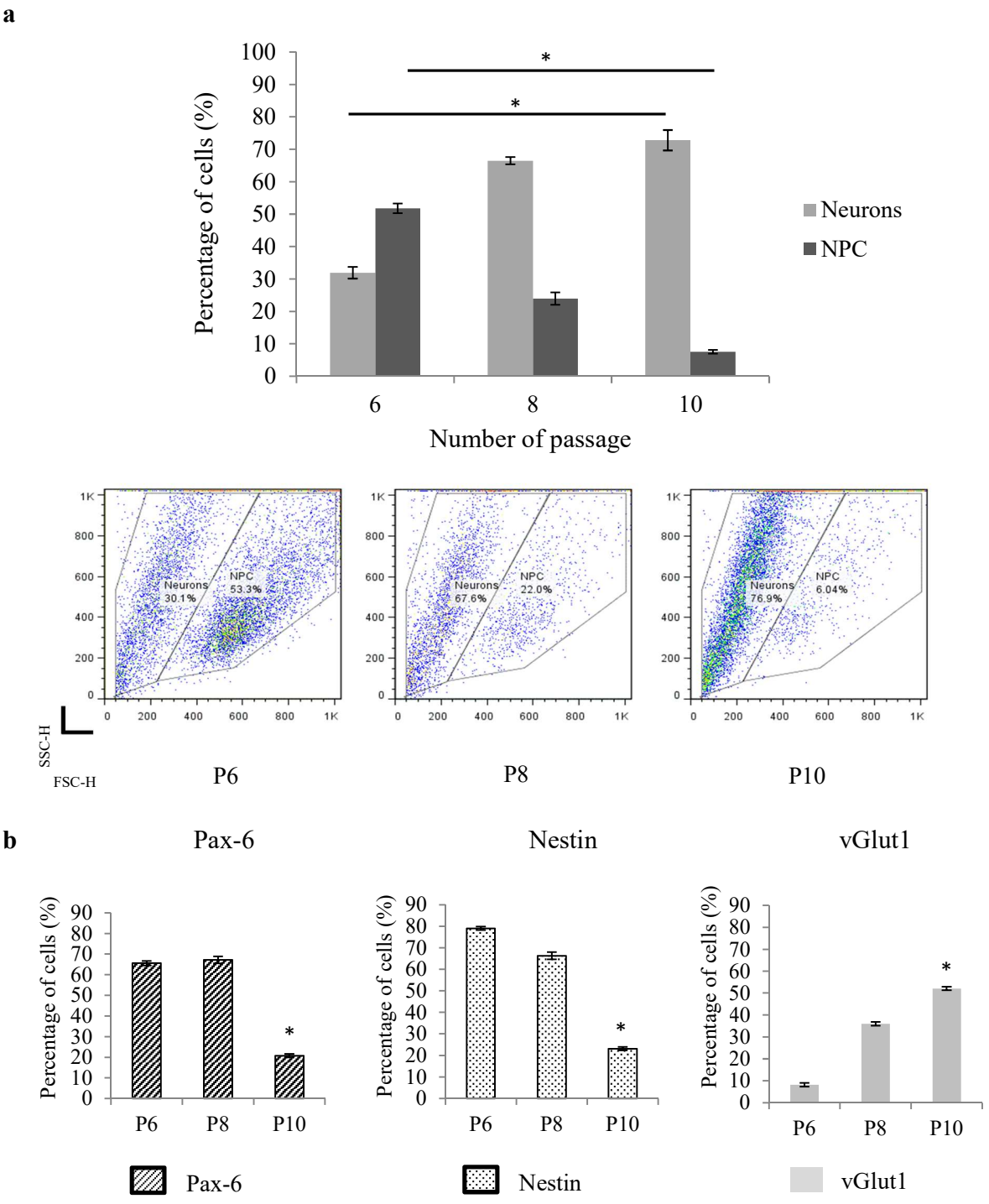

Figure 3.4: Maturation of neurons increased over passaging (P6-P10) in the culture of Axol cells.
(a) The heterogeneous Axol cells were harvested from different passages to detect their cell populations using flow cytometry (N=3). Dot plots represent the data in bar chart where cell populations toward left shift (smaller size) are neurons whilst towards right shift (larger size) indicated neural progenitor stem cells. (b) The cells were stained with progenitor stem cell markers (Pax-6 and Nestin) and neural marker (vGlut1) to further confirmed the increasing of neuronal maturation over passaging and culture (N=3). Unstained cells were used as a control and setting gate region. ANOVA test was used to determine significance. A *p-value below 0.05 was considered statistically significant. Error bars indicate standard deviation (±SD).

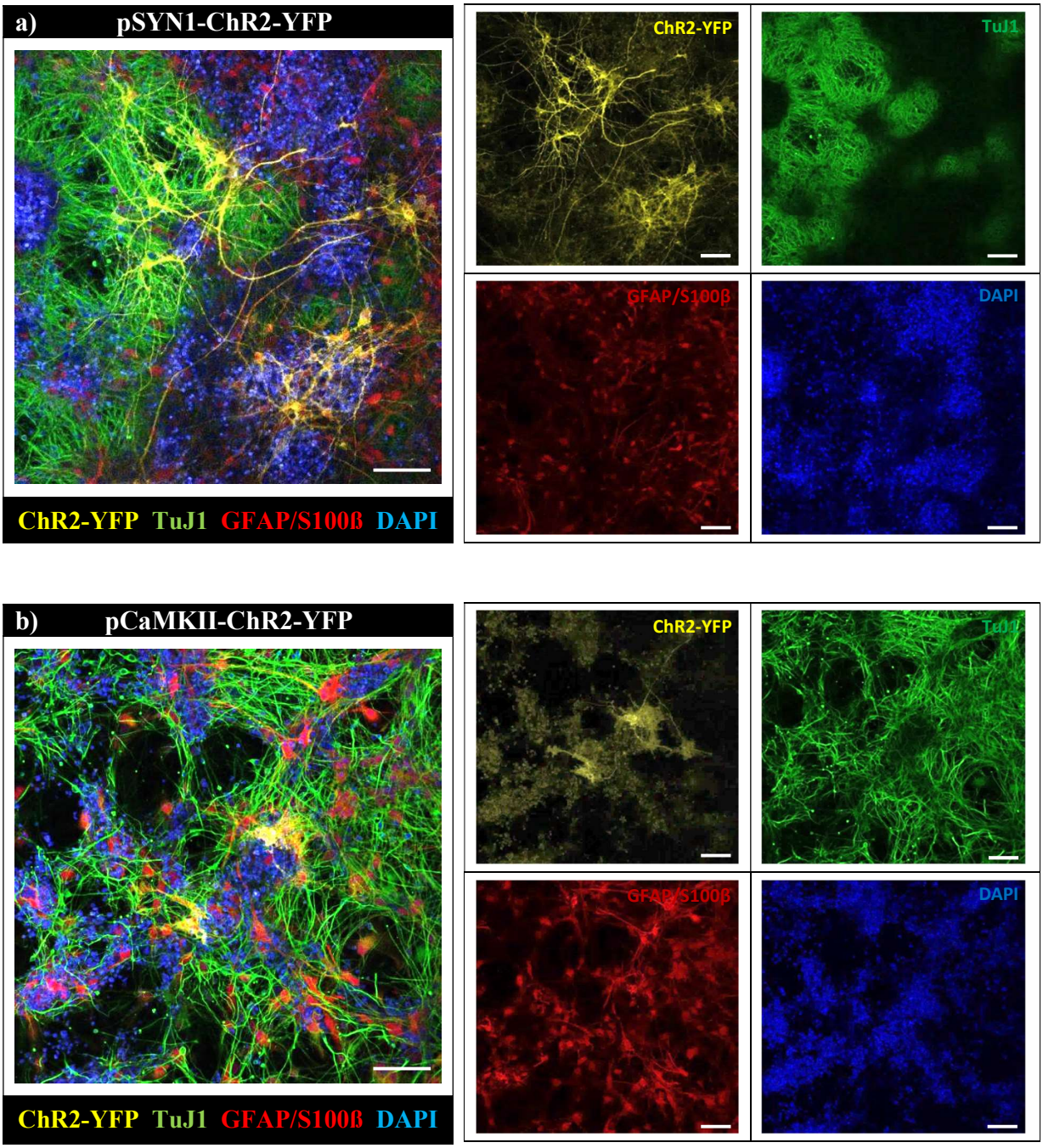

Figure 3.5: Immunofluorescent staining of human iPSC-derived neurons (Axol) demonstrates positive expression of TuJ1, GFAP/S100β and ChR2-YFP under the control of SYN1 and CaMKII promoter. Axol cells containing (a) pSYN1-ChR2-YFP and (b) pCaMKII-ChR2-YFP were cultured on a laminin coated 24-well, glass-bottom plate and matured in Axol differentiation and maintenance medium for 3–6 weeks. The cells were fixed, permeabilised and stained with neural markers TuJ1 (green) and astrocytes GFAP/S100ß (red) to identify the cell subtypes. ChR2-YFP was expressed in yellow whilst DAPI stained the nuclei blue. Fluorescence images were captured using confocal microscopy (Zeiss-LSM 710) and processed with ZEN light 2011 software. Scale bar: 50 µm.

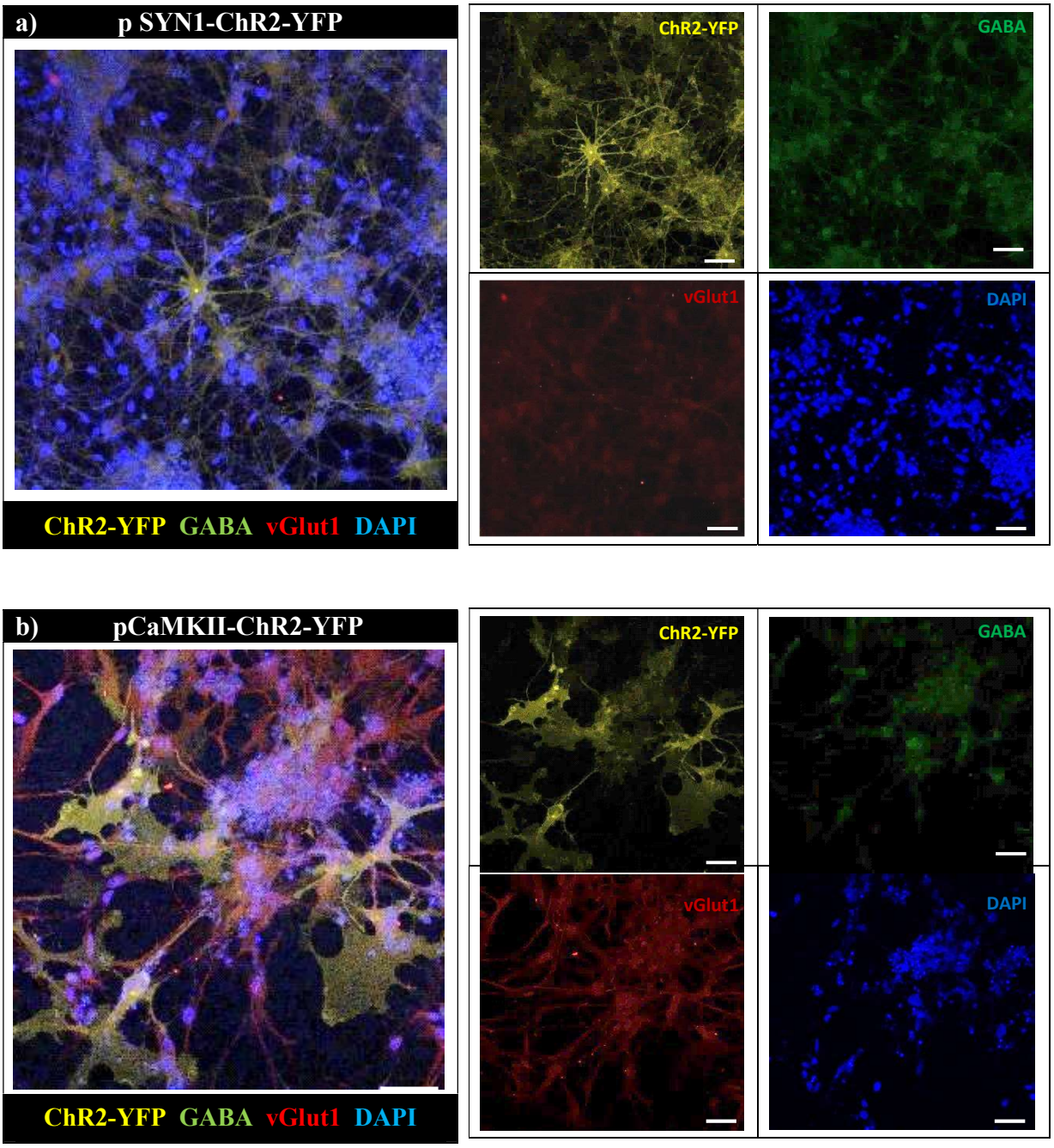

Figure 3.6: Phenotypic characterisation of human iPSC-derived neurons (Axol) demonstrates positive expression of GABA, vGlut1 and ChR2-YFP under the control of SYN1 and CaMKII promoter.
Axol cells containing (a) pSYN1-ChR2-YFP and (b) pCaMKII-ChR2-YFP were cultured on a laminin coated 24-well, glass-bottom plate and matured in Axol differentiation and maintenance medium for 3–6 weeks. The cells were fixed, permeabilised and stained with neural markers GABA (green) and vGlut1 (red) to identify the presence of inhibitory and excitatory neurons, repsectively. ChR2-YFP expressed in yellow whilst DAPI stained the nuclei blue. Fluorescence images were captured using confocal microscopy (Zeiss-LSM 710) and processed with ZEN light 2011 software. Scale bar: 50 µm.

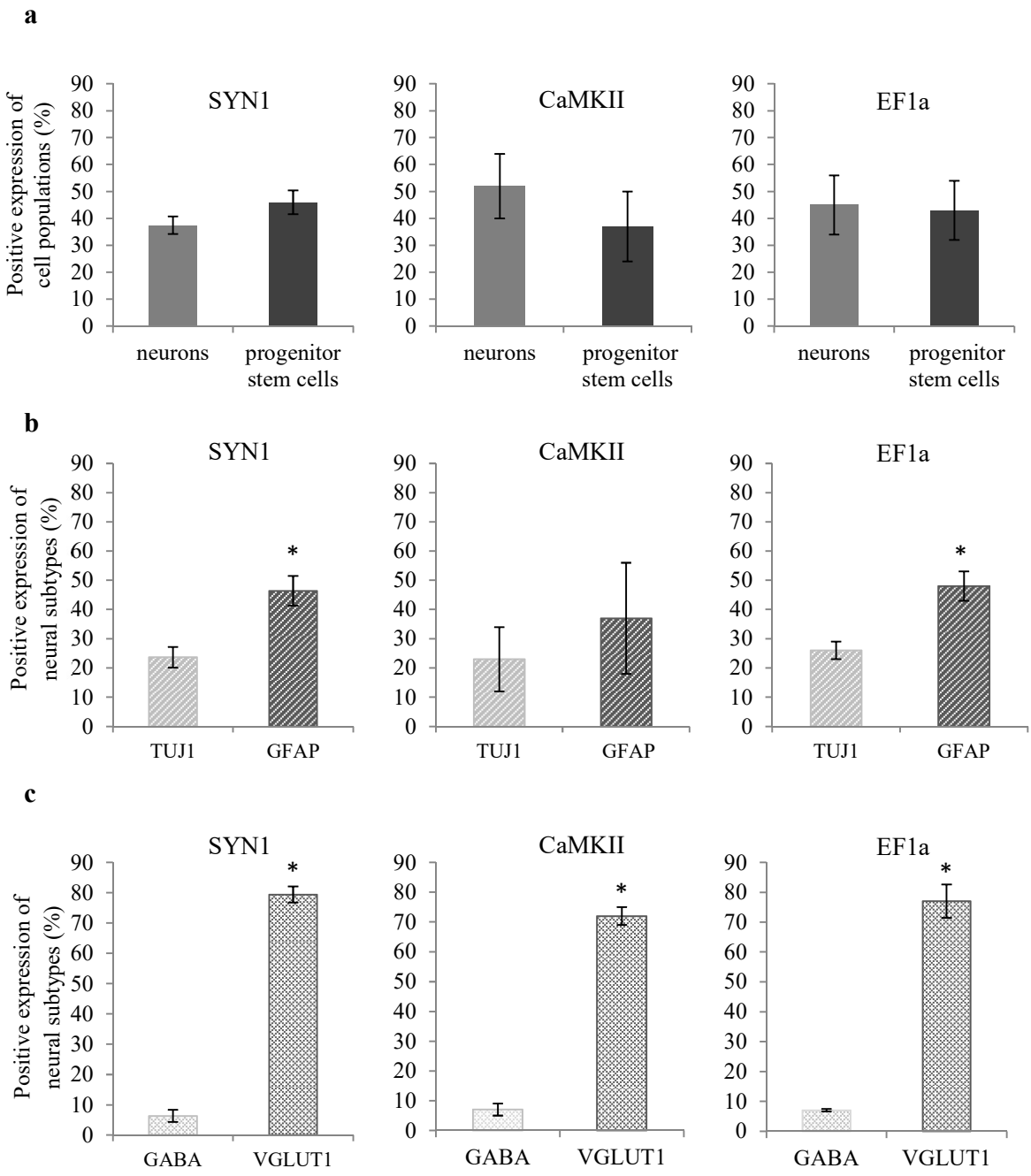

Figure 3.7: Flow cytometry analysis of human iPSC-derived neurons (Axol) to distinguish the heterogeneous cell population and the sub-classes of neurons.
(a) Mature neurons and progenitor stem cells are present in the transduced cells. The cells were trypsinised from a single well of culture plate, neutralised with culture medium, fixed, permeabilised and then analysed by flow cytometry. Unstained cells were used as a control as well as for setting gating region. (b) TuJ1 and GFAP positive cells are present in the mature neuron population. (c) GABA and vGlut1 indicated the presence of inhibitory and excitatory neurons in TuJ-1 positive population. Quantification is shown of at least three independent experimental repeats (N=3). Student's t-test was used to determine significance. A *p*-value below 0.05 was considered statistically significant; error bars indicate standard deviation (±SD).

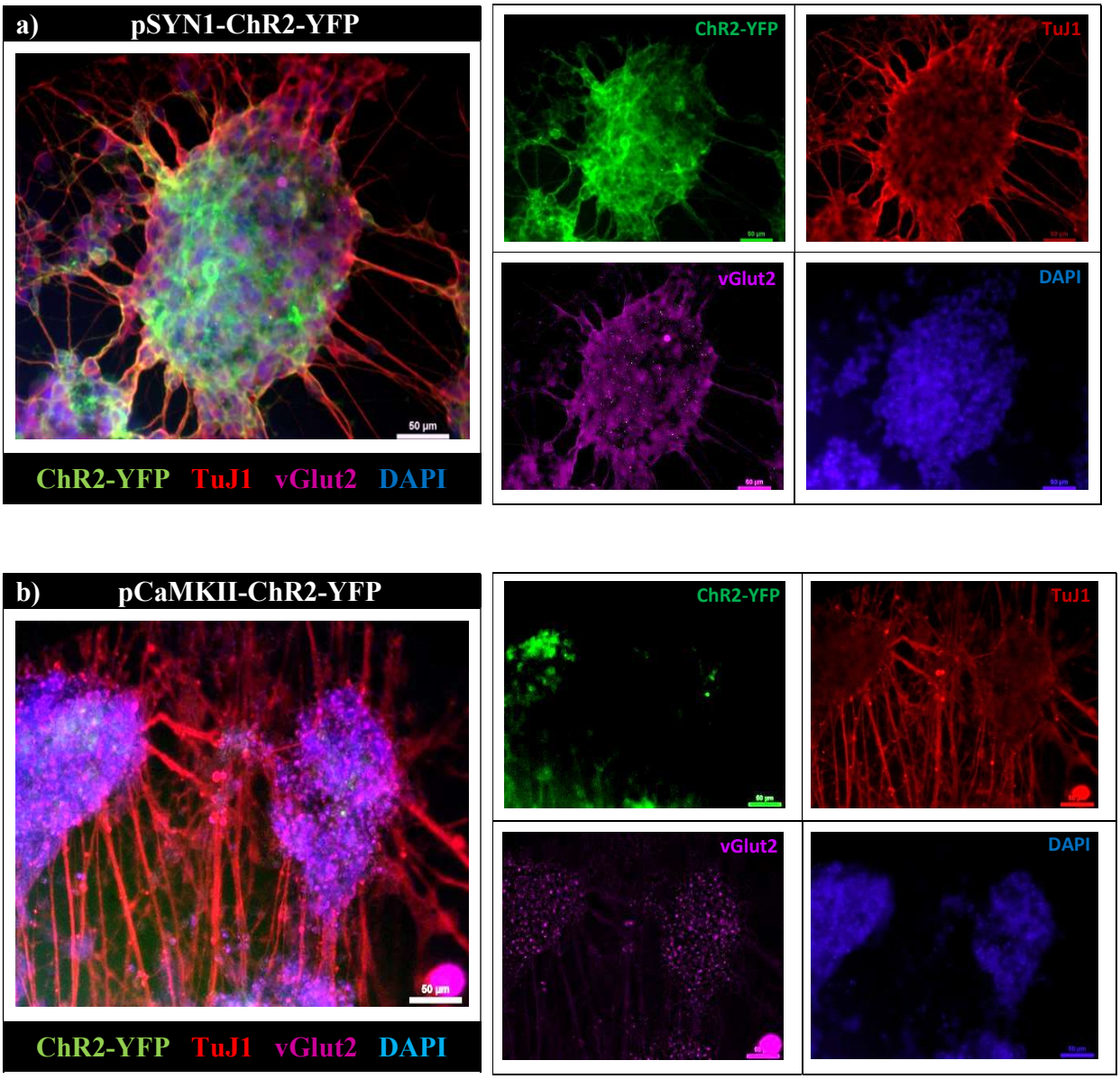

Figure 3.8: Immunofluorescent staining of human neuroblastoma cells (SY5Y) demonstrates positive expression of TuJ1, vGlut2 and ChR2-YFP under the control of SYN1 and CaMKII promoter.
SY5Y cells containing (a) pSYN1-ChR2-YFP and (b) pCaMKII-ChR2-YFP were cultured on a laminin coated 24-well, glass-bottom plate in the complete medium after differentiation. The cells were fixed, permeabilised and stained with neural markers, TuJ1 (red) and vGlut2 (magenta, dotted morphology) to identify the neural subtypes. ChR2-YFP was expressed in green whilst DAPI stained the nuclei blue. Fluorescence images were captured using confocal microscopy (Zeiss-LSM 710) and processed with ZEN light 2011 software. Scale bar: 50 µm.

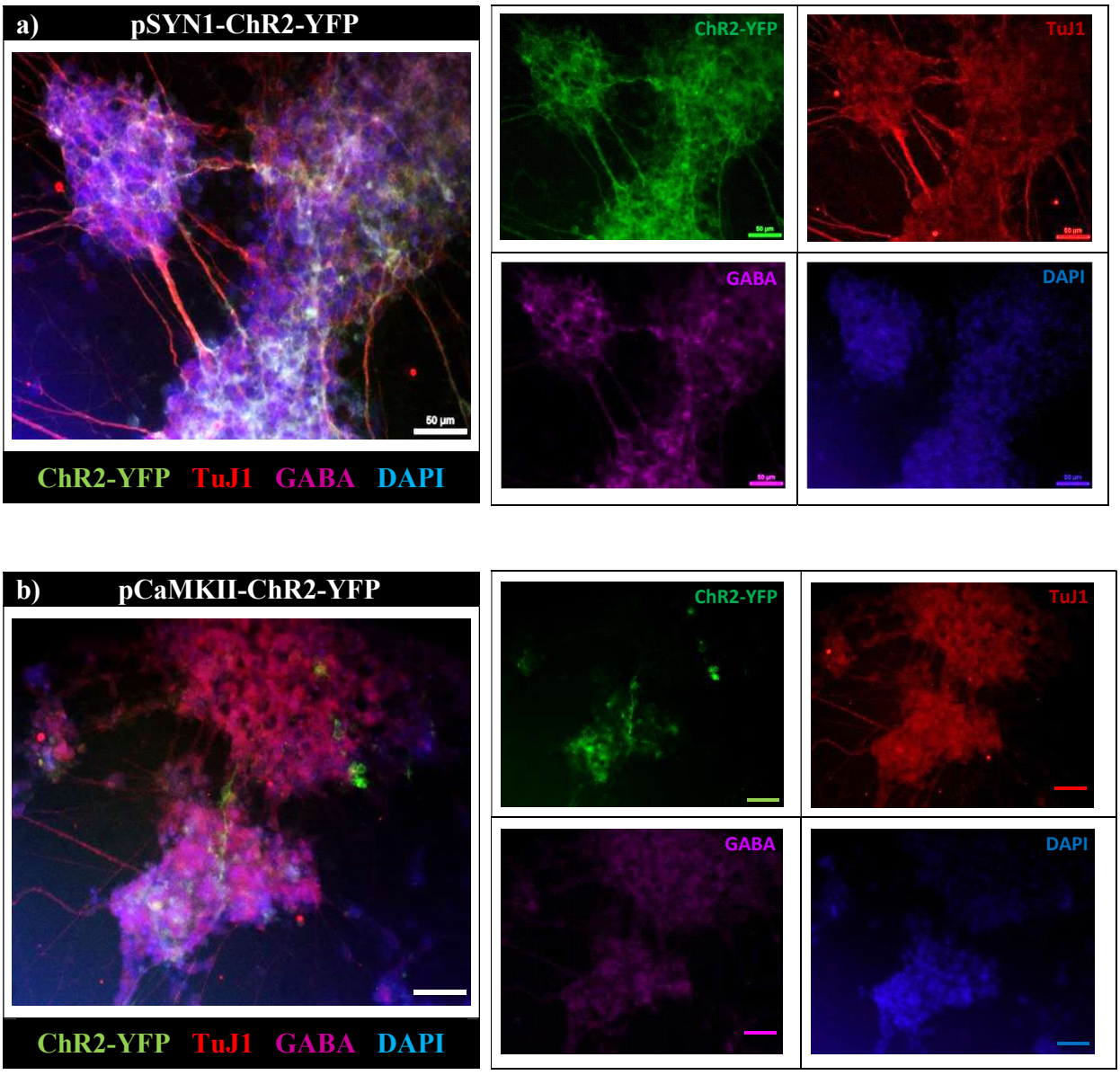

Figure 3.9: Phenotypic characterisation of human neuroblastoma cells (SY5Y) demonstrates low expression of GABA but strong expression of TuJ1, and ChR2-YFP positive was driven by SYN1 and CaMKII promoter.
SY5Y cells containing (a) pSYN1-ChR2-YFP and (b) pCaMKII-ChR2-YFP were cultured on laminin coated 24-well, glass-bottom plate in the complete neural culture medium. The cells were fixed, permeabilised and stained with neural markers TuJ1 (red) and GABA (magenta) to identify the presence of mature neurons GABAergic neurons). ChR2-YFP was expressed in green whilst DAPI stained the nuclei blue. Fluorescence images were captured using confocal microscopy (Zeiss-LSM 710) and processed with ZEN light 2011 software. Scale bar: 50 µm.

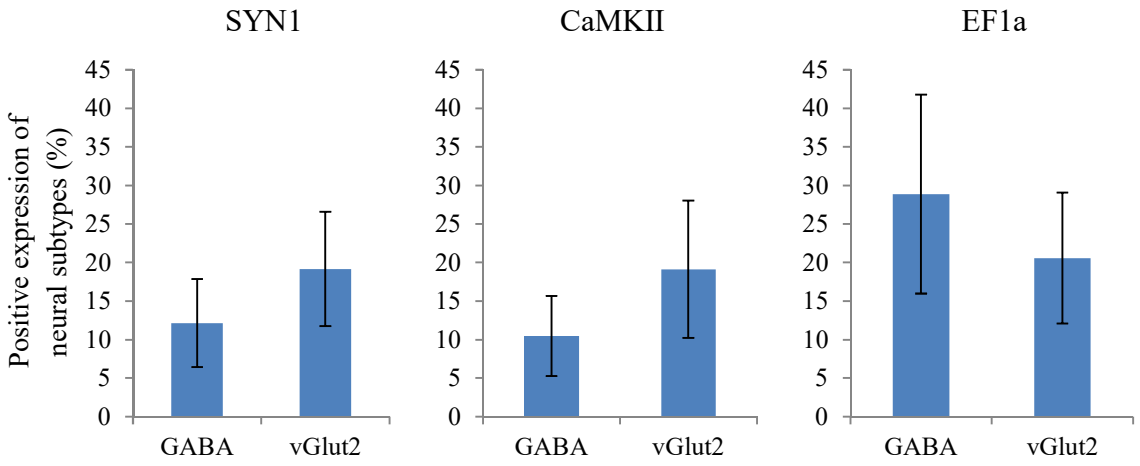

Figure 3.10: GABAergic and glutamatergic neurons are present in the transduced SY5Y cells with low percentage.

Flow cytometry analysis of human neuroblastoma cells (SY5Y) to quantify neuronal sub-classes. The cells were harvested from a single well of culture plate, neutralised with culture medium, fixed and permeabilised prior analysed with flow cytometry. Unstained cells were used as a control as well as for setting gating region. Quantification is shown of at least three independent experimental repeats (N=3). No significant of difference between GABA and vGlut2 positive cells found in transduced SY5Y. Student's t-test was used to determine significance. Error bars indicate standard deviation (±SD).

3.3 Discussion

Delivery of ChR2-YFP into neurons derived from human iPSCs (Axol) and neuroblastoma (SY5Y) cells was mediated by lentiviruses. Transduction at MOI-2 and MOI-1 (M2H2 and M1H1) followed by re-infection did not induce significant cell death but achieved high expression of ChR2. ChR2 was localised in the cell membrane and distributed along the neurites. Rapti et al. has compared the major viral vectors of AAV, adenoviruses and lentiviruses using different undifferentiated cells (hPSCs: hES2, H9, hiPS31.3, hiPS24.1) and differentiated cells (cardiomyocyte derivatives) [270]. Their findings agreed that lentiviral vectors transduced all cell types with moderate efficiency. Infection of hPSCs with AAVs resulted in cell death but high transduction efficiency was reported in differentiated cells. Conversely, adenoviral vectors were proven efficient in all cell types. Stroh et al. reported that reinfection with lentivirus (ChR2-EF1a) did not alter the gene expression profile. Their ChR2-ESC-derived neurons displayed strong ChR2-expression, mature neuronal morphology and positive expression of vGlut2 marker [271], parallel with the results demonstrated in our study using lentivirus transduction on ChR2-iPSC-derived neurons (Axol-13 and Axol-15 cell lines).

SY5Y cells demonstrated high viability and low cytotoxicity after lentiviral transduction, attributed to the cell line's robustness and rapid rate of recovery from cell stress. Cells expressed membrane bound ChR2-YFP when its expression was regulated by the SYN1 and EF1a promoters, however, far fewer cells expressing ChR2-YFP were observed under the control of CAMKII promoter. This suggests that CaMKII is weakly activated in SY5Y cells - as similarly reported by other researchers in *in vivo* studies (Fig. 3.3b-c) [267, 269]. In Axol culture, Ch2R-YFP expression driven by the SYN1 promoter was strongly expressed at 7 day-post-infection, whereas CaMKII promoter driven expression only significantly increased after 14 day-post-infection (Fig. 3.1b).

Several promoters have been tested *in vivo* by other research groups recently. For example, in rat cortical pyramidal neurons [272], the SYN1 promoter was reported to be the most efficient promoter for driving expression during the second postnatal week, whereas the CaMKII promoter was the strongest driver of expression from the third postnatal week [273]. These reports are in line with other findings, where the CaMKII promoter was found to drive expression later than the SYN1 promoter after transduction in both *in vitro* and *in vivo* investigations.

Following transduction, Axol neural progenitor cells were differentiated to distinct neuronal phenotypes with positive expression of neuron-specific tubulin (TuJ1) and astrocytes markers (S100B/GFAP) (Fig. 3.5). The mature neuronal subtypes, glutamatergic and GABAergic cells were observed, indicating the presence of excitatory and inhibitory neurons (Fig. 3.6). The mature cultures were found to contain a higher number of glutamatergic neurons (72-79%) and a lower number of GABAergic neurons (6-7%) (Fig.3.7c). Similar results supporting these findings have been reported by Yu et al. [274], where a human hippocampal neural population consisted of predominantly glutamatergic neurons (85%) together with a smaller proportion of GABAergic neurons (15%). The human cerebral cortex has been found to contain approximately 80% excitatory, glutamatergic neurons, thought to be generated by cortical stem and progenitor cells, and 20% GABAergic inhibitory interneurons, thought to migrate from outside of the cortex during development [235].

Transduced SY5Y cells showed positive expression for neural cytoskeletal tubulin, (TuJ1 – showing branching neurites), glutamatergic neurons (vGlut2 in dotted morphology), GABAergic neurons (GABA) and ChR2-YFP (Fig. 3.8 and 3.9). Approximately 10% of the differentiated SY5Y cells were GABAergic neurons and 20% were glutamatergic neurons with no significant differences observed between cell morphologies. The subpopulations and number of mature

neurons in the differentiated SY5Y cells were dependent on the treatment used to induce differentiation. For instance, sequential treatment of the SH-SY5Y human neuroblastoma cell line with retinoic acid (RA) and BDNF conducted by other researchers has yielded homogeneous populations of fully differentiated human neuron-like cells or mature neurons. The differentiated cells enter apoptotic cell death when BDNF is removed from the culture medium [245]. BDNF and NGF are known to act on specific tropomyosin receptor kinases [275] which activate intracellular kinase signalling cascades, making synergistic effects on downstream effectors to induce expression of neuro-specific proteins after differentiation.

In SY5Y cells, following differentiation, a number of neural cells could not be classified by glutamatergic or GABABergic protein markers. Accordingly, a subpopulation of the remaining cells could be dopaminergic neurons. As described by several other authors, when the differentiation protocol are started with RA treatment for 14 days or less [276], followed by the use of mitotic inhibitors to eliminate the proliferating subpopulation, the SY5Y cells elongate and exhibit branching that morphologically resembles primary rodent dopaminergic neurons [277]. Initial results suggest that ChR2 expression within these cells was driven by the pan-neuronal SYN1 promoter, but not by the CaMKII promoter, which is in line with the later finding in chapter 5 demonstrated highly active calcium transient of ChR2-positive SY5Y cells was driven by SYN1 promoter.

The experiments in this chapter have shown that lentiviruses mediate successful delivery of ChR2-YFP in neurons derived from human iPSCs and neuroblastoma cells. Efficient cell targeting using neural-specific promoters was achieved, however to produce high number of ChR2-positive cells may require more mature neurons in the culture. Characterisation of neuron cellular subtypes using immunofluorescent staining and flow cytometry analysis have further

confirmed the cell types in the culture such as the presence of inhibitory neurons (GABAergic cells), excitatory neurons (glutamatergic cells), astrocytes and progenitor stem cells. The neuronal functions of these optogenetically modified cells (e.g. whether they are responsive to the light stimulation) are unknown and therefore demand further investigation. Results in this chapter also led to the assessment and comparison of the two promoters, SYN1 and CaMKII. Their performance and responsive to light stimulation in generating neuronal activity upon illumination were reported in chapter 5.

Optogenetic targeting approach has been used for *in vivo* and *in vitro* study, but until now there is no application that uses neuron-specific promoters to generate *in-vitro* 3D neural culture model. In the next chapter, a 3D culture system was developed using modified alginate hydrogels to evaluate its potential in supporting cell survival and allowing neural networks to be light-stimulated.

4.0 Functionalised alginate hydrogel as a generic platform for 3D culture of hPSCs and specialised into neurons

Introduction:

The use of human pluripotent stem cells (hPSCs) in tissue engineering and regenerative medicine has become increasingly important due to its great potency. These cells reside in specialised microenvironments which regulate their self-renewal, long-term maintenance and differentiation [278, 279]. It has been reported that within the microenvironment, although cell-cell interaction and extrinsic factors are crucial, the role of extracellular matrix (ECM) cannot be neglected as it is critical to promote stem cell attachment and response to the surrounding cues [85, 280]. Thus studies of hPSC microenvironment and ECM appear to be of paramount importance.

The native ECM proteins such as collagen IV, laminin, fibronectin, entactin and perlecan [281] have been demonstrated to modulate pluripotency, proliferation and viability of hPSCs through the interaction with cell surface receptors known as integrins [282, 283]. For example, integrins $\alpha_5\beta_1$ and $\alpha_v\beta_3$ have been identified to recognise fibronectin and vitronectin which contain the key tripeptide sequence of RGD [100, 109]. The use of synthetic RGD peptides in 3D culture seems promising alternative to the above mentioned ECM proteins and the commonly used Matrigel [105]. In order to avoid batch-to-batch variation, eliminate undefined components and risk of pathogen transmission due to their derivation from human or animal tissue [284], peptide-functionalised biomaterials have been increasingly utilised to mimic the microenvironment of hPSCs. However, the development of specific matrix components in a defined culture condition is still a major challenge [107, 285, 286].

Hydrogels made of collagens and hyaluronic acid (HA) have been used for the culture of undifferentiated hPSCs as well as differentiation of mesenchymal stem cells (MSCs) [198] and

hESCs. However, alginate hydrogel is suitable for cell encapsulation and scale-up of hPSCs. This natural polymer is well-defined and tunable for modification to allow cell attachment and maintenance [212, 287]. The formation of alginate hydrogel involves reaction with divalent cations such as Ca^{2+}, Ba^{2+} and Sr^{2+}, it can be covalently modified with cell adhesion ligands (such as RGD-containing peptides), mediated by carbodiimide hydrochloride (EDC) chemistry in order to promote cell anchorage and matrix interaction (Fig. 4.1) [288]. The approach is stable and may results in high affinity cell recognition within the alginate microcapsule beads.

The presence of dying and dead cells can release chemokines that provoke undesired inflammatory or immune responses [289, 290]. Cell death could be further minimised using small-molecule inhibitors. Rho-associated protein kinase inhibitor (ROCKi), and caspase inhibitor (Z-VAD-FMK/ZVAD) have been reported to prevent apoptosis in the monolayer cultured cells successfully [148, 291]. However, their deployment in the 3D hydrogel system to increase the viability and long-term growth of hESCs has not been fully demonstrated. ROCKi has been shown in the literature to be responsible for regulating cell morphology and attachment by altering actin cytoskeleton [147, 148, 292]. ROCKi inhibits actin-myosin contraction to avoid membrane blebbing by reducing the phosphorylation of myosin light chain (MLC) [293, 294]. Meanwhile, synthetic peptide ZVAD is a predominantly caspase-1 and -3 inhibitor that irreversibly binds to the catalytic site of caspase proteases which play important roles in the effector event during apoptosis [261].

This chapter is focused on the development of a generic 3D culture platform which mimics the native microenvironment to support the growth of hESCs/iPSCs and specialised into neurons derived from these cells. RGD-alginate hydrogels incorporated with ROCKi/ZVAD were evaluated in this study (model refer to Fig. 4.1c) on cell growth and viability. Due to its biocompatibility and chemically versatile, alginates are suitable for cGMP manufacture. The

alginate hydrogels in the present study were fabricated and characterised to fulfill quality requirement such as physical properties including adequate bead size, spherical morphology, and swelling and degradation profiles. Since alginate alone without modification may unable to provide optimal microenvironment for cell adhesion particularly hPSCs, therefore the effects of peptide conjugation, protein incorporation and the ability of ROCKi/ZVAD to support cell viability in the 3D culture system were assessed.

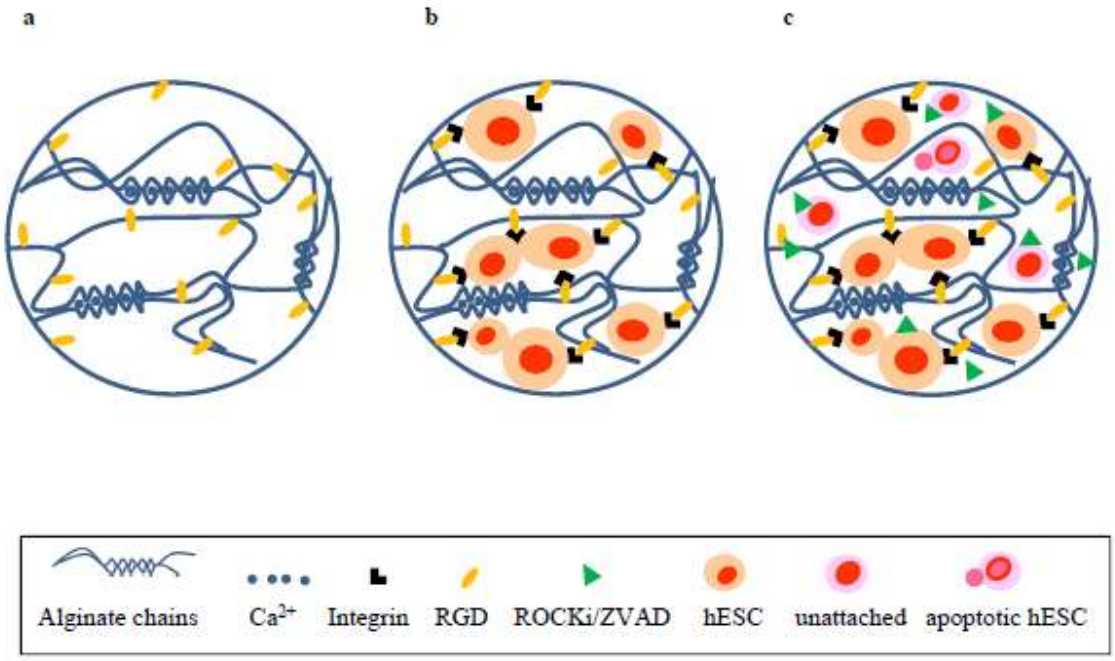

Figure 4.1: Schematic of functionalised-alginate bead and the interactions of cell-hydrogel in different conditions

(a) Alginate chains crosslink with calcium ions to form an 'egg-box' model and covalently modified with RGD peptides. (b) Encapsulation of hPSCs in RGD-modified alginate bead, integrins intercede cell adhesion to RGD sequence in the matrix. (c) Small molecule ROCKi is deployed to treat unattached single cells; alternatively, ZVAD is entrapped within the RGD-modified alginate to block the apoptosis pathway, allowing encapsulated cells to remain viable.

4.1 Fabrication factors alter physical properties of alginate hydrogel

4.1.1 Concentrations and flow rates regulate the bead diameter

Alginate beads were optimised to produce suitable bead diameter and morphology for embryonic stem cell culture. Diameters ranging from approximately 700 - 2500 µm were obtained from alginate derived from high guluronic acid or G content (UP-MVG) (Fig. 4.2). Bead diameter was adjusted by changing alginate concentrations and flow rates. A significant correlation between the two parameters was identified: the higher the flow rate, the smaller the bead diameter. The bead diameter increased constantly and proportionally to the concentration at lower flow rates (2 and 2.5 ml/min). The data indicated that the highest flow rate set at 3 ml/min in the study plays a critical role in reducing the bead diameter in all concentrations. However, the bead morphology and satellite fraction content were modulated by the concentration. The beads produced rounder shapes at higher concentrations than lower concentrations, the formation of satellites was only found at 1.2% (Fig. 4.3).

Small bead with less than 1000 µm is favourable for decreasing diffusion distance and for increasing surface-to-volume ratio. Therefore, alginate derived from 1.8% high G content (UP-MVG) at a flow rate of 3 ml/min with average diameter 800 µm was identified to satisfy the quality requirements: bead integrity, size, spherical morphology and with no presence of satellite fraction.

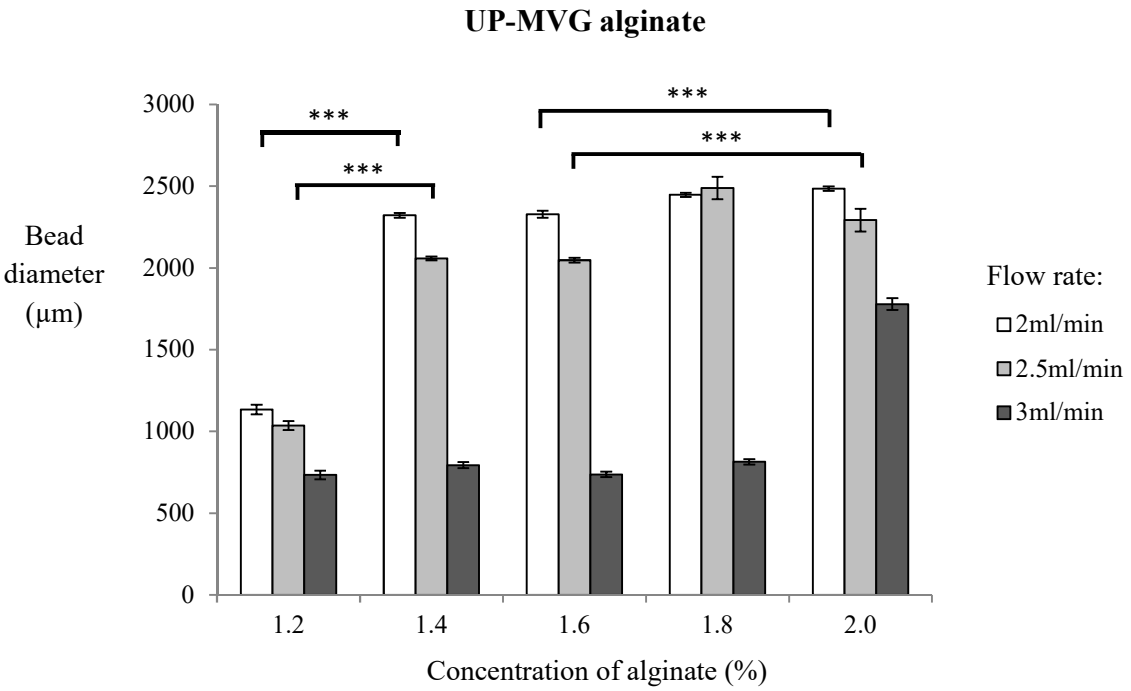

Figure 4.2: The effect of alginate concentration (%) and flow rate (ml/min) on the diameter of beads derived from different types of alginate (UP-MVG, n=50).

The alginate beads achieved smallest size at the highest flow rate (3 ml/min) in the concentrations of 1.2-1.8%. The study was performed in three independent experiments. Significance was tested by two-way ANOVA *** = $p<0.001$; error bars denote standard error of the mean (±SEM).

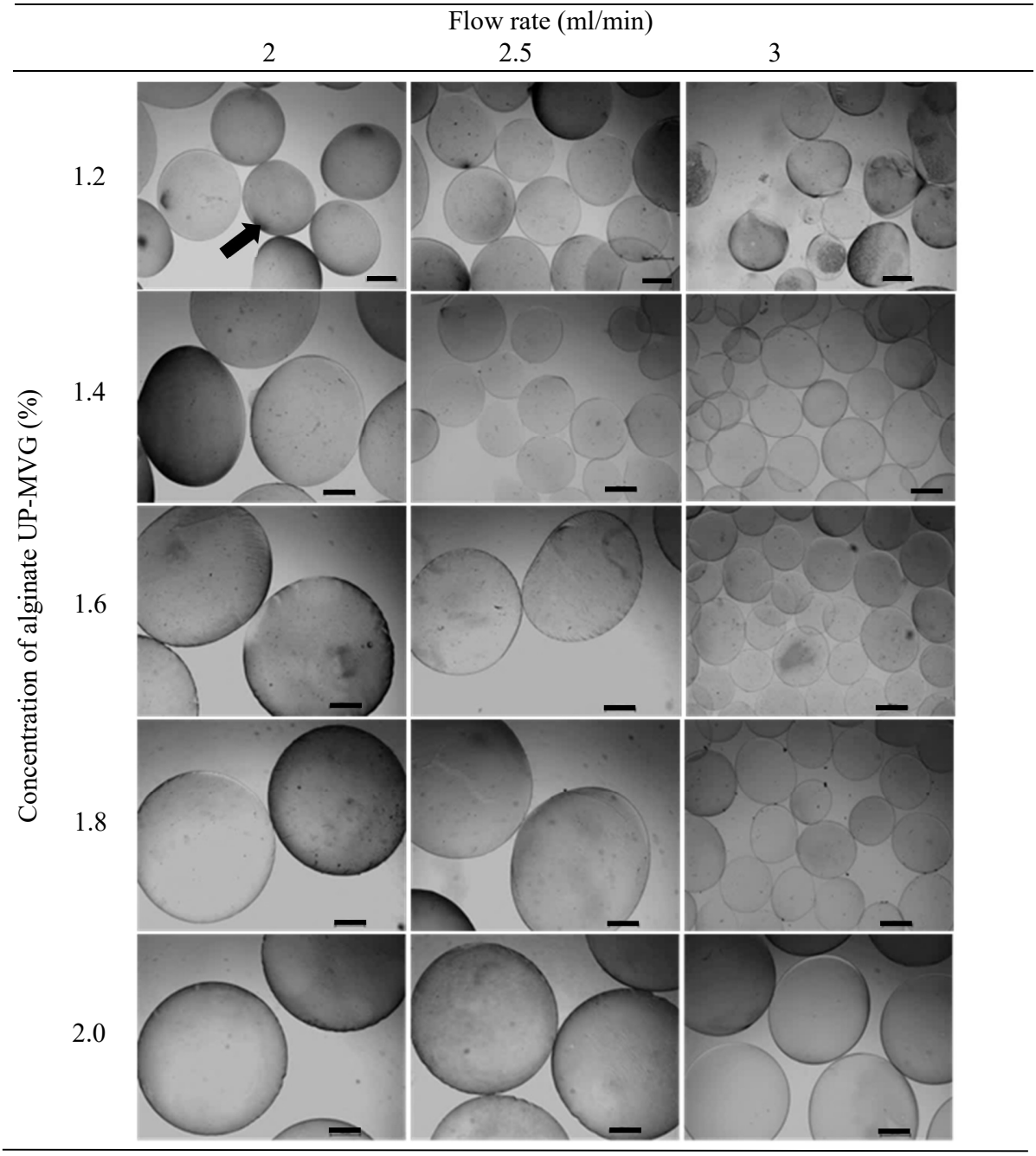

Figure 4.3: Physical morphology of UP-MVG alginate beads synthesised at different concentrations of alginate and flow rates.

Concentrations of 1.2% – 2.0% alginates formed smaller beads at flow rate 3 ml/min. Formation of satellite fraction (arrow) appeared at the lowest concentration of 1.2%. Figure shows representative images depicting the entire population of alginate beads (n=15) under a fluorescence microscope (Nikon Eclipse T_i-E, Japan). Scale bar: 500 µm.

4.1.2 Swelling and *in vitro* degradation profiles

In order to support longer period of cell culture, swelling and *in vitro* degradation profiles of alginate hydrogel are important to reveal the bead integrity and the effect of incubation on the physical properties. The swelling properties of alginate hydrogels were examined by measuring the change in hydrogel weight during incubation under physiological conditions (in a PBS solution, pH 7.4 at 37 °C). As observed, 1.8% alginate beads show a higher swelling ratio than 1.2% and RGD functionalised alginate, undergoing a weight increase until day 3 before decreasing (Fig. 4.4a). This behavior was anticipated as hydrogels are able to swell in aqueous solutions [295, 296]. The longer swelling period and the higher ratio achieved by 1.8% alginate was attributed to the higher polymer concentration [297-299]. It is noticeable that 1.2% alginate and RGD alginate possessed a more constant swelling profile; the swelling ratio increased from day 1-3, decreased and reached equilibrium at day 14.

The *in vitro* degradation profile of alginate was assessed using the same buffer solution as the swelling test. The highest weight loss is recorded on day 1 for 1.2% alginate but 1.8% alginate remained lower and constant between 3 - 5% of weight loss throughout the period of observation (Fig. 4.4b). The degradation of 1.2% alginate was greater than that of 1.8% alginate and RGD alginate at day 1 before decreasing due to the lower polymer concentration which formed a less rigid polymeric network structure, subsequently the bead size reduced and dissolved within 14 days. However, 1.8% alginate and RGD alginate possessed higher integrity and maintained their bead morphology which is required in long-term culture and differentiation.

a

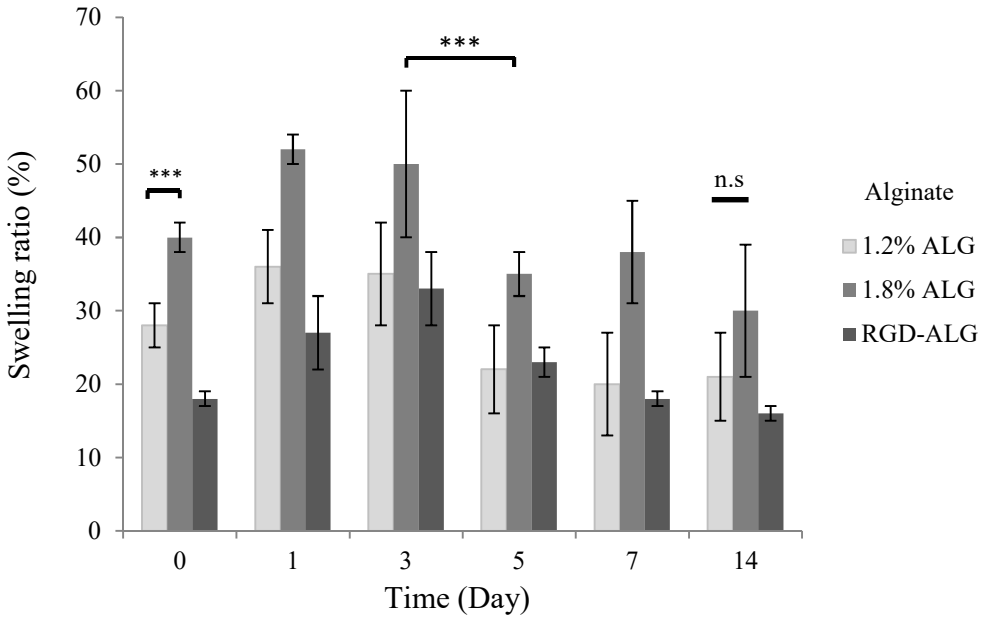

b

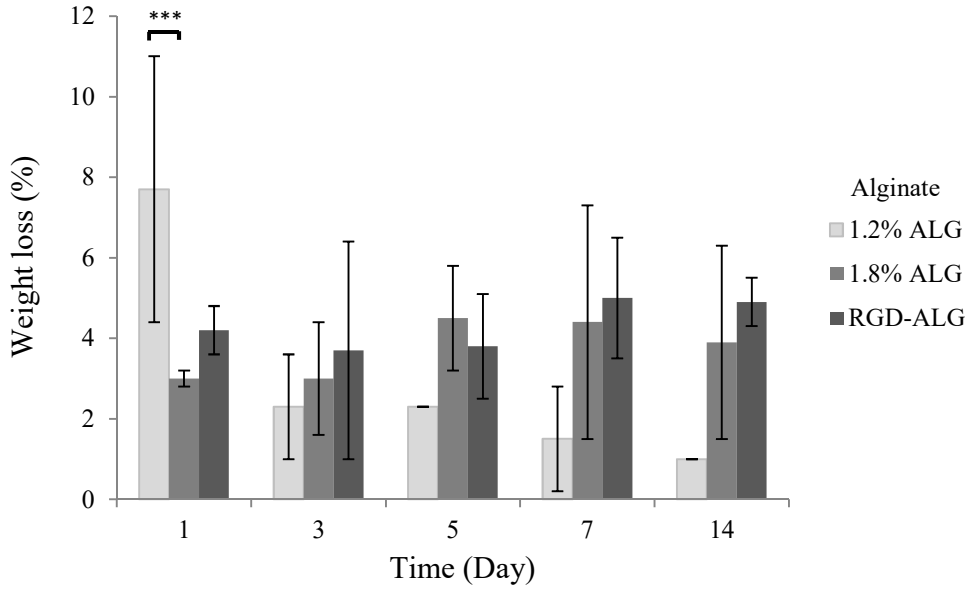

Figure 4.4: Swelling and *in vitro* degradation profile of 1.2 and 1.8 (w/v%) of alginate (UP-MVG).

(a) Higher swelling properties were demonstrated by 1.8% alginate than 1.2% and RGD-ALG at different time courses, all reached equilibrium on day-14 of incubation. (b) Alginate at 1.2% showed significant weight loss compared to 1.8% on day-1 of the study. Alginate beads at 1.8% and RGD-ALG are more consistent whilst 1.2% alginate demonstrated highest weight loss on day-1 which may lead to bead de-polymerisation throughout the incubation period, (n=3); error bars represent standard deviation (±SD).

4.1.3 Protein diffusion in alginate depends on the size and concentration of protein

Further characterisation of the alginate beads after functionalisation with proteins allows an estimation of protein amount that is required for incorporation. For example, entrapped BSA protein (Mw 66 kDa, r_s=3.6 nm), a middle size of solute was gradually dispersed into the surrounding in all concentrations. After 7 days of incubation, about 40-50% of incorporated BSA (5 – 80 µg/ml) still retained within the alginate beads (Fig. 4.5a). The results showed that the alginate outer layer is permeable, and could enable consistent mass transfer and exchange of gas and nutrients. Figure 4.5b reveals that low concentration of LN (Mw 850 kDa, with 3 identical short arm = 37 nm and 1 long arm = 75 nm in cruci-shape structure) at 5 and 10 µg/ml remained at approximately 1.5 and 4 µg/ml, respectively after 24 hours and completely diffused to the medium thereafter. On the contrary, 20, 40 and 80 µg/ml of incorporated LN were retained at approximately 5.4, 12.9 and 9.3 µg/ml in the alginate on day 7 of the study. The 20 µg/ml or higher concentrations of LN displayed a slow diffusion profile than lower concentrations, and hence 20 µg/ml was identified to be sufficient for functional conjugation. The large cruci-shape LN may unable to be re-uptake by the alginate hydrogel after diffused into the surrounding medium. Moreover, its diffusion constant rate is higher than BSA that explains lower amount of LN than BSA remained in the beads on day 7.

a

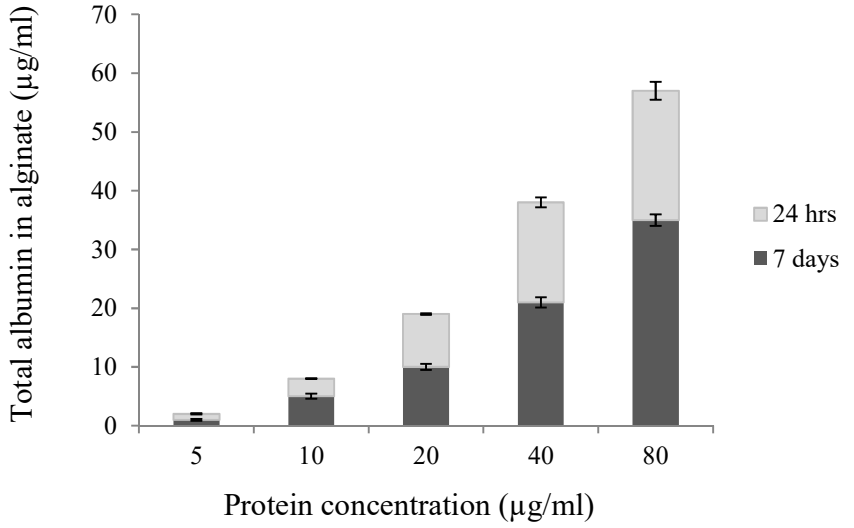

b

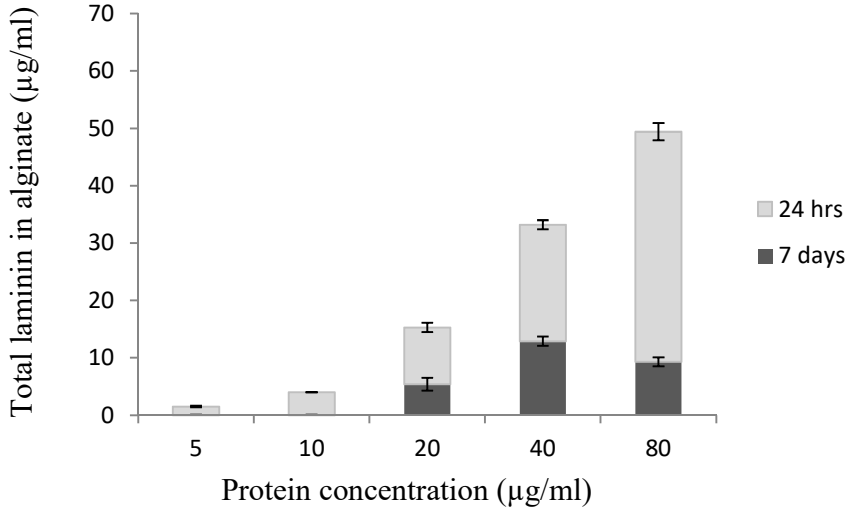

Figure 4.5: Total (a) bovine serum albumin (BSA) and (b) laminin (LN) detected within the alginate beads by comparing different concentrations used for alginate incorporation.

(a) After 7 days of incubation, approximately 50-60% of the entrapped BSA diffused into the surrounding medium. (b) Concentrations of LN at 5 and 10 ug/ml were found to diffuse completely from the alginate after 7 days of incubation. A minimum 20 µg/ml of LN is retained within the alginate for approximately 5.4%, (n=3). The alginate beads were encapsulated with BSA and LN at different concentrations (5, 10, 20, 40 and 80 ug/ml), incubated in the PBS at 37°C and removed from the buffer on day 1 and 7 for advance protein assay analysis (ADV01).

4.2 RGD functionalised alginate supports cell growth and survival

4.2.1 Encapsulated cells (hESCs and astrocytes) show high viability

The alginate hydrogels were functionalised with RGD peptide and their potential to promote human embryonic stem cells (hESCs) viability as well as *in vitro* biocompatibility were tested with 3D culture of hESCs. The growth of hESCs is very sensitive to the microenvironment and changes of the niche [300]. RGD-alginate appeared to support higher viability of hESCs (HUES-2) when compared to unmodified alginate. Cells were initially encapsulated within alginate at a density of 2×10^6 cells/ml and the total viable cells were measured by live-dead cell staining along the time course. Cell viability of HUES-2 in RGD-alginate were significantly increased ($p < 0.01$) on day 14 when compared to unmodified alginate and to the early stage (day 3) of 3D culture (Fig. 4.6). In contrast, HUES-2 in unmodified alginate decreased significantly ($p < 0.01$) and reached the lowest viability on day 14. The results indicated that conjugated RGD peptide enhanced HUES-2 attachment and viability in 3D alginate beads. A control group using glial cells (astrocytes) in unmodified alginate as a different cell type was included in this study. The viability of astrocytes increased and remained high throughout the culture period, allowing formation of distinct aggregates within the alginate beads (Fig. 4.7). Alginate hydrogel was therefore confirmed as non-toxic to brain cells, astrocytes [286, 301]; however the unmodified alginate was unable to support hESCs which presumably required a more stringent microenvironment to survive.

a

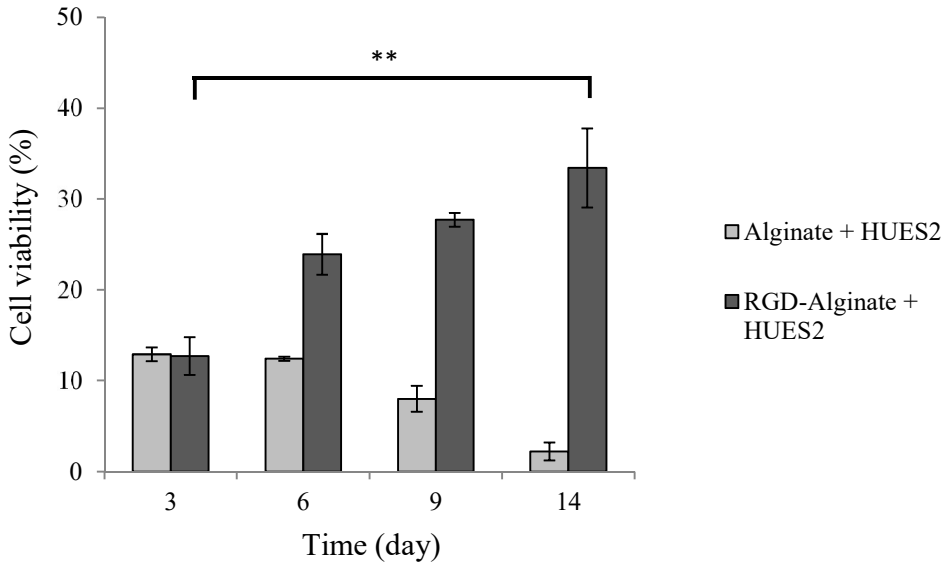

b

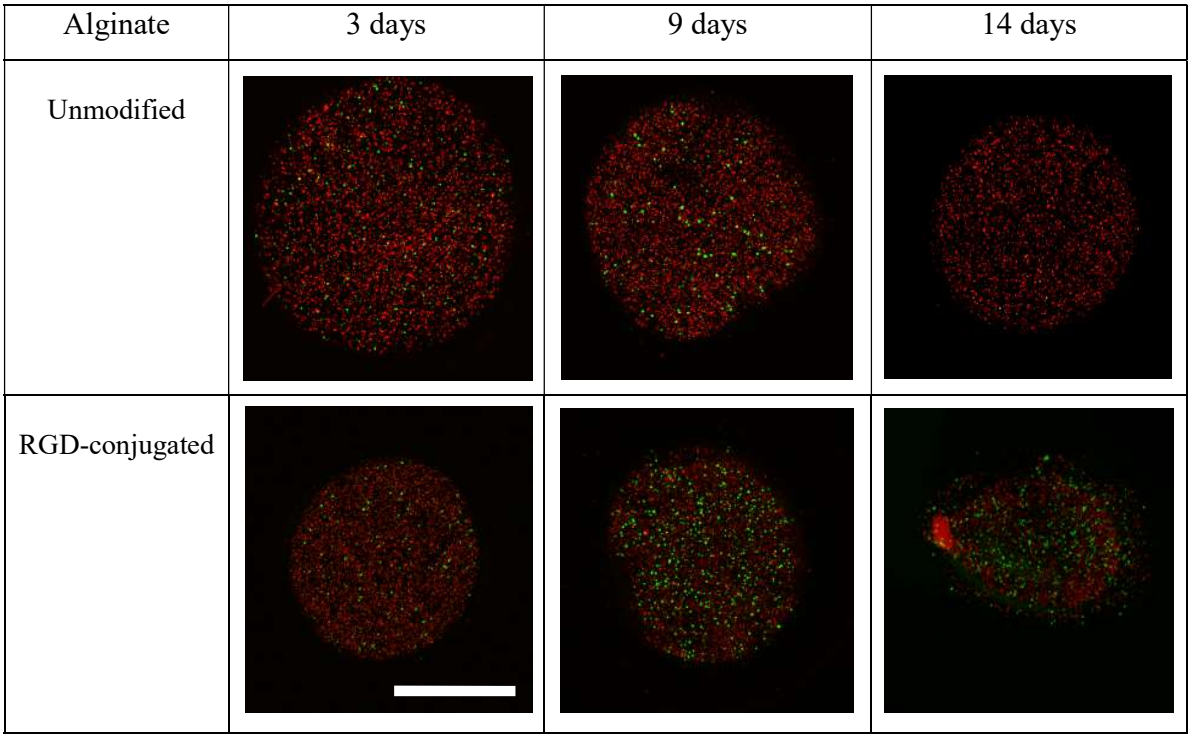

Figure 4.6: 3D culture of hESCs in RGD-alginate show higher viability than unmodified alginate.
RGD-alginate beads support cell viability of HUES-2, (n=3). Error bars represent standard deviation (±SD). (b) Confocal images revealed an even distribution of hESCs within RGD-alginate beads and the viable cells appeared in very small aggregates. Calcein-AM stained for live cells (green); propidium iodide, PI stained for dead cells (red). Images were captured using confocal microscopy (Zeiss-LSM 710) and processed with ZEN light 2011 software. Scale bar: 500 µm.

a

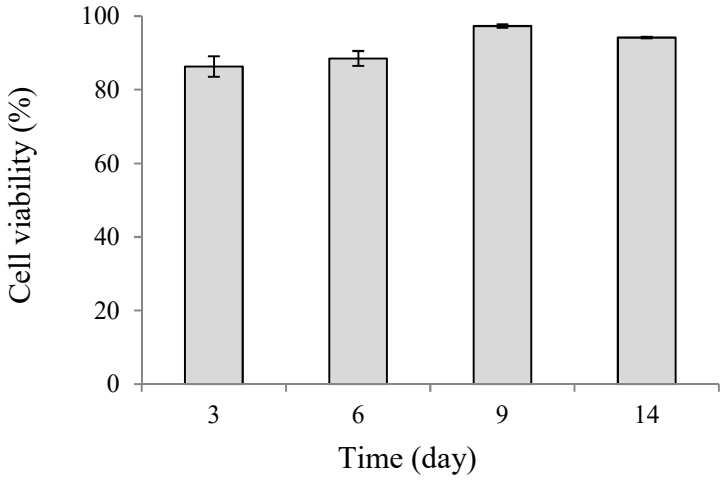

b

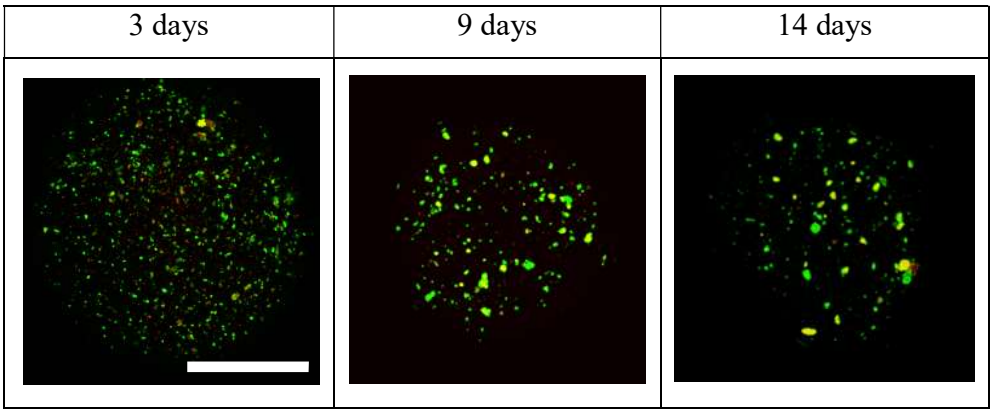

Figure 4.7: 3D culture of glial cells (astrocytes) in unmodified alginate hydrogels demonstrates high cell viability.

(a) The viability of astrocytes in the unmodified alginate system increased from 86% to 97%. (n=3). Error bars denote standard deviation (±SD). (b) Confocal images revealed uniform distribution of astrocytes within the alginate beads which formed in aggregates when time progressed. Calcein-AM stained for live cells (green); propidium iodide, PI stained for dead cells (red). Images were captured using confocal microscopy (Zeiss-LSM 710) and processed with ZEN light 2011 software. Scale bar: 500 µm.

4.2.2 Cell death in 3D culture can be rescued by small molecules

Cell death in 3D culture system may cause by apoptosis and/or necrosis. Efforts to block the apoptosis pathways have been shown in monolayer cultures in order to increase cell viability. Therefore, two type of small molecules ZVAD (inhibit caspase 3 and 7 of apoptotic pathway) and ROCKi, Y-27632 (inhibit rho-associated protein kinase pathway) were applied in this study to prevent cell death. Apart from cell viability, caspase 3 activity (as a measure for apoptosis) in identical cells–RGD-alginate constructs with the incorporation of small molecules was evaluated. In the presence of ZVAD alone, a high proportion of HUES-2 released from the beads was found viable (77.8%) with a low cytotoxic and apoptotic signal (2.6%), whilst approximately 14.7% of cells showed necrosis (Fig. 4.8). However, standard treatment using ROCKi alone supported cell viability up to 54.1% in alginate beads, and demonstrated a high number of dead cells (3% apoptotic cell and 41.2% of necrotic cells). Previous *in vitro* studies involving ROCKi (Y-27632) at 10 μM has been demonstrated to strongly inhibit other kinases such as protein kinase C-related kinase 2 (PRK2), mitogen-, stress-activated protein kinase-1 (MSK1), leucine-rich repeat protein kinase-2 (LRRK2) and MAPK-interacting protein kinases-1 (MNK1), these multiple inhibitions at a same time might explain the decrease in the number of viable cells [302, 303].

Dead cells may attribute to cell disruption due to mechanical pressure and enzymatically dissolving alginate beads in the process of cell de-capsulation. Surprisingly, the combination of ZVAD and ROCKi was found to induce higher cell death (53.6%) than single treatment although the number of apoptotic cells was recorded as low as approximately 2%. The combination of these two inhibitors may not achieve the expectation to increase cell survival because the effect of small molecules and their combination is concentration-dependent.

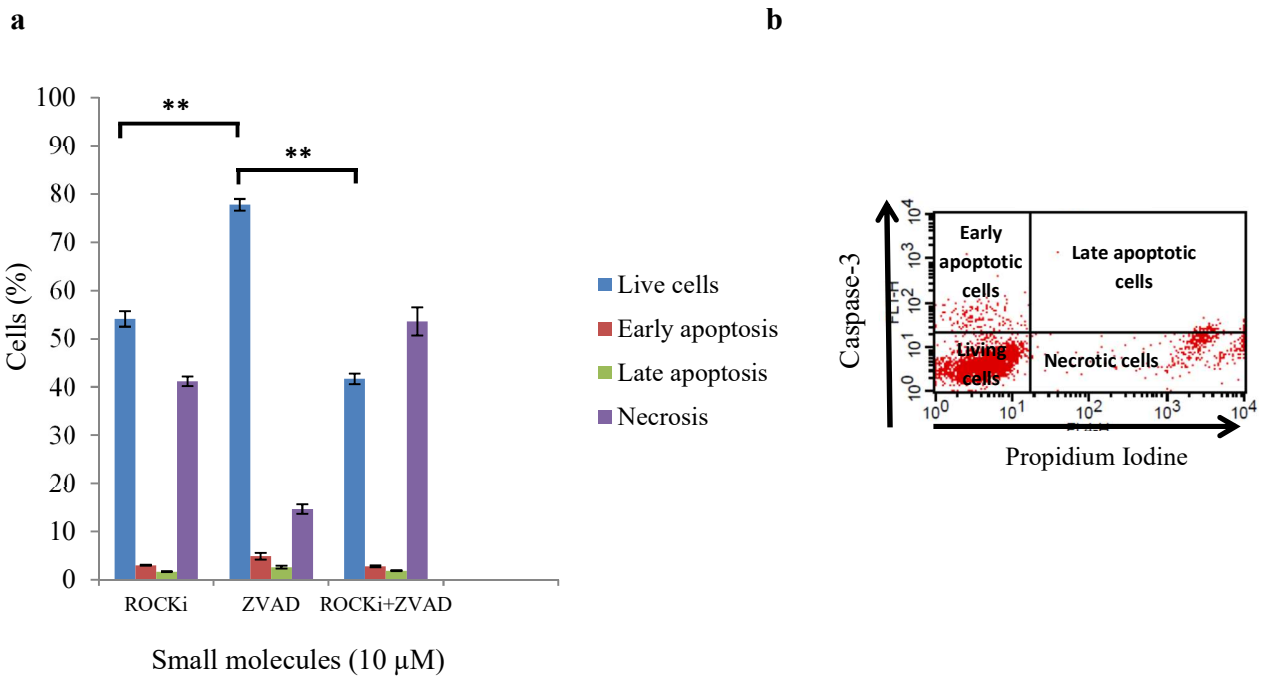

Figure 4.8: Rescue encapsulated hESCs from death using small molecules ROCKi and ZVAD.

The cells show high viability with less dead cells (apoptotic and necrotic cells) in ZVAD treatment. (a) ROCKi (control), ZVAD and ZVAD + ROCKi were used to treat the encapsulated cells in 3D RGD-alginate after being dissociated from 2D culture. Final concentration of each inhibitor is 10 uM in the RGD-alginate hydrogel (n=3), and the significance was tested by two-way ANOVA, **=$p<0.01$. Error bars denote standard deviation (±SD). (b) Flow cytometry analysis of hESCs after being treated with small molecules, de-capsulated from RGD-alginate and stained with caspase-3 and PI, was displayed in a dot plot. The quadrant shows populations of cells in percentage, and the results were presented in a bar chart in figure 4.9a (n=3).

4.3 3D culture systems were developed for neurons

4.3.1 Cell viability increased in 3D culture but decreased in longer culture period

Despite the use of alginate beads in this study, several 3D systems were developed aimed at the culture of neurons. Channel-alginate (Ch-Alg) and microcarrier-alginate (Mc-Alg) systems were seeded with neuroblastoma (SY5Y) including a 2D culture on alginate surface as a control. These systems may permit neuronal network development and extension as well as to support cell viability. SY5Y cells showed high viability in Ch-Alg, Mc-Alg and Alg beads on day 1, and the cell viability remained 14 times higher than initial seeding density up to day 3.

Results show that Ch-Alg supports cell viability and proliferation in the culture longer than other groups (up to 7 days) before decreasing as observed on day 14 (Fig. 4.9a). Live-dead cell staining and IMARIS software further revealed the localisation of live/dead cells within the systems (Fig. 4.9b). Ch-Alg supports dense and even cell attachment whilst Mc-Alg had higher dead cells located in the center of the construct. In alginate beads, cell viability of encapsulated SY5Y cells gradually decreased from day 1 to day 14, all viable and dead cells are distributed uniformly within the beads (Fig. 4.10). Bright field and fluorescence images of the cells in these 3D culture systems were attached in Appendix 8. Results suggest that Ch-Alg and bead systems may suitable for the culture of neurons derived from hPSCs, allowing neurite extension and permit light penetration for stimulation on the optogenetically modified cells

a

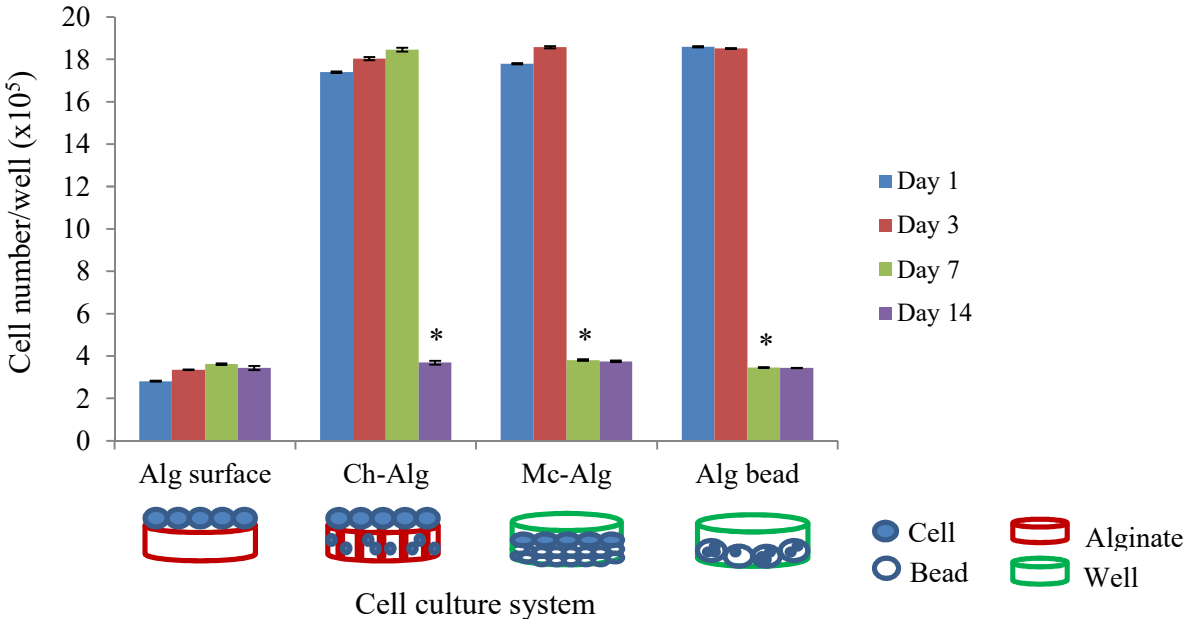

b

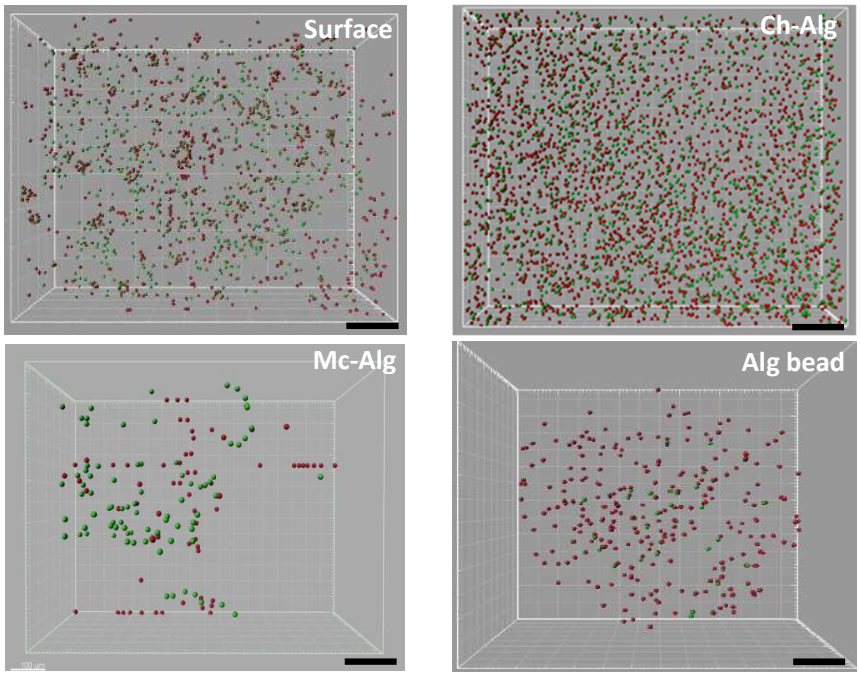

Figure 4.9: Cell viability and distribution of SY5Y cells in different 3D culture systems.
(a) Ch-Alg system supports higher cell viability in longer culture period (Day 7) than other groups. Presto blue assay was used to measure cell metabolism activity that correlates to cell viability and proliferation. ANOVA test was used to determine significance. A *p-value below 0.05 was considered statistically significant. Error bars indicate standard deviation (±SD). (b) On day 14, live and dead cell distribution in 3D culture systems demonstrated localisation of dead cells (red) in the core of Mc-Alg system. The alginate beads have functionalised with RGD. Live cells were stained green (Calcein-AM); dead cells were stained red (PI). A series of Z-stack images were taken using fluorescence microscopy (Nikon T_i Eclipse, Japan) and processed with IMARIS software (Bitplane, UK). Scale bar: 300 µm.

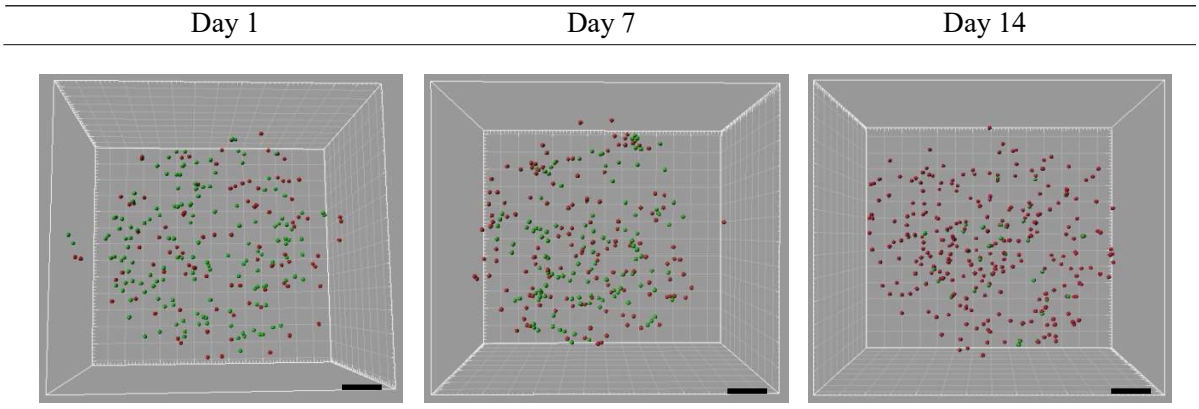

Figure 4.10: Cell viability and localisation of encapsulated SY5Y cells in the RGD-alginate beads from day 1 to day14.

Cells are uniformly spread within the construct, remained viable at 50% on day 7 before decreasing**.** Live-dead cell staining (Calcein-AM) was performed. A series of z-stack images were captured using fluorescent microscopy (Nikon T_i Eclipse, Japan), and processed with IMARIS software (Bitplane, UK). Live cells were stained green whilst dead cells were stained red. Scale bar: 200 µm.

4.3.2 ChR2-YFP expression remained when transferred to 3D culture system

The optogenetically modified cells generated in chapter 3 were cultured and treated in 2D; further investigation on the potential to establish a 3D culture network model derived from these cells in 2D culture was performed by encapsulation of the cells in our earlier developed RGD-alginate beads. Under the confocal microscope, Axol and SY5Y cells transduced with ChR2 were found to stably express (YFP labelled with green colour) without being affected by the culture environment and thickness of the beads. The transduced cells appeared in spherical aggregates within the 3D alginate beads, however no outgrowth of neurites was observed in the RGD-alginate bead after 24 hours of encapsulation (Fig. 4.11).

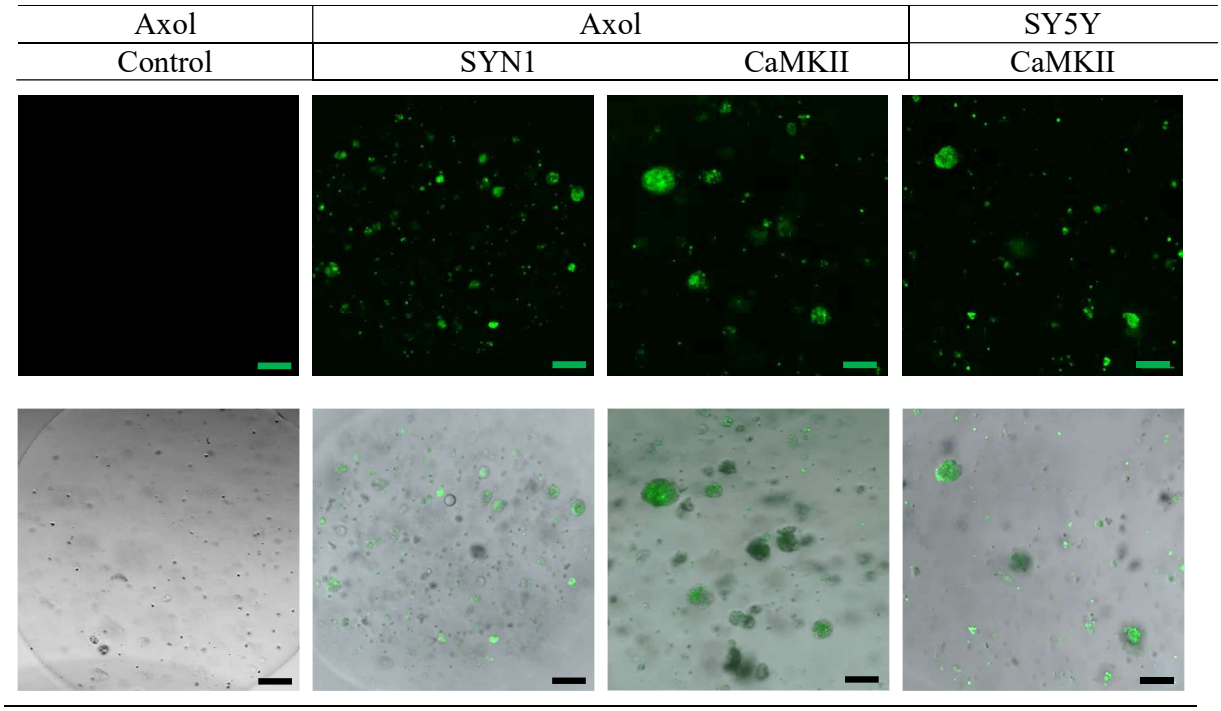

Figure 4.11: ChR2-YFP positive expression of Axol and SY5Y cells was retained in 3D culture system.

Optogenetically modified Axol and SY5Y cells cultured in 2D were enzymatically detached and encapsulated with RGD-alginate beads. The cell-RGD-alginate constructs were examined using a confocal microscope (Zeiss-LSM 710) to investigate the expression of ChR2-YFP, cell morphology and distribution within the 3D culture system. Non-transduced Axol cells were used as a control. Scale bar: 100 µm.

4.4 Discussion

Peptide-modified alginate scaffolds can be used as a biocompatible matrix suitable for the encapsulation and culture of hESCs [288, 304]. Functionalised alginate (RGD-alginate with ROCKi) was investigated as a generic 3D platform that provided a defined microenvironment for hESC adherence, survival and maintenance. The potential of alginate hydrogel for culturing neurons was also assessed through the encapsulation of astrocytes and neuroblastoma cell line (SY5Y cells).

The physical properties of alginate hydrogel including the bead size, sphericity and consistency of formation are correlated to chemical composition. The proportion of guluronic to mannuronic acid residues in alginate is deemed critical. Alginate containing a higher percentage of guluronic acid or G block (UP-MVG) forms stiffer gels and rounder beads, such that the beads maintain their physical properties for longer during cell culture. However, alginate rich in mannuronic acid residues (for example LG-A2158) comprises only short G-blocks leading to soft and easily fractured gel networks, and the beads that form are weaker, deformed, and disintegrate more easily with time. Detail results of LG-A2158 alginate with its disadvantages were presented in Appendix 9.

Kendall et al. found that microspheres produced from highly purified alginates such as UP-MVG have far less morphological imperfections, resulting in smaller size and rounder beads [305], making them more suitable for long term cell culture. For this high molecular weight alginate (UP-MVG), it was found that increasing the concentration of alginate correlated directly to an increase in bead size (2 and 2.5 ml/min). Flow rate also exerts a significant influence on reducing the bead size ($P < 0.01$), such that the highest flow rate investigated (3 ml/min) produced the smallest beads at 1.8% (w/v) alginate concentration with an average bead diameter of 800µm (Fig. 4.2 and 4.3). This optimised bead size was chosen for cell encapsulation, as it the small dimeter of the bead

allows for rapid nutrient and gas diffusion through the alginate. This bead size is within the range reported by Gautier et al. where glucose, ammonia and vitamin B was found to rapidly diffuse across the outer layer of 600 - 1000 µm diameter alginate beads [306].

Degradation of alginate is mediated by calcium and sodium ion exchange in the local environment and not by cleavage of molecular bonds [307]. The rate of degradation of alginate hydrogels is dependent on the physiologic pH of the surrounding medium and the initial ionic strength of the solution used for cross-linking. It has been demonstrated that alginate hydrogels cross-linked at pH 6 or 7 can more stably maintain a swelling ratio close to 1 than those cross-linked at pH 8 [308]. Likewise, both 1.2% and 1.8% (w/v) UP-MVG alginate hydrogels cross-linked at pH 7 and incubated in a solution that approximated *in vivo* conditions were found susceptible to both excessive shrinking and swelling throughout the 14 days investigated. The rate of degradation of 1.2% (w/v) alginate was highest on day 1 of incubation, resulting in rapid weight loss, before slowing to an average rate of loss from day 3 onwards (Fig. 4.4b).

Conversely, 1.8% (w/v) alginate swelled faster than 1.2% (w/v) alginate, reaching equilibrium and stability only after a longer 14-day incubation period (Fig. 4.4a). This could in part be explained by the higher polymer concentration within the 1.8% (w/v) hydrogel resulting in an initial relatively lower water content. When the beads transferred to PBS, this led to a greater osmotic pressure from the PBS into the hydrogel [296, 298]. The hydrogel volume subsequently expands as the void regions of the polymer network fill with PBS until an equilibrium state is reached. This type of increase swelling may enhance cellular viability within the hydrogel, facilitating mass transfer, waste and oxygen exchange via enlarged scaffold pores.

Interestingly, RGD coupled alginate (3-5% w/v) possessed a similar swelling profile to 1.2% (w/v) alginate whilst also having a constant degradation rate similar to 1.8% (w/v) alginate

throughout the 14-day incubation. The presence of RGD with positive charge bind to the negative charge of water molecules has increased the hydrophilic of alginate hydrogel, stabilised the structure with lower swelling and constant degradation profile. A recent study that investigated swelling of OMA-9, a photo-crosslinked alginate hydrogel formed at 2% (w/v), indicated similar swelling kinetics to the data presented here, with an initial swelling ratio of 40x on day-1, increasing to 50x on day-3 after which an equilibrium was reached, and swelling was unchanged throughout the rest of the 14-day study [299]. However, the degradation profile of OMA-9 was much higher (20-50% loss throughout) in comparison to the lower and consistent degradation profile observed for both 1.8% (w/v) alginate and RGD-alginate used in this study.

The diffusion and release of entrapped biological factors (i.e. growth factors and ECM proteins) from alginate hydrogels over time is influenced by how these factors physically and ionically interact with the cross-linked network. Diffusion of calcium ions out of the alginate matrix decreases the number of ionic crosslinks binding the gel together, such that the size of pores increases leading to the formation of larger channels and pathways through the hydrogel. Whilst small biological factors continue to diffuse through the gel unhindered, the diffusion rate of previously hindered medium-sized factors increases, whilst larger factors such as laminin protein remain entrapped until pore size increases sufficiently to affect transport. This model does not account for the ionic interaction between alginate and the entrapped factors – which can also act separately to slow or increase the rate of factor transport. In the present study, diffusion of differing concentrations of a medium sized solute (BSA) from the alginate beads demonstrated that the most rapid diffusion occurred within the first 24 hours of incubation. Approximately 40-50% of the initial encapsulated amount of BSA protein still retained within the alginate after 7 days of incubation (Fig. 4.5a). This may in part be coincidental on the swelling profile during incubation,

where the initial rapid swelling effect facilitated the transport of entrapped BSA. Similar trends have been reported that the diffusion rate of BSA in alginate and agarose hydrogels increases within the first 30 days of culture and then remains constant over the next 30 days [309]. Furthermore, the large solute (IgG) was reportedly withheld in the hydrogels over 60 days. However, the findings reported in chapter 4 suggest that the rate of diffusion of laminin (LN) from the alginate beads was also dependent on the initial concentration. It was found that a minimum concentration of 20 µg/ml was required for efficient incorporation, as well as to delay complete diffusion (Fig. 4.5b). As LN conforms and binds strongly to scaffold material and surfaces, it is not unexpected that a proportion of LN will remain within the beads, and it follows that a sufficient minimum coating amount can be determined that will support the expansion of hESCs, as exemplified by the coating of LN onto dextran microcarriers [309, 310].

The culture conditions for hESCs were optimised by assessing the impact of different cell seeding densities and different culture media on the survival of hESCs in alginate beads. Culture medium is a crucial parameter in the cultivation of hESCs, and there is a trend towards the use of fully defined media such as mTeSR1 and STEMPRO [311, 312]. In recent reports of 3D culture, hESCs survived and maintained their pluripotency in STEMPRO medium on laminin- and vitronectin-coated microcarriers, where results were comparable to use of MEFs and conditioned medium [310]. In addition, the use of ROCKi is beneficial for hESC culture and recovery following encapsulation in unmodified alginate [313]. Use of this small molecule enhances initial cell attachment, which has a role in regulating actin organisation and focal contact within the substrate [293, 294]. This may lead to the formation of small aggregates or clusters of cells in the beads as observed in the confocal images (Fig. 4.6b).

In order to mimic the native microenvironment, HUES-2 cells were encapsulated within RGD-alginate beads and cultured under chemically-defined conditions (mTeSR1 + ROCKi) (Fig. 4.1c). Cell viability of HUES-2 cells in RGD-alginate was higher than in unmodified alginate during long-term culture (14 days). Stem cell viability increased gradually from day-3 due to proliferation and approximately 30% of cells remained viable at day-14 in RGD-alginate. Astrocytes, a more robust cell type used as a control group, had significantly higher cell viability in unmodified alginate bead. These results suggest that alginate alone is unable to provide an optimal microenvironment for the growth of hPSCs although it can support survival of other cell types.

It is thought that the presence of RGD ligands facilitate cell-integrin binding, promote HUES-2 cells adherence and growth within the alginate beads. The RGD sequence has been widely applied in biomaterials field since being identified as a primary attachment cue by Pierschbacher and Ruoslahti [134, 286, 314]. This sequence binds primarily to the $\alpha_5\beta_3$ and $\alpha_5\beta_1$ integrin receptors found on a variety of cell types. Encapsulated single HUES-2 cells survived for up to 14 days in culture in RGD-alginate, and appeared in relatively small aggregates instead of large aggregates interconnected by tight connections as demonstrated in other reports [315]. It suggest that HUES-2 cells may require a higher amount of RGD than other cell types or cell lines, as indicated by findings reported in a recent study using HUES-7 cells [283, 316].

Despite the presence of RGD motifs within the alginate, cell death still occurred when using alginate beads to culture hESCs because upon dissociation and encapsulation, RGD does not involve in the blocking of the pro-apoptotic mechanisms activated in hPSCs. The present study investigated on the use of small molecule inhibitors (ROCKi and ZVAD) to prevent cell death. In the modified 3D system based on RGD-alginate, incorporation of ZVAD supported higher cell

viability (77.8%) than ROCKi alone (54.1%) at the same concentration of 10 μM (Fig. 4.8). A higher percentage of dead cells were observed in cultures treated with ROCKi with/without ZVAD in comparison to cultures treated with ZVAD alone. ZVAD can prevent apoptosis when bind to the active catalytic sites of caspase 3/7 or the process end of the large subunit of caspase 9. Although ROCKi (Y-27632) is well-known and found to block Rho-associated coiled kinase (ROCK) efficiently, it simultaneous inhibition onto other kinases may contribute to low viable cells [302, 303]. In contrast to other stem cell types, continuous supplementation of human adipose stem cell (ADSC) cultures with Y-27632 led to decreased numbers of cells and decreased global metabolic viability as shown by Lamas et al. This small molecule is concentration-dependent and significant for 10 μM and 20 μM [152].

Results also suggest that most cell death in the 3D culture system may be attributed to the extrinsic factors rather than reflecting the effects of apoptosis inhibitors. For instance, cells in alginate solution might experience stretching forces due to extensional flow through syringe extrusion, which may subsequently lead to acute cell death. Aguado et al. observed that both pressure drop and linear shear flow were uncorrelated to cell death (cell viability > 90%), but only 58.7% of cells survived when subjected to extensional flow [317, 318]. Thus, alginate hydrogel may be unable to provide complete mechanical protection from the damage caused by extensional flow during the extrusion and cell encapsulation processes. Moreover, cell disruption could also occur during de-capsulation. In this study, the results indicate that the incorporation of ZVAD alone may rescue cells from apoptosis but not from necrosis.

In summary, a 3D culture platform mimics the native microenvironment to support the growth of hESCs was developed i.e. RGD-alginate hydrogel incorporated with ROCKi. This functionalised alginate hydrogel fulfilled quality requirement, demonstrating an adequate bead size

(800 μm) and spherical morphology. The effects of peptide conjugation, protein incorporation and the ability of ROCKi/ZVAD to support cell viability in the 3D culture system were characterised. The cells formed in aggregates, however, whether proliferation or migration plays the role in this formation is yet to evaluate and therefore this limitation is important for future investigation. Another 3D culture system, Ch-Alg has demonstrated high cell viability in longer culture period (Fig. 4.9 and 4.10), may provide more space and surface for cell attachment as well as migration especially for neurons. Interestingly, the expression of ChR2 was stable in the 3D alginate hydrogels (Fig. 4.11) when transferred from 2D culture, suggesting an initial success towards the development of a functional 3D neural culture model responsive to light stimulation.

5.0 Neurophysiological investigation of human neural networks in 2D and 3D cultures

Introduction:

Electrical activity is known to play a crucial role in neuronal development and synaptic function of neurons [319-321]. It is essential to evaluate neuronal function or activity of Axol cells. Light-sensitive probes (optogenetics) are recent techniques which can be used for this purpose, and can even applied to control the activity of entire populations of potential presynaptic neurons, and/or regulate the responses of potential postsynaptic neurons. The questions to address in this study are whether (i) the optogenetically modified cells derived from human iPSCs (Axol cells) and neuroblastoma (SY5Y cells) respond to light stimulation, and whether (ii) the human neural network in 2D could be cultured into a functional 3D model using RGD-alginate hydrogels.

Calcium imaging experiments are able to detect neuronal activities by optically monitoring changes in calcium (Ca^{2+}) transient. The ubiquitous presence of calcium channels in neuronal membranes and their activation by depolarisation have made possible the optical detection of calcium spikes, which can produce generalised calcium influxes that are much larger than those produced by sodium spikes [322], therefore it is possible to detect whether a neuron fired an action potential (Figure 5.1) upon light stimulation.

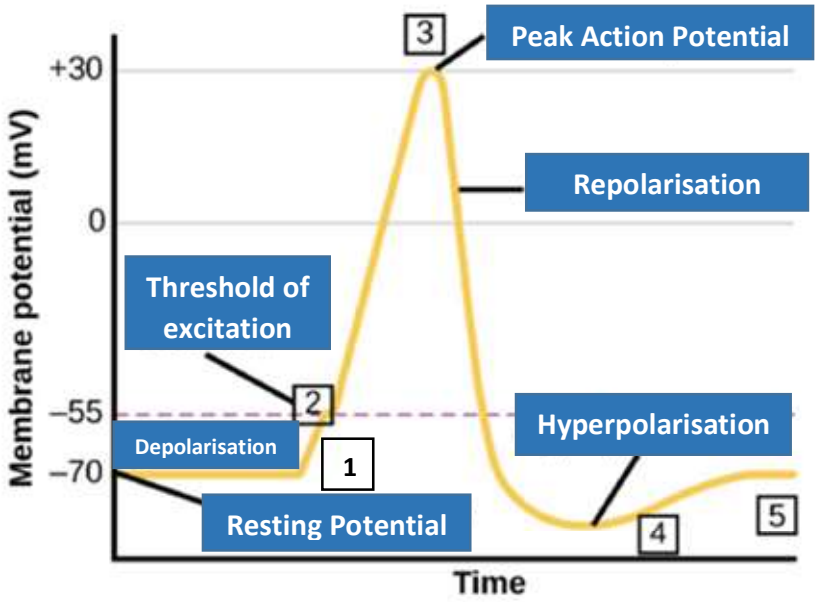

Figure 5.1: Formation of an action potential when travels down the axon.

An action potential or spike is formed as decribed in the following five stages. (1) A stimulus from a sensory cell (another neuron or light) induce the target cell at resting potential (-70 mV) to depolarise. (2) When depolarisation reached the threshold of excitation (-55 mV), Na+ channels open and trigger membrane depolarisation. (3) At the peak action potential (+30 mV), Na+ channels close but K+ channels open and release K+ ions from the cell. (4) K+ ions continue leaving the cell and the hyperpolarised membrane enters into a refractory period that unable to fire. (5) The K+ channels close and the resting potential is restored by the Na+/K+ transporter. (adapted from http://cnx.org/content/m44748/latest/Figure_35_02_03.png "OpenStax College, How Neurons Communicate. October 17, 2013." [323]

5.1 Calcium imaging as a tool for functional analysis of optogenetically modified cells

5.1.1 Optimisation of calcium dye loading and staining efficiency

The calcium indicator, Cal-590™ is a homogeneous fluorescence-based assay tool for detecting intracellular calcium mobilisation. Similar to the existing X-Rhod-1 AM, these ester dyes are non-fluorescent in solution upon cellular uptake and intracellular de-esterification, fluorescence is then emitted after chelating cytosolic calcium. Yet concentrations of dye vary between protocols and the exact loading requirements on our cell types are not well defined. It is thus important to characterise the role of different concentrations in order to maximize dye loading and staining efficiency for the best imaging output.

Under the confocal microscope imaging, no auto-fluorescence was detected in the unstained cells at 594 nm (Fig. 5.3). The results suggest that calcium detection can be increased by using high concentrations of Cal-590^{TM} (dissolved in DMSO and low concentration of pluronic acid, PF127). The optimal signal was achieved at 10 uM of Cal-590^{TM} whilst poor uptake of dye was clearly shown at low concentrations of 1 and 4 uM (Fig. 5.3a-c). When examined under high magnification (63x oil lens) (Fig. 5.3b), incomplete hydrolysed esters was not found in the cytosol (compartmentalisation artefacts). This could happen due to low cytosolic esterase concentration after long incubation times or when high extracellular probe concentrations are used. The expression of ChR2-SYN1 was seen at the cell membrane (Fig. 5.3b) indicated success integration of this membrane protein at the ion channels through lentiviral transduction.

Moreover, a positive indicator ionomycin (an ionophore) was added to trigger calcium across the plasma membrane, thereby further confirm the calcium dye was loaded and stained the cells appropriately. From the recording, calcium transient was raised immediately and the intensity remained higher than without ionomycin which showed relatively less calcium activity and slow

rise waves (Fig. 5.4). Calcium transient of a single cell or region of interest (ROI) was recorded in a video and displayed in figure 5.5.

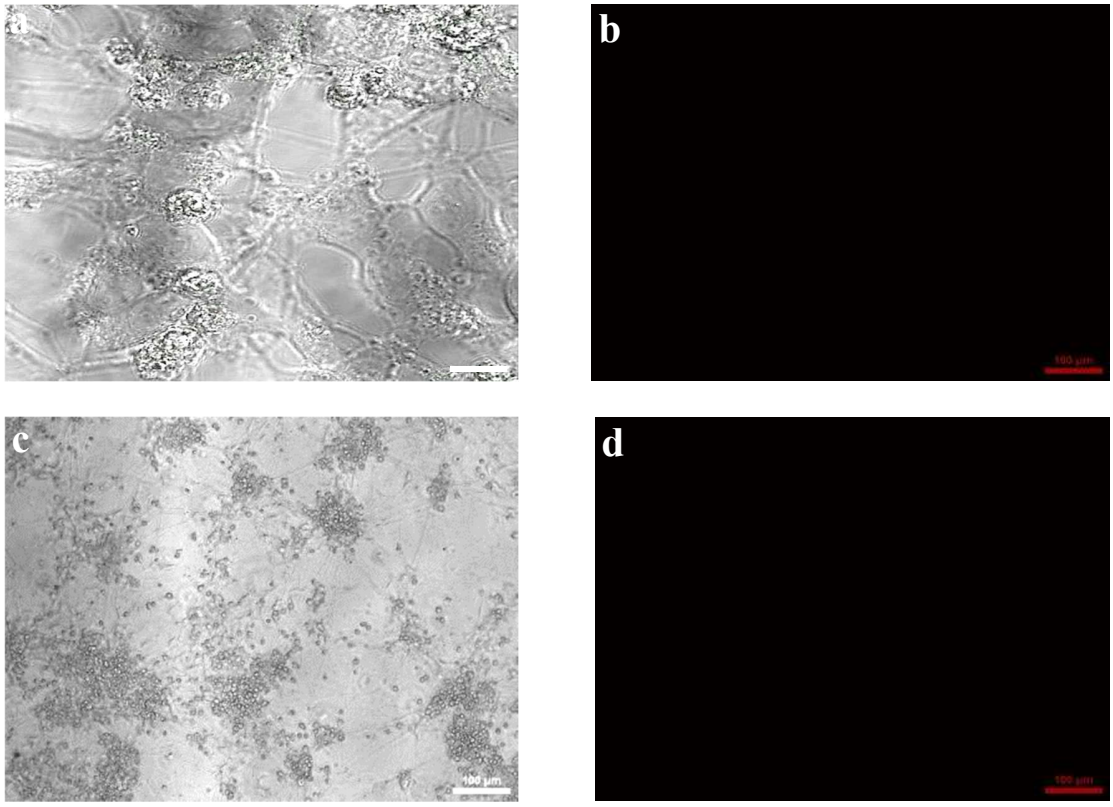

Figure 5.2: Optimisation of confocal microscope setting shows no auto-fluorescence.

(a-b) Unstained Axol cells and (c-d) unstained SY5Y cells examined with confocal microscope using laser at 594 nm (Zeiss-LSM 710). Scale bar = 100 µm.

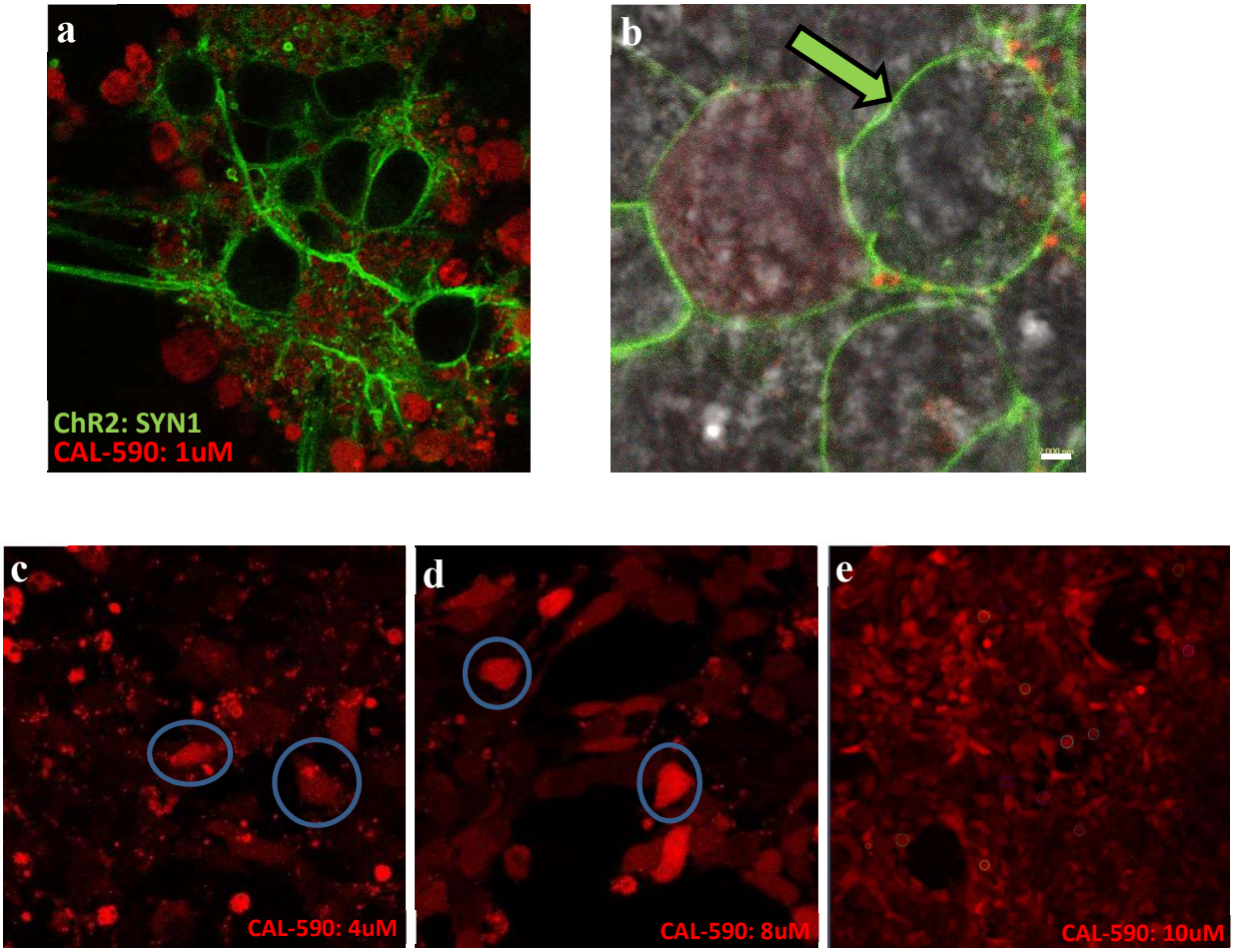

Figure 5.3: The concentration of calcium dye (CAL-590) at 10 µM contributes to optimal calcium staining and fluorescence signal.

The Axol cells were transduced with pSYN1-ChR2-YFP and cultured in a light protected glass-bottom plate. The cells were rinsed with ACSF buffer before loaded with different concentrations of CAL-590 at (a,b) 1 µM, (c) 4 µM, (d) 8 µM and (e) 10 µM. The cells were incubated at room temperature for 45 min, rinsed and replaced with filtered ACSF. Images of the staining were viewed using confocal microscopy at excitation wavelength of 594 nm (Zeiss-LSM 710). CAL-590 stained the cells in red. Calcium transient of a single cell or region of interest (ROI) was marked in blue circle (Magnification: a,c,d = 40x, b = 63x and e = 20x).

a

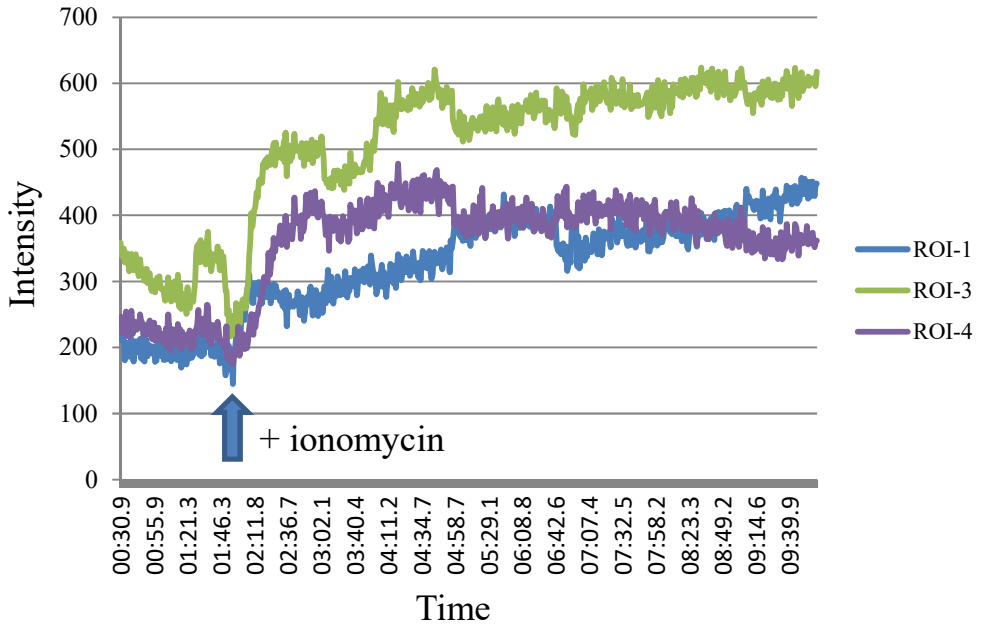

b

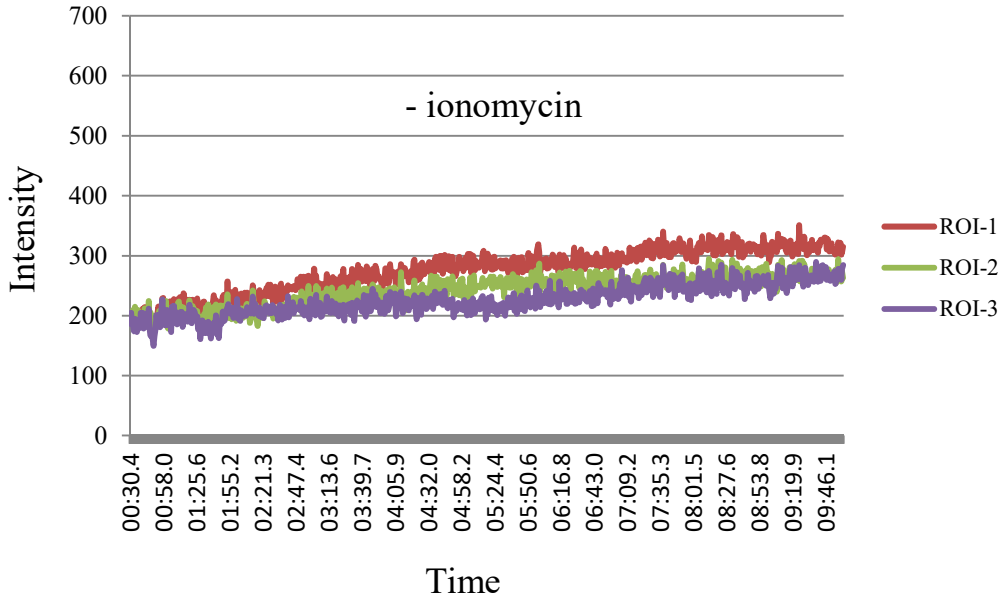

Figure 5.4: Further evaluation of loading and staining of calcium dye using a positive indicator.

(a) Positive indicator ionomycin was added during calcium imaging (arrow: adding time point), calcium influx was triggered subsequently increased calcium transient immediately and the intensity was recorded using a fluorescence microscope in a 10 min movie (Nikon Eclipse T_i-E, Japan). (b) A comparison without ionomycin showed slow calcium waves and small calcium activity throughout imaging. ROI: region of interest/single cell selected in the culture, results of 3 single cells (ROIs) were presented.

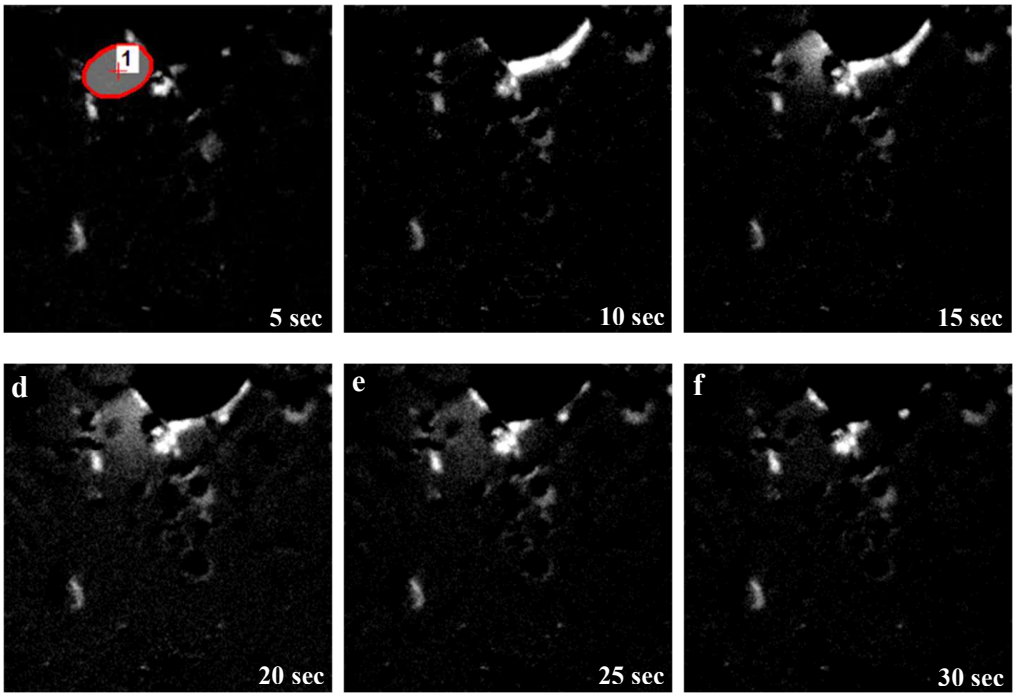

Figure 5.5: Region of interest-1 (ROI-1) marked a single Axol cell in a serial of calcium transient, where a single spike was generated in 30 second of video recording.

The expression was driven by CAMKII promoter upon light stimulation at 470 nm. Images and video were captured with confocal microscope using laser at 594 nm (Zeiss-LSM 710).

5.1.2 Classification of calcium events obtained from calcium imaging

Cells from different region of interest (ROIs) were imaged continuously over 5 min and classified based on the properties of calcium events observed. The ROIs were distinguished into the following categories reflecting either slow or fast rising phase events, active or inactive cells and the train of action potential (Fig. 5.6) [321]:

1. Calcium waves:
    a. Inactive – cells with no calcium activity
    b. Slow undefined – cells with less calcium activity, the type of calcium spikes is hardly distinguished
    c. Slow rise – cells with slow calcium activity, slow rising and usually consist of single spikes event
    d. Burst – cells with high calcium activity, fast rising and consist of any type of spikes (single or multipeak spikes)
    e. Mixed – cells with calcium activity which have a mixed spike, both single and multipeak spikes
2. Calcium spikes:
    a. Single spikes
    b. Multipeak spikes
3. Action potential (AP):
    a. Single – a single spike in slow rise waves
    b. Repetitive – repetition of calcium spikes in single spikes, multipeak spikes or a mixed of both

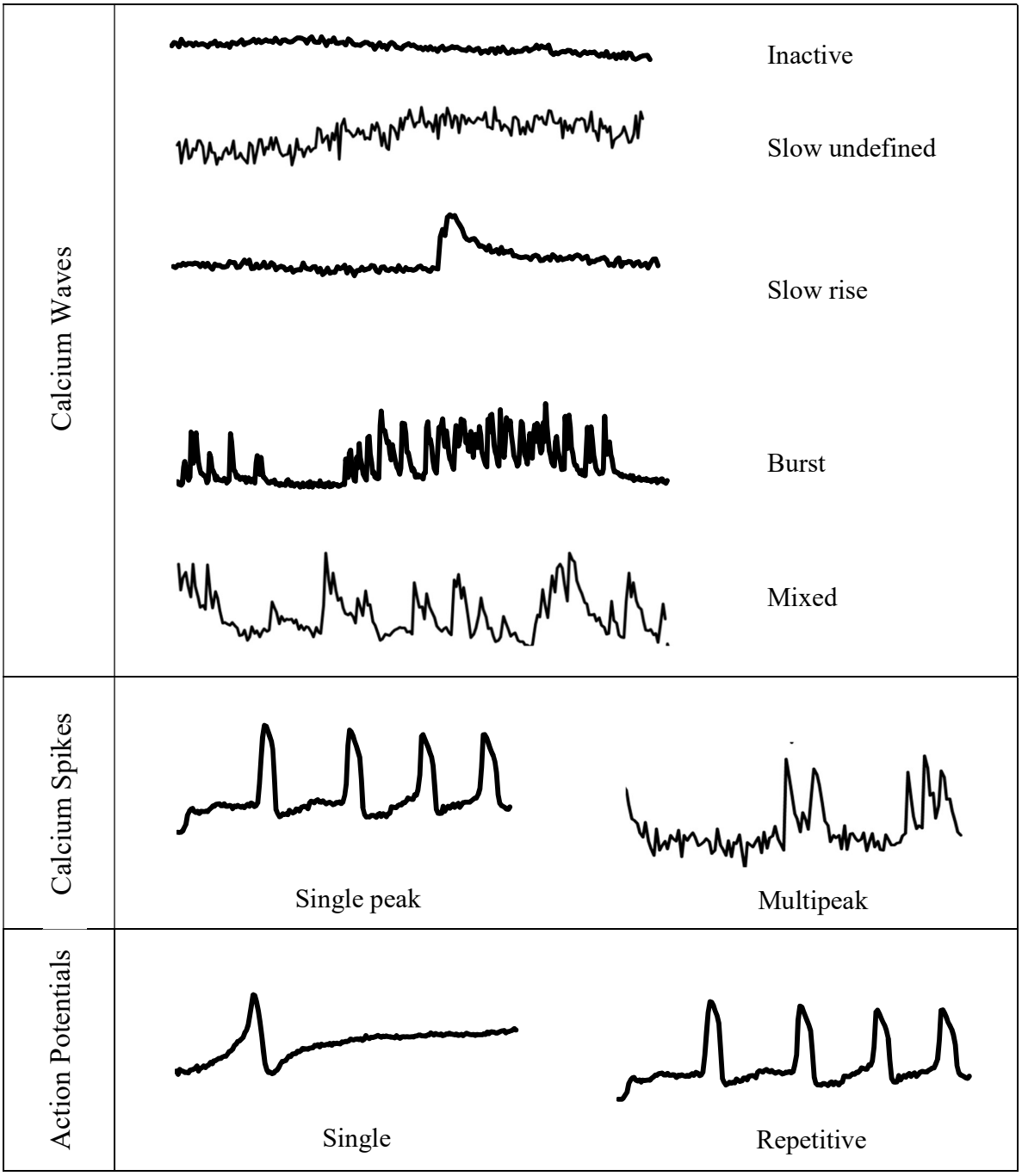

Figure 5.6: The traces represent typical examples of calcium imaging time series over 5 min from different ROIs which were classified based on the calcium events.

Three main categories of ROIs were distinguished: (1) calcium waves which were (i) inactive, (ii) slow undefined, (iii) slow rise, (iv) burst and (v) mixed, (2) calcium spikes in (i) single peak and (ii) multipeak, and (3) action potentials exhibited either (i) single or (ii) repetitive calcium transient.

5.2 Strong expression of ChR2-YFP in the primary neurons of mouse E14.5 upon stimulation as a positive control

Primary neurons of mouse E14.5 were used as a positive control in comparison to Axol and SY5Y cells for functional neuron analysis using calcium imaging. Upon light stimulation, neurons containing pSYN1-Ch2R-YFP expressed synchronous and repetitive action potentials (APs), showing burst waves and single spikes. The non-stimulated neurons showed irregular, mixed and slow waves (Fig. 5.7). When compared to pCaMKII-ChR2-YFP, the cells expressed mixed APs, demonstrating mixed calcium waves with single and multipeak spikes after stimulation (Fig. 5.8). Both SYN1 and CaMKII promoters were functional when tested in primary neurons, however, SYN1 promoter appeared as a strong neural-specific promoter, exhibiting active synchronous calcium firing.

In control experiments using unmodified primary neurons, light stimulation has no effect onto the cells due to the absence of opsin (ChR2-YFP). All the cells exhibited repetitive APs, implying mature electrical activity. In addition, typical calcium waves (burst and mixed waves) and calcium spikes (mixed of single and multipeak) were recorded in the 5 min of imaging (Fig. 5.9). Interestingly, when compared to transduced primary neurons without light stimulation (Fig. 5.7 and 5.8), less calcium events were observed than control groups. The introduction of transgene ChR2 using lentiviral transduction may interfere the neuronal activity of modified primary neurons.

Further analysis of selected 40 ROIs or single cells revealed that upon light stimulation, slow rise waves have reduced to 50% and transformed to burst, mixed and undefined waves in the cells under the control of SYN1 promoter (Fig. 5.10). Conversely, burst and mixed waves were slightly increased to 11 of ROIs whilst 29 ROIs were categorised as slow rise waves in the cells containing CaMKII promoter. Upon light stimulation, multipeak spikes ($P<0.01$) and single spikes

($p<0.05$) were increased significantly in both pSYN1-ChR2-YFP and pCaMKII-ChR2-YFP transduced cells (ROIs=40, n=3). Results suggest that SYN1 is a stronger promoter than CaMKII. Furthermore, the distinct pattern of neuronal activities that derived from mature neurons was identified (i.e. single spikes, burst and mixed calcium waves).

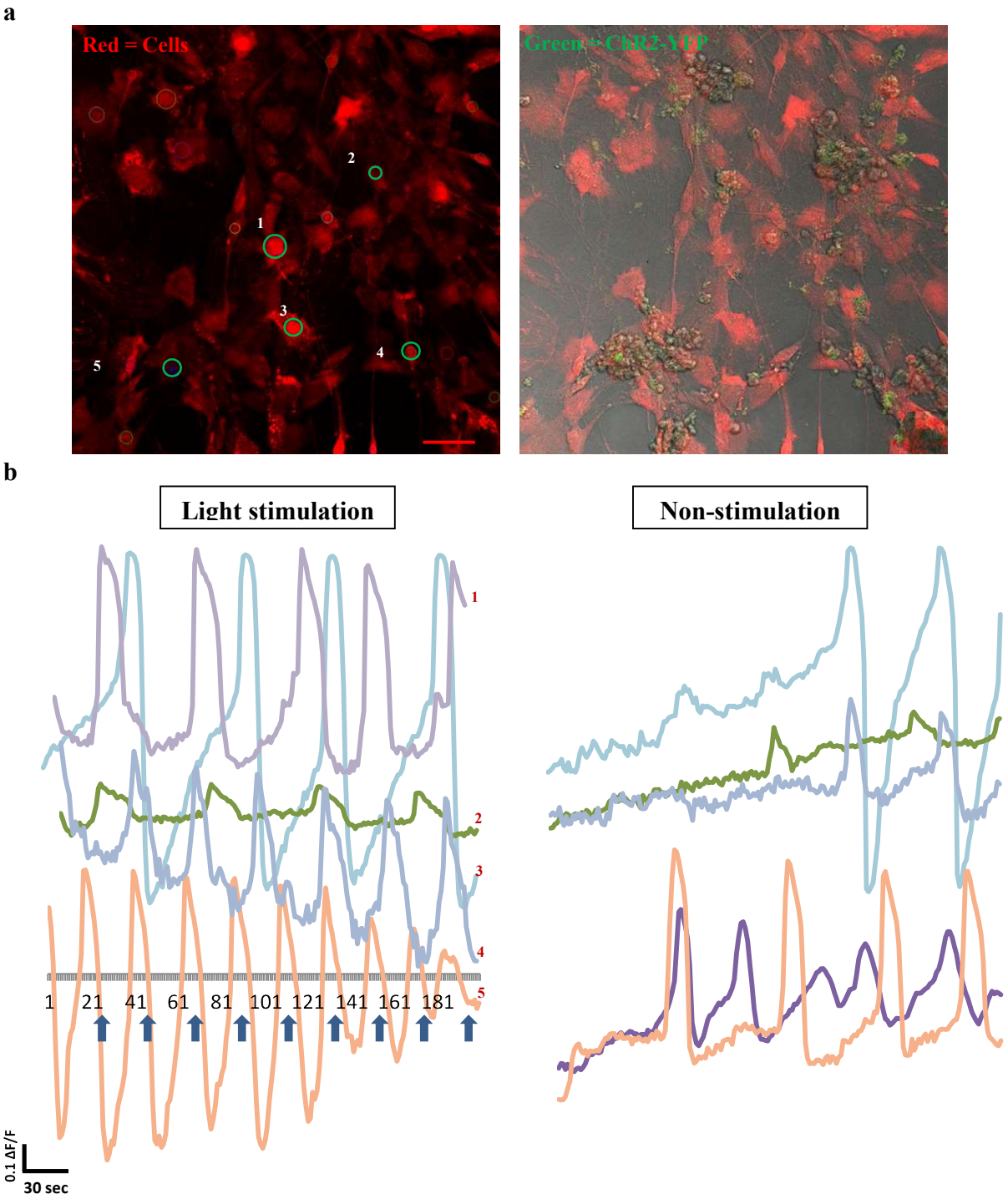

Figure 5.7: Neuron-ChR2-YFP driven by SYN1 promoter is responsive to light stimulation, raised more repetitive APs than non-stimulated neurons.
(a) Primary neurons were stained with calcium dye (red) and the region of interests (ROIs) or single cells were labelled with number (left). pSYN1-ChR2-YFP was expressed (green) in the culture and the location was shown in a merged image of bright field and fluorescence micrograph (right). (b) The cells were selected from the ROIs as marked in figure a (left), and stimulated with laser at 488 nm every 30 sec (200 frames), the fluorescence intensity was normalised to the level of baseline fluorescence measured before the onset of the calcium signal (ΔF/F). Arrow: light stimulation; circle: region of interest (ROI). Scale bar: 50 µm.

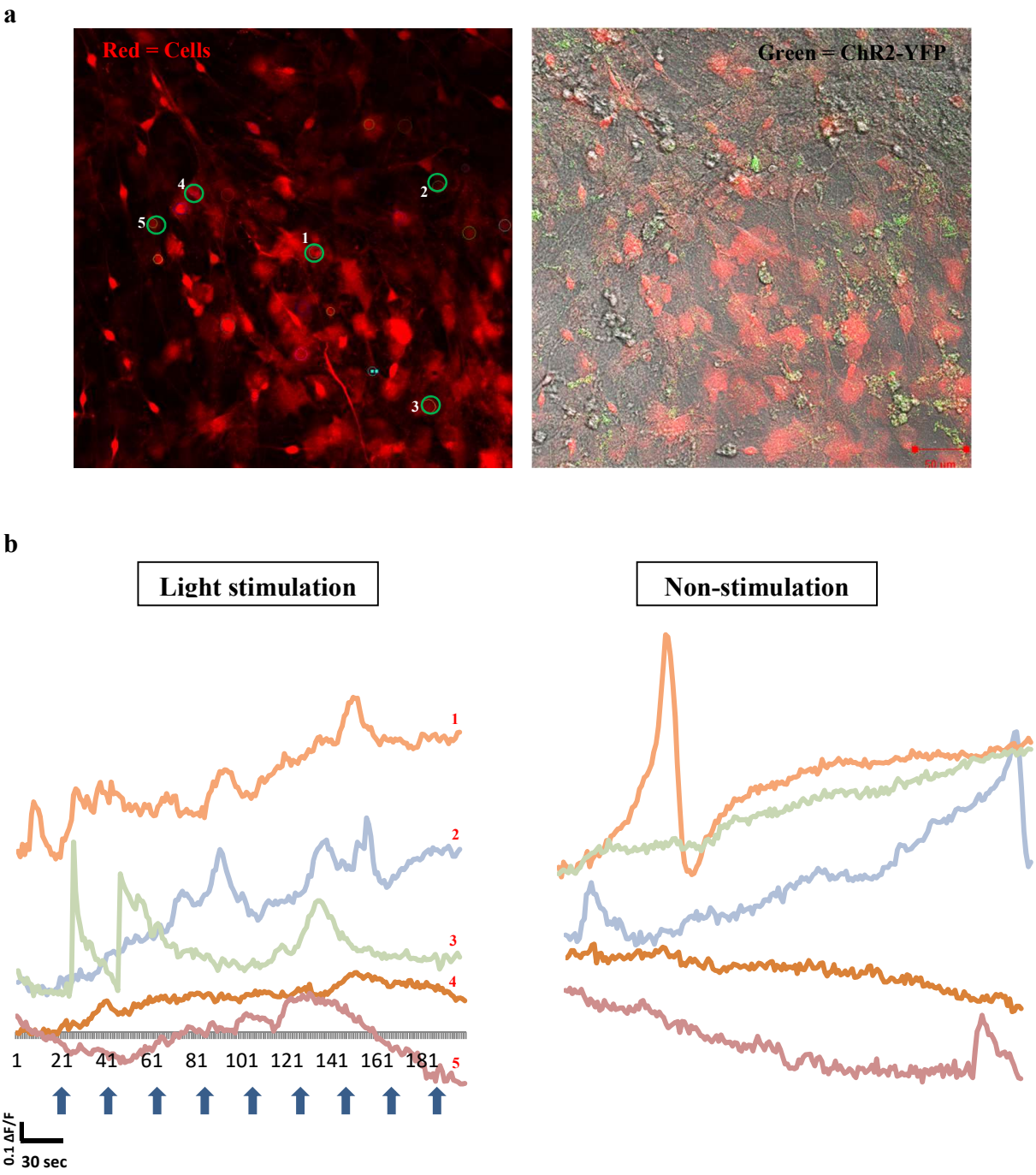

Figure 5.8: Neuron-ChR2-YFP driven by CaMKII promoter is responsive to light stimulation.

(a) Primary neurons were stained with calcium dye (red) and the region of interests (ROIs) or single cells were labelled with number (left). pCaMKII-ChR2-YFP was expressed (green) in the culture and the location was shown in a merged image of bright field and fluorescence micrograph (right). (b) The cells were selected from the ROIs marked in figure a (left), and stimulated with laser at 488 nm every 30 sec (200 frames), the fluorescence intensity was normalised to the level of baseline fluorescence measured before the onset of the calcium signal (ΔF/F). Arrow: light stimulation; circle: region of interest (ROI). Scale bar: 50 µm.

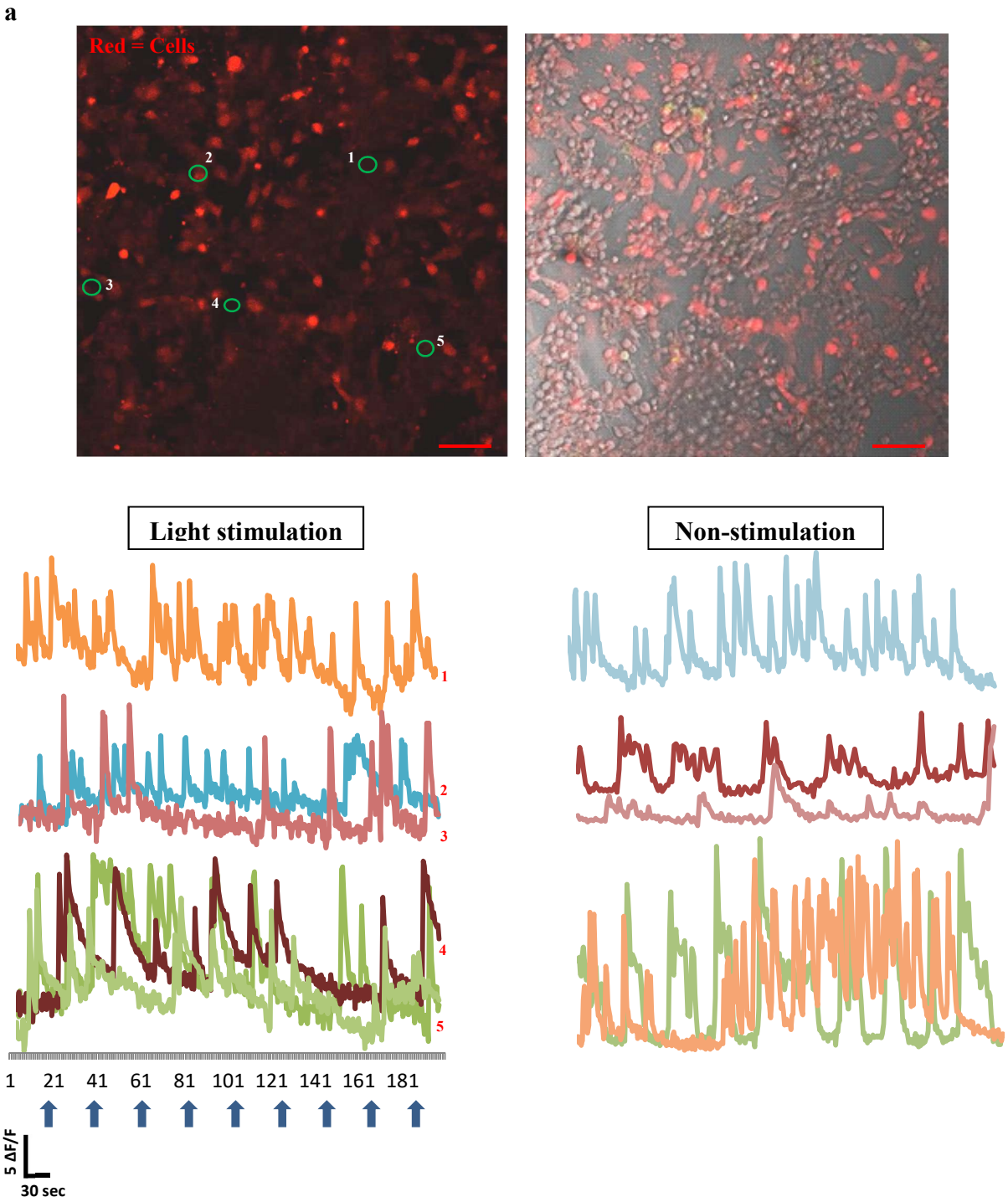

Figure 5.9: Primary neurons without optogenetically modification serve as a control, demonstrated typical calcium spikes of mature neurons.

(a) Primary neurons stained with calcium dye (red) and the region of interests (ROIs) or single cells were labelled with number (left). No expression of ChR2-YFP (green) was observed in the culture as shown in a merged image of bright field and fluorescence micrograph (right). (b) The spontaneous calcium firing of non-stimulated cells was recorded (right). The cells were selected from the ROIs and stimulated with laser at 488 nm every 30 sec (200 frames) (left). The fluorescence intensity was normalised to the level of baseline fluorescence measured before the onset of the calcium signal (ΔF/F). Arrow: light stimulation. Scale bar: 50 µm.

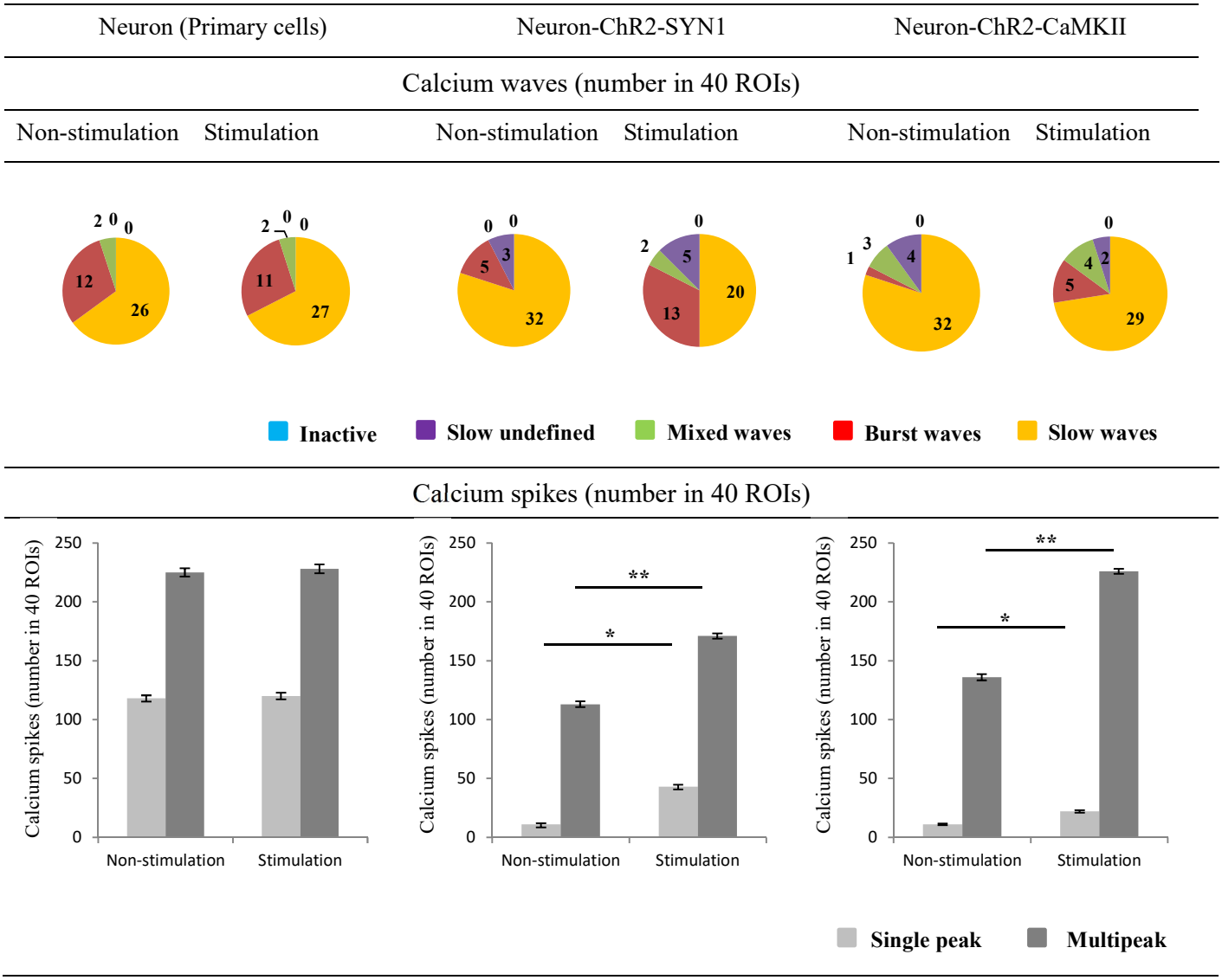

Figure 5.10: Primary neurons - ROIs were distinguished with five types of calcium waves (pie charts) and further identified with two types of calcium spikes (bar charts) to evaluate their action potentials upon light stimulation (refer Fig. 5.6)

Calcium waves were analysed from the ROIs of non-stimulated and stimulated primary cells which have been transduced (Neuron-ChR2-SYN1 and Neuron-ChR2-CaMKII) and non-transduced (Neuron) (ROIs=40, n=3). Higher number of burst waves and multipeak spikes were found in the cells under the control of SYN1 promoter upon stimulation.
Calcium spikes (single and multipeak) were identified from the selected 40 ROIs in the pie chart (ROIs=40, n=3). Significance was tested by two-way ANOVA * = $p<0.05$; P** value = < 0.01. Error bars represent standard deviation (±SD).

5.3 Human iPSC-derived neurons (Axol) and neuroblastoma cells (SY5Y) expressed ChR2 and generated calcium activity following light stimulation

5.3.1 Axol-ChR2-YFP cells driven by CaMKII promoter performed better than SYN1 promoter

Human iPSC-derived neurons (Axol) were transduced with lentiviruses containing the SYN1 and CaMKII promoters regulating the expression of ChR2-YFP. Upon light stimulation, the cells with ChR2-YFP expression driven by SYN1 (pSYN1-ChR2-YFP) give raise to calcium spikes, displaying slow and mixed calcium waves (Fig. 5.11). The slow broad transients are consistent with early developing neurons. On the contrary, non-stimulated cells showed few spontaneous calcium activities with slow and undefined calcium waves. Glutamatergic neurons targeted promoter CaMKII has generated higher calcium transient and synchronous firing than pSYN1-ChR2-YFP (Fig. 5.12). Burst spikes and mixed calcium waves were demonstrated in 5 min of recording. Results showed that CaMKII promoter performed better than the SYN1 promoter. This data is convincing when further analysis of 40 ROIs revealed that upon light stimulation, a significantly increased number of multipeak spikes was found in the cells expressing ChR2-YFP driven by CaMKII (pCaMKII-ChR2-YFP) ($P<0.01$; $n=3$). In addition, a number of slow rise waves has transformed to burst and mixed waves (Fig. 5.13).

5.3.2 SY5Y-ChR2-YFP cells driven by SYN1 promoter performed better than CaMKII promoter

An additional cell type, neuroblastoma (SY5Y) cells was used for a comparison study. Before lentiviral transduction, the cells were treated and differentiated with retinoic acid (RA) to increase neuron maturation as well as to increase calcium firing. With ChR2-YFP expression driven by SYN1 promoter, synchronous calcium firing in mixed waves consisting of both single and multipeak spikes was observed upon light stimulation (Fig. 5.14). SY5Y cells with ChR2-YFP

expression regulated by the CaMKII promoter also induce calcium influx when stimulated with light, slow and mixed calcium waves were displayed in figure 5.15. In contrast, slow undefined and inactive calcium waves were recorded in non-stimulated SY5Y culture. Results show that SY5Y cells containing pSYN1-ChR2-YFP and pCaMKII-ChR2-YFP are responsive to light stimulation, however, pSYN1-ChR2-YFP activated higher calcium transients than pCaMKII-ChR2-YFP. Further analysis of 40 ROIs revealed that upon light-stimulation, the number of multipeak spikes were increased significantly in cells containing pSYN1-ChR2-YFP ($P<0.01$; $n=3$), inactive and slow rise waves have transformed to a higher number of slow undefined, burst and mixed waves (Fig. 5.16).

When compared to the negative control groups i.e. non-transduced Axol (Fig. 5.17a) and non-transduced SY5Y cells (Fig. 5.17b), slow undefined and inactive calcium waves were found in non-stimulated cells as well as stimulated, no increase of calcium activity was observed upon light stimulation. Results indicate that Axol and SY5Y cells may consist of very early developing neurons which have slow calcium activity, however, successful targeting of neurons and triggering neuronal activity using cell type-specific promoters have achieved.

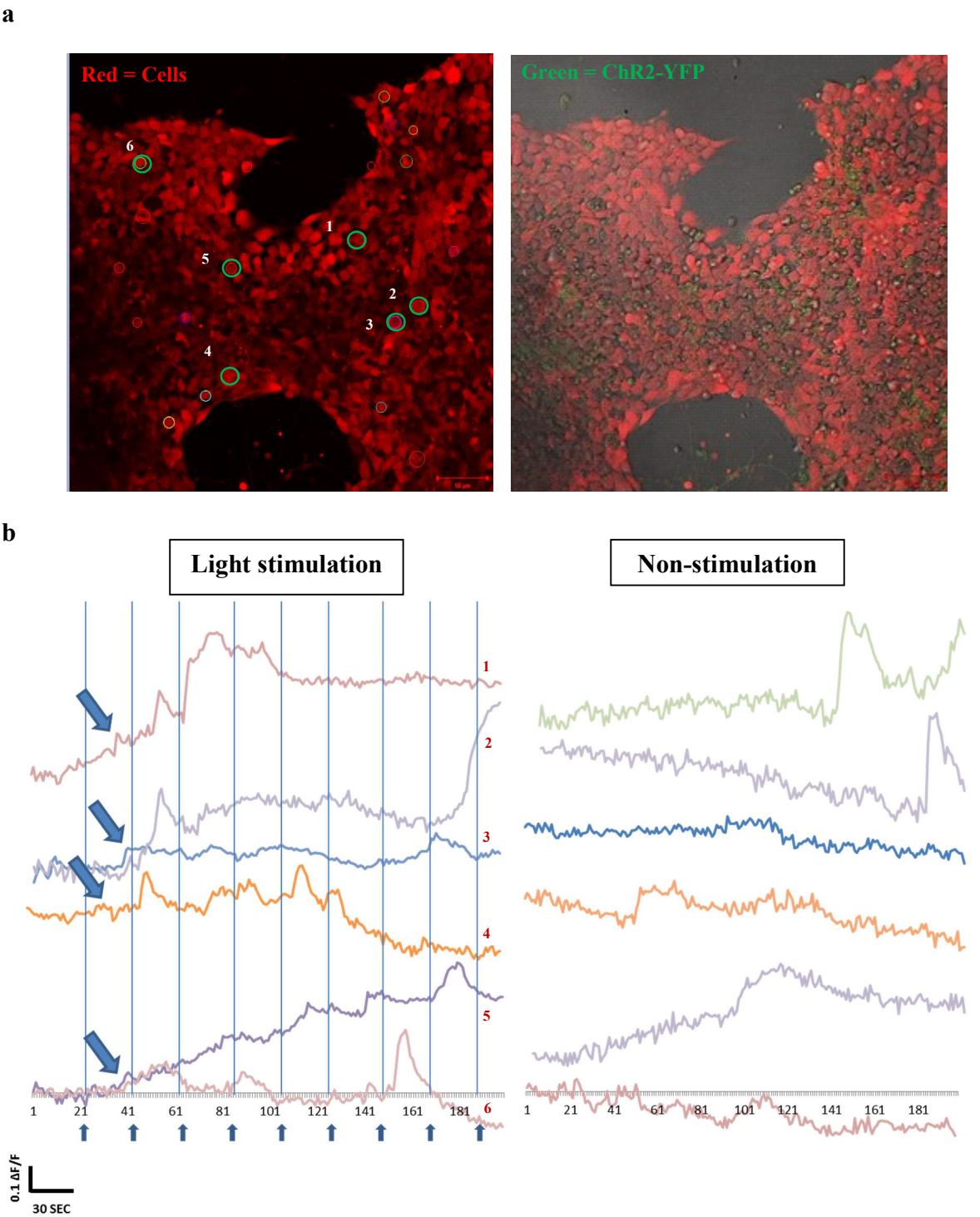

Figure 5.11: Axol-ChR2-YFP driven by SYN1 promoter is responsive to light stimulation.
(a) Axol cells were stained with calcium dye (red) and the region of interests (ROIs) or selected single cells were labelled with number (left). pSYN1-ChR2-YFP was expressed (green) in the culture and the location was shown in a merged image of bright field and fluorescence micrograph (right). (b) The cells were selected from the ROIs as marked in figure a, and stimulated with laser at 488 nm every 30 sec (200 frames) , the fluorescence intensity was normalised to the level of baseline fluorescence measured before the onset of the calcium signal (ΔF/F). Arrow: activated calcium spikes; small arrow: light stimulation; circle: region of interest (ROI). Scale bar: 50 µm.

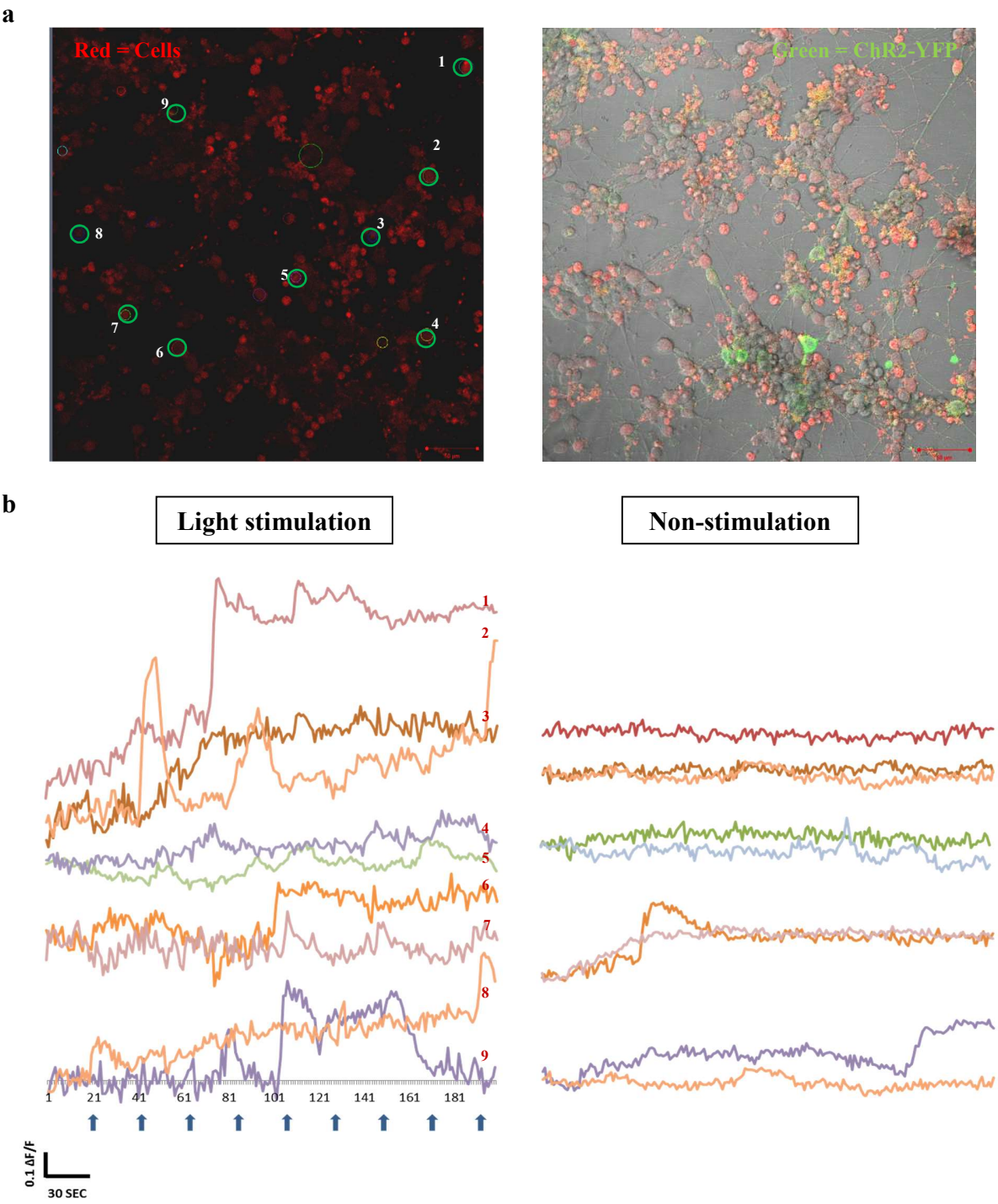

Figure 5.12: Axol-ChR2-YFP driven by CaMKII promoter is responsive to light stimulation.
(a) Axol cells were stained with calcium dye (red) and the region of interests (ROIs) or selected single cells were labelled with number (left). pCaMKII-ChR2-YFP was expressed (green) in the culture and the location was shown in a merged image of bright field and fluorescence micrograph (right). (b) The cells were selected from the ROIs as marked in figure a, and stimulated with laser at 488 nm every 30 sec (200 frames), the fluorescence intensity was normalised to the level of baseline fluorescence measured before the onset of the calcium signal (ΔF/F). Small arrow: light stimulation; circle: region of interest (ROI). Scale bar: 50 µm.

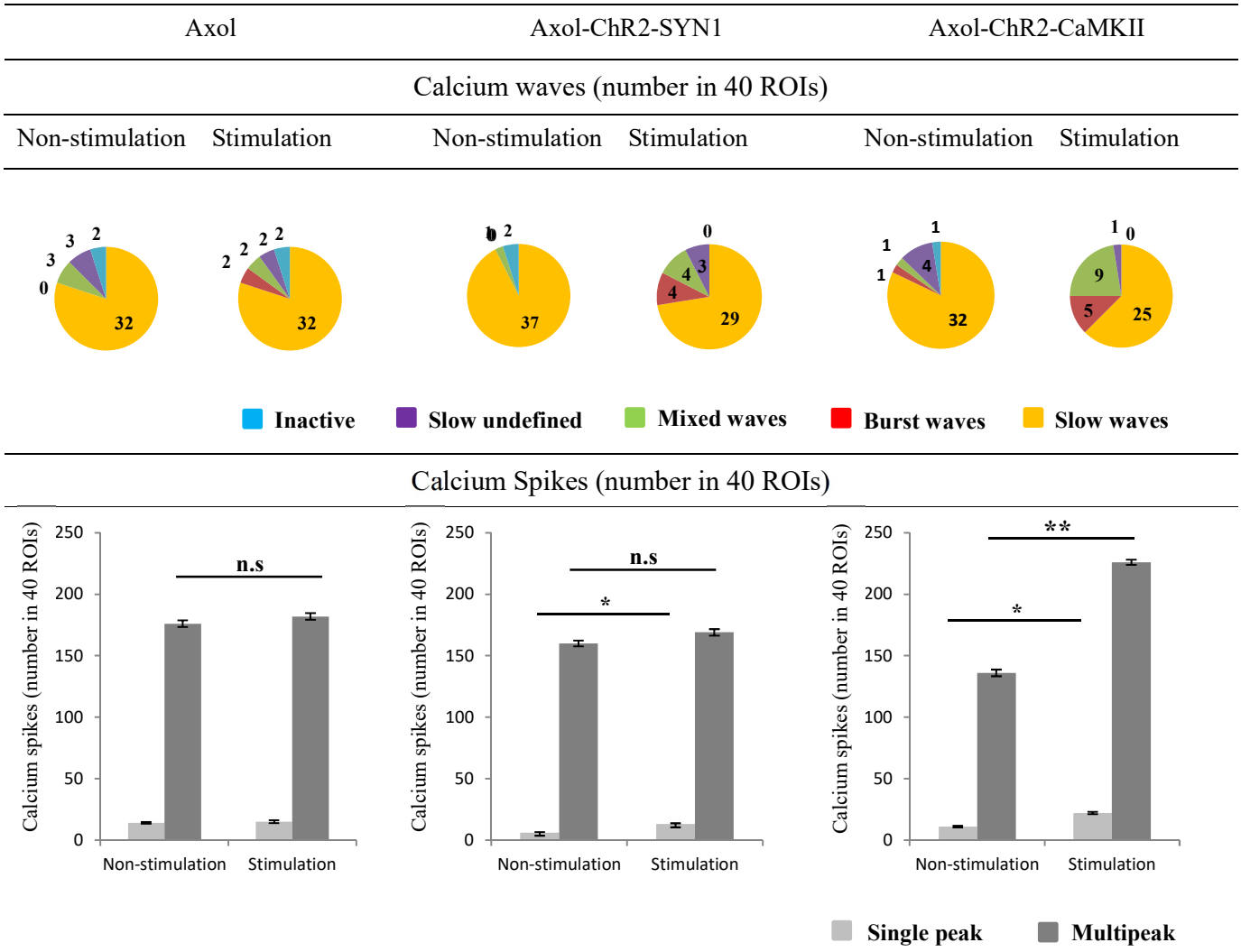

Figure 5.13: Axol cells - ROIs were distinguished with five types of calcium waves (pie charts) and further identified with two types of calcium spikes (bar charts) to evaluate their action potentials upon light stimulation (refer Fig. 5.6)

Calcium waves were analysed from the ROIs of non-stimulated and stimulated cells derived from transduced cells (Axol-ChR2-SYN1 and Axol-ChR2-CaMKII) and non-transduced cells (Axol) (ROIs=40, n=3). Higher number of burst waves and multipeak spikes were found in the cells under the control of CaMKII promoter upon stimulation.
Calcium spikes (single and multipeak) were identified from the selected 40 ROIs in the pie chart (ROIs=40, n=3). Significance was tested by two-way ANOVA * = $p<0.05$; n.s denoted a non-significant value and error bars represent standard deviation (±SD).

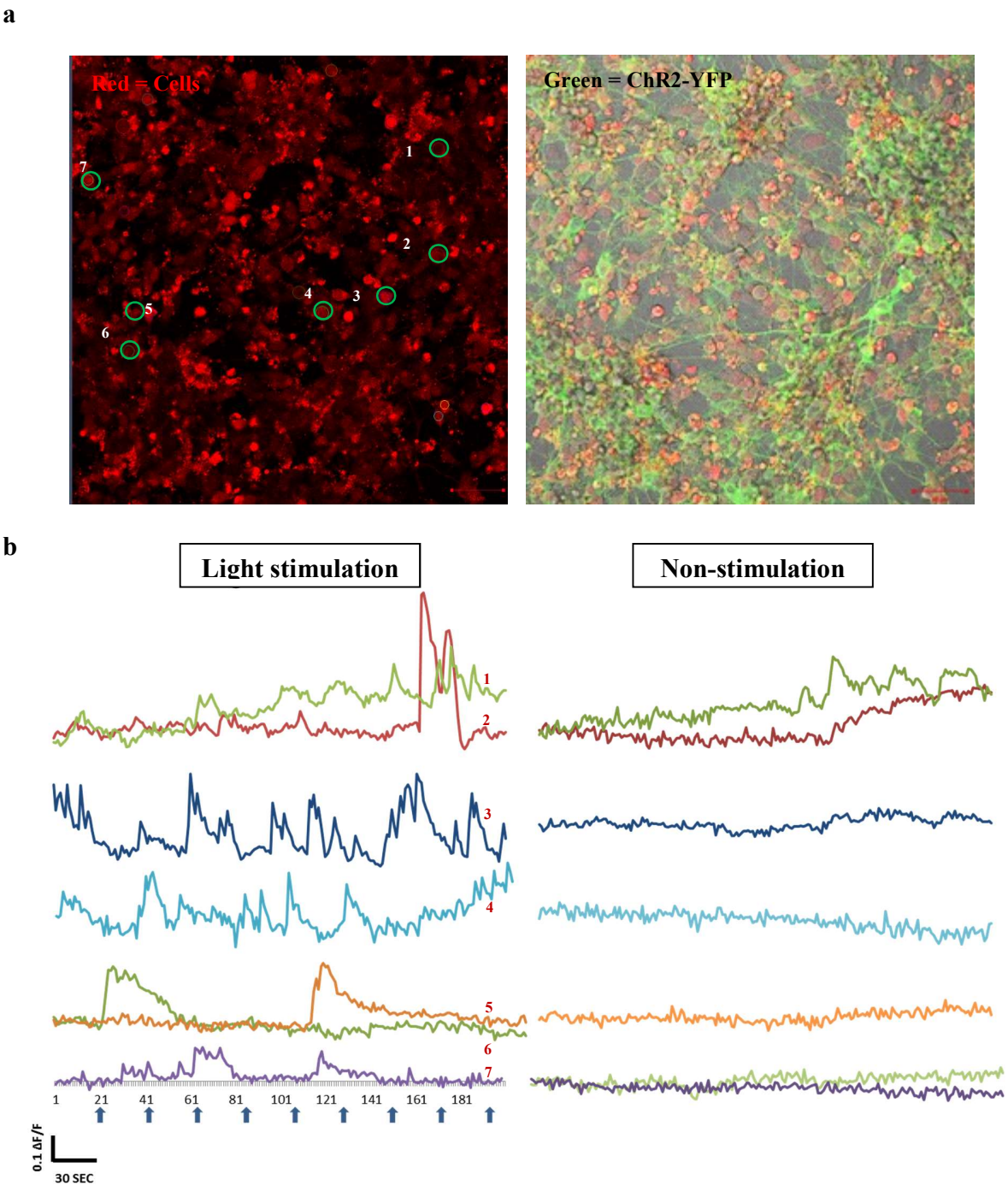

Figure 5.14: SY5Y-ChR2-YFP driven by SYN1 promoter is responsive to light stimulation.
(a) SY5Y cells were stained with calcium dye (red) and the region of interests (ROIs) or selected single cells were labelled with number (left). pSYN1-ChR2-YFP was expressed (green) in the culture and the location was shown in a merged image of bright field and fluorescence micrograph (right). (b) The cells were selected from the ROIs as marked in figure a, and stimulated with laser at 488 nm every 30 sec (200 frames), the fluorescence intensity was normalised to the level of baseline fluorescence measured before the onset of the calcium signal (ΔF/F). Small arrow: light stimulation; circle: region of interest (ROI). Scale bar: 50 µm.

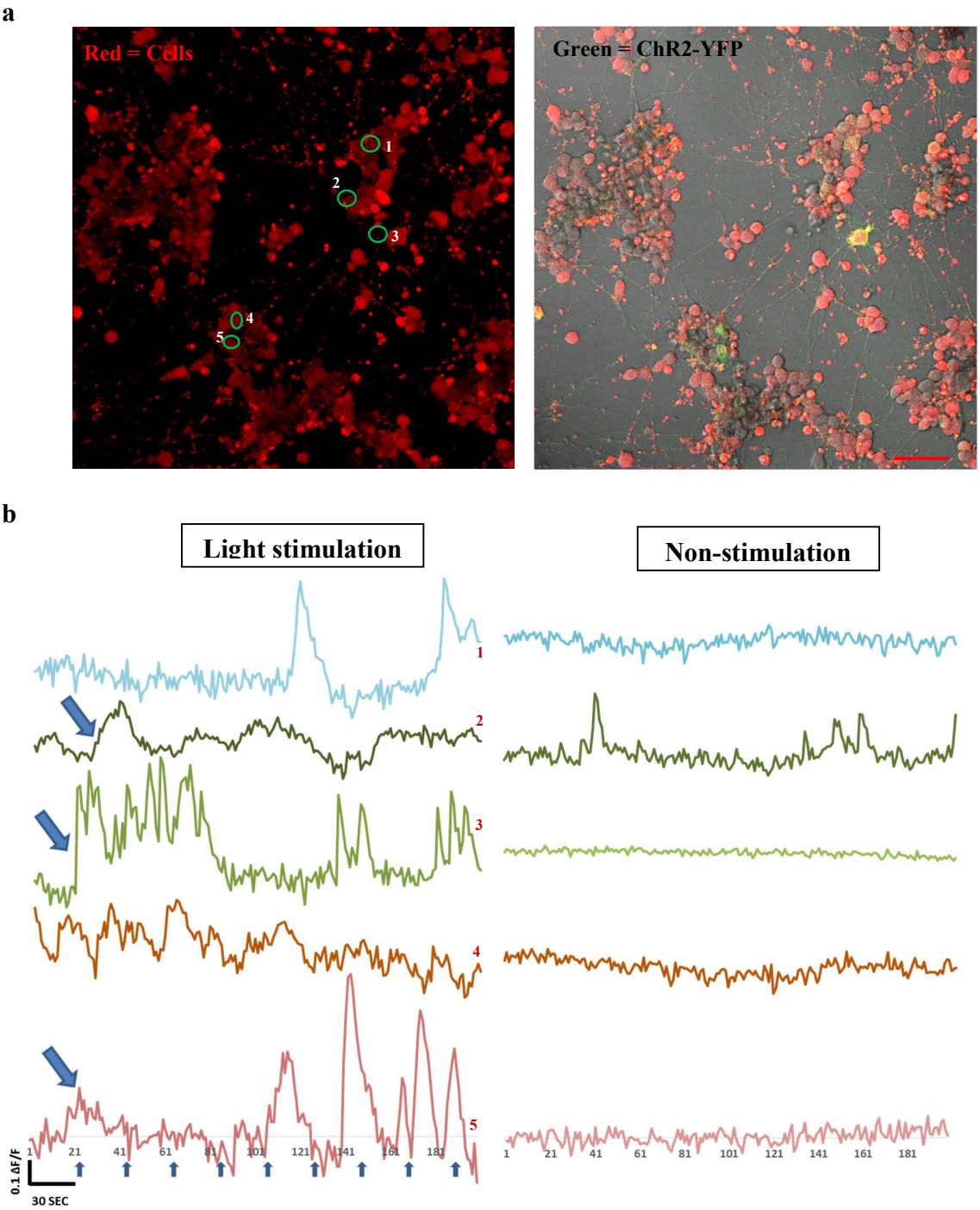

Figure 5.15: SY5Y-ChR2-YFP driven by CaMKII promoter is responsive to light stimulation.
(a) SY5Y cells were stained with calcium dye (red) and the region of interests (ROIs) or selected single cells were labelled with number (left). pCaMKII-ChR2-YFP was expressed (green) in the culture and the location was shown in a merged image of bright field and fluorescence micrograph (right). (b) The cells were selected from the ROIs as marked in figure a, and stimulated with laser at 488 nm every 30 sec (200 frames), the fluorescence intensity was normalised to the level of baseline fluorescence measured before the onset of the calcium signal (ΔF/F). Arrow: activated calcium spikes; small arrow: light stimulation; circle: region of interest (ROI). Scale bar: 50 µm.

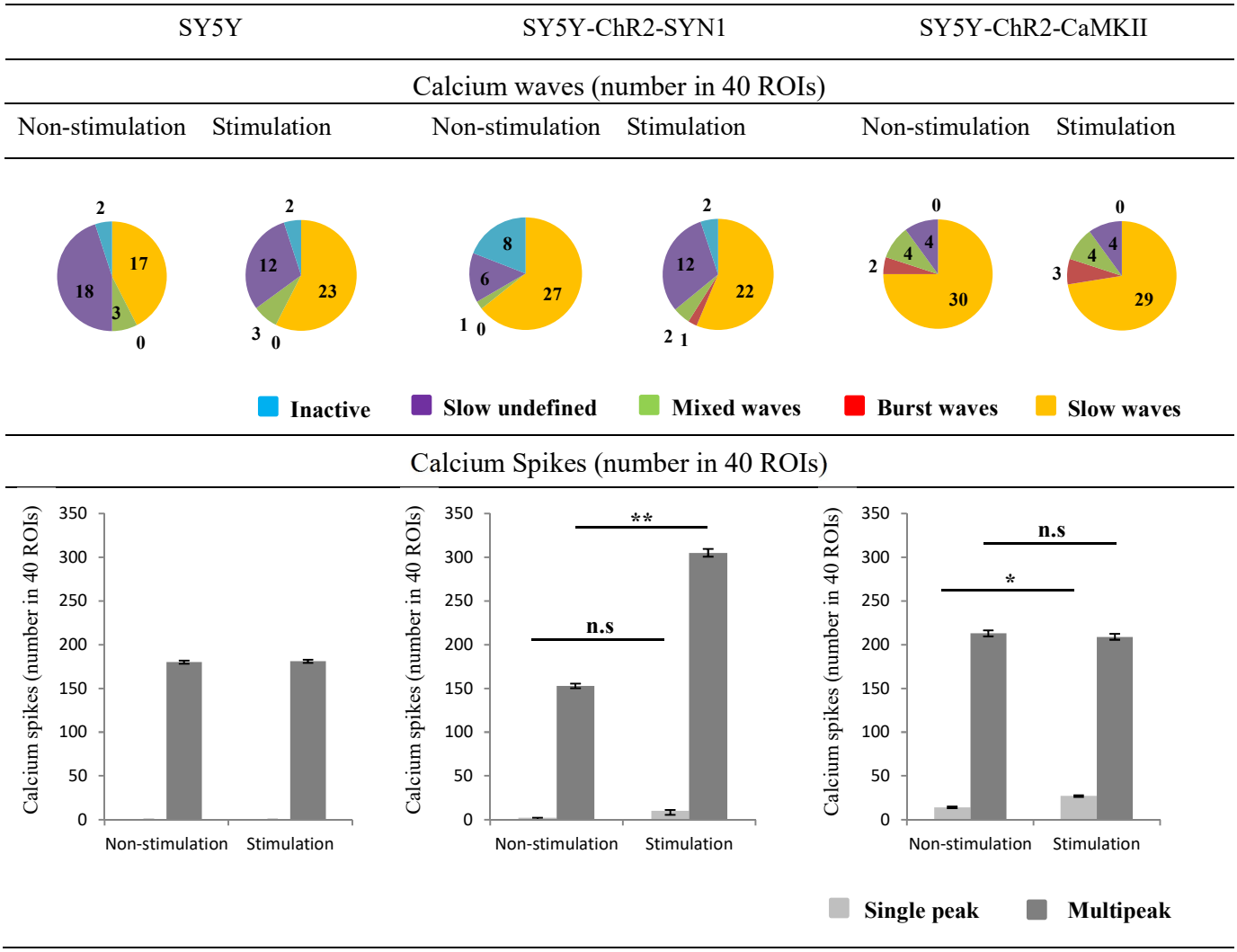

Figure 5.16: SY5Y cells - ROIs were distinguished with five types of calcium waves (pie charts) and further identified with two types of calcium spikes (bar charts) to evaluate their action potentials upon light stimulation (refer Fig. 5.6)

Calcium waves were analysed from the ROIs of non-stimulated and stimulated cells derived from transduced cells (SY5Y-ChR2-SYN1 and SY5Y-ChR2-CaMKII) and non-transduced cells (SY5Y) (ROIs=40, n=3). Number of slow waves reduced and multipeak spikes increased were found in the cells under the control of SYN1 promoter upon stimulation.
Calcium spikes (single and multipeak) were identified from the selected 40 ROIs in the pie chart (ROIs=40, n=3). Significance was tested by two-way ANOVA * = $p<0.05$; P** value = < 0.01; n.s denoted a non-significant value. Error bars represent standard deviation (±SD).

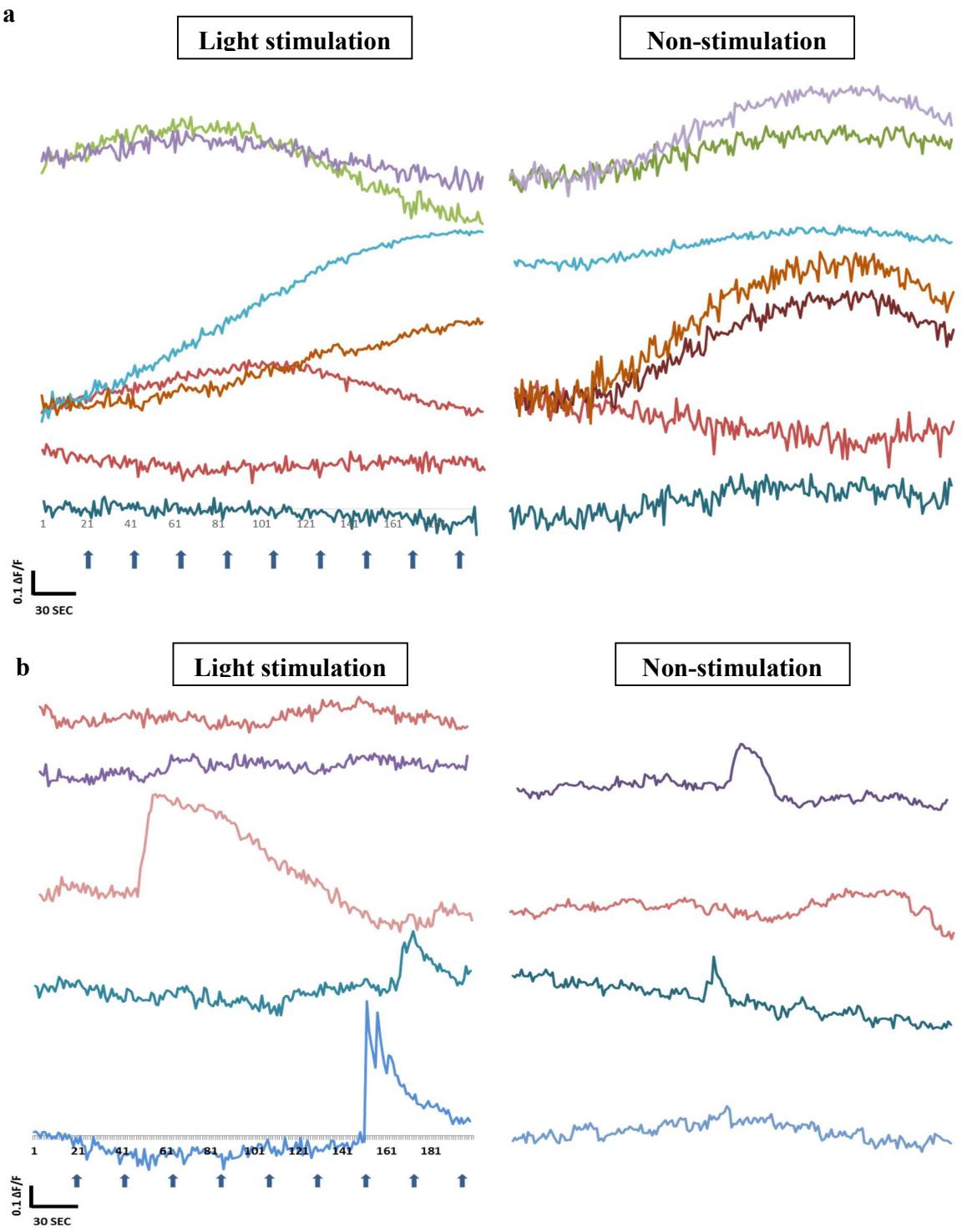

Figure 5.17: Non-transduced cells were served as a negative control in the study.
(a) Axol cells and (b) SY5Y cells were stained with calcium dye (CAL-590, 10 µM at room temperature) and the spontaneous calcium firing was recorded (right). The cells were selected from the ROIs and stimulated with laser at 488 nm every 30 sec (200 frames) (left). The fluorescence intensity was normalised to the level of baseline fluorescence measured before the onset of the calcium signal (ΔF/F). Arrow: light stimulation. Scale bar: 50 µm.

5.4 Application of calcium imaging in a 3D culture model

Calcium imaging has been established and optimised for the functional analysis of neuronal network in 2D culture (refer section 5.0 – 5.1). In chapter 4, a 3D culture system (functionalised alginate hydrogel) was improved to support different type of neurons; however neuronal activities of these cells encapsulated in alginate hydrogel system have not been investigated. The final section of this study is to investigate calcium activity of neurons (Axol) in a 3D model.

Optogenetically modified Axol cells encapsulated in alginate respond to light stimulation and the active cells with action potentials were detected using calcium imaging (Fig. 5.18). In the 3D systems, Axol cells containing pCaMKII-ChR2-YFP (number of active cells in: channel system = 16; bead system = 12) expressed higher calcium transients compared to pSYN1-ChR2-YFP (number of active cells in: channel system = 10; bead system = 10) (Fig. 5.19a).

Further analysis of total 34 active cells on calcium spikes demonstrated an increased number of single spikes in Axol cells under the control of CaMKII promoter only in the channel system (Fig. 5.19b). However, RGD-alginate beads showed increase single spikes in the cells under the control of both SYN1 and CaMKII promoters ($P<0.05$).

Upon light-stimulation, the neuronal function of Axol cells in 3D culture system demonstrated mixed of single and multipeak spikes. In line with the findings on 2D culture, cells containing pCaMKII-ChR2-YFP were found to generate higher calcium transient and calcium spikes than pSYN1-ChR2-YFP particularly in 3D channel system. Conversely, RGD-alginate beads showed similar calcium events in the cells containing pCaMKII-ChR2-YFP and pSYN1-ChR2-YFP when stimulated with light.

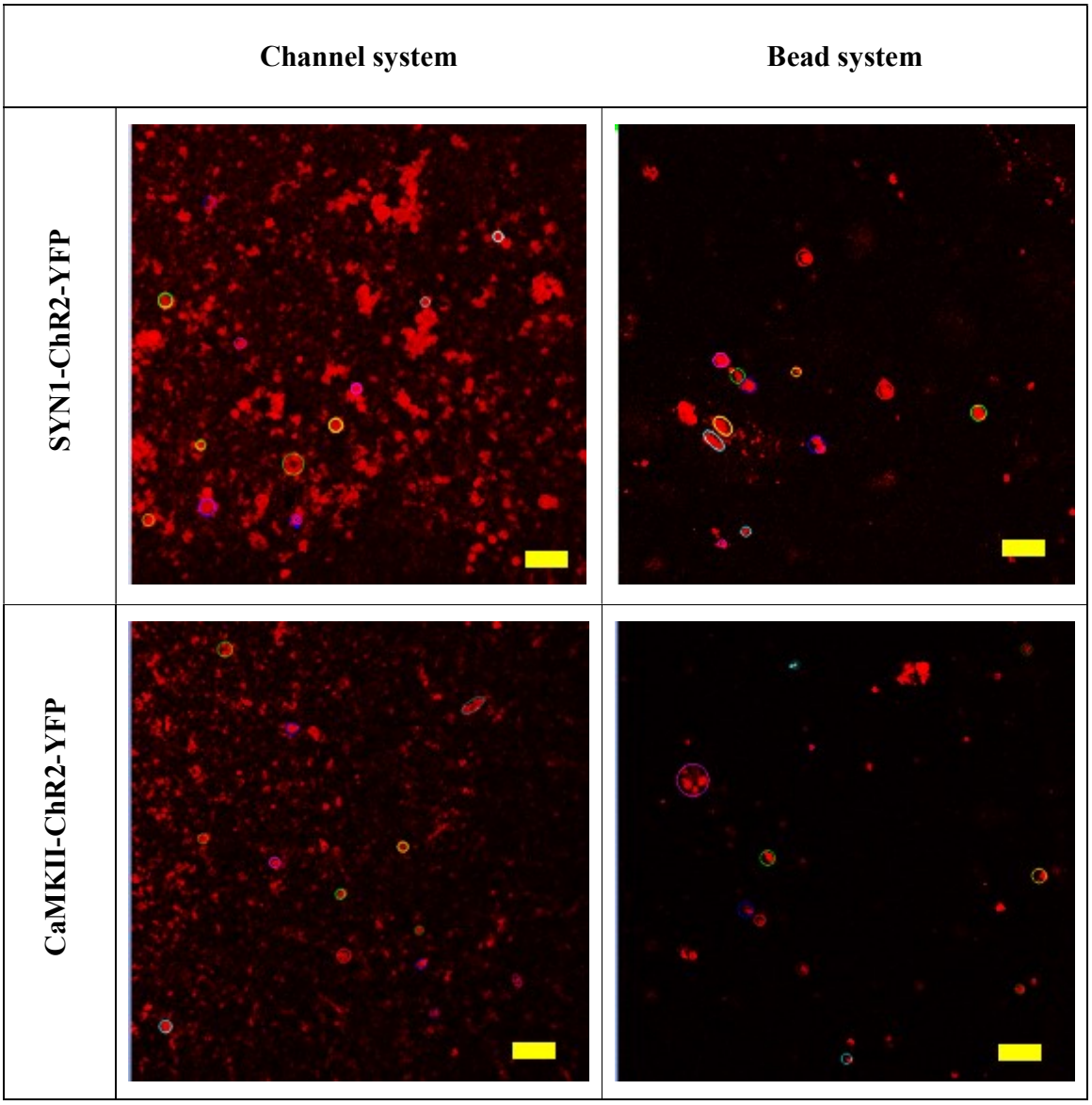

Figure 5.18: Axol cells cultured in channel system and bead system take up the calcium dye (CAL-590).

The cells in 3D culture systems were stained red (CAL-590). The alginate hydrogels are transparent allowing detection of calcium transient. Selected ROIs were further analysed to identify the number of active cells and type of calcium spikes. Images were captured using confocal microscopy (Zeiss-LSM 710) and processed with ZEN light 2011 software. Circle: region of interest. Scale bar: 100 µm.

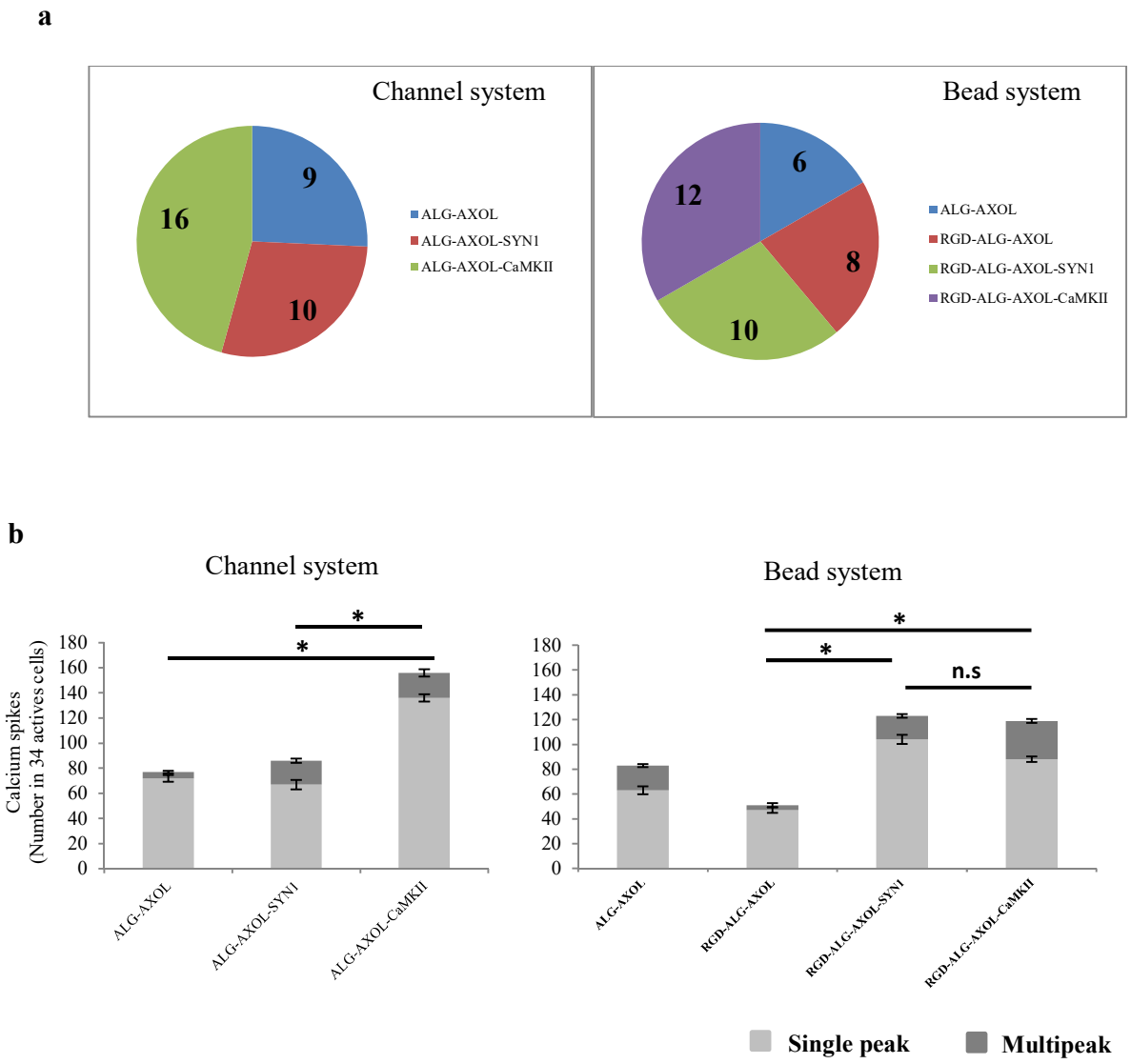

Figure 5.19: Both channel and bead systems demonstrated (a) highest number of active cells and (b) increase number of calcium spikes in Axol-ChR2-YFP under the control of CaMKII promoter.

(a) Data shows the number of active cells (generate action potentials) obtained in the culture containing different promoters, with most active cells expressed under the control of CaMKII promoter in both channel and bead system. The cells were encapsulated in channel system (alginate, ALG) and bead system (RGD-alginate, RGD-ALG), stained with calcium dye and imaged using confocal microscopy (Zeiss-LSM 710). (b) 34 active cells were selected from the ROIs (N=3) and stimulated with light before further analysed the type and number of calcium spikes. Significance was tested by two-way ANOVA * = $p<0.05$; n.s denoted a non-significant value. Error bars represent standard deviation (±SD).

5.5 Discussion

Previous studies have shown that murine ESC- and hESC-derived neurons display basic neurophysiological activity in culture, such as action potential (AP) firing and synaptic currents [76, 324-326]. The neuronal activity of hPSC-derived neurons (Axol) expressing ChR2 driven by the SYN1 and CaMKII promoters was assessed by calcium imaging in the present study. Optimal calcium signals and efficient staining of CAL-590 was achieved at a concentration of 10 µM (optimised with 1% Pluronic-F127) (Fig.5.3). Both Axol and SY5Y cells expressing ChR2 were responsive to light stimulation, giving different firing pattern and calcium events.

In general, light stimulation raised more repetitive APs than non-stimulation. Normal repetitive pattern of neuronal activity was shown in primary mouse neurons (E14.5) indicated that membrane depolarisation was triggered by light with specific neuronal subtype has been successfully targeted by SYN1 and CaMKII promoter. When compared to non-stimulated primary mouse neurons (non-transduced/wild type), non-stimulated Axol and SY5Y cells with ChR2 expression have generated a lower number of repetitive APs and mixed waves were observed (Fig. 5.7-5.9). These results imply that neuronal function of Axol and SY5Y cells may require longer time to recover after being optogenetically modified and passaged in the culture. These cells were differentiated from hiPSCs and neuroblastoma cells which later appeared as early formed neurons with less AP firing than wild type.

Further findings of this study suggest that the response of different cell types is correlated to the cell-type specific promoters used to target ChR2 expression. For example, in Axol neurons, ChR2 expression driven by the CaMKII promoter (associated to glutamatergic neurons) resulting in higher levels of calcium activity and calcium spikes upon light stimulation than with ChR2 expression driven by the SYN1 promoter (Fig. 5.11-5.13). Specifically, bursting and mixed

calcium waves were increased. Conversely, a higher level of calcium flux was observed in SY5Y neurons expressing ChR2 that driven by the SYN1 (pan-neuronal promoter, associated to GABAergic neurons). A significant increase of multipeak spikes with mixed, burst and undefined calcium waves ($p<0.01$) was observed (Fig. 5.14-5.16).

In comparison to other studies, Weick et al. have utilised SYN1 promoter [266] to drive ChR2 expression in hESC-derived neurons with a variety of neurotransmitter phenotypes. Light stimulation of these cells expressing ChR2 could reliably drive AP frequencies (5-30Hz) depending on cell maturity. ChR2 stimulation induced post-synaptic currents in glutamatergic and GABAergic neurons both *in vitro* and *in vivo* (within transplanted tissue) for at least six months. This agrees with the results in this thesis, in that cell-type specific targeting using promoters to label GABAergic and glutamatergic neurons may depend on the maturity of neurons and their quantity in the culture. Cell type, maturation of neurons and neural subtype are the key factors that contribute to the different findings on the neural network activities between Axol and SY5Y cells. CaMKII worked better in Axol cells possibly in part to the neuronal maturation achieved in higher passages and longer cultures. Nevertheless, pan neuronal promoter pSYN1-ChR2-YFP performed better than pCaMKII-ChR2-YFP in SY5Y cells because low number of glutamatergic neurons was found in the culture.

Some recent studies have used iPSC-derived neurons to show the integration of stem cell graft–host neural circuits. In an *in vitro* model of epileptic tissue, Avaliani, N. et al. reported that 6-week differentiation of hiPSC-derived self-renewing neuroepithelial stem cells showed functional afferent synaptic input [327]. Following by selective stimulation of host neurons in transgenic mice with ChR2 expression, the transplanted cells received afferent input from the host brain 6 months after grafting.

On the other hand, Colasante, G. and colleagues have direct-differentiated functional GABAergic interneurons from mouse fibroblasts (by transcription factors such as Foxg1, Sox2, Ascl1, Dlx5, and Lhx6). The cells were demonstrated functionally transmitting and synaptically linked to the host neuronal networks. This competency was confirmed using optogenetics strategy to activate interneurons that transduced with ChR2-expressing lentivirus [328].

The goal to create *in vitro* models of neural networks that closely resemble those found *in vivo* has been a challenge. Several groups have worked on efficient neural differentiation but mostly in 2D culture system. For example, Shi, Y. et al. cultured and directly differentiated cells on poly-ornithine and laminin-coated plates. They found that hPSC-derived cortical neurons showed neuronal activity, and began to form physical synapses before and even after the genesis of astrocytes [222]. We reported here for the first time the generation of a 3D *in vitro* model of neural networks by using alginate hydrogel combined with optogenetic targeting. The findings indicate that hiPSC-derived neurons (Axol) exhibiting selectively driven expression of ChR2 were responsive to light stimulation in the RGD-alginate bead system, increased similar number of calcium spikes in SYN1 and CaMKII regulated Axol cells (Fig. 5.19). However, CaMKII performed better than SYN1 in the alginate channel system upon light stimulation with higher calcium events recorded. The transparent 3D alginate systems not only support survival of Axol cells, but permit penetration of light for ChR2 activation. These advantages allow recording of neurophysiological activity through the visualisation of calcium transients using either calcium imaging or genetically encoded calcium indicators (GECIs).

6.0 General Discussion and Future Perspectives

6.1 General Discussion

6.1.1 General findings

Chapter 3:

a) ChR2 was successfully delivered into the targeted cells (Axol and SY5Y) and the expression was mediated by lentiviruses.

b) Transduction conditions of high MOI and re-infection (M2H2 and M1H1) produce strong ChR2 signals. Re-infection does not trigger cell death of Axol and SY5Y cells after lentiviral transduction as the cells remained high viability (Axol: > 80%; SY5Y: > 85%).

c) ChR2 expression was triggered by SYN1 promoter, demonstrating higher expression than CaMKII. However, ChR2 driven by CaMKII promoter exhibits its highest expression level on day 14 after transduction, indicated as the best time point for the application of light-stimulation.

d) Expression of ChR2 in SY5Y cells driven by CaMKII promoter is lower than other promoters, indicating a possibility as a weak promoter.

e) Maturity of the neurons derived from hiPSCs required efficient neural differentiation and a pro-long culture (higher passage) to generate higher number of mature neurons in the population whilst reduce the presence of neural progenitor stem cells.

f) In optogenetically modified Axol cells, the presence of glutamatergic neurons is higher than GABAergic neurons. However, in SY5Y neuroblastoma cell culture, the presence of glutamatergic neurons is similar in number to GABAergic neurons.

Chapter 4:

a) Concentration and flow rate exert significant effects on the size of alginate beads. In low flow rate (e.g. 2 and 2.5 ml/min), increasing the concentration of alginate correlated directly to an increase in bead size. However, the highest flow rate (3 ml/min) reduced the bead size significantly in all concentrations, produced the smallest beads at 1.8% (w/v) alginate concentration with an average diameter of 800µm.

b) Chemical composition of alginate such as high content of guluronic acid and low mannuronic acid including high purity has resulting in the formation of smaller size and rounder beads, making them more suitable for encapsulation and long-term 3D cell culture.

c) 1.8% alginate bead demonstrates higher swelling profile but constant weight loss (degradation: 3-5% throughout the study) when compared to 1.2% which underwent rapid degradation since day 1. Interestingly, RGD conjugated alginate possesses similar swelling profile as 1.2% alginate but constant weigh loss as shown by 1.8% alginate. Higher swelling indicated uptake of higher water content whilst slower degradation profile prevent disintegration of the alginate, suitable for use in long-term culture.

d) There are two factors in regulating protein diffusion within the 3D alginate beads, i.e. (i) molecular weight and structure, and (ii) concentration. BSA is a smaller molecular weight solute that remained higher amount within the 3D alginate bead when compared to laminin, this may due to swelling and uptake of surrounding medium which occurred throughout 7 days of incubation. In addition, increasing concentration of proteins has delayed diffusion rate.

e) Cell type shows different performance in 3D culture. The results reveal that alginate without modification can support astrocytes and SY5Y (neuroblastoma) due to the robustness of these cells, however, hPSCs (HUES-2 and hiPSC-derived neurons, Axol) survived better in RGD modified alginate incorporated with small molecules (ROCKi or ZVAD).

Chapter 5:

a) Electrophysiology using calcium imaging to analyse calcium function of optogenetically modified cells (Axol and SY5Y) was optimised. Improved calcium dye Cal-590 required high concentration, 10 µM for efficient staining to obtain optimal calcium signal although lower concentrations between 0.5 – 4 µM were reported and recommended in other studies.
b) The standard control primary neurons derived from mouse E14.5 were transduced, expressed ChR2 positive and exhibited typical synchronised neural firing upon light stimulation for both SYN1 and CaMKII promoters. Results further indicated that SYN1 and CaMKII promoters are functioning; successfully targeted glutamatergic and GABAergic neurons.
c) 3D culture systems (alginate: channel and bead system) allow detection of calcium signals of the seeded cells, expression of ChR2 was stable in 3D after transferred from 2D culture.

6.1.2 Specific findings

Chapter 3:

Axol and SY5Y cells are successfully modified using optogenetic approach in 2D though lentiviral transduction.

CaMKII promoter which has a lower expression signal was identified as a weak promoter when compared to SYN1 and universal promoter EF1a. However, its application and respond to light stimulation were further confirmed in chapter 5.

Chapter 4:

Functionalised alginate hydrogel provide an enhanced culture microenvironment for hESCs and different neural cell types. Cell viability of hESCs (HUES-2) and SY5Y cells in the 3D culture system was increased when the bio-inert alginate was conjugated with RGD. Both channel system (more spaces have created within the hydrogel) and bead system support survival of SY5Y cells and retained stably ChR2 expression of Axol and SY5Y cells.

Cell death in 3D culture induced by apoptosis can be blocked by ROCKi (54.1%), surprisingly small molecule ZVAD increase cell viability (77.8%), higher than ROCKi at 10 μM. The combination of ROCKi and ZVAD showed approximately 60% of death cells, which may attribute to the concentrations and the possibility of external force including cell disruption during encapsulation-decapsulation. Further evaluation with different concentrations (range from 1-20 μM) and time of treatment (4 -120 hours) are suggested to be included in the future studies.

Chapter 5:

Neuronal activity in response to light stimulation is highly driven by the CaMKII promoter in Axol cells and the SYN1 promoter in SY5Y cells. In Axol cells, more action potentials were observed in CaMKII driven ChR2-expression, generated a higher number of burst and mixed

calcium waves when compared to non-transduced cells. In SY5Y cells, however, more action potentials were observed in SYN1 driven ChR2-expression. Results further confirmed that the differentiated cell population in SY5Y consisting of less glutamatergic neurons. Therefore, pan neuronal promoter SYN1 performed more efficiently in targeting the mixed population of neurons derived from SY5Y. Results also agree that higher glutamatergic neurons than GABAergic neurons present in Axol cells (derived from hiPSCs) since higher calcium activity was triggered in the cells under the control of CaMKI promoter which targeted the excitatory neurons.

Significant increase of calcium spikes driven by CaMKII promoter was observed in both channel and bead alginate system. In alginate beads, SYN1 promoter performed equivalent to CaMKII upon light stimulation. Results suggest that optogenetically modified Axol cells derived from hiPSCs were successfully cultured in a 3D model.

6.2 Conclusions

The results presented in this thesis have shown that lentiviruses mediated successful delivery of ChR2-YFP into neurons derived from human iPSCs (Axol cells) and neuroblastoma (SY5Y cells). Efficient optogenetic targeting using neural-specific promoters SYN1 and CaMKII is also dependent on the increase of mature cells over passages. CaMKII promoters targeted higher proportion of glutamatergic neurons.

The second part of this thesis has shown a functionalised hydrogel, RGD-alginate incorporated with small molecule ROCKi was developed, enable 3D culture of human pluripotent stem cells (hESCs), neural derivatives (Axol cells) and neurons (SY5Y cells) (Fig. 4.1). As shown in chapter 4, a syringe extrusion method with liquid flow was successfully adjusted at the highest flow rate (3 ml/min) and a concentration of 1.8% UP-MVG alginate was used to produce spherical microbeads with average 800 μm in diameter. Furthermore, the 3D alginate bead and channel system retained the expression of ChR2 when the optogenetically modified cells being transferred from 2D culture.

In this study, a functional 2D neural culture model was established using ChR2 expressing human neurons. When transferred to RGD-alginate hydrogels, a functional neural network was successfully cultured in 3D. As detailed in chapter 5, pCaMKII-ChR2-YFP exhibited higher neuronal activity in Axol cells than pSYN1-ChR2-YFP, vice versa pSYN1-ChR2-YFP was found to exhibit more calcium events in SY5Y cells. CaMKII is confirmed as a weak promoter but was proven functional when tested with primary neurons. In conclusion, optogenetics enable the assessment of neuronal activity of differentiated neurons from hiPSCs in a 3D alginate hydrogel model.

6.3 Future Perspectives

6.3.1 Improving neural networks by efficient differentiation and co-culturing with astrocytes

Results presented in this thesis show a link between neuron maturity (cell type), efficiency of specific cell targeting (cell-type specific promoters) and neuronal function (calcium flux an AP firing). The maturation of neurons derived from hPSCs and SY5Y cells is crucial because increased maturation is necessary to give rise to more functional glutamatergic and GABAergic neurons, allowing optogenetic targeting with neural-specific promoters such as CaMKII (excitatory cell promoter) and SYN1 (pan neuronal promoter). Synchronous calcium firing with repetitive APs was demonstrated by primary rodent neurons investigated in this study, whilst Axol and SY5Y cells produced early developing neurons. Cell type and neuronal differentiation play an important role in developing functional neural networks. Alternate differentiation medium and protocols that can efficiently drive Axol and SY5Y to become more mature neurons should be considered in the future. For instance, Bardy et al. have recently discovered that certain amino acids (such as glycine and glutamate) are ligands for neurotransmission receptors that suppress neuronal activity and should be removed or reduced [321]. Another method to mature cultured hiPSC-derived neurons (Axol) and SY5Y cells as well as to increase their neuronal activity is to co-culture with astrocytes. Synapse maturation occurs more rapidly in the presence of physical contact with astrocytes [329].

6.3.2 Refine the hydrogel model for a defined and robust culture system

In chapter 4, it has been shown that RGD-alginate hydrogels that incorporated with small molecules ROCKi or ZVAD increased long term viability of human pluripotent stem cells. However, apoptotic and necrotic cells were found in both alginate and RGD-alginate beads, and

in particularly for the cells treated with the combination of both ROCKi and ZVAD. It would be interesting to investigate if the concentrations of these two small molecules and proportions could be optimised to prevent apoptosis in 3D culture system. Since the use of ZVAD inhibitor alone has demonstrated a superior result than ROCKi, further investigation and application of ZVAD should perform in the future study. Moreover, the microenvironment of alginate hydrogels can be enhanced by using RGD peptides with appropriate conformation or spacing and conjugation density to support an optimal level of hPSC adhesion, spreading and proliferation. Peptides other than RGD are also worth exploring if their use can further increase cell-cell and cell-ECM interactions. One of the limitations in this project is that the use of static culture conditions results in an inability to precisely control forces and exchange of oxygen, nutrients, and wastes within a 3D system. An alternative approach would be to use the dynamic culture conditions or bioreactors that create an optimal culture environment suitable for supporting cell proliferation.

6.3.3 The investigation of neural networks in 3D hydrogels combined calcium imaging with multielectrode array (MEA) recording

The results reported in this thesis suggest that neural networks can be cultured in a 3D alginate system, and that ChR2 expression in encapsulated Axol cells can drive the cells to be responsive to light stimulation. The neuronal activity in 3D hydrogel model with ChR2 expression driven by CaMKII and SYN1 promoters was recorded by calcium imaging. Investigating neural networks required a suitable functional evaluation method. Calcium imaging was successfully set up in this study for 2D and 3D imaging, it was found to be deemed suitable for alginate hydrogels which are transparent thus allowing penetration of both calcium dyes and laser light. It is possible to gather a rapid and accurate picture of whole network activity through use of MEA that record from the lower layers of 3D neural cultures. The combination of calcium imaging and MEA analysis would provide further details on the neurological activity of the cells with optical

stimulation being less invasive to the samples and permitting real-time and multi-point measurement. Therefore, future work should involve both the use of MEA system to rapidly record network electrical activity (where feasible) together with the use of calcium imaging for the investigation of neuronal activity in 3D. Initial set up of MEA and the preliminary data are attached in Appendix 10. In addition, the standard and conventional method, patch clamp should be included for the investigation of functional connectivity of the neurons.

References

1. Deisseroth, K., Optogenetics. *Nature methods* **2011,** 8, (1), 26-9.
2. Boyden, E. S.; Zhang, F.; Bamberg, E.; Nagel, G.; Deisseroth, K., Millisecond-timescale, genetically targeted optical control of neural activity. *Nature neuroscience* **2005,** 8, (9), 1263-8.
3. Crick, F. H., Thinking about the brain. *Scientific American* **1979,** 241, (3), 219-32.
4. Zhang, F.; Gradinaru, V.; Adamantidis, A. R.; Durand, R.; Airan, R. D.; de Lecea, L.; Deisseroth, K., Optogenetic interrogation of neural circuits: technology for probing mammalian brain structures. *Nature protocols* **2010,** 5, (3), 439-56.
5. Mei, Y.; Zhang, F., Molecular tools and approaches for optogenetics. *Biological psychiatry* **2012,** 71, (12), 1033-8.
6. Zhang, F.; Vierock, J.; Yizhar, O.; Fenno, L. E.; Tsunoda, S.; Kianianmomeni, A.; Prigge, M.; Berndt, A.; Cushman, J.; Polle, J.; Magnuson, J.; Hegemann, P.; Deisseroth, K., The microbial opsin family of optogenetic tools. *Cell* **2011,** 147, (7), 1446-57.
7. Lozier, R. H.; Bogomolni, R. A.; Stoeckenius, W., Bacteriorhodopsin: a light-driven proton pump in Halobacterium Halobium. *Biophysical journal* **1975,** 15, (9), 955-62.
8. Chow, B. Y.; Han, X.; Boyden, E. S., Genetically encoded molecular tools for light-driven silencing of targeted neurons. *Progress in brain research* **2012,** 196, 49-61.
9. Nagel, G.; Ollig, D.; Fuhrmann, M.; Kateriya, S.; Musti, A. M.; Bamberg, E.; Hegemann, P., Channelrhodopsin-1: a light-gated proton channel in green algae. *Science* **2002,** 296, (5577), 2395-8.
10. Nagel, G.; Szellas, T.; Huhn, W.; Kateriya, S.; Adeishvili, N.; Berthold, P.; Ollig, D.; Hegemann, P.; Bamberg, E., Channelrhodopsin-2, a directly light-gated cation-selective membrane channel. *Proceedings of the National Academy of Sciences of the United States of America* **2003,** 100, (24), 13940-5.
11. Fenno, L.; Yizhar, O.; Deisseroth, K., The development and application of optogenetics. *Annual review of neuroscience* **2011,** 34, 389-412.
12. Muller, M.; Bamann, C.; Bamberg, E.; Kuhlbrandt, W., Projection structure of channelrhodopsin-2 at 6 A resolution by electron crystallography. *Journal of molecular biology* **2011,** 414, (1), 86-95.
13. Zhang, F.; Wang, L. P.; Boyden, E. S.; Deisseroth, K., Channelrhodopsin-2 and optical control of excitable cells. *Nature methods* **2006,** 3, (10), 785-92.
14. Nagel, G.; Brauner, M.; Liewald, J. F.; Adeishvili, N.; Bamberg, E.; Gottschalk, A., Light activation of channelrhodopsin-2 in excitable cells of Caenorhabditis elegans triggers rapid behavioral responses. *Current biology : CB* **2005,** 15, (24), 2279-84.
15. Schroll, C.; Riemensperger, T.; Bucher, D.; Ehmer, J.; Voller, T.; Erbguth, K.; Gerber, B.; Hendel, T.; Nagel, G.; Buchner, E.; Fiala, A., Light-induced activation of distinct modulatory neurons triggers appetitive or aversive learning in Drosophila larvae. *Current biology : CB* **2006,** 16, (17), 1741-7.
16. Petreanu, L.; Huber, D.; Sobczyk, A.; Svoboda, K., Channelrhodopsin-2-assisted circuit mapping of long-range callosal projections. *Nature neuroscience* **2007,** 10, (5), 663-8.
17. Arenkiel, B. R.; Peca, J.; Davison, I. G.; Feliciano, C.; Deisseroth, K.; Augustine, G. J.; Ehlers, M. D.; Feng, G., In vivo light-induced activation of neural circuitry in transgenic mice expressing channelrhodopsin-2. *Neuron* **2007,** 54, (2), 205-18.
18. Adamantidis, A. R.; Zhang, F.; Aravanis, A. M.; Deisseroth, K.; de Lecea, L., Neural substrates of awakening probed with optogenetic control of hypocretin neurons. *Nature* **2007,** 450, (7168), 420-4.
19. Dugue, G. P.; Akemann, W.; Knopfel, T., A comprehensive concept of optogenetics. *Progress in brain research* **2012,** 196, 1-28.
20. LaLumiere, R. T., A new technique for controlling the brain: optogenetics and its potential for use in research and the clinic. *Brain stimulation* **2011,** 4, (1), 1-6.

21. Gunaydin, L. A.; Yizhar, O.; Berndt, A.; Sohal, V. S.; Deisseroth, K.; Hegemann, P., Ultrafast optogenetic control. *Nature neuroscience* **2010,** 13, (3), 387-92.
22. Berndt, A.; Yizhar, O.; Gunaydin, L. A.; Hegemann, P.; Deisseroth, K., Bi-stable neural state switches. *Nature neuroscience* **2009,** 12, (2), 229-34.
23. Lin, J. Y., A user's guide to channelrhodopsin variants: features, limitations and future developments. *Experimental physiology* **2011,** 96, (1), 19-25.
24. Schoenenberger, P.; Gerosa, D.; Oertner, T. G., Temporal control of immediate early gene induction by light. *PloS one* **2009,** 4, (12), e8185.
25. Kleinlogel, S.; Feldbauer, K.; Dempski, R. E.; Fotis, H.; Wood, P. G.; Bamann, C.; Bamberg, E., Ultra light-sensitive and fast neuronal activation with the Ca(2)+-permeable channelrhodopsin CatCh. *Nature neuroscience* **2011,** 14, (4), 513-8.
26. Lin, J. Y., Optogenetic excitation of neurons with channelrhodopsins: light instrumentation, expression systems, and channelrhodopsin variants. *Progress in brain research* **2012,** 196, 29-47.
27. Reichel, M. B.; Bainbridge, J.; Baker, D.; Thrasher, A. J.; Bhattacharya, S. S.; Ali, R. R., An immune response after intraocular administration of an adenoviral vector containing a beta galactosidase reporter gene slows retinal degeneration in the rd mouse. *The British journal of ophthalmology* **2001,** 85, (3), 341-4.
28. Sakamoto, T.; Kimura, H.; Scuric, Z.; Spee, C.; Gordon, E. M.; Hinton, D. R.; Anderson, W. F.; Ryan, S. J., Inhibition of experimental proliferative vitreoretinopathy by retroviral vector-mediated transfer of suicide gene. Can proliferative vitreoretinopathy be a target of gene therapy? *Ophthalmology* **1995,** 102, (10), 1417-24.
29. Miyoshi, H.; Takahashi, M.; Gage, F. H.; Verma, I. M., Stable and efficient gene transfer into the retina using an HIV-based lentiviral vector. *Proceedings of the National Academy of Sciences of the United States of America* **1997,** 94, (19), 10319-23.
30. Lotery, A. J.; Derksen, T. A.; Russell, S. R.; Mullins, R. F.; Sauter, S.; Affatigato, L. M.; Stone, E. M.; Davidson, B. L., Gene transfer to the nonhuman primate retina with recombinant feline immunodeficiency virus vectors. *Human gene therapy* **2002,** 13, (6), 689-96.
31. Walther, W.; Stein, U., Cell type specific and inducible promoters for vectors in gene therapy as an approach for cell targeting. *Journal of molecular medicine* **1996,** 74, (7), 379-92.
32. Bi, A.; Cui, J.; Ma, Y. P.; Olshevskaya, E.; Pu, M.; Dizhoor, A. M.; Pan, Z. H., Ectopic expression of a microbial-type rhodopsin restores visual responses in mice with photoreceptor degeneration. *Neuron* **2006,** 50, (1), 23-33.
33. Wang, J.; Hasan, M. T.; Seung, H. S., Laser-evoked synaptic transmission in cultured hippocampal neurons expressing channelrhodopsin-2 delivered by adeno-associated virus. *Journal of neuroscience methods* **2009,** 183, (2), 165-75.
34. Zhu, P.; Aller, M. I.; Baron, U.; Cambridge, S.; Bausen, M.; Herb, J.; Sawinski, J.; Cetin, A.; Osten, P.; Nelson, M. L.; Kugler, S.; Seeburg, P. H.; Sprengel, R.; Hasan, M. T., Silencing and un-silencing of tetracycline-controlled genes in neurons. *PloS one* **2007,** 2, (6), e533.
35. Shevtsova, Z.; Malik, J. M.; Michel, U.; Bahr, M.; Kugler, S., Promoters and serotypes: targeting of adeno-associated virus vectors for gene transfer in the rat central nervous system in vitro and in vivo. *Experimental physiology* **2005,** 90, (1), 53-9.
36. Palmer, A. E.; Tsien, R. Y., Measuring calcium signaling using genetically targetable fluorescent indicators. *Nature protocols* **2006,** 1, (3), 1057-65.
37. Wallace, D. J.; Meyer zum Alten Borgloh, S.; Astori, S.; Yang, Y.; Bausen, M.; Kugler, S.; Palmer, A. E.; Tsien, R. Y.; Sprengel, R.; Kerr, J. N.; Denk, W.; Hasan, M. T., Single-spike detection in vitro and in vivo with a genetic Ca2+ sensor. *Nature methods* **2008,** 5, (9), 797-804.
38. Miesenbock, G.; De Angelis, D. A.; Rothman, J. E., Visualizing secretion and synaptic transmission with pH-sensitive green fluorescent proteins. *Nature* **1998,** 394, (6689), 192-5.
39. Burger, C.; Gorbatyuk, O. S.; Velardo, M. J.; Peden, C. S.; Williams, P.; Zolotukhin, S.; Reier, P. J.; Mandel, R. J.; Muzyczka, N., Recombinant AAV viral vectors pseudotyped with viral capsids from serotypes 1, 2, and 5 display differential efficiency and cell tropism after delivery to different regions of

the central nervous system. *Molecular therapy : the journal of the American Society of Gene Therapy* **2004,** 10, (2), 302-17.
40. Tenenbaum, L.; Chtarto, A.; Lehtonen, E.; Velu, T.; Brotchi, J.; Levivier, M., Recombinant AAV-mediated gene delivery to the central nervous system. *The journal of gene medicine* **2004,** 6 Suppl 1, S212-22.
41. Sun, J. Y.; Chatterjee, S.; Wong, K. K., Jr., Immunogenic issues concerning recombinant adeno-associated virus vectors for gene therapy. *Current gene therapy* **2002,** 2, (4), 485-500.
42. Yates, F.; Daley, G. Q., Progress and prospects: gene transfer into embryonic stem cells. *Gene therapy* **2006,** 13, (20), 1431-9.
43. Pfeifer, A.; Ikawa, M.; Dayn, Y.; Verma, I. M., Transgenesis by lentiviral vectors: lack of gene silencing in mammalian embryonic stem cells and preimplantation embryos. *Proceedings of the National Academy of Sciences of the United States of America* **2002,** 99, (4), 2140-5.
44. Dottori, M.; Tay, C.; Hughes, S. M., Neural development in human embryonic stem cells-applications of lentiviral vectors. *Journal of cellular biochemistry* **2011,** 112, (8), 1955-62.
45. Jang, J. E.; Shaw, K.; Yu, X. J.; Petersen, D.; Pepper, K.; Lutzko, C.; Kohn, D. B., Specific and stable gene transfer to human embryonic stem cells using pseudotyped lentiviral vectors. *Stem cells and development* **2006,** 15, (1), 109-17.
46. Mazarakis, N. D.; Azzouz, M.; Rohll, J. B.; Ellard, F. M.; Wilkes, F. J.; Olsen, A. L.; Carter, E. E.; Barber, R. D.; Baban, D. F.; Kingsman, S. M.; Kingsman, A. J.; O'Malley, K.; Mitrophanous, K. A., Rabies virus glycoprotein pseudotyping of lentiviral vectors enables retrograde axonal transport and access to the nervous system after peripheral delivery. *Human molecular genetics* **2001,** 10, (19), 2109-21.
47. Cannon, J. R.; Sew, T.; Montero, L.; Burton, E. A.; Greenamyre, J. T., Pseudotype-dependent lentiviral transduction of astrocytes or neurons in the rat substantia nigra. *Experimental neurology* **2011,** 228, (1), 41-52.
48. Liu, B. H.; Wang, X.; Ma, Y. X.; Wang, S., CMV enhancer/human PDGF-beta promoter for neuron-specific transgene expression. *Gene therapy* **2004,** 11, (1), 52-60.
49. Nettelbeck, D. M.; Jerome, V.; Muller, R., A strategy for enhancing the transcriptional activity of weak cell type-specific promoters. *Gene therapy* **1998,** 5, (12), 1656-64.
50. Lee, J. H.; Durand, R.; Gradinaru, V.; Zhang, F.; Goshen, I.; Kim, D. S.; Fenno, L. E.; Ramakrishnan, C.; Deisseroth, K., Global and local fMRI signals driven by neurons defined optogenetically by type and wiring. *Nature* **2010,** 465, (7299), 788-92.
51. Sohal, V. S.; Zhang, F.; Yizhar, O.; Deisseroth, K., Parvalbumin neurons and gamma rhythms enhance cortical circuit performance. *Nature* **2009,** 459, (7247), 698-702.
52. Gloster, A.; Wu, W.; Speelman, A.; Weiss, S.; Causing, C.; Pozniak, C.; Reynolds, B.; Chang, E.; Toma, J. G.; Miller, F. D., The T alpha 1 alpha-tubulin promoter specifies gene expression as a function of neuronal growth and regeneration in transgenic mice. *The Journal of neuroscience : the official journal of the Society for Neuroscience* **1994,** 14, (12), 7319-30.
53. Forss-Petter, S.; Danielson, P. E.; Catsicas, S.; Battenberg, E.; Price, J.; Nerenberg, M.; Sutcliffe, J. G., Transgenic mice expressing beta-galactosidase in mature neurons under neuron-specific enolase promoter control. *Neuron* **1990,** 5, (2), 187-97.
54. Sasahara, M.; Fries, J. W.; Raines, E. W.; Gown, A. M.; Westrum, L. E.; Frosch, M. P.; Bonthron, D. T.; Ross, R.; Collins, T., PDGF B-chain in neurons of the central nervous system, posterior pituitary, and in a transgenic model. *Cell* **1991,** 64, (1), 217-27.
55. Thomson, J. A.; Itskovitz-Eldor, J.; Shapiro, S. S.; Waknitz, M. A.; Swiergiel, J. J.; Marshall, V. S.; Jones, J. M., Embryonic stem cell lines derived from human blastocysts. *Science* **1998,** 282, (5391), 1145-7.
56. Thomson, J. A.; Kalishman, J.; Golos, T. G.; Durning, M.; Harris, C. P.; Becker, R. A.; Hearn, J. P., Isolation of a primate embryonic stem cell line. *Proceedings of the National Academy of Sciences of the United States of America* **1995,** 92, (17), 7844-8.
57. Bongso, A.; Fong, C. Y.; Ng, S. C.; Ratnam, S., Isolation and culture of inner cell mass cells from human blastocysts. *Human reproduction* **1994,** 9, (11), 2110-7.

58. Villa-Diaz, L. G.; Ross, A. M.; Lahann, J.; Krebsbach, P. H., Concise review: The evolution of human pluripotent stem cell culture: from feeder cells to synthetic coatings. *Stem cells* **2013,** 31, (1), 1-7.
59. Niwa, H.; Miyazaki, J.; Smith, A. G., Quantitative expression of Oct-3/4 defines differentiation, dedifferentiation or self-renewal of ES cells. *Nature genetics* **2000,** 24, (4), 372-6.
60. Chambers, I.; Colby, D.; Robertson, M.; Nichols, J.; Lee, S.; Tweedie, S.; Smith, A., Functional expression cloning of Nanog, a pluripotency sustaining factor in embryonic stem cells. *Cell* **2003,** 113, (5), 643-55.
61. Boyer, L. A.; Lee, T. I.; Cole, M. F.; Johnstone, S. E.; Levine, S. S.; Zucker, J. P.; Guenther, M. G.; Kumar, R. M.; Murray, H. L.; Jenner, R. G.; Gifford, D. K.; Melton, D. A.; Jaenisch, R.; Young, R. A., Core transcriptional regulatory circuitry in human embryonic stem cells. *Cell* **2005,** 122, (6), 947-56.
62. International Stem Cell, I.; Adewumi, O.; Aflatoonian, B.; Ahrlund-Richter, L.; Amit, M.; Andrews, P. W.; Beighton, G.; Bello, P. A.; Benvenisty, N.; Berry, L. S.; Bevan, S.; Blum, B.; Brooking, J.; Chen, K. G.; Choo, A. B.; Churchill, G. A.; Corbel, M.; Damjanov, I.; Draper, J. S.; Dvorak, P.; Emanuelsson, K.; Fleck, R. A.; Ford, A.; Gertow, K.; Gertsenstein, M.; Gokhale, P. J.; Hamilton, R. S.; Hampl, A.; Healy, L. E.; Hovatta, O.; Hyllner, J.; Imreh, M. P.; Itskovitz-Eldor, J.; Jackson, J.; Johnson, J. L.; Jones, M.; Kee, K.; King, B. L.; Knowles, B. B.; Lako, M.; Lebrin, F.; Mallon, B. S.; Manning, D.; Mayshar, Y.; McKay, R. D.; Michalska, A. E.; Mikkola, M.; Mileikovsky, M.; Minger, S. L.; Moore, H. D.; Mummery, C. L.; Nagy, A.; Nakatsuji, N.; O'Brien, C. M.; Oh, S. K.; Olsson, C.; Otonkoski, T.; Park, K. Y.; Passier, R.; Patel, H.; Patel, M.; Pedersen, R.; Pera, M. F.; Piekarczyk, M. S.; Pera, R. A.; Reubinoff, B. E.; Robins, A. J.; Rossant, J.; Rugg-Gunn, P.; Schulz, T. C.; Semb, H.; Sherrer, E. S.; Siemen, H.; Stacey, G. N.; Stojkovic, M.; Suemori, H.; Szatkiewicz, J.; Turetsky, T.; Tuuri, T.; van den Brink, S.; Vintersten, K.; Vuoristo, S.; Ward, D.; Weaver, T. A.; Young, L. A.; Zhang, W., Characterization of human embryonic stem cell lines by the International Stem Cell Initiative. *Nature biotechnology* **2007,** 25, (7), 803-16.
63. Stevens, L. C., The biology of teratomas including evidence indicating their origin form primordial germ cells. *L' Annee biologique* **1962,** 1, 585-610.
64. Yu, J.; Vodyanik, M. A.; Smuga-Otto, K.; Antosiewicz-Bourget, J.; Frane, J. L.; Tian, S.; Nie, J.; Jonsdottir, G. A.; Ruotti, V.; Stewart, R.; Slukvin, II; Thomson, J. A., Induced pluripotent stem cell lines derived from human somatic cells. *Science* **2007,** 318, (5858), 1917-20.
65. Takahashi, K.; Tanabe, K.; Ohnuki, M.; Narita, M.; Ichisaka, T.; Tomoda, K.; Yamanaka, S., Induction of pluripotent stem cells from adult human fibroblasts by defined factors. *Cell* **2007,** 131, (5), 861-72.
66. Boer, G. J., Ethical issues in neurografting of human embryonic cells. *Theoretical medicine and bioethics* **1999,** 20, (5), 461-75.
67. Okita, K.; Ichisaka, T.; Yamanaka, S., Generation of germline-competent induced pluripotent stem cells. *Nature* **2007,** 448, (7151), 313-7.
68. Boland, M. J.; Hazen, J. L.; Nazor, K. L.; Rodriguez, A. R.; Gifford, W.; Martin, G.; Kupriyanov, S.; Baldwin, K. K., Adult mice generated from induced pluripotent stem cells. *Nature* **2009,** 461, (7260), 91-4.
69. Bjorklund, L. M.; Sanchez-Pernaute, R.; Chung, S.; Andersson, T.; Chen, I. Y.; McNaught, K. S.; Brownell, A. L.; Jenkins, B. G.; Wahlestedt, C.; Kim, K. S.; Isacson, O., Embryonic stem cells develop into functional dopaminergic neurons after transplantation in a Parkinson rat model. *Proceedings of the National Academy of Sciences of the United States of America* **2002,** 99, (4), 2344-9.
70. Kim, D. S.; Lee, J. S.; Leem, J. W.; Huh, Y. J.; Kim, J. Y.; Kim, H. S.; Park, I. H.; Daley, G. Q.; Hwang, D. Y.; Kim, D. W., Robust enhancement of neural differentiation from human ES and iPS cells regardless of their innate difference in differentiation propensity. *Stem cell reviews* **2010,** 6, (2), 270-81.
71. Cai, J.; Yang, M.; Poremsky, E.; Kidd, S.; Schneider, J. S.; Iacovitti, L., Dopaminergic neurons derived from human induced pluripotent stem cells survive and integrate into 6-OHDA-lesioned rats. *Stem cells and development* **2010,** 19, (7), 1017-23.
72. Kriks, S.; Shim, J. W.; Piao, J.; Ganat, Y. M.; Wakeman, D. R.; Xie, Z.; Carrillo-Reid, L.; Auyeung, G.; Antonacci, C.; Buch, A.; Yang, L.; Beal, M. F.; Surmeier, D. J.; Kordower, J. H.; Tabar, V.; Studer, L.,

Dopamine neurons derived from human ES cells efficiently engraft in animal models of Parkinson's disease. *Nature* **2011,** 480, (7378), 547-51.
73. Rhee, Y. H.; Ko, J. Y.; Chang, M. Y.; Yi, S. H.; Kim, D.; Kim, C. H.; Shim, J. W.; Jo, A. Y.; Kim, B. W.; Lee, H.; Lee, S. H.; Suh, W.; Park, C. H.; Koh, H. C.; Lee, Y. S.; Lanza, R.; Kim, K. S.; Lee, S. H., Protein-based human iPS cells efficiently generate functional dopamine neurons and can treat a rat model of Parkinson disease. *The Journal of clinical investigation* **2011,** 121, (6), 2326-35.
74. Swistowski, A.; Peng, J.; Liu, Q.; Mali, P.; Rao, M. S.; Cheng, L.; Zeng, X., Efficient generation of functional dopaminergic neurons from human induced pluripotent stem cells under defined conditions. *Stem cells* **2010,** 28, (10), 1893-904.
75. Ben-Hur, T.; Idelson, M.; Khaner, H.; Pera, M.; Reinhartz, E.; Itzik, A.; Reubinoff, B. E., Transplantation of human embryonic stem cell-derived neural progenitors improves behavioral deficit in Parkinsonian rats. *Stem cells* **2004,** 22, (7), 1246-55.
76. Hu, B. Y.; Weick, J. P.; Yu, J.; Ma, L. X.; Zhang, X. Q.; Thomson, J. A.; Zhang, S. C., Neural differentiation of human induced pluripotent stem cells follows developmental principles but with variable potency. *Proceedings of the National Academy of Sciences of the United States of America* **2010,** 107, (9), 4335-40.
77. Narsinh, K. H.; Sun, N.; Sanchez-Freire, V.; Lee, A. S.; Almeida, P.; Hu, S.; Jan, T.; Wilson, K. D.; Leong, D.; Rosenberg, J.; Yao, M.; Robbins, R. C.; Wu, J. C., Single cell transcriptional profiling reveals heterogeneity of human induced pluripotent stem cells. *The Journal of clinical investigation* **2011,** 121, (3), 1217-21.
78. Feng, Q.; Lu, S. J.; Klimanskaya, I.; Gomes, I.; Kim, D.; Chung, Y.; Honig, G. R.; Kim, K. S.; Lanza, R., Hemangioblastic derivatives from human induced pluripotent stem cells exhibit limited expansion and early senescence. *Stem cells* **2010,** 28, (4), 704-12.
79. Narsinh, K. H.; Plews, J.; Wu, J. C., Comparison of human induced pluripotent and embryonic stem cells: fraternal or identical twins? *Molecular therapy : the journal of the American Society of Gene Therapy* **2011,** 19, (4), 635-8.
80. Steinbeck, J. A.; Choi, S. J.; Mrejeru, A.; Ganat, Y.; Deisseroth, K.; Sulzer, D.; Mosharov, E. V.; Studer, L., Optogenetics enables functional analysis of human embryonic stem cell-derived grafts in a Parkinson's disease model. *Nature biotechnology* **2015,** 33, (2), 204-9.
81. Grealish, S.; Diguet, E.; Kirkeby, A.; Mattsson, B.; Heuer, A.; Bramoulle, Y.; Van Camp, N.; Perrier, A. L.; Hantraye, P.; Bjorklund, A.; Parmar, M., Human ESC-derived dopamine neurons show similar preclinical efficacy and potency to fetal neurons when grafted in a rat model of Parkinson's disease. *Cell stem cell* **2014,** 15, (5), 653-65.
82. Byers, B.; Lee, H. J.; Liu, J.; Weitz, A. J.; Lin, P.; Zhang, P.; Shcheglovitov, A.; Dolmetsch, R.; Pera, R. R.; Lee, J. H., Direct in vivo assessment of human stem cell graft-host neural circuits. *NeuroImage* **2015,** 114, 328-37.
83. Krencik, R.; Weick, J. P.; Liu, Y.; Zhang, Z. J.; Zhang, S. C., Specification of transplantable astroglial subtypes from human pluripotent stem cells. *Nature biotechnology* **2011,** 29, (6), 528-34.
84. Weick, J. P.; Johnson, M. A.; Skroch, S. P.; Williams, J. C.; Deisseroth, K.; Zhang, S. C., Functional control of transplantable human ESC-derived neurons via optogenetic targeting. *Stem cells* **2010,** 28, (11), 2008-16.
85. Discher, D. E.; Mooney, D. J.; Zandstra, P. W., Growth factors, matrices, and forces combine and control stem cells. *Science* **2009,** 324, (5935), 1673-7.
86. Miller, C. J.; Davidson, L. A., The interplay between cell signalling and mechanics in developmental processes. *Nature reviews. Genetics* **2013,** 14, (10), 733-44.
87. Hazeltine, L. B.; Selekman, J. A.; Palecek, S. P., Engineering the human pluripotent stem cell microenvironment to direct cell fate. *Biotechnology advances* **2013,** 31, (7), 1002-19.
88. Higuchi, A.; Ling, Q. D.; Chang, Y.; Hsu, S. T.; Umezawa, A., Physical cues of biomaterials guide stem cell differentiation fate. *Chemical reviews* **2013,** 113, (5), 3297-328.
89. Sun, Y.; Chen, C. S.; Fu, J., Forcing stem cells to behave: a biophysical perspective of the cellular microenvironment. *Annual review of biophysics* **2012,** 41, 519-42.

90. Kinney, M. A.; Hookway, T. A.; Wang, Y.; McDevitt, T. C., Engineering three-dimensional stem cell morphogenesis for the development of tissue models and scalable regenerative therapeutics. *Annals of biomedical engineering* **2014,** 42, (2), 352-67.
91. Genbacev, O.; Krtolica, A.; Zdravkovic, T.; Brunette, E.; Powell, S.; Nath, A.; Caceres, E.; McMaster, M.; McDonagh, S.; Li, Y.; Mandalam, R.; Lebkowski, J.; Fisher, S. J., Serum-free derivation of human embryonic stem cell lines on human placental fibroblast feeders. *Fertility and sterility* **2005,** 83, (5), 1517-29.
92. Li, Y.; Powell, S.; Brunette, E.; Lebkowski, J.; Mandalam, R., Expansion of human embryonic stem cells in defined serum-free medium devoid of animal-derived products. *Biotechnology and bioengineering* **2005,** 91, (6), 688-98.
93. Vallier, L.; Alexander, M.; Pedersen, R. A., Activin/Nodal and FGF pathways cooperate to maintain pluripotency of human embryonic stem cells. *Journal of cell science* **2005,** 118, (Pt 19), 4495-509.
94. Ludwig, T. E.; Levenstein, M. E.; Jones, J. M.; Berggren, W. T.; Mitchen, E. R.; Frane, J. L.; Crandall, L. J.; Daigh, C. A.; Conard, K. R.; Piekarczyk, M. S.; Llanas, R. A.; Thomson, J. A., Derivation of human embryonic stem cells in defined conditions. *Nature biotechnology* **2006,** 24, (2), 185-7.
95. Chen, G.; Hou, Z.; Gulbranson, D. R.; Thomson, J. A., Actin-myosin contractility is responsible for the reduced viability of dissociated human embryonic stem cells. *Cell stem cell* **2010,** 7, (2), 240-8.
96. Chen, G.; Gulbranson, D. R.; Hou, Z.; Bolin, J. M.; Ruotti, V.; Probasco, M. D.; Smuga-Otto, K.; Howden, S. E.; Diol, N. R.; Propson, N. E.; Wagner, R.; Lee, G. O.; Antosiewicz-Bourget, J.; Teng, J. M.; Thomson, J. A., Chemically defined conditions for human iPSC derivation and culture. *Nature methods* **2011,** 8, (5), 424-9.
97. Kleinman, H. K.; McGarvey, M. L.; Liotta, L. A.; Robey, P. G.; Tryggvason, K.; Martin, G. R., Isolation and characterization of type IV procollagen, laminin, and heparan sulfate proteoglycan from the EHS sarcoma. *Biochemistry* **1982,** 21, (24), 6188-93.
98. Mackay, A. R.; Gomez, D. E.; Cottam, D. W.; Rees, R. C.; Nason, A. M.; Thorgeirsson, U. P., Identification of the 72-kDa (MMP-2) and 92-kDa (MMP-9) gelatinase/type IV collagenase in preparations of laminin and Matrigel. *BioTechniques* **1993,** 15, (6), 1048-51.
99. Vukicevic, S.; Kleinman, H. K.; Luyten, F. P.; Roberts, A. B.; Roche, N. S.; Reddi, A. H., Identification of multiple active growth factors in basement membrane Matrigel suggests caution in interpretation of cellular activity related to extracellular matrix components. *Experimental cell research* **1992,** 202, (1), 1-8.
100. Braam, S. R.; Zeinstra, L.; Litjens, S.; Ward-van Oostwaard, D.; van den Brink, S.; van Laake, L.; Lebrin, F.; Kats, P.; Hochstenbach, R.; Passier, R.; Sonnenberg, A.; Mummery, C. L., Recombinant vitronectin is a functionally defined substrate that supports human embryonic stem cell self-renewal via alphavbeta5 integrin. *Stem cells* **2008,** 26, (9), 2257-65.
101. Rodin, S.; Domogatskaya, A.; Strom, S.; Hansson, E. M.; Chien, K. R.; Inzunza, J.; Hovatta, O.; Tryggvason, K., Long-term self-renewal of human pluripotent stem cells on human recombinant laminin-511. *Nature biotechnology* **2010,** 28, (6), 611-5.
102. Li, L.; Klim, J. R.; Derda, R.; Courtney, A. H.; Kiessling, L. L., Spatial control of cell fate using synthetic surfaces to potentiate TGF-beta signaling. *Proceedings of the National Academy of Sciences of the United States of America* **2011,** 108, (29), 11745-50.
103. Derda, R.; Li, L.; Orner, B. P.; Lewis, R. L.; Thomson, J. A.; Kiessling, L. L., Defined substrates for human embryonic stem cell growth identified from surface arrays. *ACS chemical biology* **2007,** 2, (5), 347-55.
104. Saha, K.; Mei, Y.; Reisterer, C. M.; Pyzocha, N. K.; Yang, J.; Muffat, J.; Davies, M. C.; Alexander, M. R.; Langer, R.; Anderson, D. G.; Jaenisch, R., Surface-engineered substrates for improved human pluripotent stem cell culture under fully defined conditions. *Proceedings of the National Academy of Sciences of the United States of America* **2011,** 108, (46), 18714-9.
105. Kolhar, P.; Kotamraju, V. R.; Hikita, S. T.; Clegg, D. O.; Ruoslahti, E., Synthetic surfaces for human embryonic stem cell culture. *Journal of biotechnology* **2010,** 146, (3), 143-6.

106. Melkoumian, Z.; Weber, J. L.; Weber, D. M.; Fadeev, A. G.; Zhou, Y.; Dolley-Sonneville, P.; Yang, J.; Qiu, L.; Priest, C. A.; Shogbon, C.; Martin, A. W.; Nelson, J.; West, P.; Beltzer, J. P.; Pal, S.; Brandenberger, R., Synthetic peptide-acrylate surfaces for long-term self-renewal and cardiomyocyte differentiation of human embryonic stem cells. *Nature biotechnology* **2010,** 28, (6), 606-10.
107. Villa-Diaz, L. G.; Nandivada, H.; Ding, J.; Nogueira-de-Souza, N. C.; Krebsbach, P. H.; O'Shea, K. S.; Lahann, J.; Smith, G. D., Synthetic polymer coatings for long-term growth of human embryonic stem cells. *Nature biotechnology* **2010,** 28, (6), 581-3.
108. Miyazaki, T.; Futaki, S.; Suemori, H.; Taniguchi, Y.; Yamada, M.; Kawasaki, M.; Hayashi, M.; Kumagai, H.; Nakatsuji, N.; Sekiguchi, K.; Kawase, E., Laminin E8 fragments support efficient adhesion and expansion of dissociated human pluripotent stem cells. *Nature communications* **2012,** 3, 1236.
109. Baxter, M. A.; Camarasa, M. V.; Bates, N.; Small, F.; Murray, P.; Edgar, D.; Kimber, S. J., Analysis of the distinct functions of growth factors and tissue culture substrates necessary for the long-term self-renewal of human embryonic stem cell lines. *Stem cell research* **2009,** 3, (1), 28-38.
110. Harb, N.; Archer, T. K.; Sato, N., The Rho-Rock-Myosin signaling axis determines cell-cell integrity of self-renewing pluripotent stem cells. *PloS one* **2008,** 3, (8), e3001.
111. Nagaoka, M.; Si-Tayeb, K.; Akaike, T.; Duncan, S. A., Culture of human pluripotent stem cells using completely defined conditions on a recombinant E-cadherin substratum. *BMC developmental biology* **2010,** 10, 60.
112. Mei, Y.; Saha, K.; Bogatyrev, S. R.; Yang, J.; Hook, A. L.; Kalcioglu, Z. I.; Cho, S. W.; Mitalipova, M.; Pyzocha, N.; Rojas, F.; Van Vliet, K. J.; Davies, M. C.; Alexander, M. R.; Langer, R.; Jaenisch, R.; Anderson, D. G., Combinatorial development of biomaterials for clonal growth of human pluripotent stem cells. *Nature materials* **2010,** 9, (9), 768-78.
113. Klim, J. R.; Fowler, A. J.; Courtney, A. H.; Wrighton, P. J.; Sheridan, R. T.; Wong, M. L.; Kiessling, L. L., Small-molecule-modified surfaces engage cells through the alphavbeta3 integrin. *ACS chemical biology* **2012,** 7, (3), 518-25.
114. Derda, R.; Musah, S.; Orner, B. P.; Klim, J. R.; Li, L.; Kiessling, L. L., High-throughput discovery of synthetic surfaces that support proliferation of pluripotent cells. *Journal of the American Chemical Society* **2010,** 132, (4), 1289-95.
115. Irwin, E. F.; Gupta, R.; Dashti, D. C.; Healy, K. E., Engineered polymer-media interfaces for the long-term self-renewal of human embryonic stem cells. *Biomaterials* **2011,** 32, (29), 6912-9.
116. Musah, S.; Morin, S. A.; Wrighton, P. J.; Zwick, D. B.; Jin, S.; Kiessling, L. L., Glycosaminoglycan-binding hydrogels enable mechanical control of human pluripotent stem cell self-renewal. *ACS nano* **2012,** 6, (11), 10168-77.
117. Nandivada, H.; Villa-Diaz, L. G.; O'Shea, K. S.; Smith, G. D.; Krebsbach, P. H.; Lahann, J., Fabrication of synthetic polymer coatings and their use in feeder-free culture of human embryonic stem cells. *Nature protocols* **2011,** 6, (7), 1037-43.
118. Lambshead, J. W.; Meagher, L.; O'Brien, C.; Laslett, A. L., Defining synthetic surfaces for human pluripotent stem cell culture. *Cell regeneration* **2013,** 2, (1), 7.
119. Ekblom, P.; Lonai, P.; Talts, J. F., Expression and biological role of laminin-1. *Matrix biology : journal of the International Society for Matrix Biology* **2003,** 22, (1), 35-47.
120. Miner, J. H.; Yurchenco, P. D., Laminin functions in tissue morphogenesis. *Annual review of cell and developmental biology* **2004,** 20, 255-84.
121. Kallunki, P.; Sainio, K.; Eddy, R.; Byers, M.; Kallunki, T.; Sariola, H.; Beck, K.; Hirvonen, H.; Shows, T. B.; Tryggvason, K., A truncated laminin chain homologous to the B2 chain: structure, spatial expression, and chromosomal assignment. *The Journal of cell biology* **1992,** 119, (3), 679-93.
122. Iivanainen, A.; Kortesmaa, J.; Sahlberg, C.; Morita, T.; Bergmann, U.; Thesleff, I.; Tryggvason, K., Primary structure, developmental expression, and immunolocalization of the murine laminin alpha4 chain. *The Journal of biological chemistry* **1997,** 272, (44), 27862-8.
123. Miner, J. H.; Lewis, R. M.; Sanes, J. R., Molecular cloning of a novel laminin chain, alpha 5, and widespread expression in adult mouse tissues. *The Journal of biological chemistry* **1995,** 270, (48), 28523-6.

124. Yurchenco, P. D.; Quan, Y.; Colognato, H.; Mathus, T.; Harrison, D.; Yamada, Y.; O'Rear, J. J., The alpha chain of laminin-1 is independently secreted and drives secretion of its beta- and gamma-chain partners. *Proceedings of the National Academy of Sciences of the United States of America* **1997,** 94, (19), 10189-94.
125. Doi, M.; Thyboll, J.; Kortesmaa, J.; Jansson, K.; Iivanainen, A.; Parvardeh, M.; Timpl, R.; Hedin, U.; Swedenborg, J.; Tryggvason, K., Recombinant human laminin-10 (alpha5beta1gamma1). Production, purification, and migration-promoting activity on vascular endothelial cells. *The Journal of biological chemistry* **2002,** 277, (15), 12741-8.
126. Kortesmaa, J.; Yurchenco, P.; Tryggvason, K., Recombinant laminin-8 (alpha(4)beta(1)gamma(1)). Production, purification,and interactions with integrins. *The Journal of biological chemistry* **2000,** 275, (20), 14853-9.
127. Meng, Y.; Eshghi, S.; Li, Y. J.; Schmidt, R.; Schaffer, D. V.; Healy, K. E., Characterization of integrin engagement during defined human embryonic stem cell culture. *FASEB journal : official publication of the Federation of American Societies for Experimental Biology* **2010,** 24, (4), 1056-65.
128. Miyazaki, T.; Futaki, S.; Hasegawa, K.; Kawasaki, M.; Sanzen, N.; Hayashi, M.; Kawase, E.; Sekiguchi, K.; Nakatsuji, N.; Suemori, H., Recombinant human laminin isoforms can support the undifferentiated growth of human embryonic stem cells. *Biochemical and biophysical research communications* **2008,** 375, (1), 27-32.
129. Manton, K. J.; Richards, S.; Van Lonkhuyzen, D.; Cormack, L.; Leavesley, D.; Upton, Z., A chimeric vitronectin: IGF-I protein supports feeder-cell-free and serum-free culture of human embryonic stem cells. *Stem cells and development* **2010,** 19, (9), 1297-305.
130. Xu, C.; Inokuma, M. S.; Denham, J.; Golds, K.; Kundu, P.; Gold, J. D.; Carpenter, M. K., Feeder-free growth of undifferentiated human embryonic stem cells. *Nature biotechnology* **2001,** 19, (10), 971-4.
131. Amit, M.; Itskovitz-Eldor, J., Feeder-free culture of human embryonic stem cells. *Methods in enzymology* **2006,** 420, 37-49.
132. Frisch, S. M.; Ruoslahti, E., Integrins and anoikis. *Current opinion in cell biology* **1997,** 9, (5), 701-6.
133. Ruoslahti, E., RGD and other recognition sequences for integrins. *Annual review of cell and developmental biology* **1996,** 12, 697-715.
134. Hersel, U.; Dahmen, C.; Kessler, H., RGD modified polymers: biomaterials for stimulated cell adhesion and beyond. *Biomaterials* **2003,** 24, (24), 4385-4415.
135. Koivunen, E.; Wang, B.; Ruoslahti, E., Phage libraries displaying cyclic peptides with different ring sizes: ligand specificities of the RGD-directed integrins. *Bio/technology* **1995,** 13, (3), 265-70.
136. Li, X.; Liu, X.; Josey, B.; Chou, C. J.; Tan, Y.; Zhang, N.; Wen, X., Short laminin peptide for improved neural stem cell growth. *Stem cells translational medicine* **2014,** 3, (5), 662-70.
137. Orive, G.; Anitua, E.; Pedraz, J. L.; Emerich, D. F., Biomaterials for promoting brain protection, repair and regeneration. *Nature reviews. Neuroscience* **2009,** 10, (9), 682-92.
138. LeBaron, R. G.; Athanasiou, K. A., Extracellular matrix cell adhesion peptides: functional applications in orthopedic materials. *Tissue engineering* **2000,** 6, (2), 85-103.
139. Geiger, B.; Bershadsky, A., Assembly and mechanosensory function of focal contacts. *Current opinion in cell biology* **2001,** 13, (5), 584-92.
140. Hynes, R. O., Integrins: versatility, modulation, and signaling in cell adhesion. *Cell* **1992,** 69, (1), 11-25.
141. Boudreau, N. J.; Jones, P. L., Extracellular matrix and integrin signalling: the shape of things to come. *The Biochemical journal* **1999,** 339 (Pt 3), 481-8.
142. Schwartz, M. A., Integrin signaling revisited. *Trends in cell biology* **2001,** 11, (12), 466-70.
143. Ying, Q. L.; Wray, J.; Nichols, J.; Batlle-Morera, L.; Doble, B.; Woodgett, J.; Cohen, P.; Smith, A., The ground state of embryonic stem cell self-renewal. *Nature* **2008,** 453, (7194), 519-23.
144. Silva, J.; Smith, A., Capturing pluripotency. *Cell* **2008,** 132, (4), 532-6.

145. Tsutsui, H.; Valamehr, B.; Hindoyan, A.; Qiao, R.; Ding, X.; Guo, S.; Witte, O. N.; Liu, X.; Ho, C. M.; Wu, H., An optimized small molecule inhibitor cocktail supports long-term maintenance of human embryonic stem cells. *Nature communications* **2011,** 2, 167.
146. Hanna, J.; Cheng, A. W.; Saha, K.; Kim, J.; Lengner, C. J.; Soldner, F.; Cassady, J. P.; Muffat, J.; Carey, B. W.; Jaenisch, R., Human embryonic stem cells with biological and epigenetic characteristics similar to those of mouse ESCs. *Proceedings of the National Academy of Sciences of the United States of America* **2010,** 107, (20), 9222-7.
147. Ohgushi, M.; Sasai, Y., Lonely death dance of human pluripotent stem cells: ROCKing between metastable cell states. *Trends in cell biology* **2011,** 21, (5), 274-82.
148. Watanabe, K.; Ueno, M.; Kamiya, D.; Nishiyama, A.; Matsumura, M.; Wataya, T.; Takahashi, J. B.; Nishikawa, S.; Nishikawa, S.; Muguruma, K.; Sasai, Y., A ROCK inhibitor permits survival of dissociated human embryonic stem cells. *Nature biotechnology* **2007,** 25, (6), 681-6.
149. Tilson, S. G.; Haley, E. M.; Triantafillu, U. L.; Dozier, D. A.; Langford, C. P.; Gillespie, G. Y.; Kim, Y., ROCK Inhibition Facilitates In Vitro Expansion of Glioblastoma Stem-Like Cells. *PloS one* **2015,** 10, (7), e0132823.
150. Lau, C. L.; O'Shea, R. D.; Broberg, B. V.; Bischof, L.; Beart, P. M., The Rho kinase inhibitor Fasudil up-regulates astrocytic glutamate transport subsequent to actin remodelling in murine cultured astrocytes. *British journal of pharmacology* **2011,** 163, (3), 533-45.
151. Nakagawa, M.; Taniguchi, Y.; Senda, S.; Takizawa, N.; Ichisaka, T.; Asano, K.; Morizane, A.; Doi, D.; Takahashi, J.; Nishizawa, M.; Yoshida, Y.; Toyoda, T.; Osafune, K.; Sekiguchi, K.; Yamanaka, S., A novel efficient feeder-free culture system for the derivation of human induced pluripotent stem cells. *Scientific reports* **2014,** 4, 3594.
152. Lamas, N. J.; Serra, S. C.; Salgado, A. J.; Sousa, N., Failure of Y-27632 to improve the culture of adult human adipose-derived stem cells. *Stem cells and cloning : advances and applications* **2015,** 8, 15-26.
153. Xu, Y.; Zhu, X.; Hahm, H. S.; Wei, W.; Hao, E.; Hayek, A.; Ding, S., Revealing a core signaling regulatory mechanism for pluripotent stem cell survival and self-renewal by small molecules. *Proceedings of the National Academy of Sciences of the United States of America* **2010,** 107, (18), 8129-34.
154. Lin, T.; Ambasudhan, R.; Yuan, X.; Li, W.; Hilcove, S.; Abujarour, R.; Lin, X.; Hahm, H. S.; Hao, E.; Hayek, A.; Ding, S., A chemical platform for improved induction of human iPSCs. *Nature methods* **2009,** 6, (11), 805-8.
155. Burdon, T.; Stracey, C.; Chambers, I.; Nichols, J.; Smith, A., Suppression of SHP-2 and ERK signalling promotes self-renewal of mouse embryonic stem cells. *Developmental biology* **1999,** 210, (1), 30-43.
156. Callus, B. A.; Vaux, D. L., Caspase inhibitors: viral, cellular and chemical. *Cell death and differentiation* **2007,** 14, (1), 73-8.
157. Shi, Y., Caspase activation, inhibition, and reactivation: a mechanistic view. *Protein science : a publication of the Protein Society* **2004,** 13, (8), 1979-87.
158. Adams, J. M.; Cory, S., Apoptosomes: engines for caspase activation. *Current opinion in cell biology* **2002,** 14, (6), 715-20.
159. Shi, Y., Mechanisms of caspase activation and inhibition during apoptosis. *Molecular cell* **2002,** 9, (3), 459-70.
160. Huang, Y.; Park, Y. C.; Rich, R. L.; Segal, D.; Myszka, D. G.; Wu, H., Structural basis of caspase inhibition by XIAP: differential roles of the linker versus the BIR domain. *Cell* **2001,** 104, (5), 781-90.
161. Riedl, S. J.; Renatus, M.; Schwarzenbacher, R.; Zhou, Q.; Sun, C.; Fesik, S. W.; Liddington, R. C.; Salvesen, G. S., Structural basis for the inhibition of caspase-3 by XIAP. *Cell* **2001,** 104, (5), 791-800.
162. Yee, S. B.; Baek, S. J.; Park, H. T.; Jeong, S. H.; Jeong, J. H.; Kim, T. H.; Kim, J. M.; Jeong, B. K.; Park, B. S.; Kwon, T. K.; Yoon, I.; Yoo, Y. H., zVAD-fmk, unlike BocD-fmk, does not inhibit caspase-6 acting on 14-3-3/Bad pathway in apoptosis of p815 mastocytoma cells. *Experimental & molecular medicine* **2006,** 38, (6), 634-42.

163. Garcia-Calvo, M.; Peterson, E. P.; Leiting, B.; Ruel, R.; Nicholson, D. W.; Thornberry, N. A., Inhibition of human caspases by peptide-based and macromolecular inhibitors. *The Journal of biological chemistry* **1998,** 273, (49), 32608-13.
164. Riento, K.; Ridley, A. J., Rocks: multifunctional kinases in cell behaviour. *Nature reviews. Molecular cell biology* **2003,** 4, (6), 446-56.
165. Chambers, S. M.; Fasano, C. A.; Papapetrou, E. P.; Tomishima, M.; Sadelain, M.; Studer, L., Highly efficient neural conversion of human ES and iPS cells by dual inhibition of SMAD signaling. *Nature biotechnology* **2009,** 27, (3), 275-80.
166. Hwang, N. S.; Varghese, S.; Lee, H. J.; Zhang, Z.; Ye, Z.; Bae, J.; Cheng, L.; Elisseeff, J., In vivo commitment and functional tissue regeneration using human embryonic stem cell-derived mesenchymal cells. *Proceedings of the National Academy of Sciences of the United States of America* **2008,** 105, (52), 20641-6.
167. Li, Y. Q.; Liu, W.; Liu, F.; Zeng, Y.; Zuo, S. M.; Feng, S. Y.; Qi, C. X.; Wang, B. J.; Yan, X. J.; Khademhosseini, A.; Bai, J.; Du, Y. A., Primed 3D injectable microniches enabling low-dosage cell therapy for critical limb ischemia. *Proceedings of the National Academy of Sciences of the United States of America* **2014,** 111, (37), 13511-13516.
168. Choi, S. H.; Kim, Y. H.; Hebisch, M.; Sliwinski, C.; Lee, S.; D'Avanzo, C.; Chen, H. C.; Hooli, B.; Asselin, C.; Muffat, J.; Klee, J. B.; Zhang, C.; Wainger, B. J.; Peitz, M.; Kovacs, D. M.; Woolf, C. J.; Wagner, S. L.; Tanzi, R. E.; Kim, D. Y., A three-dimensional human neural cell culture model of Alzheimer's disease. *Nature* **2014,** 515, (7526), 274-U293.
169. Nawroth, J. C.; Parker, K. K., Design standards for engineered tissues. *Biotechnology advances* **2013,** 31, (5), 632-637.
170. Lancaster, M. A.; Renner, M.; Martin, C. A.; Wenzel, D.; Bicknell, L. S.; Hurles, M. E.; Homfray, T.; Penninger, J. M.; Jackson, A. P.; Knoblich, J. A., Cerebral organoids model human brain development and microcephaly. *Nature* **2013,** 501, (7467), 373-9.
171. Pasca, A. M.; Sloan, S. A.; Clarke, L. E.; Tian, Y.; Makinson, C. D.; Huber, N.; Kim, C. H.; Park, J. Y.; O'Rourke, N. A.; Nguyen, K. D.; Smith, S. J.; Huguenard, J. R.; Geschwind, D. H.; Barres, B. A.; Pasca, S. P., Functional cortical neurons and astrocytes from human pluripotent stem cells in 3D culture. *Nature methods* **2015,** 12, (7), 671-8.
172. Mariani, J.; Simonini, M. V.; Palejev, D.; Tomasini, L.; Coppola, G.; Szekely, A. M.; Horvath, T. L.; Vaccarino, F. M., Modeling human cortical development in vitro using induced pluripotent stem cells. *Proceedings of the National Academy of Sciences of the United States of America* **2012,** 109, (31), 12770-5.
173. Chen, V. C.; Couture, S. M.; Ye, J.; Lin, Z.; Hua, G.; Huang, H. I.; Wu, J.; Hsu, D.; Carpenter, M. K.; Couture, L. A., Scalable GMP compliant suspension culture system for human ES cells. *Stem cell research* **2012,** 8, (3), 388-402.
174. Amit, M.; Laevsky, I.; Miropolsky, Y.; Shariki, K.; Peri, M.; Itskovitz-Eldor, J., Dynamic suspension culture for scalable expansion of undifferentiated human pluripotent stem cells. *Nature protocols* **2011,** 6, (5), 572-9.
175. Zweigerdt, R.; Olmer, R.; Singh, H.; Haverich, A.; Martin, U., Scalable expansion of human pluripotent stem cells in suspension culture. *Nature protocols* **2011,** 6, (5), 689-700.
176. Nie, Y.; Bergendahl, V.; Hei, D. J.; Jones, J. M.; Palecek, S. P., Scalable culture and cryopreservation of human embryonic stem cells on microcarriers. *Biotechnology progress* **2009,** 25, (1), 20-31.
177. Chen, A. K.; Chen, X.; Choo, A. B.; Reuveny, S.; Oh, S. K., Critical microcarrier properties affecting the expansion of undifferentiated human embryonic stem cells. *Stem cell research* **2011,** 7, (2), 97-111.
178. Li, Y.; Liu, M.; Yan, Y.; Yang, S. T., Neural differentiation from pluripotent stem cells: The role of natural and synthetic extracellular matrix. *World journal of stem cells* **2014,** 6, (1), 11-23.
179. Nguyen, K. T.; West, J. L., Photopolymerizable hydrogels for tissue engineering applications. *Biomaterials* **2002,** 23, (22), 4307-14.

180. Lutolf, M. P.; Hubbell, J. A., Synthetic biomaterials as instructive extracellular microenvironments for morphogenesis in tissue engineering. *Nature biotechnology* **2005,** 23, (1), 47-55.
181. Butcher, J. T.; Nerem, R. M., Porcine aortic valve interstitial cells in three-dimensional culture: comparison of phenotype with aortic smooth muscle cells. *The Journal of heart valve disease* **2004,** 13, (3), 478-85; discussion 485-6.
182. Eyrich, D.; Brandl, F.; Appel, B.; Wiese, H.; Maier, G.; Wenzel, M.; Staudenmaier, R.; Goepferich, A.; Blunk, T., Long-term stable fibrin gels for cartilage engineering. *Biomaterials* **2007,** 28, (1), 55-65.
183. Masters, K. S.; Shah, D. N.; Leinwand, L. A.; Anseth, K. S., Crosslinked hyaluronan scaffolds as a biologically active carrier for valvular interstitial cells. *Biomaterials* **2005,** 26, (15), 2517-25.
184. Azab, A. K.; Orkin, B.; Doviner, V.; Nissan, A.; Klein, M.; Srebnik, M.; Rubinstein, A., Crosslinked chitosan implants as potential degradable devices for brachytherapy: in vitro and in vivo analysis. *Journal of controlled release : official journal of the Controlled Release Society* **2006,** 111, (3), 281-9.
185. Barralet, J. E.; Wang, L.; Lawson, M.; Triffitt, J. T.; Cooper, P. R.; Shelton, R. M., Comparison of bone marrow cell growth on 2D and 3D alginate hydrogels. *Journal of materials science. Materials in medicine* **2005,** 16, (6), 515-9.
186. Fang, J. Y.; Chen, J. P.; Leu, Y. L.; Wang, H. Y., Characterization and evaluation of silk protein hydrogels for drug delivery. *Chemical & pharmaceutical bulletin* **2006,** 54, (2), 156-62.
187. Dawson, E.; Mapili, G.; Erickson, K.; Taqvi, S.; Roy, K., Biomaterials for stem cell differentiation. *Advanced drug delivery reviews* **2008,** 60, (2), 215-28.
188. Sawhney, A. S.; Pathak, C. P.; Hubbell, J. A., Interfacial photopolymerization of poly(ethylene glycol)-based hydrogels upon alginate-poly(l-lysine) microcapsules for enhanced biocompatibility. *Biomaterials* **1993,** 14, (13), 1008-16.
189. Lee, S. Y.; Pereira, B. P.; Yusof, N.; Selvaratnam, L.; Yu, Z.; Abbas, A. A.; Kamarul, T., Unconfined compression properties of a porous poly(vinyl alcohol)-chitosan-based hydrogel after hydration. *Acta biomaterialia* **2009,** 5, (6), 1919-25.
190. Chirila, T. V.; Constable, I. J.; Crawford, G. J.; Vijayasekaran, S.; Thompson, D. E.; Chen, Y. C.; Fletcher, W. A.; Griffin, B. J., Poly(2-hydroxyethyl methacrylate) sponges as implant materials: in vivo and in vitro evaluation of cellular invasion. *Biomaterials* **1993,** 14, (1), 26-38.
191. Bryant, S. J.; Anseth, K. S., Hydrogel properties influence ECM production by chondrocytes photoencapsulated in poly(ethylene glycol) hydrogels. *Journal of biomedical materials research* **2002,** 59, (1), 63-72.
192. Cushing, M. C.; Anseth, K. S., Materials science. Hydrogel cell cultures. *Science* **2007,** 316, (5828), 1133-4.
193. Gerecht-Nir, S.; Cohen, S.; Ziskind, A.; Itskovitz-Eldor, J., Three-dimensional porous alginate scaffolds provide a conducive environment for generation of well-vascularized embryoid bodies from human embryonic stem cells. *Biotechnology and bioengineering* **2004,** 88, (3), 313-20.
194. Leor, J.; Gerecht, S.; Cohen, S.; Miller, L.; Holbova, R.; Ziskind, A.; Shachar, M.; Feinberg, M. S.; Guetta, E.; Itskovitz-Eldor, J., Human embryonic stem cell transplantation to repair the infarcted myocardium. *Heart* **2007,** 93, (10), 1278-84.
195. Li, Z.; Leung, M.; Hopper, R.; Ellenbogen, R.; Zhang, M., Feeder-free self-renewal of human embryonic stem cells in 3D porous natural polymer scaffolds. *Biomaterials* **2010,** 31, (3), 404-12.
196. Baharvand, H.; Hashemi, S. M.; Kazemi Ashtiani, S.; Farrokhi, A., Differentiation of human embryonic stem cells into hepatocytes in 2D and 3D culture systems in vitro. *The International journal of developmental biology* **2006,** 50, (7), 645-52.
197. Ferreira, L. S.; Gerecht, S.; Fuller, J.; Shieh, H. F.; Vunjak-Novakovic, G.; Langer, R., Bioactive hydrogel scaffolds for controllable vascular differentiation of human embryonic stem cells. *Biomaterials* **2007,** 28, (17), 2706-17.
198. Gerecht, S.; Burdick, J. A.; Ferreira, L. S.; Townsend, S. A.; Langer, R.; Vunjak-Novakovic, G., Hyaluronic acid hydrogel for controlled self-renewal and differentiation of human embryonic stem cells.

Proceedings of the National Academy of Sciences of the United States of America **2007,** 104, (27), 11298-303.
199. Toh, W. S.; Lee, E. H.; Guo, X. M.; Chan, J. K.; Yeow, C. H.; Choo, A. B.; Cao, T., Cartilage repair using hyaluronan hydrogel-encapsulated human embryonic stem cell-derived chondrogenic cells. *Biomaterials* **2010,** 31, (27), 6968-80.
200. Laflamme, M. A.; Chen, K. Y.; Naumova, A. V.; Muskheli, V.; Fugate, J. A.; Dupras, S. K.; Reinecke, H.; Xu, C.; Hassanipour, M.; Police, S.; O'Sullivan, C.; Collins, L.; Chen, Y.; Minami, E.; Gill, E. A.; Ueno, S.; Yuan, C.; Gold, J.; Murry, C. E., Cardiomyocytes derived from human embryonic stem cells in pro-survival factors enhance function of infarcted rat hearts. *Nature biotechnology* **2007,** 25, (9), 1015-24.
201. Ferreira, L.; Karp, J. M.; Nobre, L.; Langer, R., New opportunities: the use of nanotechnologies to manipulate and track stem cells. *Cell stem cell* **2008,** 3, (2), 136-46.
202. Spence, J. R.; Mayhew, C. N.; Rankin, S. A.; Kuhar, M. F.; Vallance, J. E.; Tolle, K.; Hoskins, E. E.; Kalinichenko, V. V.; Wells, S. I.; Zorn, A. M.; Shroyer, N. F.; Wells, J. M., Directed differentiation of human pluripotent stem cells into intestinal tissue in vitro. *Nature* **2011,** 470, (7332), 105-9.
203. Gerecht, S.; Townsend, S. A.; Pressler, H.; Zhu, H.; Nijst, C. L.; Bruggeman, J. P.; Nichol, J. W.; Langer, R., A porous photocurable elastomer for cell encapsulation and culture. *Biomaterials* **2007,** 28, (32), 4826-35.
204. Lee, S. T.; Yun, J. I.; Jo, Y. S.; Mochizuki, M.; van der Vlies, A. J.; Kontos, S.; Ihm, J. E.; Lim, J. M.; Hubbell, J. A., Engineering integrin signaling for promoting embryonic stem cell self-renewal in a precisely defined niche. *Biomaterials* **2010,** 31, (6), 1219-26.
205. Kraehenbuehl, T. P.; Ferreira, L. S.; Hayward, A. M.; Nahrendorf, M.; van der Vlies, A. J.; Vasile, E.; Weissleder, R.; Langer, R.; Hubbell, J. A., Human embryonic stem cell-derived microvascular grafts for cardiac tissue preservation after myocardial infarction. *Biomaterials* **2011,** 32, (4), 1102-9.
206. Levenberg, S.; Rouwkema, J.; Macdonald, M.; Garfein, E. S.; Kohane, D. S.; Darland, D. C.; Marini, R.; van Blitterswijk, C. A.; Mulligan, R. C.; D'Amore, P. A.; Langer, R., Engineering vascularized skeletal muscle tissue. *Nature biotechnology* **2005,** 23, (7), 879-84.
207. Levenberg, S.; Huang, N. F.; Lavik, E.; Rogers, A. B.; Itskovitz-Eldor, J.; Langer, R., Differentiation of human embryonic stem cells on three-dimensional polymer scaffolds. *Proceedings of the National Academy of Sciences of the United States of America* **2003,** 100, (22), 12741-6.
208. Caspi, O.; Lesman, A.; Basevitch, Y.; Gepstein, A.; Arbel, G.; Habib, I. H.; Gepstein, L.; Levenberg, S., Tissue engineering of vascularized cardiac muscle from human embryonic stem cells. *Circulation research* **2007,** 100, (2), 263-72.
209. Kraehenbuehl, T. P.; Langer, R.; Ferreira, L. S., Three-dimensional biomaterials for the study of human pluripotent stem cells. *Nature methods* **2011,** 8, (9), 731-6.
210. Smidsrod, O.; Skjak-Braek, G., Alginate as immobilization matrix for cells. *Trends in biotechnology* **1990,** 8, (3), 71-8.
211. Martinsen, A.; Skjak-Braek, G.; Smidsrod, O., Alginate as immobilization material: I. Correlation between chemical and physical properties of alginate gel beads. *Biotechnology and bioengineering* **1989,** 33, (1), 79-89.
212. Serra, M.; Correia, C.; Malpique, R.; Brito, C.; Jensen, J.; Bjorquist, P.; Carrondo, M. J.; Alves, P. M., Microencapsulation technology: a powerful tool for integrating expansion and cryopreservation of human embryonic stem cells. *PloS one* **2011,** 6, (8), e23212.
213. Chayosumrit, M.; Tuch, B.; Sidhu, K., Alginate microcapsule for propagation and directed differentiation of hESCs to definitive endoderm. *Biomaterials* **2010,** 31, (3), 505-14.
214. Dean, S. K.; Yulyana, Y.; Williams, G.; Sidhu, K. S.; Tuch, B. E., Differentiation of encapsulated embryonic stem cells after transplantation. *Transplantation* **2006,** 82, (9), 1175-84.
215. Addae, C.; Yi, X.; Gernapudi, R.; Cheng, H.; Musto, A.; Martinez-Ceballos, E., All-trans-retinoid acid induces the differentiation of encapsulated mouse embryonic stem cells into GABAergic neurons. *Differentiation; research in biological diversity* **2012,** 83, (5), 233-41.

216. Vacharathit, V.; Silva, E. A.; Mooney, D. J., Viability and functionality of cells delivered from peptide conjugated scaffolds. *Biomaterials* **2011,** 32, (15), 3721-8.
217. Rowley, J. A.; Madlambayan, G.; Mooney, D. J., Alginate hydrogels as synthetic extracellular matrix materials. *Biomaterials* **1999,** 20, (1), 45-53.
218. Lutolf, M. P., Biomaterials: Spotlight on hydrogels. *Nature materials* **2009,** 8, (6), 451-3.
219. Caliari, S. R.; Burdick, J. A., A practical guide to hydrogels for cell culture. *Nature methods* **2016,** 13, (5), 405-14.
220. Lee, K. Y.; Mooney, D. J., Hydrogels for tissue engineering. *Chemical reviews* **2001,** 101, (7), 1869-79.
221. Nicholas, C. R.; Chen, J.; Tang, Y.; Southwell, D. G.; Chalmers, N.; Vogt, D.; Arnold, C. M.; Chen, Y. J.; Stanley, E. G.; Elefanty, A. G.; Sasai, Y.; Alvarez-Buylla, A.; Rubenstein, J. L.; Kriegstein, A. R., Functional maturation of hPSC-derived forebrain interneurons requires an extended timeline and mimics human neural development. *Cell stem cell* **2013,** 12, (5), 573-86.
222. Shi, Y.; Kirwan, P.; Smith, J.; Robinson, H. P.; Livesey, F. J., Human cerebral cortex development from pluripotent stem cells to functional excitatory synapses. *Nature neuroscience* **2012,** 15, (3), 477-86, S1.
223. Martini, F.; Bartholomew, E. F.; Ober, W. C., *Essentials of anatomy & physiology*. 5th ed.; Benjamin Cummings: San Francisco ; London, 2010.
224. Pouton, C. W.; Haynes, J. M., Embryonic stem cells as a source of models for drug discovery. *Nature reviews. Drug discovery* **2007,** 6, (8), 605-16.
225. Conti, L.; Pollard, S. M.; Gorba, T.; Reitano, E.; Toselli, M.; Biella, G.; Sun, Y.; Sanzone, S.; Ying, Q. L.; Cattaneo, E.; Smith, A., Niche-independent symmetrical self-renewal of a mammalian tissue stem cell. *PLoS biology* **2005,** 3, (9), e283.
226. Hook, L.; O'Brien, C.; Allsopp, T., ES cell technology: an introduction to genetic manipulation, differentiation and therapeutic cloning. *Advanced drug delivery reviews* **2005,** 57, (13), 1904-17.
227. Zhao, S.; Maxwell, S.; Jimenez-Beristain, A.; Vives, J.; Kuehner, E.; Zhao, J.; O'Brien, C.; de Felipe, C.; Semina, E.; Li, M., Generation of embryonic stem cells and transgenic mice expressing green fluorescence protein in midbrain dopaminergic neurons. *The European journal of neuroscience* **2004,** 19, (5), 1133-40.
228. Ying, Q. L.; Stavridis, M.; Griffiths, D.; Li, M.; Smith, A., Conversion of embryonic stem cells into neuroectodermal precursors in adherent monoculture. *Nature biotechnology* **2003,** 21, (2), 183-6.
229. Elkabetz, Y.; Panagiotakos, G.; Al Shamy, G.; Socci, N. D.; Tabar, V.; Studer, L., Human ES cell-derived neural rosettes reveal a functionally distinct early neural stem cell stage. *Genes & development* **2008,** 22, (2), 152-65.
230. Davidson, K. C.; Jamshidi, P.; Daly, R.; Hearn, M. T.; Pera, M. F.; Dottori, M., Wnt3a regulates survival, expansion, and maintenance of neural progenitors derived from human embryonic stem cells. *Molecular and cellular neurosciences* **2007,** 36, (3), 408-15.
231. Dottori, M.; Pera, M. F., Neural differentiation of human embryonic stem cells. *Methods in molecular biology* **2008,** 438, 19-30.
232. Itskovitz-Eldor, J.; Schuldiner, M.; Karsenti, D.; Eden, A.; Yanuka, O.; Amit, M.; Soreq, H.; Benvenisty, N., Differentiation of human embryonic stem cells into embryoid bodies compromising the three embryonic germ layers. *Molecular medicine* **2000,** 6, (2), 88-95.
233. Barberi, T.; Klivenyi, P.; Calingasan, N. Y.; Lee, H.; Kawamata, H.; Loonam, K.; Perrier, A. L.; Bruses, J.; Rubio, M. E.; Topf, N.; Tabar, V.; Harrison, N. L.; Beal, M. F.; Moore, M. A.; Studer, L., Neural subtype specification of fertilization and nuclear transfer embryonic stem cells and application in parkinsonian mice. *Nature biotechnology* **2003,** 21, (10), 1200-7.
234. Denham, M.; Thompson, L. H.; Leung, J.; Pebay, A.; Bjorklund, A.; Dottori, M., Gli1 is an inducing factor in generating floor plate progenitor cells from human embryonic stem cells. *Stem cells* **2010,** 28, (10), 1805-15.
235. Shi, Y.; Kirwan, P.; Livesey, F. J., Directed differentiation of human pluripotent stem cells to cerebral cortex neurons and neural networks. *Nature protocols* **2012,** 7, (10), 1836-46.

236. Ma, L.; Liu, Y.; Zhang, S. C., Directed differentiation of dopamine neurons from human pluripotent stem cells. *Methods in molecular biology* **2011,** 767, 411-8.
237. Marchetto, M. C.; Muotri, A. R.; Mu, Y.; Smith, A. M.; Cezar, G. G.; Gage, F. H., Non-cell-autonomous effect of human SOD1 G37R astrocytes on motor neurons derived from human embryonic stem cells. *Cell stem cell* **2008,** 3, (6), 649-57.
238. Roy, N. S.; Cleren, C.; Singh, S. K.; Yang, L.; Beal, M. F.; Goldman, S. A., Functional engraftment of human ES cell-derived dopaminergic neurons enriched by coculture with telomerase-immortalized midbrain astrocytes. *Nature medicine* **2006,** 12, (11), 1259-68.
239. Perrier, A. L.; Tabar, V.; Barberi, T.; Rubio, M. E.; Bruses, J.; Topf, N.; Harrison, N. L.; Studer, L., Derivation of midbrain dopamine neurons from human embryonic stem cells. *Proceedings of the National Academy of Sciences of the United States of America* **2004,** 101, (34), 12543-8.
240. Lorson, C. L.; Rindt, H.; Shababi, M., Spinal muscular atrophy: mechanisms and therapeutic strategies. *Human molecular genetics* **2010,** 19, (R1), R111-8.
241. Ebert, A. D.; Yu, J.; Rose, F. F., Jr.; Mattis, V. B.; Lorson, C. L.; Thomson, J. A.; Svendsen, C. N., Induced pluripotent stem cells from a spinal muscular atrophy patient. *Nature* **2009,** 457, (7227), 277-80.
242. Maroof, A. M.; Keros, S.; Tyson, J. A.; Ying, S. W.; Ganat, Y. M.; Merkle, F. T.; Liu, B.; Goulburn, A.; Stanley, E. G.; Elefanty, A. G.; Widmer, H. R.; Eggan, K.; Goldstein, P. A.; Anderson, S. A.; Studer, L., Directed differentiation and functional maturation of cortical interneurons from human embryonic stem cells. *Cell stem cell* **2013,** 12, (5), 559-72.
243. Vanderhaeghen, P., Generation of cortical neurons from pluripotent stem cells. *Progress in brain research* **2012,** 201, 183-95.
244. Agholme, L.; Lindstrom, T.; Kagedal, K.; Marcusson, J.; Hallbeck, M., An in vitro model for neuroscience: differentiation of SH-SY5Y cells into cells with morphological and biochemical characteristics of mature neurons. *Journal of Alzheimer's disease : JAD* **2010,** 20, (4), 1069-82.
245. Encinas, M.; Iglesias, M.; Liu, Y.; Wang, H.; Muhaisen, A.; Cena, V.; Gallego, C.; Comella, J. X., Sequential treatment of SH-SY5Y cells with retinoic acid and brain-derived neurotrophic factor gives rise to fully differentiated, neurotrophic factor-dependent, human neuron-like cells. *Journal of neurochemistry* **2000,** 75, (3), 991-1003.
246. Esper, R. M.; Pankonin, M. S.; Loeb, J. A., Neuregulins: versatile growth and differentiation factors in nervous system development and human disease. *Brain research reviews* **2006,** 51, (2), 161-75.
247. Gerecke, K. M.; Wyss, J. M.; Carroll, S. L., Neuregulin-1beta induces neurite extension and arborization in cultured hippocampal neurons. *Molecular and cellular neurosciences* **2004,** 27, (4), 379-93.
248. Moore, T. B.; Sidell, N.; Chow, V. J.; Medzoyan, R. H.; Huang, J. I.; Yamashiro, J. M.; Wada, R. K., Differentiating effects of 1,25-dihydroxycholecalciferol (D3) on LA-N-5 human neuroblastoma cells and its synergy with retinoic acid. *Journal of pediatric hematology/oncology* **1995,** 17, (4), 311-7.
249. Sarkanen, J. R.; Nykky, J.; Siikanen, J.; Selinummi, J.; Ylikomi, T.; Jalonen, T. O., Cholesterol supports the retinoic acid-induced synaptic vesicle formation in differentiating human SH-SY5Y neuroblastoma cells. *Journal of neurochemistry* **2007,** 102, (6), 1941-52.
250. Reddy, C. D.; Patti, R.; Guttapalli, A.; Maris, J. M.; Yanamandra, N.; Rachamallu, A.; Sutton, L. N.; Phillips, P. C.; Posner, G. H., Anticancer effects of the novel 1alpha, 25-dihydroxyvitamin D3 hybrid analog QW1624F2-2 in human neuroblastoma. *Journal of cellular biochemistry* **2006,** 97, (1), 198-206.
251. Myers, T. A.; Nickerson, C. A.; Kaushal, D.; Ott, C. M.; Honer zu Bentrup, K.; Ramamurthy, R.; Nelman-Gonzalez, M.; Pierson, D. L.; Philipp, M. T., Closing the phenotypic gap between transformed neuronal cell lines in culture and untransformed neurons. *Journal of neuroscience methods* **2008,** 174, (1), 31-41.
252. Glitsch, M. D., Spontaneous neurotransmitter release and Ca2+--how spontaneous is spontaneous neurotransmitter release? *Cell calcium* **2008,** 43, (1), 9-15.
253. Bengtson, C. P.; Bading, H., Nuclear calcium signaling. *Advances in experimental medicine and biology* **2012,** 970, 377-405.

254. Greber, U. F.; Gerace, L., Depletion of Calcium from the Lumen of Endoplasmic-Reticulum Reversibly Inhibits Passive Diffusion and Signal-Mediated Transport into the Nucleus. *Journal of Cell Biology* **1995,** 128, (1-2), 5-14.
255. Vasiljevic, M.; Heisler, F. F.; Hausrat, T. J.; Fehr, S.; Milenkovic, I.; Kneussel, M.; Sieghart, W., Spatio-Temporal Expression Analysis of the Calcium-Binding Protein Calumenin in the Rodent Brain. *Neuroscience* **2012,** 202, 29-41.
256. Grynkiewicz, G.; Poenie, M.; Tsien, R. Y., A new generation of Ca2+ indicators with greatly improved fluorescence properties. *The Journal of biological chemistry* **1985,** 260, (6), 3440-50.
257. Mank, M.; Griesbeck, O., Genetically encoded calcium indicators. *Chemical reviews* **2008,** 108, (5), 1550-64.
258. Lancaster, M. A.; Knoblich, J. A., Organogenesis in a dish: modeling development and disease using organoid technologies. *Science* **2014,** 345, (6194), 1247125.
259. Bryson, J. B.; Machado, C. B.; Crossley, M.; Stevenson, D.; Bros-Facer, V.; Burrone, J.; Greensmith, L.; Lieberam, I., Optical control of muscle function by transplantation of stem cell-derived motor neurons in mice. *Science* **2014,** 344, (6179), 94-7.
260. Cunningham, M.; Cho, J. H.; Leung, A.; Savvidis, G.; Ahn, S.; Moon, M.; Lee, P. K.; Han, J. J.; Azimi, N.; Kim, K. S.; Bolshakov, V. Y.; Chung, S., hPSC-derived maturing GABAergic interneurons ameliorate seizures and abnormal behavior in epileptic mice. *Cell stem cell* **2014,** 15, (5), 559-73.
261. Thornberry, N. A.; Lazebnik, Y., Caspases: enemies within. *Science* **1998,** 281, (5381), 1312-6.
262. Dunnett, S. B.; Hernandez, T. D.; Summerfield, A.; Jones, G. H.; Arbuthnott, G., Graft-derived recovery from 6-OHDA lesions: specificity of ventral mesencephalic graft tissues. *Experimental brain research. Experimentelle Hirnforschung. Experimentation cerebrale* **1988,** 71, (2), 411-24.
263. Kim, J. H.; Auerbach, J. M.; Rodriguez-Gomez, J. A.; Velasco, I.; Gavin, D.; Lumelsky, N.; Lee, S. H.; Nguyen, J.; Sanchez-Pernaute, R.; Bankiewicz, K.; McKay, R., Dopamine neurons derived from embryonic stem cells function in an animal model of Parkinson's disease. *Nature* **2002,** 418, (6893), 50-6.
264. Antkowiak, M.; Torres-Mapa, M. L.; Witts, E. C.; Miles, G. B.; Dholakia, K.; Gunn-Moore, F. J., Fast targeted gene transfection and optogenetic modification of single neurons using femtosecond laser irradiation. *Scientific reports* **2013,** 3, 3281.
265. Aravanis, A. M.; Wang, L. P.; Zhang, F.; Meltzer, L. A.; Mogri, M. Z.; Schneider, M. B.; Deisseroth, K., An optical neural interface: in vivo control of rodent motor cortex with integrated fiberoptic and optogenetic technology. *Journal of neural engineering* **2007,** 4, (3), S143-56.
266. Kugler, S.; Kilic, E.; Bahr, M., Human synapsin 1 gene promoter confers highly neuron-specific long-term transgene expression from an adenoviral vector in the adult rat brain depending on the transduced area. *Gene therapy* **2003,** 10, (4), 337-47.
267. Dittgen, T.; Nimmerjahn, A.; Komai, S.; Licznerski, P.; Waters, J.; Margrie, T. W.; Helmchen, F.; Denk, W.; Brecht, M.; Osten, P., Lentivirus-based genetic manipulations of cortical neurons and their optical and electrophysiological monitoring in vivo. *Proceedings of the National Academy of Sciences of the United States of America* **2004,** 101, (52), 18206-11.
268. Nathanson, J. L.; Yanagawa, Y.; Obata, K.; Callaway, E. M., Preferential labeling of inhibitory and excitatory cortical neurons by endogenous tropism of adeno-associated virus and lentivirus vectors. *Neuroscience* **2009,** 161, (2), 441-50.
269. Rein, M. L.; Deussing, J. M., The optogenetic (r)evolution. *Molecular genetics and genomics : MGG* **2012,** 287, (2), 95-109.
270. Rapti, K.; Stillitano, F.; Karakikes, I.; Nonnenmacher, M.; Weber, T.; Hulot, J. S.; Hajjar, R. J., Effectiveness of gene delivery systems for pluripotent and differentiated cells. *Molecular therapy. Methods & clinical development* **2015,** 2, 14067.
271. Stroh, A.; Tsai, H. C.; Wang, L. P.; Zhang, F.; Kressel, J.; Aravanis, A.; Santhanam, N.; Deisseroth, K.; Konnerth, A.; Schneider, M. B., Tracking stem cell differentiation in the setting of automated optogenetic stimulation. *Stem cells* **2011,** 29, (1), 78-88.

272. Marr, R. A.; Rockenstein, E.; Mukherjee, A.; Kindy, M. S.; Hersh, L. B.; Gage, F. H.; Verma, I. M.; Masliah, E., Neprilysin gene transfer reduces human amyloid pathology in transgenic mice. *The Journal of neuroscience : the official journal of the Society for Neuroscience* **2003,** 23, (6), 1992-6.
273. van Hooijdonk, L. W.; Ichwan, M.; Dijkmans, T. F.; Schouten, T. G.; de Backer, M. W.; Adan, R. A.; Verbeek, F. J.; Vreugdenhil, E.; Fitzsimons, C. P., Lentivirus-mediated transgene delivery to the hippocampus reveals sub-field specific differences in expression. *BMC neuroscience* **2009,** 10, 2.
274. Yu, D. X.; Di Giorgio, F. P.; Yao, J.; Marchetto, M. C.; Brennand, K.; Wright, R.; Mei, A.; McHenry, L.; Lisuk, D.; Grasmick, J. M.; Silberman, P.; Silberman, G.; Jappelli, R.; Gage, F. H., Modeling hippocampal neurogenesis using human pluripotent stem cells. *Stem cell reports* **2014,** 2, (3), 295-310.
275. Barbacid, M., Neurotrophic factors and their receptors. *Current opinion in cell biology* **1995,** 7, (2), 148-55.
276. Nicolini, G.; Miloso, M.; Zoia, C.; Di Silvestro, A.; Cavaletti, G.; Tredici, G., Retinoic acid differentiated SH-SY5Y human neuroblastoma cells: an in vitro model to assess drug neurotoxicity. *Anticancer research* **1998,** 18, (4A), 2477-81.
277. Constantinescu, R.; Constantinescu, A. T.; Reichmann, H.; Janetzky, B., Neuronal differentiation and long-term culture of the human neuroblastoma line SH-SY5Y. *Journal of neural transmission. Supplementum* **2007**, (72), 17-28.
278. Scadden, D. T., The stem-cell niche as an entity of action. *Nature* **2006,** 441, (7097), 1075-9.
279. Morrison, S. J.; Spradling, A. C., Stem cells and niches: mechanisms that promote stem cell maintenance throughout life. *Cell* **2008,** 132, (4), 598-611.
280. Guilak, F.; Cohen, D. M.; Estes, B. T.; Gimble, J. M.; Liedtke, W.; Chen, C. S., Control of stem cell fate by physical interactions with the extracellular matrix. *Cell stem cell* **2009,** 5, (1), 17-26.
281. Votteler, M.; Kluger, P. J.; Walles, H.; Schenke-Layland, K., Stem cell microenvironments--unveiling the secret of how stem cell fate is defined. *Macromolecular bioscience* **2010,** 10, (11), 1302-15.
282. Prowse, A. B.; Chong, F.; Gray, P. P.; Munro, T. P., Stem cell integrins: implications for ex-vivo culture and cellular therapies. *Stem cell research* **2011,** 6, (1), 1-12.
283. Kalaskar, D. M.; Downes, J. E.; Murray, P.; Edgar, D. H.; Williams, R. L., Characterization of the interface between adsorbed fibronectin and human embryonic stem cells. *Journal of the Royal Society, Interface / the Royal Society* **2013,** 10, (83), 20130139.
284. Martin, M. J.; Muotri, A.; Gage, F.; Varki, A., Human embryonic stem cells express an immunogenic nonhuman sialic acid. *Nature medicine* **2005,** 11, (2), 228-32.
285. Heydarkhan-Hagvall, S.; Gluck, J. M.; Delman, C.; Jung, M.; Ehsani, N.; Full, S.; Shemin, R. J., The effect of vitronectin on the differentiation of embryonic stem cells in a 3D culture system. *Biomaterials* **2012,** 33, (7), 2032-40.
286. Hwang, N. S.; Varghese, S.; Zhang, Z.; Elisseeff, J., Chondrogenic differentiation of human embryonic stem cell-derived cells in arginine-glycine-aspartate-modified hydrogels. *Tissue engineering* **2006,** 12, (9), 2695-706.
287. Sidhu, K.; Kim, J.; Chayosumrit, M.; Dean, S.; Sachdev, P., Alginate microcapsule as a 3D platform for propagation and differentiation of human embryonic stem cells (hESC) to different lineages. *Journal of visualized experiments : JoVE* **2012**, (61).
288. Lee, K. Y.; Mooney, D. J., Alginate: properties and biomedical applications. *Progress in polymer science* **2012,** 37, (1), 106-126.
289. Chen, K.; Huang, J.; Gong, W.; Iribarren, P.; Dunlop, N. M.; Wang, J. M., Toll-like receptors in inflammation, infection and cancer. *International immunopharmacology* **2007,** 7, (10), 1271-85.
290. Marshak-Rothstein, A.; Rifkin, I. R., Immunologically active autoantigens: the role of toll-like receptors in the development of chronic inflammatory disease. *Annual review of immunology* **2007,** 25, 419-41.
291. Heng, B. C.; Clement, M. V.; Cao, T., Caspase inhibitor Z-VAD-FMK enhances the freeze-thaw survival rate of human embryonic stem cells. *Bioscience reports* **2007,** 27, (4-5), 257-64.

292. Gauthaman, K.; Fong, C. Y.; Bongso, A., Effect of ROCK inhibitor Y-27632 on normal and variant human embryonic stem cells (hESCs) in vitro: its benefits in hESC expansion. *Stem cell reviews* **2010,** 6, (1), 86-95.
293. Hu, E.; Lee, D., Rho kinase as potential therapeutic target for cardiovascular diseases: opportunities and challenges. *Expert opinion on therapeutic targets* **2005,** 9, (4), 715-736.
294. Elmore, S., Apoptosis: a review of programmed cell death. *Toxicologic pathology* **2007,** 35, (4), 495-516.
295. Fedorovich, N. E.; Alblas, J.; de Wijn, J. R.; Hennink, W. E.; Verbout, A. J.; Dhert, W. J., Hydrogels as extracellular matrices for skeletal tissue engineering: state-of-the-art and novel application in organ printing. *Tissue engineering* **2007,** 13, (8), 1905-25.
296. Gaharwar, A. K.; Dammu, S. A.; Canter, J. M.; Wu, C. J.; Schmidt, G., Highly extensible, tough, and elastomeric nanocomposite hydrogels from poly(ethylene glycol) and hydroxyapatite nanoparticles. *Biomacromolecules* **2011,** 12, (5), 1641-50.
297. Chan, A. W.; Neufeld, R. J., Modeling the controllable pH-responsive swelling and pore size of networked alginate based biomaterials. *Biomaterials* **2009,** 30, (30), 6119-29.
298. Davidovich-Pinhas, M.; Bianco-Peled, H., A quantitative analysis of alginate swelling. *Carbohydrate polymers* **2010,** 79, (4), 1020-1027.
299. Andersen, T.; Melvik, J. E.; Gaserod, O.; Alsberg, E.; Christensen, B. E., Ionically gelled alginate foams: Physical properties controlled by type, amount and source of gelling ions. *Carbohydrate polymers* **2014,** 99, 249-256.
300. Gattazzo, F.; Urciuolo, A.; Bonaldo, P., Extracellular matrix: a dynamic microenvironment for stem cell niche. *Biochimica et biophysica acta* **2014,** 1840, (8), 2506-19.
301. Lee, K. Y.; Mooney, D. J., Hydrogels for tissue engineering. *Chemical reviews* **2001,** 101, (7), 1869-1879.
302. Green, K. N.; Smith, I. F.; Laferla, F. M., Role of calcium in the pathogenesis of Alzheimer's disease and transgenic models. *Sub-cellular biochemistry* **2007,** 45, 507-21.
303. Carroll, J. C.; Rosario, E. R.; Chang, L.; Stanczyk, F. Z.; Oddo, S.; LaFerla, F. M.; Pike, C. J., Progesterone and estrogen regulate Alzheimer-like neuropathology in female 3xTg-AD mice. *The Journal of neuroscience : the official journal of the Society for Neuroscience* **2007,** 27, (48), 13357-65.
304. Hsiong, S. X.; Boontheekul, T.; Huebsch, N.; Mooney, D. J., Cyclic arginine-glycine-aspartate peptides enhance three-dimensional stem cell osteogenic differentiation. *Tissue engineering. Part A* **2009,** 15, (2), 263-72.
305. Kendall, W. F.; Darrabie, M. D.; El-Shewy, H. M.; Opara, E. C., Effect of alginate composition and purity on alginate microspheres. *Journal of microencapsulation* **2004,** 21, (8), 821-828.
306. Gautier, A.; Carpentier, B.; Dufresne, M.; Vu Dinh, Q.; Paullier, P.; Legallais, C., Impact of alginate type and bead diameter on mass transfers and the metabolic activities of encapsulated C3A cells in bioartificial liver applications. *European cells & materials* **2011,** 21, 94-106.
307. Bajpai, S. K.; Sharma, S., Investigation of swelling/degradation behaviour of alginate beads crosslinked with Ca2+ and Ba2+ ions. *React Funct Polym* **2004,** 59, (2), 129-140.
308. Chawla, K.; Yu, T. B.; Liao, S. W.; Guan, Z. B., Biodegradable and Biocompatible Synthetic Saccharide-Peptide Hydrogels for Three-Dimensional Stem Cell Culture. *Biomacromolecules* **2011,** 12, (3), 560-567.
309. Shoichet, M. S.; Li, R. H.; White, M. L.; Winn, S. R., Stability of hydrogels used in cell encapsulation: An in vitro comparison of alginate and agarose. *Biotechnology and bioengineering* **1996,** 50, (4), 374-381.
310. Heng, B. C.; Li, J.; Chen, A. K. L.; Reuveny, S.; Cool, S. M.; Birch, W. R.; Oh, S. K. W., Translating Human Embryonic Stem Cells from 2-Dimensional to 3-Dimensional Cultures in a Defined Medium on Laminin- and Vitronectin-Coated Surfaces. *Stem cells and development* **2012,** 21, (10), 1701-1715.

311. Xu, C. H.; Inokuma, M. S.; Denham, J.; Golds, K.; Kundu, P.; Gold, J. D.; Carpenter, M. K., Feeder-free growth of undifferentiated human embryonic stem cells. *Nature biotechnology* **2001,** 19, (10), 971-974.
312. Ludwig, T. E.; Levenstein, M. E.; Jones, J. M.; Berggren, W. T.; Mitchen, E. R.; Frane, J. L.; Crandall, L. J.; Daigh, C. A.; Conard, K. R.; Piekarczyk, M. S.; Llanas, R. A.; Thomson, J. A., Derivation of human embryonic stem cells in defined conditions. *Nature biotechnology* **2006,** 24, (2), 185-187.
313. Chayosumrit, M.; Tuch, B.; Sidhu, K., Alginate microcapsule for propagation and directed differentiation of hESCs to definitive endoderm. *Biomaterials* **2010,** 31, (3), 505-514.
314. Pierschbacher, M. D.; Ruoslahti, E., Cell Attachment Activity of Fibronectin Can Be Duplicated by Small Synthetic Fragments of the Molecule. *Nature* **1984,** 309, (5963), 30-33.
315. Wan, A. C. A.; Tai, B. C. U.; Schumacher, K. M.; Schumacher, A.; Chin, S. Y.; Ying, J. Y., Polyelectrolyte complex membranes for specific cell adhesion. *Langmuir : the ACS journal of surfaces and colloids* **2008,** 24, (6), 2611-2617.
316. Derda, R.; Li, L. Y.; Orner, B. P.; Lewis, R. L.; Thomson, J. A.; Kiessling, L. L., Defined substrates for human embryonic stem cell growth identified from surface arrays. *ACS chemical biology* **2007,** 2, (5), 347-355.
317. Aguado, B. A.; Mulyasasmita, W.; Su, J.; Lampe, K. J.; Heilshorn, S. C., Improving Viability of Stem Cells During Syringe Needle Flow Through the Design of Hydrogel Cell Carriers. *Tissue Eng Pt A* **2012,** 18, (7-8), 806-815.
318. Tanzeglock, T.; Soos, M.; Stephanopoulos, G.; Morbidelli, M., Induction of Mammalian Cell Death by Simple Shear and Extensional Flows. *Biotechnology and bioengineering* **2009,** 104, (2), 360-370.
319. Spitzer, N. C., Electrical activity in early neuronal development. *Nature* **2006,** 444, (7120), 707-12.
320. Hanse, E.; Seth, H.; Riebe, I., AMPA-silent synapses in brain development and pathology. *Nature reviews. Neuroscience* **2013,** 14, (12), 839-50.
321. Bardy, C.; van den Hurk, M.; Eames, T.; Marchand, C.; Hernandez, R. V.; Kellogg, M.; Gorris, M.; Galet, B.; Palomares, V.; Brown, J.; Bang, A. G.; Mertens, J.; Bohnke, L.; Boyer, L.; Simon, S.; Gage, F. H., Neuronal medium that supports basic synaptic functions and activity of human neurons in vitro. *Proceedings of the National Academy of Sciences of the United States of America* **2015,** 112, (20), E2725-34.
322. Smetters, D.; Majewska, A.; Yuste, R., Detecting action potentials in neuronal populations with calcium imaging. *Methods* **1999,** 18, (2), 215-21.
323. Barnett, M. W.; Larkman, P. M., The action potential. *Practical neurology* **2007,** 7, (3), 192-7.
324. Johnson, M. A.; Weick, J. P.; Pearce, R. A.; Zhang, S. C., Functional neural development from human embryonic stem cells: accelerated synaptic activity via astrocyte coculture. *The Journal of neuroscience : the official journal of the Society for Neuroscience* **2007,** 27, (12), 3069-77.
325. Wernig, M.; Zhao, J. P.; Pruszak, J.; Hedlund, E.; Fu, D.; Soldner, F.; Broccoli, V.; Constantine-Paton, M.; Isacson, O.; Jaenisch, R., Neurons derived from reprogrammed fibroblasts functionally integrate into the fetal brain and improve symptoms of rats with Parkinson's disease. *Proceedings of the National Academy of Sciences of the United States of America* **2008,** 105, (15), 5856-61.
326. Wu, H.; Xu, J.; Pang, Z. P.; Ge, W.; Kim, K. J.; Blanchi, B.; Chen, C.; Sudhof, T. C.; Sun, Y. E., Integrative genomic and functional analyses reveal neuronal subtype differentiation bias in human embryonic stem cell lines. *Proceedings of the National Academy of Sciences of the United States of America* **2007,** 104, (34), 13821-6.
327. Avaliani, N.; Sorensen, A. T.; Ledri, M.; Bengzon, J.; Koch, P.; Brustle, O.; Deisseroth, K.; Andersson, M.; Kokaia, M., Optogenetics reveal delayed afferent synaptogenesis on grafted human-induced pluripotent stem cell-derived neural progenitors. *Stem cells* **2014,** 32, (12), 3088-98.
328. Colasante, G.; Lignani, G.; Rubio, A.; Medrihan, L.; Yekhlef, L.; Sessa, A.; Massimino, L.; Giannelli, S. G.; Sacchetti, S.; Caiazzo, M.; Leo, D.; Alexopoulou, D.; Dell'Anno, M. T.; Ciabatti, E.; Orlando, M.; Studer, M.; Dahl, A.; Gainetdinov, R. R.; Taverna, S.; Benfenati, F.; Broccoli, V., Rapid

Conversion of Fibroblasts into Functional Forebrain GABAergic Interneurons by Direct Genetic Reprogramming. *Cell stem cell* **2015,** 17, (6), 719-34.
329. Chung, W. S.; Allen, N. J.; Eroglu, C., Astrocytes Control Synapse Formation, Function, and Elimination. *Cold Spring Harbor perspectives in biology* **2015,** 7, (9), a020370.
330. Tian, N.; Copenhagen, D. R., Visual stimulation is required for refinement of ON and OFF pathways in postnatal retina. *Neuron* **2003,** 39, (1), 85-96.

Appendices

Appendix 1 – List of materials and reagents

Materials/Reagents	Producer
1 ml syringes	BD BIOSCIENCE
0.5 mm needles	BD BIOSCIENCE
1.5 ml Eppendorf tube	EPPENDORF
15 ml falcon tubes	CORNING
50 ml falcon tubes	CORNING
75 cm^2 flasks	CORNING
225 cm^2 flasks	CORNING
96-well flat bottom plates	CORNING
96-well v-bottom plates	CORNING
6-well plates	CORNING
24-well plates	IBIDI
Accutase	INVITROGEN
Advanced protein assay (ADVA01)	INVITROGEN
Axol neural differentiation-XF medium	AXOL BIOSCIENCE
Axol neural maintenance-XF medium	AXOL BIOSCIENCE
Axol plating-XF medium	AXOL BIOSCIENCE
B-27 supplement	GIBCO
BD matrigel	THEMOFISHER
BDNF	PEPROTECH
BSA	PEPROTECH
$CaCl_2$	SIGMA
CAL-590 AM	ATT BIOQUEST
cytofix/cytoperm solution	BD BIOSCIENCE
D-glucose	SIGMA
DMEM	GIBCO
DMSO	SIGMA
EDC	SIGMA
FBS	INVITROGEN
FGF	INVITROGEN
HD5a bacteria	INVTROGEN
Ionomycin	SIGMA
KCl	SIGMA
KOSR	INVITROGEN
Laminin 2020	SIGMA
LB	SIGMA
LG-A2158 alginate	SIGMA
L-Glutamine	INVITROGEN
lipofectamine-2000	INVITROGEN
Live-dead cell staining kit	SIGMA

Materials/Reagents	Producer
MES buffer	SIGMA
$MgCl_2.6H_2O$	SIGMA
Mitomycin C	SIGMA
mTeSR1 medium	STEMCELL TECHNOLOGIES
N-2 supplement	GIBCO
NaCl	SIGMA
NaH_2PO_4	SIGMA
Neurobasal medium	GIBCO
NGF	PEPROTECH
Opti-MEM I reduced serum medium	INVITROGEN
Paraformaldehyde	SIGMA
PBS	SIGMA
Penicillin/streptomycin (pen-strep)	GIBCO
Perm/wash solution	BD BIOSCIENCE
Plasmid purification kit	QIAGEN
plasmids (pSPAX2 or pMD2.G)	INVITROGEN
Pluronic F-127	SIGMA
Poly-L-ornithine solution	SIGMA
Presto blue assay	INVTROGEN
QuickTiter™ Lentivirus Titer Kit	CELL BIOLABS
RA	SIGMA
EcoR1, Not1 and HindIII restriction enzyme	NEW ENGLAND BIOLABS
RGD peptide	PEPROTECH
ROCKi, Y-27632	CALBIOCHEM
RPMI 1640 medium	GIBCO
ß-Mercaptoethanol	SIGMA
Sulfo-NHS	SIGMA
Syringe pump	HARVARD APPARATUS
Trypan Blue solution 0.4%	SIGMA
Trypsin-EDTA	INVITROGEN
UP-MVG alginate	PRONOVA BIOMEDICAL
X-Rhod-1 AM	INVITROGEN
Z-VAD-FMK	ENZO LIFE SCIENCES

Appendix 2 - List of medium

1. MEF medium

MEF Medium (500 ml)	Concentration (ml)
DMEM	445
10% FBS	50
1% MEM Non-essential amino acids (NEAA) (10 mM, 100x)	5
1% pen-strep (100x, optional)	

2. hESC medium

hESC Medium (500 ml)	Concentration (ml)
DMEM/F-12	390
20% KOSR	100
2 mM L-Glutamine (200 mM, 100x)	5
0.1 mM MEM Non-essential amino acids (NEAA) (10 mM, 100x)	5
0.1 mM ß-Mercaptoethanol (14.3 M)	0.0035
4 ng/ml FGF (4 µg/ml)*	0.5
1% pen-strep (100x, optional)	

*Freshly add

3. SY5Y maintenance medium

Maintenance Medium (500 ml)	Concentration (ml)
RPMI 1640 medium	440
10% FBS	50
0.1 mM MEM Non-essential amino acids (NEAA) (10 mM, 100x)	5
1% pen-strep (100x)	5

4. SY5Y complete medium

Complete Medium (500 ml)	Concentration (ml)
RPMI 1640 medium	440
10% FBS	50
0.1 mM MEM Non-essential amino acids (NEAA) (10 mM, 100x)	5
1% pen-strep (100x)	5
Retinoic acid (50 µM)	0.5

5. SY5Y differentiation medium

Differentiation Medium (1,000 ml)	Concentration (ml)
DMEM/F-12	475
0.5% N-2 supplement (100X)	5
0.5% B-27 supplement (50X)	10
0.1% BDNF *	1
1% pen-strep (100x)	10
Neurobasal media	500

*Freshly add

6. HEK 293FT complete medium (500 ml)

Complete Medium (500 ml)	Concentration (ml)
DMEM (high glucose)	430
10% FBS	50
0.1 mM MEM Non-essential amino acids (NEAA) (10 mM, 100x)	5
2 mM L-glutamine (200 mM, 100x)	5
1 mM MEM sodium pyruvate (100 mM, 100x)	5
1% pen-strep (optional, 100x)	5
Antibiotic	500 g/ml
Freezing medium (100 ml)	
90% complete medium	90
10% DMSO	10

7. Virus production medium

Transfection Medium (500 ml)	Concentration (ml)
Opti-MEM	485
1% GlutaMAX (100x)	5
1 mM MEM sodium pyruvate (100 mM, 100x)	5
1% pen-strep (100x)	5

8. Imaging buffer

Artificial cerebrospinal fluid, ACSF (50 ml)	Concentration (mg)
$CaCl_2$ (1.1 mM)	6.10
D-glucose (20 mM)	180.00
KCl (4.2 mM)	15.65
$MgCl_2$ (0.3mM)	1.43
$MgSO_4$ (0.4 mM)	2.41
NaCl (121 mM)	353.50
NaH_2PO_4 (0.5 mM)	3.60
$NaH_2PO_4.H_2O$ (0.45 mM)	3.20
$NaHCO_3$ (29 mM)	121.80

Appendix 3 – Vector map of SYN1 and CaMKII promoter

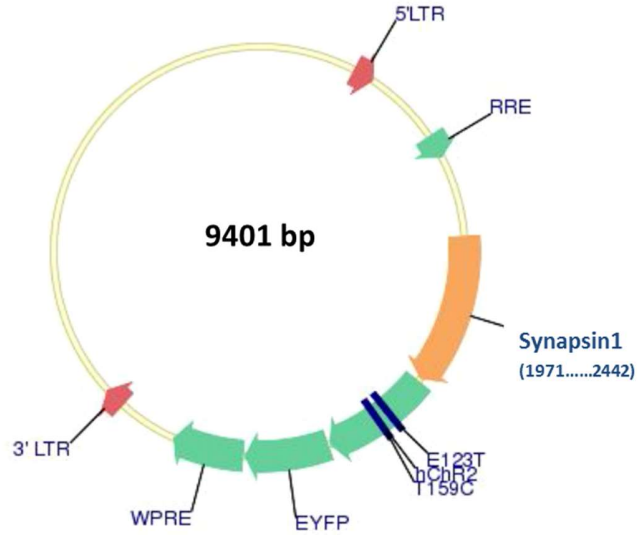

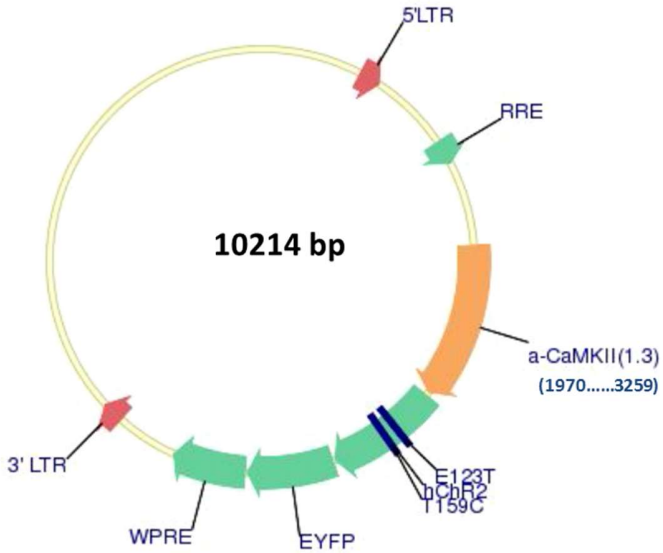

Appendix 4 - List of antibodies

Primary antibody	Dilution	Provider
Tuj1	1:1000	abcam, Cambridge, UK
GABA-B-R1	1:50	abcam, Cambridge, UK
S100B	1:200	abcam, Cambridge, UK
GFAP	1:2500	abcam, Cambridge, UK
vGlut1	1:100	abcam, Cambridge, UK

Secondary antibody	Dilution	Provider
Alexa Fluor®649-conjugated goat-anti rabbit	1:500	Invitrogen, Life Technologies, USA
Alexa Fluor®568-conjugated goat anti-mouse	1:500	Invitrogen, Life Technologies, USA
Alexa Fluor®488-conjugated goat anti-rabbit	1:500	Invitrogen, Life Technologies, USA
Alexa Fluor®649-conjugated goat anti-rabbit	1:500	Invitrogen, Life Technologies, USA
PerCP-Cy5.5-conjugated goat anti-mouse IgG_{2a}	1:400	Santa Cruz Biotechnology, USA

Appendix 5 – Amino acid analysis

Amino Acid Analysis

Printed 03/02/2015
A22356 R1 S Lee.xls

Alta code **A22356 R1**
Sample name **S1**
Analysis after hydrolysis, 24 hours at 110°C

Units / mg

AA	nmole / mg	ug / mg	mg / mg	g / 100g
Cysteic acid[1]	–	–	–	–
Hydroxyproline[1]	–	–	–	–
Aspartic acid	11	1.3	0.0013	0.13
Threonine	–	–	–	–
Serine	8.5	0.74	0.00074	0.074
Glutamic acid	0.43	0.055	0.000055	0.0055
Proline	–	–	–	–
Glycine	21	1.2	0.0012	0.12
Alanine	0.12	0.0087	0.0000087	0.00087
Cystine	–	–	–	–
Valine	–	–	–	–
Methionine	–	–	–	–
Isoleucine	–	–	–	–
Leucine	0.14	0.016	0.000016	0.0016
Tyrosine	–	–	–	–
Phenylalanine	–	–	–	–
Histidine	0.58	0.079	0.000079	0.0079
Tryptophan[1]	–	–	–	–
Lysine	0.14	0.018	0.000018	0.0018
Arginine	8.8	1.4	0.0014	0.14
Totals	51	4.8	0.0048	0.48

sample notes: Some amino acids detectable at levels on the boundary of levels of quantification. Making identification uncertain.

Notes about amino acid analysis:-
* on chromatogram denotes unknown, co-eluting or unsure assignment.
Asn and Gln are completely converted to Asp and Glu during the acid hydrolysis of the protein.
The values for Thr and Ser have been corrected for hydrolysis losses of 5% and 10% respectively.
Trp usually suffers complete loss during acid hydrolysis and is not normally quantified.
Cys is usually observed as cystine and its recovery is variable using standard hydrolysis conditions.
The values for His are sometimes affected by co-eluting compounds from the sample.
The reported values have been rounded off to either 2 or 3 significant figures, depending on peak size.

Note 1. Although listed, values for these compounds are only assigned when specific analysis has been requested.

Appendix 6 – Flow cytometry analysis of ChR2 expression

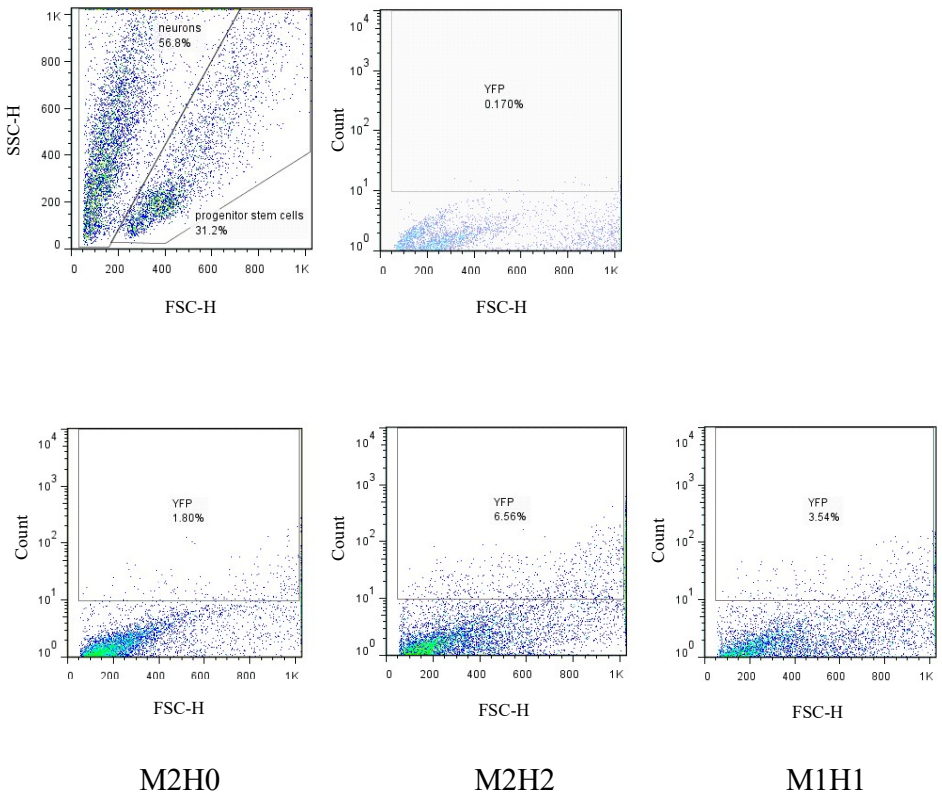

Figure 6.1: Transduced Axol cells show positive ChR2 expression (%) driven by SYN1 promoter at different MOI on 7 day-post-infection.

Negative expression was found in non-transduced cells which were used as a control (top right).

Appendix 7 – Flow cytometry analysis of hiPSC-derived neurons (Axol cells)

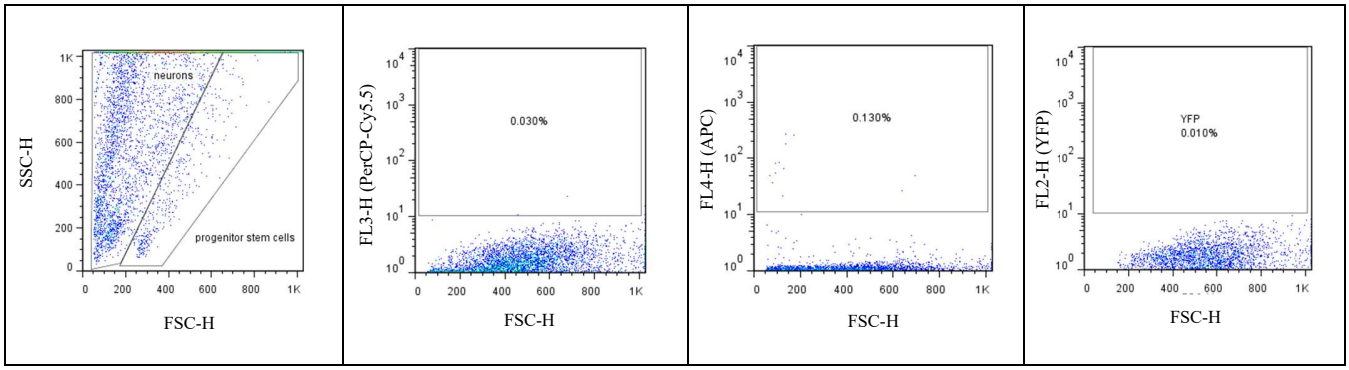

Figure 6.2: Unstained and non-transduced Axol cells were used as a control.

Negative expression was shown in cells labelled with PerCP-Cy5.5 (Tuj1 and GABA markers) and APC (GFAP and VGLUT1 markers) and YFP (ChR2).

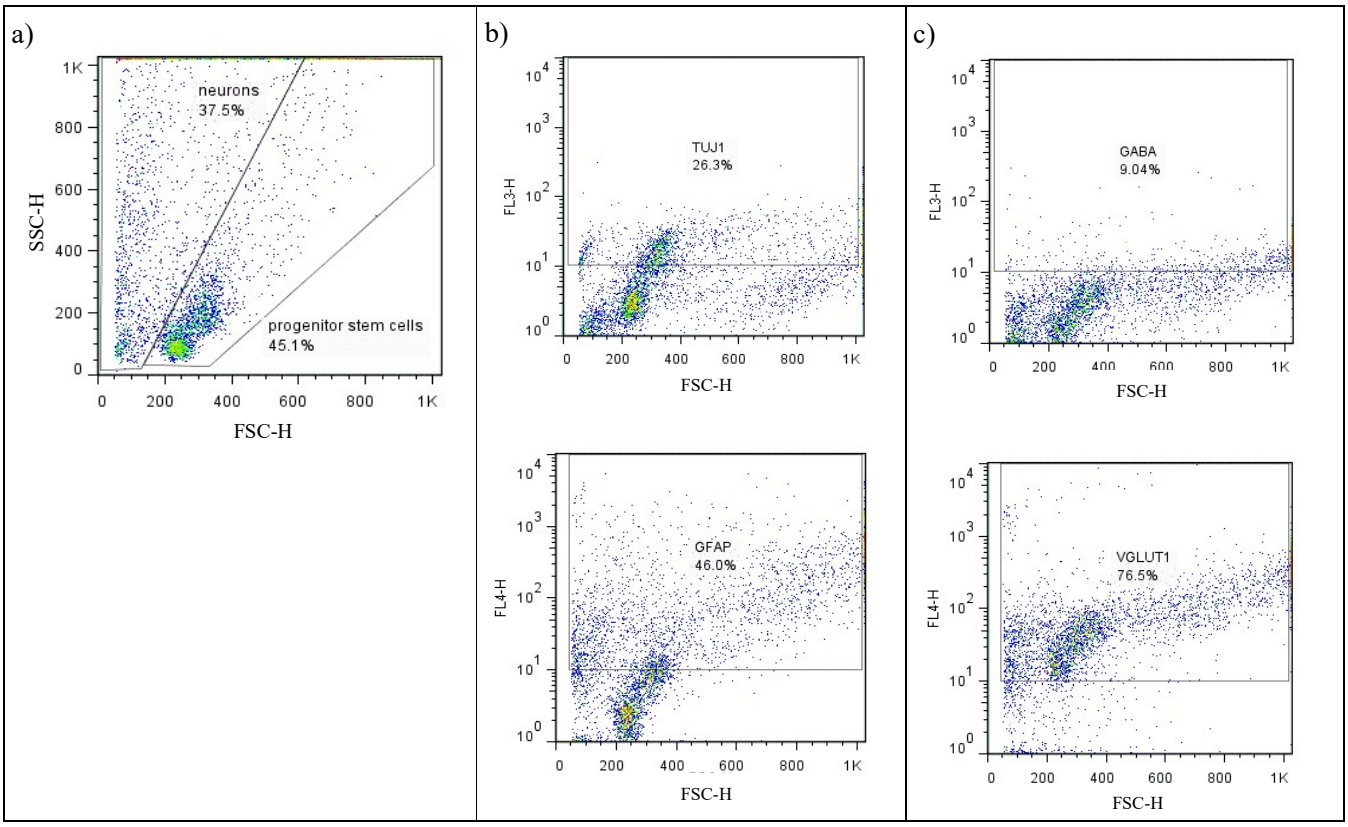

Figure 6.3: pSYN1-ChR2-YFP driven Axol cells show heterogeneous population and the sub-classes of neurons are identified.

(a) neurons and progenitor stem cells, (b) TuJ1 positive for mature neurons and GFAP positive for astrocytes in the neuron population, (c) GABA positive for GABAergic neurons and VGLUT1 positive for glutamatergic neurons in the mature neuron population.

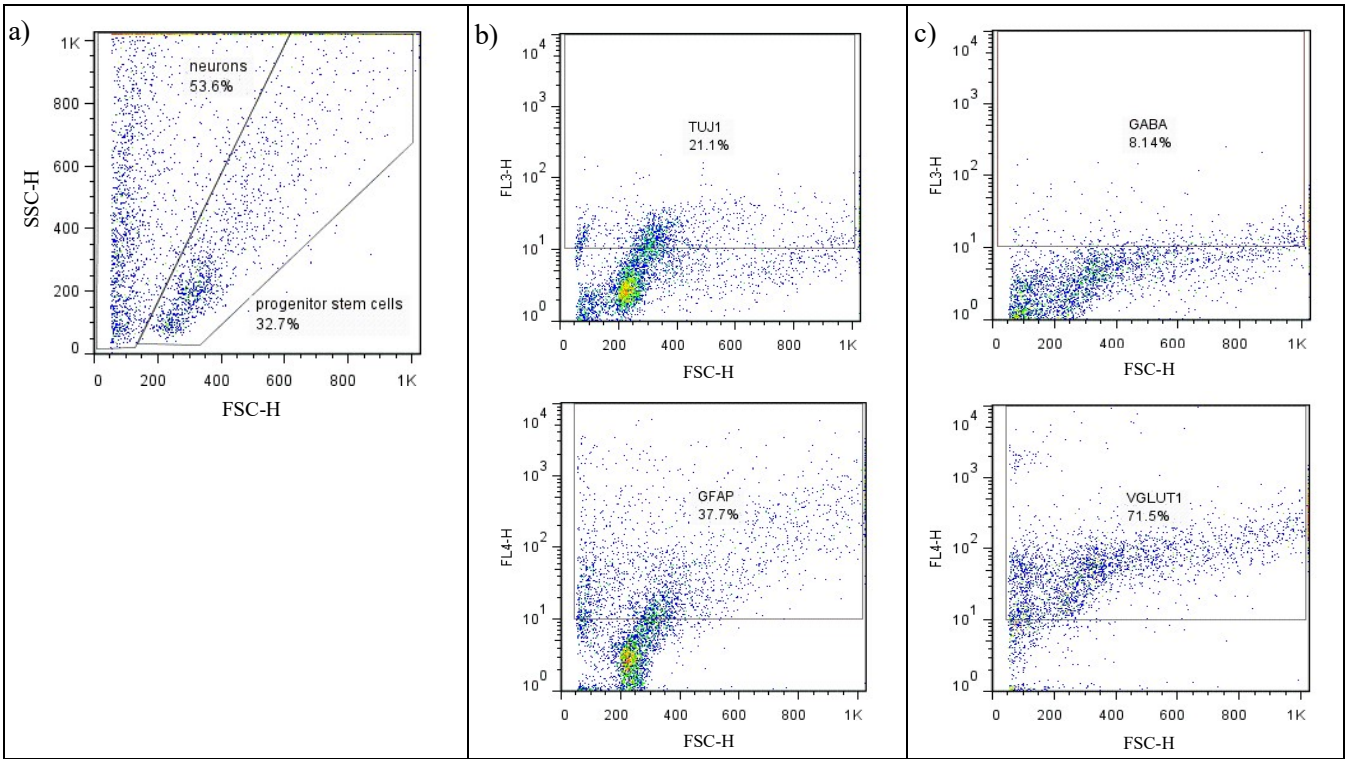

Figure 6.4: pCaMKII-ChR2-YFP driven Axol cells show heterogeneous population and the sub-classes of neurons are identified.

(a) neurons and progenitor stem cells, (b) TuJ1 positive for mature neurons and GFAP positive for astrocytes in the neuron population, (c) GABA positive for GABAergic neurons and VGLUT1 positive for glutamatergic neurons in the mature neuron population.

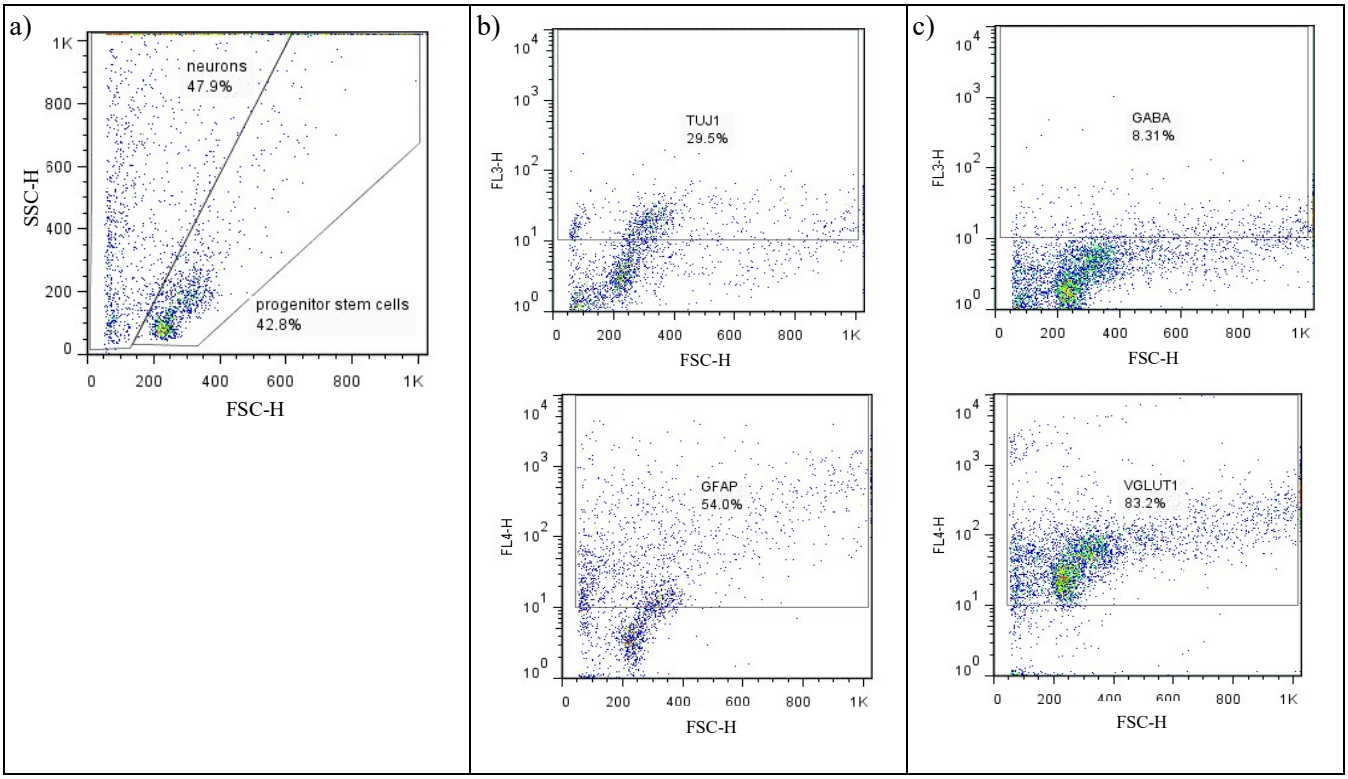

Figure 6.5: pEF1a-ChR2-YFP driven Axol cells show heterogeneous population and the sub-classes of neurons are identified.

(a) neurons and progenitor stem cells, (b) TuJ1 positive for mature neurons and GFAP positive for astrocytes in the neuron population, (c) GABA positive for GABAergic neurons and VGLUT1 positive for glutamatergic neurons in the mature neuron population.

Appendix 8 – Bright field and fluorescence images of SY5Y cells in the 3D culture systems

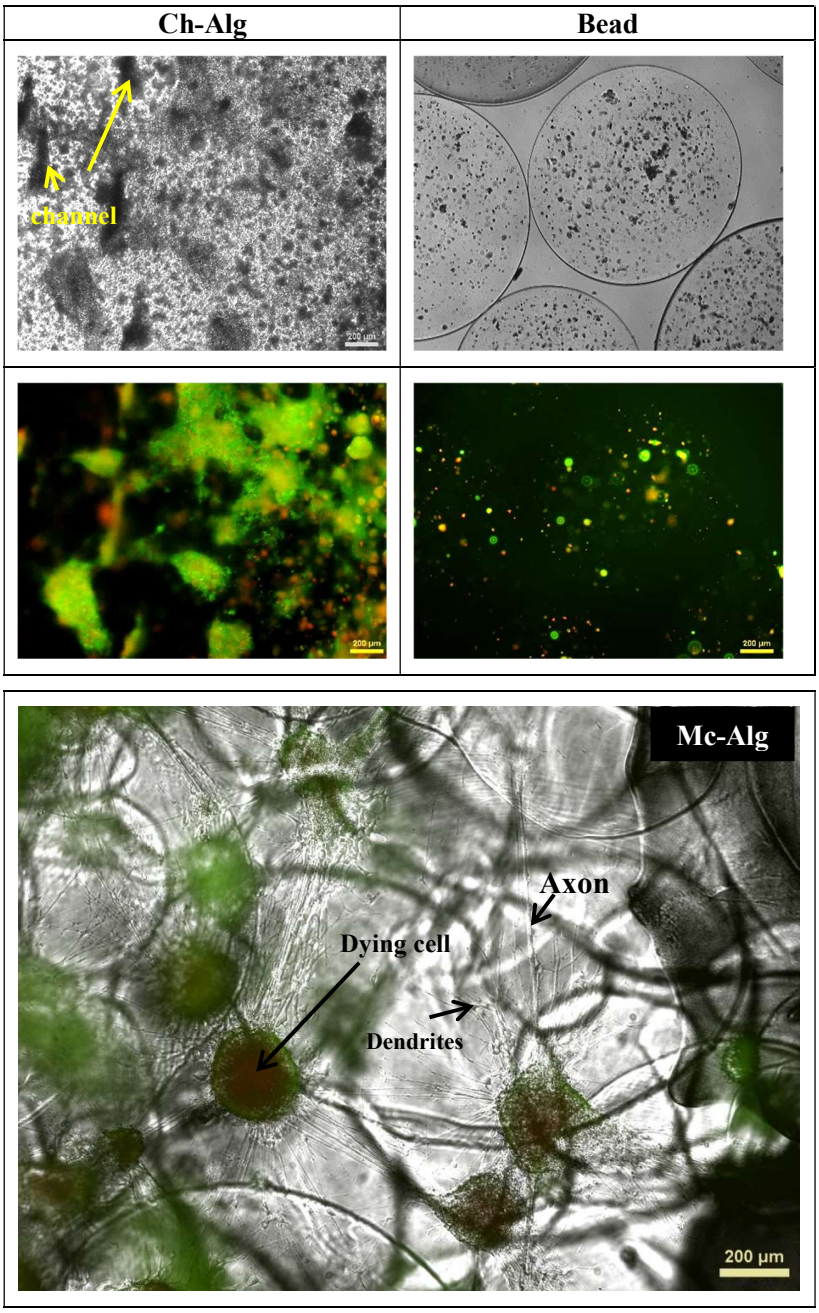

Figure 6.6: Live-dead cell staining of SY5Y cells in different 3D culture system at day 14.

The cells attached to the surface of alginate whilst dendrites and axon were branching into the channels of Ch-Alg and spaces between Mc-Alg. The cells encapsulated in beads however, formed in small aggregates without neurite extension. Live cells stained in green; dead cells stained in red. Fluorescence imaging of cells was performed using fluorescence microscopy (Nikon Eclipse T_i-E, Japan). Scale bar: 200 µm

Appendix 9 – Size and physical morphology of alginate (LG-A2158)

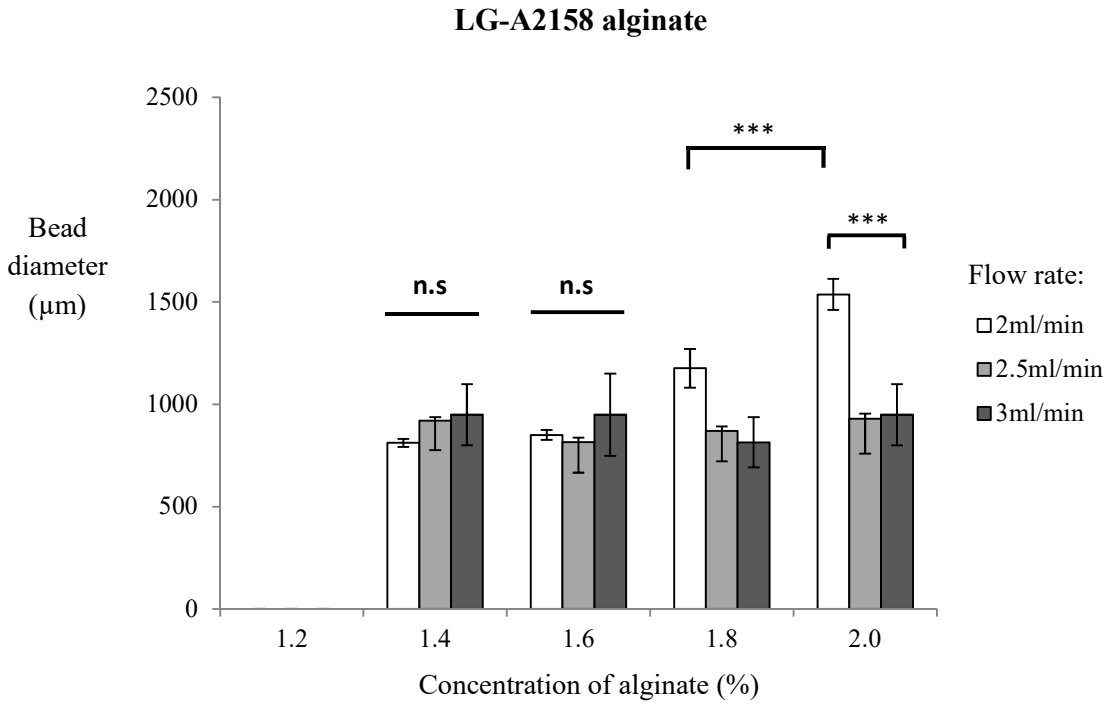

Figure 6.7: The effect of alginate concentration (%) and flow rate (ml/min) on the diameter of beads derived from different type of alginate (LG-A2158, n=50).

A concentration of 1.2% alginate formed clumps of irregular shape preventing diameter measurement. No significant differences in bead size were detected at concentrations of 1.4 and 1.6% alginate in all flow rates except 2 ml/min for 1.8 and 2.0%. The study was performed in three independent experiments. Significance was tested by two-way ANOVA *** = $p<0.001$; error bars denote standard error of the mean (±SEM).

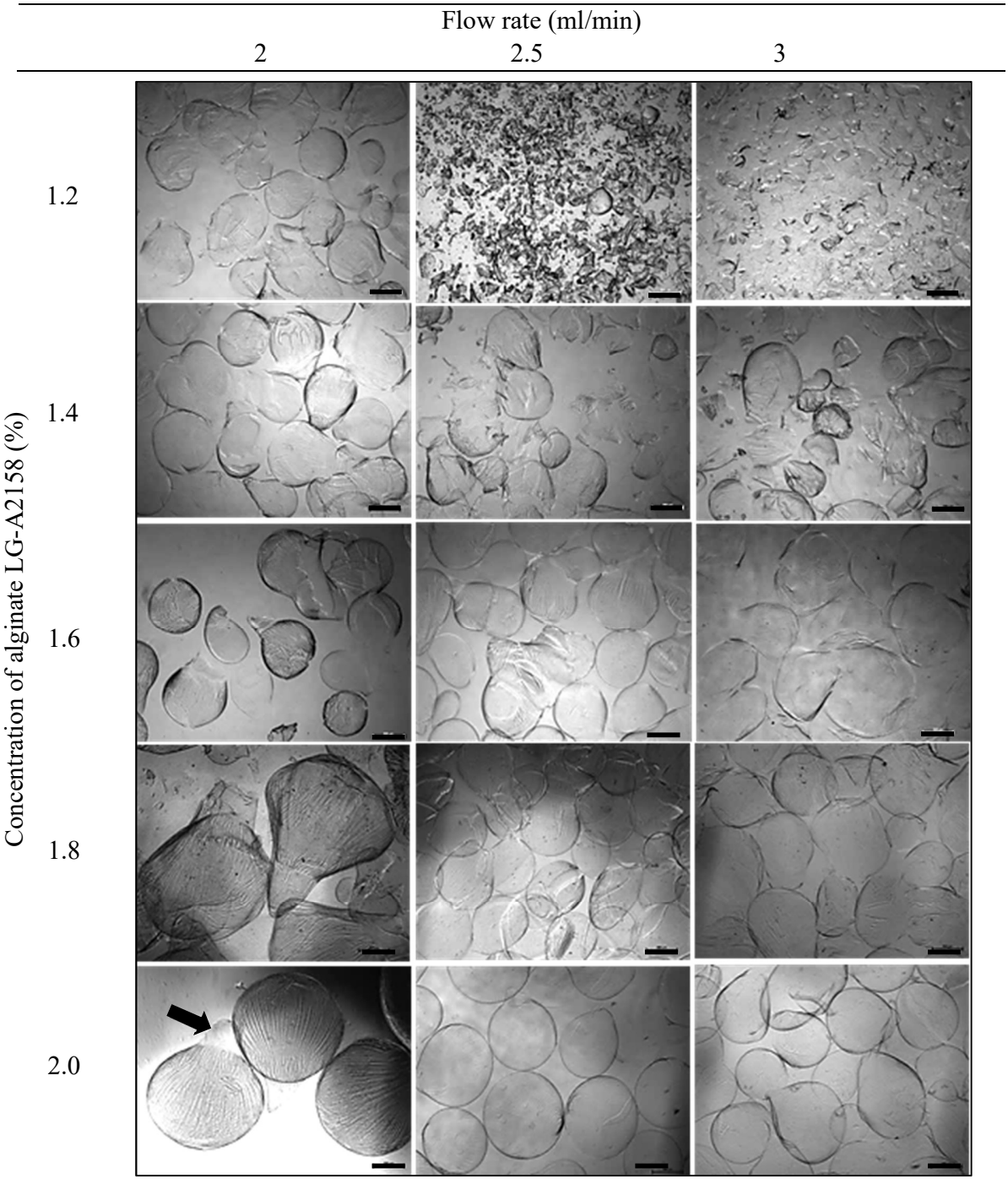

Figure 6.8: Morphology of LG-A2158 alginate beads with low G content derived from different concentrations of alginate and flow rates.
Non-spherical alginate hydrogel beads were produced at concentration of 1.2% whilst ovoid beads with tails or satellite fractions (arrow) formed at concentrations of 1.4% – 2.0%. Figure shows representative images depicting the entire population of alginate beads (n=15) under a fluorescence microscope (Nikon Eclipse T_i-E, Japan). Scale bar: 500 µm.

Appendix 10 – An initial set up: Functional study of 2D neural network using multielectrode array (MEA) recordings

Methods and Materials:

The multielectrode array recordings were based on the procedures reported by Tian, N. et al [330]. Briefly, the cells in the well were placed in the MEA-265 multielectrode array recording chamber of 30 μm diameter electrodes spaced 200 μm apart (Multi Channel System MCS GmbH, Reutlingen, Germany). Recordings were started after the cells were positioned in the recording chamber. The interval between onsets of each light stimulus was 1-5 sec. The signals were filtered between 200 Hz (low cut off) and 20 kHz (high cut off).

Preliminary results:

Multielectrode array analysis (MEA) is another tool used to measure network response to light-addressed stimulation of ChR2-positive or ChR2-negative neurons. Two types of cells were seeded on the MEA microchip in this study i.e Axol cells and SY5Y cells. Action potential (AP) is observed within 14 days after the seeding of Axol cells. The cells were detached from MEA microchip before 21 days of recording (Fig. 6.9a). However, some of the SY5Y cells are still remained attach on the microchip and therefore allowing initial data to be collected (Fig. 6.9b). Results show increasing APs in SY5Y cells containing pSYN1-ChR2-YFP from 13.5 (day 14) to 64.5 (day 21), indicated that maturation of neuron is proportional to the time. When compared to SY5Y cells containing pCaMKII-ChR2-YFP on day 21, pSYN1-ChR2-YFP demonstrated 2 fold higher of APs, again suggesting that SYN1 is a strong promoter which targeted more neuronal cells than excitatory neuron-specific CaMKII promoter. Cell detachment from MEA microchip is a major drawback which needs to be resolved for future set up.

a

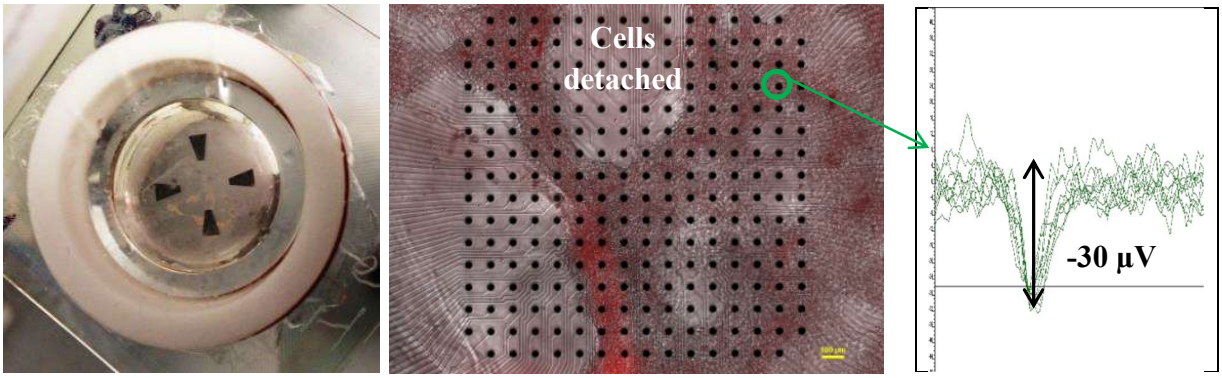

b

Time (Day)	SY5Y	SY5Y-ChR2-SYN1	SY5Y-ChR2-CaMKII
14	48	13.5	Nil
21	Nil (cells detached)	64.5	37

Figure 6.9: Multielectrode array (MEA) analysis of optogenetically modified SY5Y cells in the culture over time.

(a) Cells were seeded on the MEA microchip with 256 arrays of electrodes. Current major issue encountered is detachment of seeded cells (Axol and SY5Y) from the surface of MEA dish after lentiviral transduction (middle). The cells could not sustain longer culture (>21 days) on the MEA microchip, hence further recording of higher time point was unable to achieve. An example of action potential or spike obtained from an electrode output at maximum average rate of firing at 0.16 Hz was displayed (right) (b) Number of spike generated upon light stimulation (LED 470 nm) at 100 ms (Frequency/15 min) was shown in the table.